PUBLISCIENCE

A RESEARCH JOURNAL OF HIGH SCHOOL RESEARCH

VOLUME 4 ISSUE 1

AUGUST 2021

EDITORIAL BOARD

DISCLAIMER

Publiscience (ISSN: 2619-7359) is published annually by the Research Unit of Philippine Science High School – Western Visayas Campus, Brgy. Bito-on, Jaro, Iloilo City spearheaded by the Editorial Board composed of Batch 2021 students.

Please address all matters regarding exchange of publications to the Editors-in-Chief of the Publiscience Editorial Board of Philippine Science High School – Western Visayas Campus, Brgy. Bito-on, Jaro, Iloilo City, Philippines.

Mail: The Editors-in-Chief
Publiscience
Philippine Science High School
Western Visayas Campus
Brgy Bito-on, Jaro, Iloilo City
5000 Philippines

Trunklines: *Director's Office Direct Line*
+63-33-3295644

Registrar's Office Direct Line
+63-33-3290501

+63-33-5014335
+63-33-5014133

E-mail: publiscience@wvc.pshs.edu.ph

The views and opinions expressed by the authors in their articles do not reflect the views and opinions of the Editorial Board, the academic unit, the institution, and the agency. The articles have been rigorously reviewed by their fellow scholars, respective advisers, the research teachers, the Research Academic Unit Head, a three-person defense panel, the Editorial Board, and two external reviewers; nonetheless, readers must exercise caution in citing the articles herein. The journal is more tolerant in publishing articles. Published here are studies performed by high school students. Please refer to the review process in the Research Program page.

You may visit the website for the softcopy of the journal and previous issue via the QR code or by visiting: http://publiscience.org/

ABOUT THE COVER

The cover features bunker fuel on foil. Bunker fuel, which powers marine vessels, is the most common type of oil in oil spill incidents. A heavy fuel oil that evaporates only in small percentages and has a higher viscosity relative to other oil types, it is highly persistent in environments where it is not supposed to be in. Just like bunker fuel, our persistence in the most uncanny and difficult situations makes us float on top. No obstacle can easily absorb our energy to push us to giving up. Instead, we take it as a challenge to improve ourselves, becoming victors in the end.

ABOUT PSHS

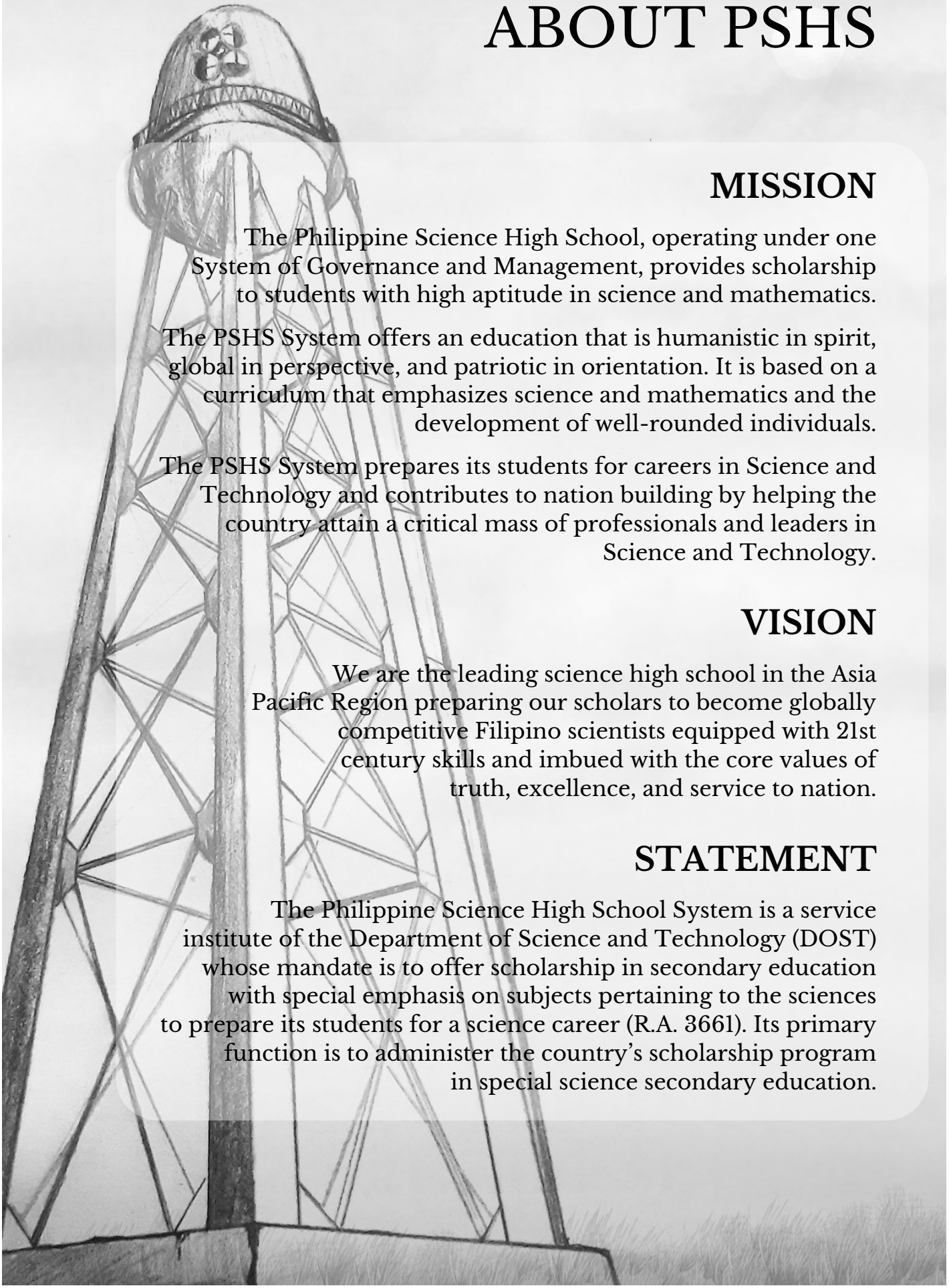

MISSION

The Philippine Science High School, operating under one System of Governance and Management, provides scholarship to students with high aptitude in science and mathematics.

The PSHS System offers an education that is humanistic in spirit, global in perspective, and patriotic in orientation. It is based on a curriculum that emphasizes science and mathematics and the development of well-rounded individuals.

The PSHS System prepares its students for careers in Science and Technology and contributes to nation building by helping the country attain a critical mass of professionals and leaders in Science and Technology.

VISION

We are the leading science high school in the Asia Pacific Region preparing our scholars to become globally competitive Filipino scientists equipped with 21st century skills and imbued with the core values of truth, excellence, and service to nation.

STATEMENT

The Philippine Science High School System is a service institute of the Department of Science and Technology (DOST) whose mandate is to offer scholarship in secondary education with special emphasis on subjects pertaining to the sciences to prepare its students for a science career (R.A. 3661). Its primary function is to administer the country's scholarship program in special science secondary education.

Be a PSHS Scholar today!

RACE (Requirements for Admission, Criteria and Evaluation)

- **2-stage** selection procedure.
    1. Determining applicant's **predicted NCE grade** (PNG) based on **final grades** in Science and Mathematics in Grade 5.
    2. Writing skills test through an **essay submission** and the **applicant's academic rank** at the end of Grade 5.
- Applicants will be **ranked** based on final score.
- Top **240** applicants – Principal Qualifiers to PSHS – MC.
- Top **90 or 120** applicants – Principal Qualifiers to PSHS Regional Campuses (depending on quota).

Admission requirements

- Final grade of **85% or better** in Science and Mathematics
- **Filipino citizen** (with no pending applications)
- Born **on or after** August 1, 2006
- **First time** to take the DOST-PSHS National Competitive Exam
- **Satisfactory** character rating
- **Good health and fit to handle** the program

Perks of being a PSHS scholar

- Recipient of a **globally-competitive education** specializing in Science, Technology, Engineering, and Mathematics (**STEM**).
- **Science Immersion Program** (SIP) – experience working in science and technology institutions, both here and abroad.
- **SCALE** (Service, Creativity, Action, and Leadership Program) – engagement in non-STEM fields to complement intensive STEM curriculum and develop well-rounded skills.
- Chance to exhibit and hone globally-competitive skills in national and international **events / competitions.**

FOREWORD

PUBLISCIENCE is a collection of the research works of the graduating scholars of Philippine Science High School- Western Visayas Campus (PSHS-WVC). This is the final output of students by the end of their Research 3 subject. As a requirement for graduation, this year's publication is the fourth volume of at most 34 different studies in the areas of agriculture, aquaculture, computer science, environmental science and health, materials science and technology, microbiology and biochemistry, and spatial analysis. PSHSWVC takes pride to be the very first and still is the only PSHS Campus that has successfully published all the Science and Technology Research works of its graduating scholars. This legacy is continued through the hard work of our scholars with support and guidance from our Research Unit. Publiscience is a testament of our scholars' pursuit for excellence. Congratulations to our Research Unit and our Batch 2021!

SHENA FAITH M. GANELA
Campus Director III

* * *

Congratulations Batch 2021 in your Publiscience! Researches are not meant to be kept and displayed in the bookshelves and gather clouds of dust rather it has to be shared with the academic community through publications. The publication of your research works is a sterling example of what every researcher must achieve. Indeed, accomplishing this gigantic task requires more than just material resources but also loads of patience, dedication and determination.

Amidst all the challenges, you have taught yourself the most valuable lesson in life and that is to bring out the best version of yourself in accomplishing any task, overcoming difficulties and finding solutions to problems.

My heart is filled with pride and happiness because you are now, more than ever equipped and ready to accomplish bigger tasks, overcome more obstacles and find solutions to bigger problems.

May your experiences give you wisdom, may your passion burn bright and move you to learn more and do more, and may your efforts be rewarded all for the glory of God and for your country.

Congratulations. Ingat lagi.

ROLANDO S. LIBUTAQUE
Curriculum Instruction Division Chief

* * *

THE RESEARCH PROGRAM

The research program is a three-year undertaking that aims to inculcate the scholars with the quality and skills becoming of a world-class Filipino scientist. Each year starting from Grade 10 focuses on an aspect of research paramount to the growth of scholars in becoming leading figures in their respective fields.

RESEARCH 1

Research as a subject is introduced in Grade 10. It is the formative year for the budding researcher with in-depth discussions on the Scientific Method, and the Research Process. Particularly, it introduces scholars in topic selection, literature search, research design, and paper presentation. Scholars were also taught the basics of writing a proposal, and a research paper – both in instruction, and in practice. Each group or work unit is composed of at most five members with general topics provided by the Research 1 teachers. Research 1 culminates with the paper presentation of the Grade 10 scholars in *Pagsuguidadon*.

RESEARCH 2

Research 2 is the reinforcement year in Grade 11. The writing of the proposal, and the research paper are further scrutinized in this year. Each section of a standard research paper: abstract, introduction, method, results, discussion, and conclusion are more pronounced in the syllabus. Research 2 is performed in work units of, at most, three. Scholars are allowed to select any topic in alignment with their science options and/or elective under the supervision of their advisers, propose and defend their proposal to a panel, develop and/or enhance skills related to the study, perform the method outlined in their proposal, and report their findings in a full-fledged research paper. Research 2 concludes with the presentation of the results in the final defense.

RESEARCH 3

Research 3 is the culminating year of the research curriculum. It is reserved for Grade 12 scholars who organize activities and events that share their respective study's findings, including but not limited to: research presentation (*Pagbantala*), poster presentation (*Pagbalandra*), seminar-workshop (*Pahisayod*), and community science conference (*Pagwaragwag*) with more events described at the end of this journal. This very journal is a fruit of the previous two batches' research experience. Research 3 focuses on finalizing the study and networking the results. It focuses on community-oriented approach in making science more accessible. This is evident in the oral and poster presentations for students and professionals, workshops and seminars for high school students, and gamification of each study for elementary students during the aforementioned events. Each study is given the opportunity to be published in this journal, provided that they have accomplished the review process outlined at the left.

The Research Review Process

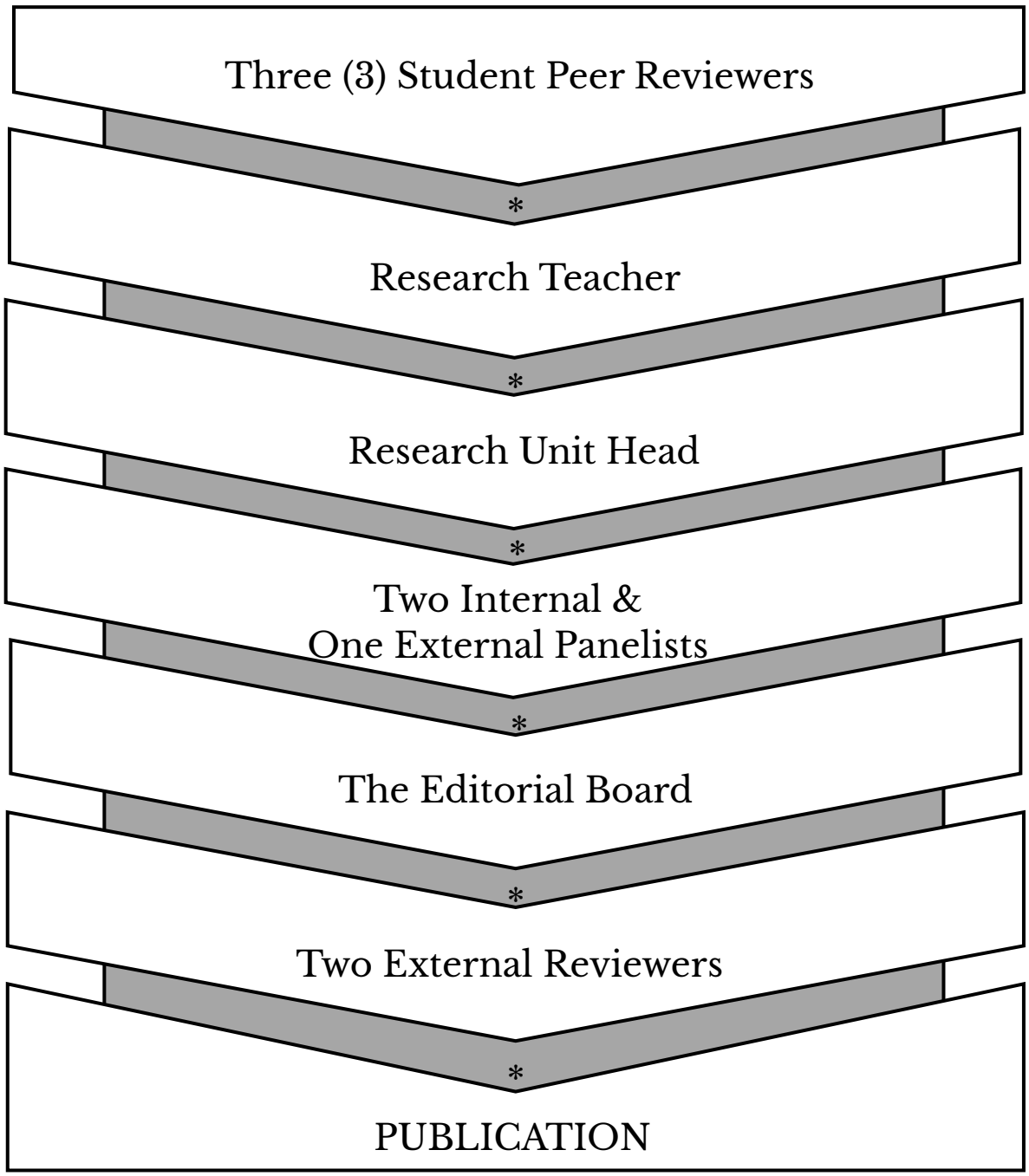

***Research Adviser**

Since research advisers are the co-authors of the journal article, they need to be updated with or review the article after each change.

THE RESEARCH COMMITTEE

The Research Committee is tasked with ensuring the quality of all research projects produced by the Batch 2021 scholars, performed from the 10th to the 12th grade. It is headed by the Research Unit Head who oversees and approves all research work and composed of the research teachers who handle the Research class for a specific school year and grade level and the research advisers who provide guidance, insight, and assistance in a consulting capacity in their fields of expertise. The Science Research Assistants (SRA) manage the different labs, apparatuses, equipment, and reagents for the use of the scholars in the conduct of their respective studies.

* * *

RESEARCH UNIT HEAD

Aris C. Larroder

RESEARCH 3 TEACHERS SY 2020–2021

Aris C. Larroder **Catherine Joy A. Mediodia** **Ramon Angelo N. Sinco**

RESEARCH 2 TEACHERS SY 2019–2020

Athenes Joy Presno-Aban **Julnafe B. Libo-on** **Zennifer L. Oberio**

RESEARCH 1 TEACHERS SY 2018–2019

Mialo P. Bautista **Harold P. Mediodia** **Lovie Grace A. Nzeakor**

RESEARCH ADVISERS

BIOLOGICAL SCIENCES & MICROBIOLOGY

Andrea Lucyle M. Bela-ong **Maria Deanna Jolito** **Fernando Christian G. Jolito III**
Julnafe B. Libo-on **Catherine Joy A. Mediodia** **Harold P. Mediodia**
Virna Jane M. Navarro **Angelo P. Olvido** **Zennifer Oberio**

CHEMISTRY & INTEGRATED SCIENCE

Michael Patrick M. Padernal **Ramon Angelo N. Sinco**

PHYSICS & ENGINEERING

David Bryan P. Lao **Aris C. Larroder** **Xavier Romy Braña**

COMPUTER SCIENCE &TECHNOLOGY

Eisen Ed C. Briones **Maria Milagrosa A. Nulla** **Gerald U. Salazar**

STATISTICS TEACHERS

Charmaigne D. Aguirre **Ma. Romy Alexis C. Consulta** **Myrna B. Libutaque**

SCIENCE RESEARCH ASSISTANT (SRA)

CHEMISTRY	INSTRUMENTATION	MICROBIOLOGY	PHYSICS
Leilani C. Estilo	**Mark V. Rosales**	**Rusty A. Balcoba**	**Gabriel Z. Bermejo**
	Amafe B. Gavile	**Cherry Rose D. Haro**	**Rusty A. Balcoba**

REVIEWERS AND PANELISTS

The research curriculum of PSHS - WVC is predominantly composed of highly immersive activities that develop the scholars' skills as researchers and scientific communicators. From Grade 10, the scholars experience the rigors of having to defend their proposals and, ultimately, their final paper.

PAGSUGUIDADON

PAGSUGUIDADON, from the Hiligaynon word *suguid* or "to report", is the culminating event for the Grade 10 Research curriculum. Scholars present and defend their paper to a three-person panel, composed of two invited panelists and a faculty member of PSHS-WVC. The papers are presented in five clusters with each study's overarching theme as the basis of grouping.

INVITED PANELISTS

Hannah Valencia
UNIVERSITY OF SAN AGUSTIN

Emily Singbenco
ASSUMPTION ILOILO

Paolo Cabañero
WESTERN INSTITUTE OF TECHNOLOGY

Ardee Caro
DEPARTMENT OF EDUCATION – BAROTAC NUEVO

May Sansait
ILOILO SCIENCE AND TECHNOLOGY UNIVERSITY

Homer Gumban
ALEJANDRO FIRMEZA MEMORIAL NATIONAL HIGH SCHOOL

Mathew Tubola
UNIVERSITY OF SAN AGUSTIN

Micah Lojera
SOUTHEAST ASIAN FISHERIES DEVELOPMENT CENTER

Early Sol Gadong
UNIVERSITY OF THE PHILIPPINES - VISAYAS

Sarah Liezl Lacaden
FREELANCE PROGRAMMER

PSHS-WV FACULTY

Ramon Angelo Sinco
SESSION 1

Catherine Joy Mediodia
SESSION 2

Andrea Lucyle Bela-ong
SESSION 3

Angelo Olvido
SESSION 4

David Bryan Lao
SESSION 5

PAGBANTALA

PAGBANTALA, from the Hiligaynon word *bantala* or "to inform", is the oral presentation of the scholars' studies to a panel of experts composed of an invited panelist, an alumni, and a faculty member of PSHS - WVC. For the SY 2020-2021, the studies were presented in 7 clusters namely: Aquaculture, Agriculture, Plant Chemistry, Satellite Imagery, a combination of categories (Agriculture, Aquaculture, and Satellite Imagery), and Computer Science and Technology (ordered below left to right, top to bottom).

INVITED PANELISTS

Peter Palma
SOUTHEAST ASIAN FISHERIES DEVELOPMENT CENTER

Irene R. Betalas
UNIVERSITY OF THE PHILIPPINES - VISAYAS

Phillip Raymund R. De Oca
BACOLOD CITY NATIONAL HIGH SCHOOL

Carlo Chris Apurillo
PHILIPPINE SCIENCE HIGH SCHOOL - EASTERN VISAYAS CAMPUS

Evans Sansolis
WEST VISAYAS STATE UNIVERSITY

Raphael Kevin Nagal
DEPARTMENT OF EDUCATION - DIVISION OF AKLAN

Mary Sol Baldevarrona
ILOILO STATE COLLEGE OF FISHERIES

PSHS-WV ALUMNI

Micah Lojera
SOUTHEAST ASIAN FISHERIES DEVELOPMENT CENTER

Rhyll Joy Balinas
PSHS-WVC BATCH 2015

Neil Phillip Poral
PSHS-WVC BATCH 2014

Jobi Subosa
NATIONAL INSTITUTE OF MOLECULAR BIOLOGY AND BIOTECHNOLOGY

John Dale Dianala
UNIVERSITY OF THE PHILIPPINES - DILIMAN

Gregory Parcon
ADVANCED WORLD SOLUTIONS INC.

Vincent Errick Itucal
CHI-X GLOBAL TECHNOLOGY (PHILIPPINES) INC.

PSHS-WVC FACULTY

Virna Navarro
AQUACULTURE

Angelo Olvido
AGRICULTURE

Erika Eunice P. Salvador
PLANT CHEMISTRY

Ma. Deanna Jolito
MICROBIOLOGY AND ENVIRONMENTAL SCIENCE

David Bryan Lao
SATELLITE IMAGERY

Andrea Lucyle Bela-ong
AGRICULTURE, AQUACULTURE, AND SATELLITE IMAGERY

Gerald Salazar
COMPUTER SCIENCE AND TECHNOLOGY

THE FINAL DEFENSE

The **FINAL DEFENSE** is the final step towards the end of the research curriculum. The scholars invite one external expert and two PSHS - WVC faculty to compose a three-person panel to assess the merits and validity of their findings. The final defense panel recommends revisions to the study's manuscript as well as continually review the same until approval.

INVITED PANELISTS

Ariel Blanco **Ian Kendrich Fontanilla** **Jeark Principe**
UNIVERSITY OF THE PHILIPPINES – DILIMAN

Michael Russelle Alvarez **Rowena Carpio** **Milagrosa Martinez - Goss**
UNIVERSITY OF THE PHILIPPINES – LOS BAÑOS

Teodora Bagarinao **Peter Palma**
SOUTHEAST ASIAN FISHERIES DEVELOPMENT CENTER

Melissa June Paderog - Ariego
UNIVERSITY OF SAN AGUSTIN

Corazon Arroyo
DEPARMENT OF AGRICULTURE – REGION VI

Mary Jane Calagui
CAGAYAN STATE UNIVERSITY

Gabrielle Troy Cuevas
UNIVERSITY OF THE PHILIPPINES – VISAYAS

Grace delos Reyes
AKLAN CATHOLIC COLLEGE

Gerard Dumancas
LOUISIANA STATE UNIVERSITY – ALEXANDRIA

Anthony Joseph Lucero
DEPARTMENT OF SCIENCE AND TECHNOLOGY - PAGASA

John Jowil Orquia
UNIVERSITY OF ANTIQUE

Edsel Peña
UNIVERSITY OF SOUTH CAROLINA

Stephen Sabinay
WEST VISAYAS STATE UNIVERSITY

Jerson Sala
5TH DISTRICT PROVINCE OF ILOILO

Julie Ann Acebuque Salido
AKLAN STATE UNIVERSITY

Cristie Sumbilla
NEW LUCENA NATIONAL COMPREHENSIVE HIGH SCHOOL

Isabelle Tingzon
THINKING MACHINES

PSHS-WVC FACULTY

Fernando Christian Jolito III **Ma. Deanna Jolito** **Julnafe Libo-on**
Catherine Joy Mediodia **Virna Jane Navarro** **Angelo Olvido**
BIOLOGICAL SCIENCES UNIT

Athenes Joy Presno-Aban **Elizalde Miguel Flores**
Erika Eunice Salvador **Michael Patrick Padernal** **Ramon Angelo Sinco**
CHEMISTRY AND INTEGRATED SCIENCES UNIT

Raphael Eric Yturralde **Xavier Romy Braña** **Oliver Fuentespina**
Aris Larroder
PHYSICAL SCIENCES UNIT

Eisen Ed Briones **Jose Vicente Tan** **Maria Millagrosa Nulla**
COMPUTER SCIENCE AND TECHNOLOGY UNIT

David Bryan Lao **Zennifer Oberio**
MATHEMATICS UNIT

THE EXTERNAL REVIEWERS

THE EXTERNAL REVIEWERS are practitioners of scientific fields recommended by the Research Unit and invited by the Editorial Board to assess the merit and substance of each of the published papers. These individuals serve as the final reviewers prior to an article's publication. Before the publication of this section, their identities are anonymous to the authors.

Bee Gee Belle Agustin
AKLAN STATE UNIVERSITY, PHL

Aldrean Paul Alogon
WESLEYAN UNIVERSITY, USA

John Rafael Ambag
UNIVERSITY OF THE PHILIPPINES - DILIMAN, PHL

Artoni Kevin Ang
NAGOYA INSTITUTE OF TECHNOLOGY, JPN

Christine Marie Angos-Banaszek
CHARLES ROSS & SON COMPANY, USA

Romie Angelo Azur
UNIVERSITY OF THE PHILIPPINES - DILIMAN, PHL

Jenny Babon
HARVARD UNIVERSITY, USA

Justin Enrique Banusing
UNIVERSITY OF WASHINGTON, USA

Juan Paolo Lorenzo Gerardo Barrios
DURHAM UNIVERSITY, GBR

Diana Mae Calde
UNIVERSITY OF THE PHILIPPINES - DILIMAN, PHL

Alexis Richard Claridades
UNIVERSITY OF SEOUL, KOR

Myke Wallace Cohen
ARIZONA STATE UNIVERSITY, USA

Marlon Conato
UNIVERSITY OF THE PHILIPPINES - DILIMAN, PHL

Cris Jericho Cruz
KOREA ADVANCED INSTITUTE OF SCIENCE, KOR

Roldan De Guia
INSTITUTE OF MOLECULAR GENETICS, CZE

Christian Deo Deguit
UNIVERSITY OF THE PHILIPPINES - MANILA, PHL

Ina Dela Fuente
UNIVERSITY OF CONNECTICUT, USA

Yevgeny Aster Dulla
INTRALINK JAPAN, JPN

Emil Emmanuel Estilo
HIROSHIMA UNIVERSITY, JPN

Philip Caesar Flores
UNIVERSITY OF THE PHILIPPINES - DILIMAN, PHL

Riel Carlo Ingeniero
GEOMER HELMHOLTZ CENTRE FOR OCEAN RESEARCH, DEU

Angelo Jamerlan
GACHON UNIVERSITY, KOR

Ma. Christina Jamerlan
NEURAL MECHANICS INC., PHL

Santiago Emil A. Joson IV
UNIVERSITY OF THE PHILIPPINES - DILIMAN, PHL

Sami Juanico
UNIVERSITY OF THE PHILIPPINES VISAYAS FOUNDATION INC., PHL

Chricel Lattao
UNIVERSITY OF SANTO TOMAS, PHL

Joseph Simon Madrinan
PHILIPPINE SCIENCE HIGH SCHOOL - WESTERN VISAYAS, PHL

Ellazar Niangar
GENERAL MOTORS GLOBAL FUEL CELL ACTIVITIES, USA

Lurylee Olarte
PANAY ENERGY DEVELOPMENT CORPORATION, PHL

Jacqueline Ponteres
ASPEN TECHNOLOGY AUSTRALIA PTY LTD, AUS

Marmelou Popes
UNIVERSITY OF THE PHILIPPINES - DILIMAN, PHL

Ben Joshua Porras
UNIVERSITY OF THE PHILIPPINES - DILIMAN, PHL

Peter Paolo Rivera
UNIVERSITY OF EAST ANGLIA, GBR

Leo Albert Sala
J. HEYROVSKY INSTITUTE OF PHYSICAL CHEMISTRY, CZE

Jaya Lavalle Sitjar
NATIONAL CHENG KUNG UNIVERSITY, TWN

Alexandria Sombiro
UNIVERSITY OF THE PHILIPPINES - DILIMAN, PHL

Varsolo Sunio
YONDU, INC., PHL

Liezel Tamon
MRC WETHERALL INSTITUTE OF MOLECULAR MEDICINE, GBR

John Noel Viaña
AUSTRALIAN NATIONAL CENTRE, AUS

TABLE OF CONTENTS

i. About the Cover
ii. About PSHS
iii. Foreword
iv. Research Program
v. Research Committee
vi. Panelists and Reviewers
Pagsuguidadon
Pagbantala
Final Defense
Publiscience External Reviewers
vii. Preface, Dedication

I. **ENVIRONMENTAL SCIENCE AND HEALTH** 1

Climatological analysis of the Southwest Monsoon (Habagat) in Type 1 Climate Areas in the Philippines from 1949–2018 2

Microplastics in farmed oysters (*Crassostrea iredalei*) from Capiz, Philippines 8

Evaluation of the larvicidal efficacy of *Artocarpus heterophyllus* (jackfruit) rags and rind ethanolic crude extracts against third to early fourth instar *Aedes aegypti* larvae 14

Reduction of acrolein concentrations in palm cooking oil emissions through the addition of *Muntingia calabura* (aratiles) leaf extract to inhibit lipid peroxidation 20

II. **MATERIAL SCIENCE AND TECHNOLOGY** 26

Comparison in yield of the microwave-assisted method and conventional method in *Zea mays* var. *ceratina* (glutinous corn) cobs cellulose fiber extraction 27

Development of a reduced nanoporous graphene oxide membrane synthesized from *Oryza sativa* husk using the Tour method for the reduction of salt ions 32

III. **MICROBIOLOGY AND BIOCHEMISTRY** 38

Formulation and evaluation of antibacterial gel incorporated with *Stachytarpheta jamaicensis* crude ethanolic leaf extract against *Staphylococcus aureus* 39

Molecular docking of selected phytochemicals from malunggay (*Moringa oleifera*) against the chromosomal trehalose-6-phosphate phosphatase (PDB ID: 6CJ0) enzyme of *Pseudomonas aeruginosa* 45

IV. **AGRICULTURE** 51

The effect of humic acid and inorganic fertilizer application on the growth and yield of *Ipomoea reptans* Poir. (kangkong) 52

Effects of hydropriming on the germination of *Oryza sativa* L. NSIC Rc 216 (rice) under sodium chloride (NaCl) stress 58

Effects of powdered chicken eggshells as a soil amendment on the vegetative growth of *Vigna radiata* 63

Comparison of the percent adsorption of raw corn husk and raw rice husk for bunker fuel 67

V. **AQUACULTURE** 71

Sodium lactate as a potential preservative to green mussel meat 72

DNA barcoding of freshwater gastropods found in the upstream of Jalaur River in Barangay Garangan, Calinog, Central Philippines 77

Effect of different irradiance levels on the growth of the cyanobacterium *Lyngbya majuscula* 82

VI. **COMPUTER SCIENCE** 87

Developing a neural network that uses satellite imagery to estimate carbon dioxide emissions in the Philippines 88

Evaluating the ripening stages of *Musa acuminata* × *balbisiana* (Saba) using 2D-image analysis 93

Using a sssNet Convolutional Neural Network (CNN) with Support Vector Machine (SVM) algorithm to identify formalin presence in images of eyes of *Chanos chanos* (milkfish) 99

VII. **SPATIAL ANALYSIS** 105

Assessment of soil erosion risk within the Maasin Watershed Forest Reserve, Iloilo, Philippines using the Revised Universal Soil Loss Equation (RUSLE) and Geographical Information System (GIS) 106

Mapping and calculation of the shoreline change in selected areas in Tigbauan, Iloilo, Philippines using remote sensing and geographic information systems (GIS) techniques 112

Research Events: *Pagbantala, Pagbalandra, Paghinun-anon, Pahisayod*

Research Events: *Pagwaragwag, Paindis-indis, Pagpabalhag, Pagsuguidadon*

Keyword Index

Institutional Partners

PREFACE

It is our pleasure to present the fourth volume of Publiscience, the annual, peer-reviewed research journal of PSHS-WVC. Publiscience is a joint effort of the scholars and the Research Unit to communicate the results of the scholars' studies. In line with the PSHS mission and vision, the publication cultivates their research skills in preparation for them to become world-class Filipino scientists. Since the establishment of the journal in 2018, the scholars have strived to innovate and improve the aspects of the journal. For this volume, the *Pagpasanyog* or the improvement entails transparency on the conduct of the studies, by providing readers open-view access to supplementary data supporting the results and including the submission, approval, and publication dates of the articles.

The fourth volume of Publiscience contains 20 Science and Technology (S&T) studies venturing into topics such as Biology, Chemistry, and Engineering. The journal articles are clustered into seven (7) areas, namely: (1) Environmental Science and Health, (2) Material Science and Technology, (3) Microbiology and Biochemistry, (4) Agriculture, (5) Aquaculture, (6) Computer Science, and (7) Spatial Analysis.

Lastly, this volume was published during a period of great hardship and uncertainty. Essentially, it has considerably affected the conduct of research studies—the greatest obstacle in the research process. Despite the odds, the PSHS-WVC scholars persevered to publish the research articles, all in the pursuit of truth, passion for excellence, and commitment to service. This serves as our testament that research can be conducted during unfavorable circumstances. The pandemic has indeed highlighted the significance of research in society, and it is and will always be the advocacy of Publiscience to promote the pursuance of research to be of service to the people.

THE EDITORIAL BOARD

* * *

DEDICATION

This journal is dedicated to all the learners and teachers,
who struggled during these difficult times yet study and teach
to satisfy the thirst for knowledge and love for learning and the DOST Secretary,
Fortunato de la Peña, for spearheading the scientific efforts in dealing with the pandemic.

CLUSTER ONE

ENVIRONMENTAL SCIENCE AND HEALTH

Red is the color of blood, symbolizing our deeper connection to our environment and planet. The gem is in the shape of a drop of blood for the same reason. As such, if we are to keep living on this earth, we have to keep track of the environment's status and find ways to solve environmental problems. One of the biggest aims of environmental science is to find solutions to such problems. The striking color of red therefore also inspires and motivates us to take action and work towards this aim.

These studies tackle varying environmental issues. As such, they can be associated with one of the following agendas: the Aquatic, Agriculture, and Natural Resources (AANR) Research and Development Agenda, and the Disaster Risk Reduction and Climate Change Adaptation (DRR & CCA) Research and Development Agenda. This is because the studies are generally aligned with the objectives of the former agenda, while one study has objectives and has aspects more related to the priorities of the latter agenda.

BASED ON: Harmonized National Research and Development Agenda (HNRDA)

Publiscience Vol. 4 Issue 1

Climatological analysis of the Southwest Monsoon (Habagat) in Type 1 Climate Areas in the Philippines from 1949–2018

POLINA S. ESPINO, ALYSA MARIE M. ONG, DANIELLE MARI J. YORAC, and JULNAFE B. LIBO-ON

Philippine Science High School Western Visayas Campus - Department of Science and Technology (DOST-PSHSWVC), Brgy. Bito-on, Jaro, Iloilo City 5000, Philippines

Article Info

Submitted: May 10, 2021
Approved: Aug 11, 2021
Published: Aug 30, 2021

Keywords:
southwest monsoon
habagat
rainfall
climatological analysis
precipitation

Abstract

The Southwest monsoon (SWM) rainfall is used in agriculture, industry, and electrical energy and fills reservoirs that supply water to households. However, it generates high levels of rainfall which can negatively affect Philippine agriculture. The historical behavior and trends of the SWM rainfall in the Philippines were identified using collected rainfall data from fourteen (14) meteorological stations situated in Type 1 climate areas of the country, where the impact of SWM is well-pronounced. The time series analysis from 1949 to 2018 for the months of June to September showed an overall increase in accumulated rainfall with a slope of +1.8047, as well as in the decadal frequencies of high precipitation event days (HPE) at the 85th, 95th, and 99th percentile with slopes of +1.0586, +0.4740, and +0.1030, respectively. The trendline for the no-rain days graph has a slope of -0.1177, indicating a decreasing trend. These findings suggest a possibility of an increase in SWM rainfall in the coming decades.

Introduction. - Heavy rainfall is considered one of the most disastrous weather extremes that greatly affect human activities and environmental systems [1]. The factors that facilitate heavy rainfall events include (i) the southward expansion of the high-pressure system to the north of the Philippines, (ii) the El Niño Southern Oscillation (ENSO), and (iii) enhanced moisture-converged cold surges [2]

The Southwest monsoon (SWM) are trade winds that bring warm and considerably humid air mass during the months of June to September every year. The Southwest monsoon (SWM) rainfall results from the passing of air over large areas of warm equatorial ocean that stimulates evaporation from its surface; as the moisture-heavy air cools, it moves north and precipitates [3]. It contributes 43% of the precipitation in the mean annual rainfall in the Philippines [4]. According to [5], the western side of the country is greatly affected by rainfall from the Southwest monsoon (SWM) during boreal summer. It also simultaneously occurs with the peak occurrence of tropical cyclones in the country which is during the months of July and August. This co-occurrence allows tropical cyclones to influence the southwesterly winds of the monsoon which contributes to an increase in the amount of precipitation during the season [4,6]. Crost et al. [7] found that an increase in rainfall during the dry season increases agricultural production, while rainfall during the wet season harms crops and produces conflict. According to the International Rice Research Institute [8], 30% of the total rice area in the country is rainfed and upland, which are heavily reliant on rainfall for crop production. However, this agricultural system is also sensitive to the variability in rainfall patterns which could bring sudden heavy rainfalls that are damaging to the crops [9]. In 2016, it was found that there is an increasing trend in economic loss and damage due to tropical cyclones [10]. Since the country is vulnerable to variations in climate and rainfall, changes in the onset and intensity of rainfall can significantly affect livelihood, food security, and economic stability, by disrupting agricultural production and damaging infrastructure [5,11].

The East Asian Monsoon and South China Sea Monsoon rainfall trends have been studied intensively over the past years [12,13,14]. However, the rainfall trends of the Southwest monsoon have received relatively little interest from the scientific community, thus the need for this research. The study of Cruz et al. [5] presented data regarding the climatological analysis of Philippine Southwest monsoon rainfall. Their examination of the rainfall extremes indicated an increasing trend in the number of days without rain and a decreasing trend in the heavy rainfall days from 1961 to 2010, which can be detected with statistical confidence. However, multiple meteorological stations have been constructed in other parts of the country since then. A shift in rainfall was also observed in different portions of the country due to the reduction of the topography of mountains, urbanization, and climate change. Hence, utilizing a wider scope of data in terms of geography and time will increase the accuracy of *Habagat* rainfall trends and patterns, thus the need for this study [15].

This observational study analyzed the trend and behavior of SWM or habagat rainfall in the

How to cite this article:
CSE: Espino PS, Ong AMM, Yorac DMJ. 2021. Climatological analysis of the Southwest Monsoon (Habagat) in Type 1 Climate Areas in the Philippines from 1949–2018. Publiscience. 4(1): 2–7.
APA: Espino, P.S., Ong, A.M.M., & Yorac, D.M.J. (2021). Climatological analysis of the Southwest Monsoon (Habagat) in Type 1 Climate Areas in the Philippines from 1949–2018. *Publiscience*, *4*(1), 2–7.

For supplementary data, contact: publiscience@wvc.pshs.edu.ph.

northwestern portion of the Philippines using rainfall data from fourteen (14) synoptic stations from 1949 to 2018. It specifically aims to:

(i) identify the high precipitation event days (HPE) where the total amount of rainfall collected in each station belongs to the upper 85th, 95th, and 99th percentile;

(ii) determine the number of days with and without rain;

(iii) present a time series analysis that will show the trend of rainfall for the past seventy (70) years in the Type 1 climate areas of the Philippines where the impact of SWM is well pronounced;

(iv) identify years where the SWM rainfall deviates from the climate mean;

(v) detect years with normal, below-normal, and above-normal rainfall using the Southwest Monsoon Rainfall Anomaly Index (SWMRAI) threshold; and

(vi) analyze the graphs and investigate the trends present in the graphs.

Methods. - The methodology used for this study was adapted from the study of Cruz et al. [5]. Total rainfall data from the years 1949–2018, collected from fourteen (14) synoptic meteorological stations—the Baguio PAGASA weather station, and thirteen (13) stations which are included in the Climate Type I of the modified Corona's climate classification—were requested from PAGASA. A time-series analysis was used to determine the historical trend and variability of the SWM rainfall. The no-rain days and high precipitation event (HPE) days were then determined and the HPE days were classified into 85th, 95th, and 99th percentiles. Using the calculated spatial average of each standardized rainfall anomaly, the Southwest monsoon Rainfall Anomaly Index (SWMRAI) for each year was obtained. Finally, using the standard deviation of the SWMRAI as the threshold, the SWM rainfall extremes were determined.

Collection of Raw Rainfall Data. The daily, monthly, and annual rainfall data that was used to determine the trends and historical behavior of the Southwest monsoon (SWM) or *Habagat* in the country are from the year 1949 to 2018. They were collected from PAGASA's fourteen (14) synoptic meteorological stations (see Table 1). In this study, the reference period for the baseline climate is from 1949 to 2018. Since the synoptic meteorological stations were not built in the same years, the months with missing data were replaced with the climatological mean of the monthly total rainfall, following the methods of Cruz et al. [5].

Table 1. Coordinates and year built of the fourteen (14) synoptic stations used to determine trends and historical behavior of the southwest monsoon in the country.

Location	Year and Month Built
Ambulong, Batangas	Jan 1951
Baguio City, Benguet	Jan 1949
Cabanatuan, Nueva Ecija	Jan 1989
Coron, Palawan	Jan 1951
Cuyo, Palawan	Jan 1951
Dagupan City, Pangasinan	Jan 1951
Iba, Zambales	Jan 1951
Laoag City, Ilocos Norte	Jan 1951
NAIA (MIA), Pasay City	Jan 1949
Port Area (MCO), Manila	Jan 1949
Puerto Princesa, Palawan	Jan 1951
San Jose, Occ. Mindoro	Jan 1981
Sangley Point, Cavite	Jan 1974
Science Garden, Quezon City	Apr 1961

Data Analysis. The time-series analysis was used to determine the historical trend and variability of the SWM rainfall. From the data provided by PAGASA, days with no rain and HPE were determined. The HPE days were then classified into 85th, 95th, and 99th percentiles, which according to Bagtasa et al. [16], are considered days with heavy rain. Using the formula adapted from Wilks [12], standardized anomalies were determined for each station per year. The Southwest monsoon Rainfall Anomaly Index (SWMRAI) for each year was then obtained using the calculated spatial average of each standardized rainfall anomaly. The standard deviation of the SWMRAI was derived and used as a threshold to determine the rainfall levels.

No-rain Days. The number of days where the rainfall collected in a station is 0 mm was determined per year and tallied per decade. A bar graph was then generated with the decadal frequencies of no-rain days for the months of June to September from 1949 to 2018 for each station.

High Precipitation Events Days. The high precipitation events (HPE) days, days with rainfall in the upper 85th, 95th, and 99th percentile, were determined using daily rainfall data from all fourteen (14) synoptic stations and were tallied per decade. They are referred to as HPE85, HPE95, and HPE99, respectively. A graph containing the decadal frequencies of HPE85 days per station was generated. The same was done for HPE95 and HPE99 days.

Standardized anomalies. A rainfall index was used to determine the annual variation of SWM rainfall per station. Rainfall data from PAGASA is expressed as a standardized anomaly so that it can be directly compared to rainfall data from different stations regardless of local conditions such as elevation and land use. Adapted from Wilks [17], the standardized anomalies are expressed as:

$$(1) \quad Z_i = \frac{x_i - \bar{x}_i}{s_{xi}}$$

Where:

x_i = SWM rainfall value at station i for a particular year
$\bar{x_i}$ = mean SWM rainfall for station i
s_{xi} = standard deviation at station i from 1949–2018

The data that were obtained from this step are 843 Z_i values – one value for each of the fourteen stations per year. The Z_i values were grouped per year and their average was calculated to obtain 70 Z_{it} values which were needed for succeeding calculation.

Southwest Monsoon Rainfall Anomaly Index. The spatial average for Z_i, the annual variation, at each station were calculated to derive a single index called the SWMRAI. For each year (t), SWMRAI is expressed as:

$$(2) \quad SWMRAI_t = \frac{1}{N}\sum_{i=1}^{N} Z_{it}$$

Where:
N = total number of stations in a particular year t
Z_{it} = standardized rainfall anomaly at year t

The data that were obtained from this step are 70 values – one SWMRAI value per year.

Standard deviation of SWMRAI. The standard deviation *s* of SWMRAI was also calculated to identify a threshold for determining the years with normal, above normal, and below-normal rainfall. The formula for standard deviation that was used is:

$$(3) \quad s = \sqrt{\frac{\sum_{i=1}^{n}(x_i - \bar{x_i})^2}{n-1}}$$

Where:
n = total number of stations
x_i = SWMRAI of each year
$\bar{x_i}$ = mean of x_i

The positive and negative *s* values were used as the upper and lower bounds. A year where the SWMRAI exceeds the positive *s* value means that the SWM rainfall at that year has above-normal rainfall and vice versa.

Standard deviation of annual rainfall data. The standard deviation of the total collected rainfall of year *t* in station *i* was calculated. A time-series graph of the SWM accumulated rainfall, taken as an average across all stations, was produced. Error bars were added to indicate the positive and negative standard deviation of annual rainfall data.

Safety Procedure. Protective measures were done to prevent the risk of file corruption as well as to ensure security. A copy of the files was downloaded directly from the email that PAGASA sent before any calculation was done and was stored in a virus-free flash drive. A copy of the original files was also uploaded to a Google drive folder, where files of calculated data were also stored.

Results and Discussion. - The average annual accumulated rainfall of all stations during the months of June to September, from the year 1949 to 2018 showed an inter-annual variability (see Figure 1). In the 70-year time series, a minimal increasing trend for the annual accumulated rainfall can be observed from its linear trend slope of +1.8047. The spatial variability which has a slope of -0.1065, however, indicates a decreasing trend. This implies that the degree to which rainfall amounts vary across time is decreasing. Great spatial variability can be observed in the years 1951, 1958, 1968, 1972, 1990, 2012, and 2018. It is also worth noting that the deviation between stations tends to be lower in years with lower accumulated rainfall. According to several studies [18,19], the observed interannual variability of rainfall is highly correlated to the effects of the El Niño Southern Oscillation. The shifting phenomenon of other monsoons in Southeast Asia also has an impact on rainfall variability [20]. Furthermore, The results for spatial variability are supported by the study of Cruz et al. [5] which also reported a decline in the linear trend of the spatial variability of total SWM rainfall from the year 1960 to 2010.

It can also be seen from Figure 1 that in 1972, the annual accumulated rainfall was significantly higher. This increase can be attributed to prolonged flood conditions due to the occurrences of tropical cyclones, further aggravated by the intensification of the SWM. The events that were primarily responsible for these conditions are Super Typhoon Rita and Typhoon Susan, which altered the monsoon winds over the Philippines. They were then succeeded by Typhoons Edeng, Gloring, Isang, and Huaning only weeks after. It is interesting to note that the 1972 great flood over Luzon occurred during an El Niño episode [21]. Villafuerte et al. [22] confirmed that with the development of El Niño in the north-central Philippines, wetter conditions during the months of July to September are expected.

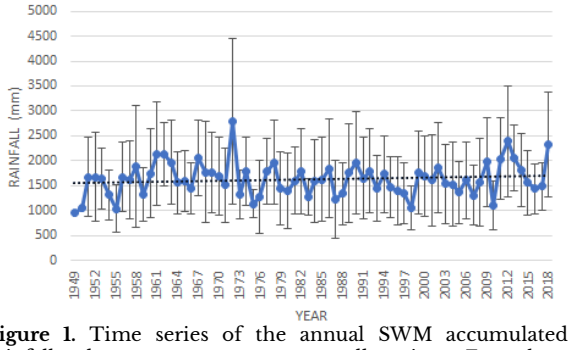

Figure 1. Time series of the annual SWM accumulated rainfall, taken as an average across all stations. Error bars indicate the standard deviation of station values. Dashed line indicates the linear trend.

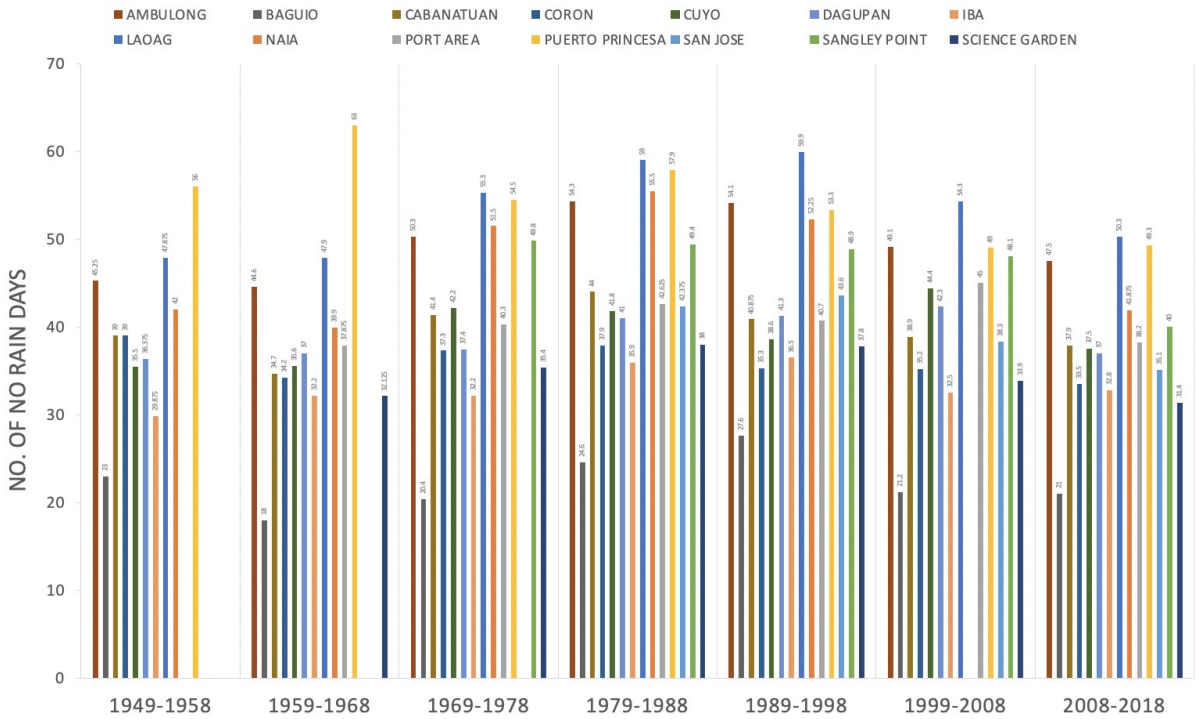

Figure 2. Decadal frequencies of no-rain days for the months of June to September from 1949 to 2018 for each station.

As seen in Figure 2, there is a decline in the frequency of no-rain days during SWM season for the past four decades (1979 to 2018), with the linear trend having a slope of -0.1177. The number of no-rain days has decreased from decades 1949–1958 and 1959–1968, increased from decades 1959–1968 to 1979–1988 and decreased from decades 1979–1988 to 2009–2018. It can be observed in the graph that in all stations, the years from 1979 to 1998 have the most number of no-rain days. Results also showed that the station in Iba received the most rain averaging 2887 mm per year, and the station in Puerto Princesa received the least rain averaging 708 mm per year for the past 70 years. Changes in the extremes are important to understand because of their climatic impact in terms of floods and droughts, which result in serious consequences especially on the agricultural and energy sectors [5].

Moreover, the decadal changes in the number of HPE days—those who are above the 85th, 95th, and 99th percentile (Figure 3)—are increasing as well. In other words, there is an overall increasing trend in the number of days belonging to the 85th, 95th, and 99th percentile rainfall throughout the decades. The slopes of their trends are +1.0586, +0.4740, and +0.1030, respectively. It can also be seen in the figures that all the trendlines have a positive slope, regardless of their percentile value. This indicates that rainfall has continually increased in terms of intensity within the 70-year period.

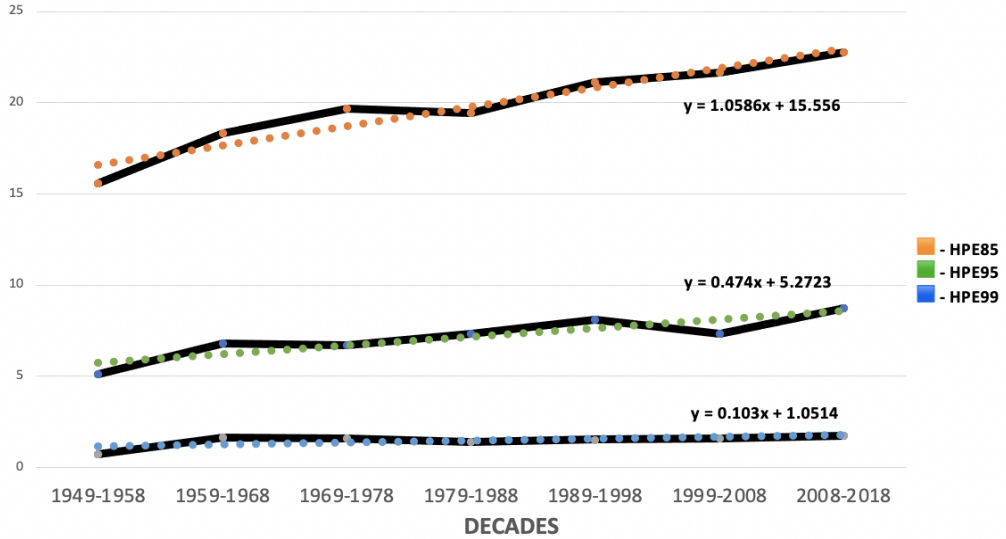

Figure 3. Overall trends of HPE85 (orange), HPE95 (green), and HPE99 (blue) days, defined as exceeding the 85th, 95th, and 99th percentile from 1949 to 2018, for the months of June to September for each station.

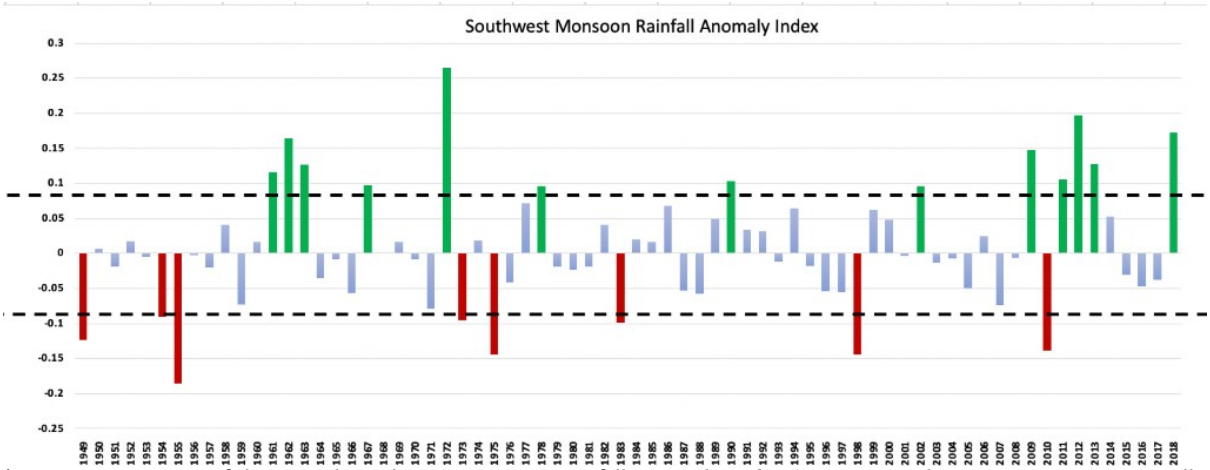

Figure 4. Time-series of the annual Southwest Monsoon Rainfall Anomaly Index (SWMRAI), taken as an average across all stations. The standard deviation of these indices (dashed line) sets the thresholds for normal rainfall. Years are classified as follows: above-normal (green), normal (blue), and below-normal (red).

Unlike the no-rain days graph, no station has consistently experienced the greatest or least HPE days. According to Cruz et al. [5], the 95th percentile of daily rainfall from the baseline climate is already considered as heavy rainfall. A negative trend in the 85th, 95th, and 99th percentiles of HPE days can be observed in their study, which is in contrast with our findings. However, this may be due to the difference in the number of stations and years analyzed. The study of Cruz et al. [5] utilized data from only 9 stations over a 50-year period, whereas this paper utilized data from 14 stations in a 70-year span.

As shown in Figure 4, the years with above-normal rainfall are 1961, 1962, 1963, 1967, 1978, 1990, 2002, 2009, 2011, 2012, 2013, and 2018, while the years with below-normal rainfall are 1949, 1954, 1955, 1973, 1975, 1983, 1998, 2010. The rest of the years are categorized under normal rainfall.

The standard deviation of SWMRAI, ±0.08460741, was used as the threshold in determining the years with above-normal and below-normal SWM rainfall. Within the 70-year period of study, 49 years were normal, 13 years were above-normal, and 8 years were below-normal. In the study of Cruz et al. [5], the majority of the years from 1961 to 2010 also fell in the normal rainfall category. Data from PAGASA was used in determining El Niño and La Niña years. Two (2) out of twelve (12) years when the Type 1 climate areas of the Philippines received above-normal rainfall, were La Niña years (1962, 1972). It is worth noting that one El Niño year (2002) belonged to the same category. One (1) out of eight (8) occurrences of below-normal rainfall were El Niño years (1983). Moreover, all except one below-normal rainfall years are La Niña years (1949, 1954, 1955, 1973, 1975, 1998, 2010). These findings show that El Niño years are not necessarily associated with below-normal rainfall, and the same idea can be applied to La Niña years as well.

Limitations. Not all stations had available rainfall data from 1949–2018 since they were constructed at different years, and some had to stop operations due to maintenance problems. This resulted in missing data in some years.

Conclusion. - During the Southwest monsoon season, there is an overall increase in the amount of rainfall and a decrease in drier days in Type 1 climate areas of the Philippines as compared to the past years. The frequency of no rain days has decreased, the trend lines observed in the frequency of high precipitation days at the 85th, 95th and 99th percentile are increasing, and the average accumulated Southwest monsoon rainfall has increased as well. The extremes in the number of no-rain days are the years from 1979 to 1998, and there are no extreme years for the number of HPE days in all three percentiles. This shows that during this period, a lot of days had zero precipitation, and for the years during this period that had above-normal rainfall, it can be inferred that precipitation was heavy during the rainy days. For the SWMRAI, 1955 is the year with the lowest recorded below-normal rainfall, while 1972 is the highest recorded above-normal rainfall value. The decrease in the frequency of no-rain days, and the increasing trend lines observed in the frequency of high precipitation days at the 85th, 95th, and 99th percentile, as well as the average accumulated Southwest monsoon rainfall shows that there is an overall increase in the amount of rainfall in the northwest portion of the Philippines during this season. It was found that whether a year falls in the below-normal, normal, or above-normal rainfall categorization is not dependent on its classification as an El Niño or La Niña event. In summary, based on the results of the data analysis, it can be concluded that there is a possibility of increased rainfall and shorter dry periods during the SWM season in future years. If the rainfall trend continues to increase in the future, heavy rainfall-related risks such as flooding and landslide occurrence are likely to escalate.

Recommendations. - Other factors such as passages of landfalling and non-landfalling tropical cyclones, wind, urbanization, and heat flux were not included in this study. An in-depth analysis on the correlation between other factors could provide better predictions for SWM rainfall. Lastly, it is recommended that sectors that are highly vulnerable to heavy rainfall, such as the agricultural sector, to regularly monitor the trend and prepare a risk management plan and risk reduction plan to help

them mitigate the negative effects of SWM in the future, since it is expected that rainfall will be heavier than previous years.

Acknowledgment. - The researchers would like to extend their gratitude to PAGASA for their punctuality in providing the rainfall data used in the study.

References

[1] Ohba M, Sugimoto S. 2019. Differences in climate change impacts between weather patterns: possible effects on spatial heterogeneous changes in future extreme rainfall. Clim Dyn. 52 (7–8). doi: 10.1007/s00382-018-4374.

[2] Olaguera LMP, Caballar ME, De Mata JC, Dagami LAT, Matsumoto J, Kubota H. 2021. Synoptic conditions and potential causes of the extreme heavy rainfall event of January 2009 over Mindanao Island, Philippines. Nat Hazards. https://doi.org/10.1007/s11069-021-04934-z.

[3] Boquet Y. 2017. A tropical archipelago. The Philippine archipelago. 37–59. doi:10.1007/978-3-319-51926-5_3.

[4] Cayanan EO, Chen TC, Argete JC, Yen MC, Nilo PD. 2011. The effect of tropical cyclones on Southwest Monsoon rainfall in the Philippines. J. Meteor. Soc. Japan. 89(A): 123–139. doi: 10.2151/jmsj.2011-A08.

[5] Cruz FT, Narisma GT, Villafuerte MQ, Cheng Chua KU, Olaguera LM. 2013. A Climatological Analysis of the Southwest Monsoon Rainfall in the Philippines. Atmos Res. 122. doi: 10.1016/j.atmosres.20 12.06.01

[6] Bagtasa, G. 2017. Contribution of Tropical Cyclones to Rainfall in the Philippines. J. Clim. 30 (10): 3621-3633. https://doi.org/10.1175/JCLI-D-16-0150.1

[7] Crost B, Duquennois C, Felter JH, Reese DI. 2018. Climate change, agricultural production and civil conflict: evidence from the Philippines. J Environ Econ Manag. 88 (2018): 379-395. https://doi.org/10.1016/j.jeem.2018.01.005.

[8] International Rice Research Institute. 2013. Rice Almanac 4th Edition. Retrieved 2021 Aug 10. Available from https://www.irri.org/resources/publications/books/rice-alamanac-4th-edition.

[9] Olesen JE, Trnka M, Kersebaum KC, Skjelvag AO, Seguine B, Peltonen-Sainiof P, Rossig F, Kozyrah J, Micale F. 2011. Impacts and adaptation of European crop production systems to climate change. Eu J Agron. 34(2):96–112. https://doi.org/10.1016/j.eja.2010.11.003.

[10] Cinco TA, de Guzman RG, Ortiz AM, Delfino RJ, Lasco R, Hilario F, Juanillo E, Barba R, Ares E. 2016. Observed Trends and Impacts of Tropical Cyclones in the Philippines. Int J Climatol. 36(14). doi: 10.1002/joc.46.

[11] Basconcillo JA. 2019. Gender and climate change adaptation: a case study of flood-prone rice-farming villages in Bulacan, Philippines. In: Paris TR, Rola-Rubzen MF, editors. Gender dimension of climate change research in agriculture: case studies in Southeast Asia. Philippines: SEARCA; Netherlands: CCAFS.

[12] Chan JCL. 2000. Tropical Cyclone Activity over the Western North Pacific Associated with El Nino and La Nina Events. J. Clim. 13(16). doi: 10.1175/1520-0442(2000)013<2960:TCAOTW>2.0.CO.

[13] Chen TC, Wang SY, Huang WR, Yen MC. 2004. Variation of the East Asian Summer Monsoon Rainfall. J. Clim. 17 (4). doi: 10.1175/1520-0442(2004)017<0744:VOTEAS>2.0.CO

[14] Zhang Y, Li J, Xue J, Zheng F, Wu R, Ha KJ, Feng J. 2019. The Relative Roles of the South China Sea Summer Monsoon and ENSO in the Indian Ocean Dipole Development. Clim Dyn. 53 (11). doi: 10.1007/s00382-019-04953.

[15] Racoma BAB, David CPC, Crisologo IA, Bagtasa G. 2016. The change in rainfall from tropical cyclones due to orographic effect of the Sierra Madre Mountain Range in Luzon, Philippines. Philipp J Sci. 145(4): 313–326.

[16] Bagtasa G. 2020. 118-year climate and extreme weather events of Metropolitan Manila in the Philippines. Int J Climatol. 40, no. 2(2020): 1228–1240.

[17] Wilks D. 1995. Statistical methods in atmospheric sciences. An introduction. Academic Press, San Diego, 467 pp.

[18] Feng J, Wang L, Chen W. 2014. How does the East Asian summer monsoon behave in the decaying phase of El Niño during different PDO phases? J Climate. 27(7): 2682–2698.

[19] Villafuerte M, Matsumoto J. 2015. Significant influences of global mean temperature and ENSO on extreme rainfall in Southeast Asia. J Climate. 28(5): 1905–1919.

[20] Loo Y, Billa L, Singh A. 2015. Effect of climate change on seasonal monsoon in Asia and its impact on the variability of monsoon rainfall in Southeast Asia. Geosci. Front. 6 (6): 817-823. https://doi.org/10.1016/j.gsf.2014.02.0.

[21] Hilario F, De Guzman R, Ortega D, Hayman P, Alexander B. 2009. El niño southern oscillation in the Philippines: impacts, forecasts, and risk management. Philipp J Dev. 66: 36(1).

[22] Villafuerte II, Marcelino Q, Matsumoto J, Akasaka I, Takahashi HG, Kubota H, Cinco TA. 2014. Long-term trends and variability of rainfall extremes in the Philippines. Atmos Res. 137(2014): 1–1.

Publiscience Vol. 4 Issue 1

Microplastics in farmed oysters (*Crassostrea iredalei*) from Capiz, Philippines

ARABELLA SHAYNE S. BRAÑA, MARIAMA LOIS P. CELESTIAL, RYNE JETHRO M. MOLINA, and CATHERINE JOY A. MEDIODIA

Philippine Science High School Western Visayas Campus - Department of Science and Technology (DOST-PSHSWVC), Brgy. Bito-on, Jaro, Iloilo City 5000, Philippines

Article Info

Submitted: May 02, 2021
Approved: Jul 24, 2021
Published: Aug 30, 2021

Keywords:
microplastic
oyster
Crassostrea iredalei
FTIR
KOH digestion

Abstract

Microplastics (plastic particles <5 mm in size) have been increasingly abundant, especially in filter-feeders. Oysters are commercially farmed and highly consumed in the Philippines. This study determined the presence of microplastics in commercial oysters (*Crassostrea iredalei*) sold in public markets from Cagay, Culajao, and Ivisan, Capiz. Thirty oysters yielded 47.6 g of meat, which were homogenized, divided into nine portions for KOH digestion, and incubated at 40 °C for 48 h. The digestates were passed through 25 µm Whatman filter paper. The retained particles were viewed under a microscope, identified by GESAMP descriptors, photographed, counted, and measured. Three residues were analyzed by FTIR spectroscopy to identify the chemical origin of the microplastics. The study confirmed the presence of microplastics in the oysters. The 38 microplastic particles were mostly fibers with some sheets. Their sizes ranged from 109 µm to 3.3 mm, and did not significantly differ among the three source locations. Only the sheet particle had a 49% match with cellophane.

Introduction. - Microplastics are plastic particles with sizes less than 5 mm that have become the most abundant pollutant in the aquatic environment [1,2]. Two types of microplastics exist: primary and secondary. Primary microplastics are those manufactured to size and secondary microplastics are tiny fragments from degraded larger plastics. Microplastics enter the seas directly as marine litter from shipping and fishing, or indirectly as solid wastes from land through rivers and estuaries [3, 4]. Encounters and interactions between microplastics and marine organisms are inevitable and problematic and such interactions will continue to increase as microplastics continue to accumulate over time [1].

Microplastics are imminent threats to marine biota because they are ingested and as a result, they have been found in the bodies of various marine animals including fishes [5,6] and bivalves [7,8], consequently causing digestive blockage, organ damage, low birth and growth rates, and reproductive failure [9,10]. Over time microplastics extend their effects to humans through the consumption of seafood [11] as a result of bioaccumulation]. The effects of microplastics on human health are unclear but the severity of adverse effects can depend on the toxicity of the chemicals used to produce the plastic [12].

There is huge potential for microplastics to adversely impact populations of marine animals and the Filipinos who consume them. Fish and other seafood account for 15.5% of the total protein intake in the Philippines [13] and the per capita consumption of crustaceans and mollusks is about 3 kg/year [14]. In 2019, Capiz is the top producer of fish and marine products in Western Visayas, including 31% of the aquaculture products from the region [15]. In Roxas City alone, mariculture areas produce about 513 metric tons of grouper, oysters, and mussels annually [16]. Thus, due to the considerable role of Capiz in producing commercial seafood, it is important to obtain data on microplastics found in farmed and marketed oysters (*Crassostrea iredalei*) from the aforementioned locale.

In summary, this study aims to identify and assess microplastics in commercial oysters (*C. iredalei*) from selected areas in Capiz. Specifically, it aims to:

(i) extract microplastics from oysters from three locations in Capiz;

(ii) describe, photograph, count, and measure the extracted microplastics;

(iii) identify the chemical origin of the microplastic particles; and

(iv) compare the microplastics found in oysters from the three locations.

The results of this study will benefit future studies that aim to further investigate and assess the

How to cite this article:
CSE: Braña AS, Celestial ML, Molina RJ. 2021. Microplastics in farmed oysters (*Crassostrea iredalei*) from Capiz, Philippines. Publiscience. 4(1): 8–13.
APA: Braña A.S., Celestial M.L., & Molina R.J.. (2021). Microplastics in farmed oysters (*Crassostrea iredalei*) from Capiz, Philippines. *Publiscience, 4*(1), 8–13.

For supplementary data, contact: publiscience@wvc.pshs.edu.ph.

presence of microplastics in marine environments and organisms. Furthermore, this study may also be a baseline for future studies concerning the occurrence of microplastics in the food chain. The use of KOH digestion adapted from Thiele et. al. [7] can be used as a reference for future bivalve tissue digestion for microplastic extraction.

Methods. - This study aims to identify and assess the presence of microplastics in *C. iredalei* through visual inspection, FTIR analysis, and statistical analysis.

Site Selection. Site selection was done through purposive sampling. Various seafood restaurants in Iloilo were contacted and inquired about their oyster supply, and most referred to Capiz as the source. Study sites were selected based on (1) the presence of oyster collectors or oyster farms; (2) availability and abundance of marketable oysters; (3) the oyster species was *C. iredalei*; and (4) presence of local sources of pollution. Three locations were then chosen- Cagay, Culajao, and Ivisan, Capiz (Figure 1) with the following latitude longitude coordinates: 11°35'47.8"N 122°46'39.2"E, 11°34'49.9"N 122°45'20.2"E, and 11°31'00.4"N 122°41'37.7"E respectively. All three locations had high levels of human populations, settlements, and commercial activities including fishing and fish farming.

Figure 1. Satellite image of the three sample locations taken using Google Maps.

Oyster Sampling. *C. iredalei* is easy to identify by its cup-shaped or slipper-shaped shell and the purple adductor muscle scar. The species identification was confirmed by the Southeast Asian Fisheries Development Center (SEAFDEC) in Tigbauan, Iloilo. Oyster samples were collected during the cool dry season (January, 2020) from a fish farm in Cagay and from the wet markets in Culajao and Ivisan, Capiz. A total of 15–20 oysters per site, all alive with shells shut tight. They were transported to PSHS-WVC and refrigerated at 3–6 °C for processing within 3 days. Ten live oysters of shell height 5–10 cm were chosen from each site sample for microplastic extraction. Oysters of this size were considered adults with well-developed digestive tracts, active feeding behavior, and high potential for ingestion of microplastics. The oysters were washed clean with tap water, blot-dried, then dissected in a laminar-flow cabinet to avoid contamination. To remove the oyster meat, the shell was opened by sliding a knife or scalpel between the valves and cutting the adductor muscle. The meat from 10 oysters from each site were pooled and weighed on an analytical balance. Oyster sizes (shell heights) did not differ significantly by location), but the larger oysters from Ivisan, Capiz yielded more meat.

Extraction of Microplastics. The pooled oyster meat from each source location was homogenized by combining the meat and divided into three equal weights in three beakers. The homogenates in nine beakers were chemically digested in a 10% w/v KOH solution at three times the meat volume [17]. The stock solution 10% KOH solution was prepared with 20 g KOH pellets dissolved in 200 ml distilled water. The homogenates were then incubated without agitation at 40°C for 48 h in an incubator (Biobase). Subsequently, the resulting digestates were poured on Whatman No. 4 qualitative filter paper with a pore size of 20–25 µm. The papers with residues were then placed in separate petri dishes, air-dried for 6 h and examined for microplastics. A blank sample, 10% KOH solution without oyster meat, was processed through all procedures to quantify possible microplastics contamination in the laboratory.

Visual Assessment by Microscopy. The residues were first subjected to visual assessment through microscopy at 40x magnification as the microplastic particles cannot be seen by the naked eye. The residues were viewed under a digital microscope connected to a laptop (Dell Inspiron 14 8th generation). Microplastics were identified and sorted by type according to the Joint Group of Experts on the Scientific Aspects of Marine Environmental Protection (GESAMP) [2] guidelines. The computer program Image Focus 4 was used to take images of the microplastics on filter papers. The microplastic particles were counted on 5x5 mm grids. The ImageJ and AmScope affiliate software were then used to measure the particle sizes.

FTIR Spectroscopy. Three of the extracted microplastics, named 'single fiber', 'fiber cluster', and 'sheet microplastic' were sent to the University of the Philippines Regional Research Center (UP-RRC) for Fourier Transform Infrared spectroscopy with a Thermo Scientific Nicolet iS5). This is in order to identify what type of plastic the microplastics originated from. The resulting FTIR spectra were compared or matched with the polymer database in the FTIR spectra library of UP-RRC. The analysis of the spectra was verified by a PSHS-WVC chemistry teacher.

Data Analysis. Data on oyster sizes and microplastic particle sizes were tabulated by source location and the means ± standard deviation were computed. The data were tested for normality via Shapiro-Wilk test. Furthermore, the means were compared by source location (one-way ANOVA at a 95% significance level). When the data were not normally distributed, the non-parametric Kruskal-Wallis test was used. All computations were done using the IBM® SPSS® Statistics v27 and RStudio© v3.6.1 software. The results were verified by a Statistics teacher from PSHS-WVC.

Safety Procedure. Use of personal protective equipment was observed during all laboratory work. Practice trials were conducted of all procedures from dissection of the oysters to extraction of microplastics

to microscopy. Furthermore, the empty oyster shells were bagged for disposal by the PSHS-WVC COOP personnel. Then, the used KOH solution was stored in plastic bottles and turned over to the Science Research Assistant at PSHS-WVC for proper disposal. Lastly, the researchers cleaned the work areas and organized the glassware after every use.

Results and Discussion. - This study aims to identify and assess microplastics in commercial oysters from selected areas in Capiz. Specifically, it aims to: (1) extract microplastics from oysters by means of KOH digestion and filtration; (2) describe, photograph, count, and measure the extracted microplastics under a digital microscope; (3) identify the chemical origin of the microplastic particles by spectroscopy; and (4) compare the microplastics found in oysters from three locations in Capiz.

Occurrence of Microplastics. A total of 38 microplastic particles were extracted from 47.6 g of meat from 30 oysters from the three sites in Capiz (Table 1). The data confirmed the occurrence of microplastics in farmed and marketed *C. iredalei* in Capiz — at least one microplastic particle per oyster regardless of source location. In other words, one microplastic particle was extracted for every 1.5 g of oyster meat.

Table 1. Counts and types of microplastic particles in oysters from three sites in Capiz, Philippines. (NO - Number of Oysters, TW - Total weight of oyster meat, TMPs - Total microplastics (NT + NS), NT - Number of threads, NS - Number of sheets)

Site	NO	TW (g)	TMPs (NT+NS)	NT	NS
Cagay	10	13.84	12	8	4
Culajao	10	15.48	15	13	2
Ivisan	10	18.28	11	10	1

This study confirmed the presence of microplastics in commercial oysters *C. iredalei* from raft farms and wet markets in Capiz, Philippines. Most particles were blue fibers, which are possibly remnants of fishing nets. Some were sheets that matched cellophane, a common packaging material. Cellophane is a polymeric cellulose film produced from processing cellulose from wood, cotton, hemp, or other sources. Some cellophane are coated with polyethylene or other polymers to make it heat sealable for automated wrapping machines. Though labeled as "biodegradable plastic," cellophane will break down completely only when being subjected to prolonged temperatures above 50 °C [10].

Particle Sizes of Microplastics. All the 38 (sum of all TMPs) extracted particles were <3.3 mm in their greatest dimension (Table 2) and thus were microplastic by definition. The smallest particle was 109 µm, which is much larger than the 20-25 µm pore size of the Whatman No. 4 filter paper that was used. The particle sizes apparently differed among locations, with mean sizes highest in Cagay and lowest in Ivisan (Table 2). However, the differences were not statistically significant (Kruskal-Wallis test, $p = 0.28$). Furthermore, a non-parametric test was used because the size data were not normally distributed (Shapiro-Wilk test, $p < 0.05$).

Table 2. Particle sizes (greatest dimension) of microplastics in oysters from three sites in Capiz. (NP - Number of Particles)

Sites	NP	Particle size (mm)			
		Min	Max	Mean	SD
Cagay	12	0.165	3.207	1.506	0.961
Culajao	15	0.123	2.928	1.266	0.967
Ivisan	11	0.109	3.260	0.951	0.975

The microplastics found in oysters in this study had particle sizes of 0.11–3.25 mm, larger than those (0.1–0.3 mm) found in green mussels in Bacoor Bay [18], but similar to those (0.56–4.58 mm) found in the waters of Pasig River [19]. Much smaller microplastics of sizes 2–6 µm adversely affected reproduction in the oysters studied by Sussarellu et. al. [20]. It remains to be determined whether smaller microplastics, and even the larger microplastics that were found, would also be harmful to *C. iredalei.*

Types and Composition. The microplastics left on the filter paper were mostly thin blue fibers but some were sheet-like and white or transparent. The 38 microplastic particles consisted of fibers (81.58%) with some sheets (18.42%) (Table 1). Digital images of the extracted microplastic particles are shown in Figure 1.

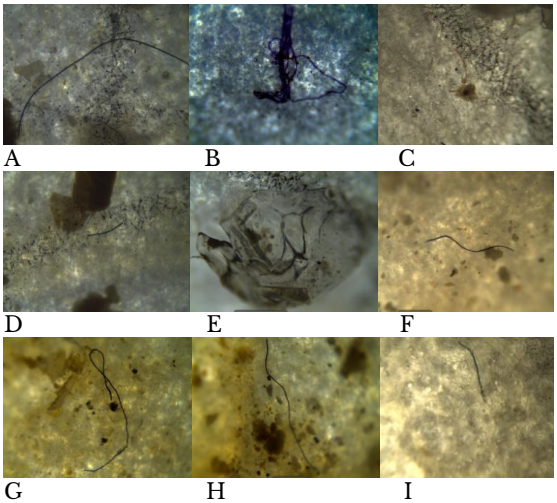

Figure 1. Microplastic particles extracted from farmed oysters from Capiz. Images taken by digital microscope of the residues on three filter papers per location. A-C Cagay; D-F Culajao; G-I Ivisan.

Indeed the study sites confirmed the extensive use of plastic nets, ropes, containers, and other gear in locations consume a variety of plastic products and packaging materials that were plainly visible as fishing and fish farming. Furthermore, it can be inferred that numerous households in the three

scattered litter: sachets of shampoo and coffee, single-use bags, wrappers, jars, etc. Markets and tourism and recreational activities were also sources of plastic pollution at the study sites.

Chemical Origin of Microplastics. The microplastics analyzed by FTIR spectroscopy are shown in Figure 5. 'Sheet microplastic' is image E. 'Single fiber' is image A and 'fiber cluster' is image G.

Figure 2 shows the FTIR spectrum of the 'sheet microplastic' together with the library matching, which yielded a 49% match with cellophane. A 49% match under normal conditions is not considered an ideal match rate, however, with the nature of these microplastic samples, it is deemed acceptable. The samples were dried insufficiently due to lack of supporting articles, and with this, saltwater residues and oxidized groups interfered in the results, thus producing a low match rate. In contrast, the FTIR spectra for 'single fiber' and 'fiber cluster' showed no match with any polymer in the database (Figures 3 and 4).

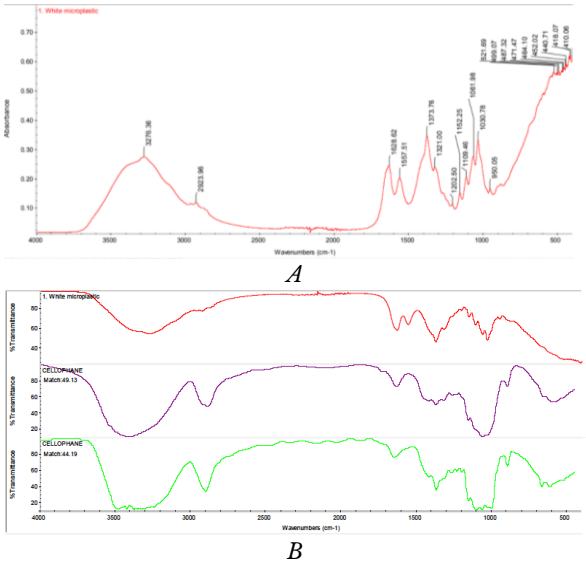

A

B

Figure 2. A The FTIR spectrum of sheet microplastic; B Library match with cellophane, 49%.

The fibers and sheets that were analyzed by FTIR spectroscopy could not be matched with any polymer in the UP-RRC spectra database. This result was probably due to insufficient drying of the fibers in the residue on the filter paper. Furthermore, the structural identity of the microplastic samples was also compromised given the changes in the chemical structures of the samples (e.g. bond breakage, etc.). Da Costa et al. [21] reported that the physical and chemical properties of a microplastic particle are affected by prolonged exposure to saltwater. The formation of oxidized groups from exposure to water results in noise when the spectroscopy test was conducted. While it is difficult to identify the primary causes of noise in spectroscopy, deficiencies in sample preparation/handling is considered a probable cause.

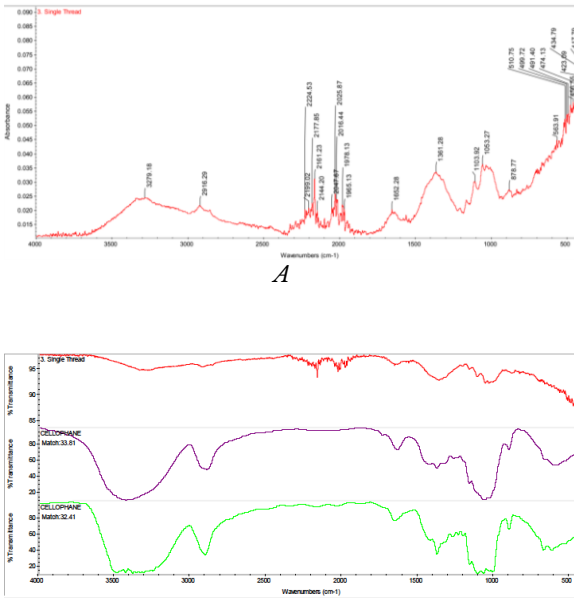

A

B

Figure 3. A The FTIR spectrum of 'single fiber' microplastic; B Library match not found.

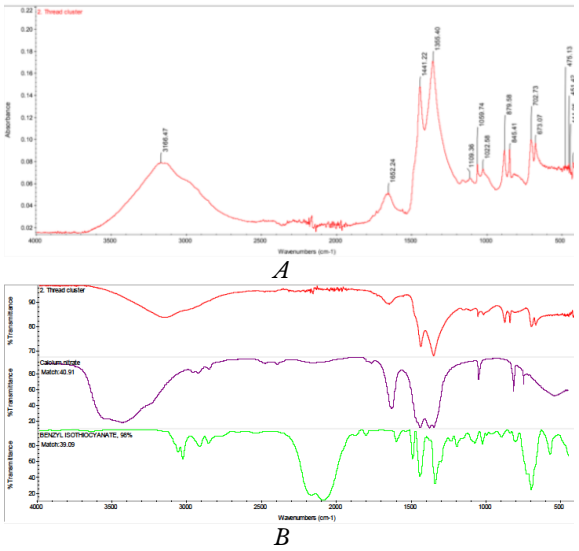

A

B

Figure 4. A The FTIR spectrum of 'fiber cluster' microplastic; B Library match not found.

Limitations. Cellulose filter paper was unavailable during the conduct of the laboratory procedures and Whatman® Grade 4 qualitative filter paper was used instead. Thus, particle retention was limited to 25 µm. Secondly, the Fourier Transform Infrared (FTIR) spectra were only compared to pre-identified polymer databases. Thus, other non-polymer spectra were not subjected for comparison.

Conclusion. - Microplastic presence was confirmed in commercial oysters *C. iredalei* collected from three various locations in Capiz with Culajao yielding the highest number of microplastics among the three locations. The abundance of microplastic fiber found and the identification of cellophane in 'white microplastic' suggest that the source of microplastics come from maritime activities such as fishing and improper disposal of household waste in the area. Statistical analysis concludes that the

location of the collection sites do not directly affect the microplastic size.

Recommendations. - To improve the study, it is recommended that cellulose filter paper with pore size lower than 25 µm should be used during filtration to enable the extraction of microplastics that have a diameter less than 25 µm. Additionally, air-drying the filter papers used during filtration at room temperature can be used as an alternative to oven-drying, which will greatly enhance the generated IR spectra as water will no longer be factored in the FTIR analysis. It is also recommended that a library match with a more extensive polymer library should be conducted to yield a more specific polymer type. Furthermore, the microplastics extracted may be weighed using more precise weighing scales to calculate microplastic abundance in milligrams microplastic/sample mass or for sediment studies, milligrams microplastic/kg^{-1} sediment. Finally, it is recommended that the results of this study are communicated to local government units to allow oyster farmers to reevaluate the conditions of their farm and create appropriate measures to reduce microplastic pollution such as imposing strict guidelines on proper waste disposal.

Acknowledgment. - We would like to extend our gratitude to Mrs. Junemie Ramos from SEAFDEC Iloilo for aiding us in the authentication of the oyster species. Likewise, we also extend our gratitude to Mr. Mark Rosales for responding to our queries and assisting us in our data presentation and analysis. Finally, we would also like to thank Mrs. Teodora Bagarinao for assisting us with our documents.

References

[1] Law KL, Thompson RC. 2014. Microplastics in the seas. Science. 345(6193): 144–145. doi:10.1126/science.1254065.

[2] GESAMP (Joint Group of Experts on the Scientific Aspects of Marine Environmental Protection). 2019. Guidelines for the Monitoring and Assessment of Plastic Litter in the Ocean. Nairobi, Kenya: United Nations Environment Programme (UNEP). p. 11–12.

[3] Eerkes-Medrano D, Thompson R, Aldridge D. 2015. Microplastics in freshwater systems: a review of the emerging threats, identification of knowledge gaps and prioritisation of research needs. 75: 63–82. https://doi.org/10.1016/j.watres.2015.02.012.

[4] Vermeiren, P, Munoz CC, Ikejima K. 2016. Sources and sinks of plastic debris in estuaries: A conceptual model integrating biological, physical and chemical distribution mechanisms. MarPollut Bull. 113: 7–16. https://doi.org/10.1016/j.marpolbul.2016.10.002.

[5] Bucol L, Romano E, Cabcaban S, Siplon LM, Madrid GC, Bucol A, Polidoro B. 2019. Microplastics in marine sediments and rabbitfish (Siganus fuscescens) from selected coastal areas of Negros Oriental, Philippines. Mar Pollut Bull. 148. https://doi.org/10.1016/j.marpolbul.2019.110685.

[6] Sarijan S, Azman S, Said MIM, Lee MH. 2019. Ingestion of microplastics by commercial fish in Skudai River, Malaysia. Environ Asia. 12(3): 75–84.http://dx.doi.org/10.14456/ea.2019.47.

[7] Li J, Yang D, Li L, Jabeen K, Shi H. 2015. Microplastics in commercial bivalves from China. Environ Pollut. 207: 190–195. https://doi.org/10.1016/j.envpol.2015.09.018.

[8] Ding J, Li JX, Sun CJ, He CF, Jiang FH, Gao FL, Zheng L. 2018. Separation and identification of microplastics in digestive systems of bivalves. Chinese J Anal Chem. 46(5): 690–697. https://doi.org/10.1016/S1872-2040(18)61086-2.

[9] Wright SL, Thompson RC, Galloway TS. 2013. The physical impacts of microplastics on marine organisms: a review. Environ. Pollut. 178: 483–492.https://doi.org/10.1016/j.envpol.2013.02.031.

[10] Cole M, Lindeque P, Fileman E, Halsband C, Galloway TS. 2015. The impact of polystyrene microplastics on feeding, function and fecundity in the marine copepod Calanus helgolandicus. Environ Sci Technol 49: 1130–1137. https://doi.org/10.1021/es504525u.

[11] Van Cauwenberghe L and Janssen CR. 2014. Microplastics in bivalves cultured for human consumption. Environ. Pollut. 193: 65–70. https://doi.org/10.1016/j.envpol.2014.06.010.

[12] Smith M, Love DC, Rochman CM, Neff RA. 2018. Microplastics in seafood and the implications for human health. Curr Environ Health Rep. 5(3): 375–386. doi: 10.1007/s40572-018-0206-z.

[13] Food and Agriculture Organization (FAO). 2020. Aquaculture growth potential in the Philippines. FAO. [accessed 2021 Mar 18]. Available from https://bit.ly/3g9lqbd.

[14] BFAR On-Line Information System. c 2018. Bureau of Fisheries and Aquatic Resources. [cited 2021 Mar 21]. Available from https://bit.ly/3pp55Db.

[15] Philippine Statistics Authority. c 2020. Capiz fishery production in 2019 [Internet]. [accessed 2021 Mar 18] https://bit.ly/3vXa94c.

[16] Baes MM. 2015. Economic analysis and adaptation measures of small-scale aquaculture in Roxas City, Capiz. University of the Philippines Visayas.

[17] Thiele CJ, Hudson MD, Russel AE. 2019. Evaluation of existing methods to extract microplastics from bivalve tissue: Adapted KOH digestion protocol improves filtration at single-digit pore size. Marine Pollution Bulletin. 142: 384–393.

https://doi.org/10.1016/j.marpolbul.2019.03.003.

[18] Argamino CR and Janairo JI. 2016. Qualitative assessment and management of microplastics in Asian green mussels (*Perna viridis*) cultured in Bacoor bay, Cavite, Philippines. Environment Asia. 9(2): 48–54. doaj.org/article:b0df33553e1b401492b3c50d526457ab.

[19] Deocaris CC, Allosada JO, Ardiente LT, Bitang LGG, Dulohan CL, Lapuz JKI, Padilla LM, Ramos VP, Padolina JBP. 2019. Occurrence of microplastic fragments in the Pasig River. H2Open Journal 2: 92–100. https://doi.org/10.2166/h2oj.2019.001.

[20] Sussarellu R, Suquet M, Thomas Y, Lambert C, Fabioux C, Pernet ME, Le Goïc N, Quillien V, Mingant C, Epelboin Y, et al. 2016. Oyster reproduction is affected by exposure to polystyrene microplastics. Proceedings of the National Academy of Sciences. 113: 2430–2435. https://doi.org/10.1073/pnas.1519019113.

[21] Da Costa J, Nunes A, Santos P, Girao A, Duarte A, Rocha Santos T. 2018. Degradation of polyethylene microplastics in seawater: insights into the environmental degradation of polymers. Journ of Environ Sci and Health. 53(9): 866–875. doi: 10.1080/10934529.2018.145.

Publiscience Vol. 4 Issue 1

Evaluation of the larvicidal efficacy of *Artocarpus heterophyllus* (jackfruit) rags and rind ethanolic crude extracts against third to early fourth instar *Aedes aegypti* larvae

BLESSY MARIE A. ALIBO, MYANNA SHAREE P. FUENTES, GYDEL FAITH A. ORBINA, and CATHERINE JOY A. MEDIODIA

Philippine Science High School Western Visayas Campus - Department of Science and Technology (DOST-PSHSWVC), Brgy. Bito-on, Jaro, Iloilo City 5000, Philippines Brgy. Bito-on, Jaro, Iloilo City 5000, Philippines

Article Info

Submitted: Apr 21, 2021
Approved: Jun 23, 2021
Published: Aug 30, 2021

Keywords:
Artocarpus heterophyllus
Aedes aegypti
biolarvicide
larvicidal bioassay
phytochemical analysis

Abstract

Artocarpus heterophyllus (jackfruit) is a shrub that has high phytochemical content in its different plant parts. However, 60% of its fruit remains underutilized. This study evaluated the larvicidal activity of the crude extracts of *A. heterophyllus* rags, rind, and combined rags and rind against third to early fourth instar *Aedes aegypti* larvae. Larvicidal bioassay was performed using concentrations ranging from 500–2500 ppm. Larval mortality data were recorded after 48 hours of exposure and were analyzed using Probit analysis. The *A. heterophyllus* rags and rind crude extracts showed high larval percent mortality rates of 70%-90%. The rind crude extract has the highest larvicidal efficacy since it has the lowest LC50 and LC90 values of 1136 ppm and 2500 ppm, respectively. The promising larvicidal activities shown by the treatments may be attributed to the abundance of triterpenes, saponins, tannins, and glycosides that was found using qualitative phytochemical analysis. Thus, the crude extracts of *A. heterophyllus* rags and rind may be used as alternatives to synthetic larvicides.

Introduction. - Dengue epidemics have increased for the past 20 years in both number and magnitude due to the rapid spread of the *Aedes aegypti* mosquito, the primary vector of dengue viruses, which thrives in highly urbanized areas [1]. The disease is one of the most significantly widespread mosquito-borne viral infections in humans [2]. Due to the lack of medical response against dengue viruses, effective vector control measures have become the sole weapon against dengue today [3]. The application of chemical insecticides to control the principal dengue vector, *Ae. aegypti*, is widespread. However, the development of resistance against these chemicals, the undesirable effects on non-target organisms, and the rise of environmental and health concerns led to the search for other alternative methods in controlling vector mosquitoes, such as the use of plants [4].

Plant-derived products have been used as insecticides in substitute for synthetic chemicals. They are less toxic, less prone to the development of resistance, and easily biodegradable [5]. The general classes of phytochemicals that they contain (sterols, triterpenes, flavonoids, alkaloids, saponins, glycosides, and tannins) are responsible for their insecticidal activity. These phytochemicals extend the postembryonic development of larvae and pupae and delay the formation of adult insects [6].

Artocarpus heterophyllus, also known as jackfruit, is a tree belonging to the mulberry family (Moraceae). It has naturalized in the tropics, particularly in Southeast Asia, and is considered an important crop in many countries such as the Philippines [7]. Only 15–20% of the ripe fruit is utilized as food [8], while 60% of the fruit which includes the rind, inner perdigones, and central core, are being thrown away as waste [9]. Thus, utilization of these parts must be done to convert these wastes into useful products [10].

Previous studies have focused on the pulp and seeds of the jackfruit and their phytochemical properties which reported that they have a high phytochemical content [11,12,13]. Moreover, the results of several studies have shown that high quantities of saponins, alkaloids, and flavonoids are present in jackfruits [11]. However, despite these pieces of information, none of the previous studies have isolated and examined the underutilized parts of jackfruit for their phytochemical content and larvicidal activity against dengue mosquito vectors,

How to cite this article:
CSE: Alibo BM, Fuentes MS, Orbina GF, Mediodia CJ. 2021. Evaluation of the larvicidal efficacy of *Artocarpus heterophyllus* (jackfruit) rags and rind ethanolic crude extracts against third to early fourth instar *Aedes aegypti* larvae. Publiscience. 4(1): 14–19.
APA: Alibo, B.M., Fuentes, M.S., Orbina, G.F., & Mediodia, C.J. (2021). Evaluation of the larvicidal efficacy of *Artocarpus heterophyllus* (jackfruit) rags and rind ethanolic crude extracts against third to early fourth instar *Aedes aegypti* larvae. *Publiscience*, *4*(1), 14–19.

For supplementary data, contact: publiscience@wvc.pshs.edu.ph.

specifically, the rags and rind of the fruit.

This study aimed to evaluate the larvicidal effect of *A. heterophyllus* crude extracts in terms of mortality rate against *Ae. aegypti* larvae. Specifically, the study aimed to:

(i) count the dead and moribund *Ae. aegypti* larvae after the treatment of *A. heterophyllus* rags, rind, and 50:50 combination crude extracts.

(ii) determine the lowest concentration of *A. heterophyllus* rags, rind, and 50:50 combination crude extracts that would yield 50% and 90% mortality rates in the larval population; and

(iii) assess and confirm the presence and abundance of phytochemicals in *A. heterophyllus* rags and rind using qualitative phytochemical analysis.

Methods. - The study conducted was experimental in nature. After the acquisition, *A. heterophyllus* rags, white or pale yellow fibrous strands surrounding the flesh, and rind, the green or yellow spiky outer skin of the fruit, were thoroughly rinsed before oven drying and powderization. The ground samples were macerated for 24 hours with constant agitation and filtered using vacuum filtration. Rotary evaporation was performed to obtain the crude extracts used in the succeeding processes. A qualitative phytochemical analysis was performed on both rags and rind samples to assess the active components. The larvicidal effect of each crude extract, against *Ae. aegypti* larvae were investigated using a larvicidal bioassay. Probit analysis was utilized to determine the LC50 and LC90 values of the crude extracts. The number of mosquito larval deaths in set-ups was recorded and counted manually after 24 hours and 48 hours of exposure.

Preparation of Samples. The samples were collected from a jackfruit vendor in Calle Real, Iloilo, and sent to the Department of Agriculture (DA) for verification. The rags and rind portion were separated, cut into smaller pieces, rinsed with distilled water, and oven-dried at 40 °C for 48 hours. The dried samples were ground into fine particles and weighed using a digital analytical balance.

Extraction. One hundred grams (100 g) of the ground samples were macerated in 1000 mL of 95% ethanol in amber glass bottles for 24 hours at room temperature. The solutions were mixed in batches using a magnetic stirrer and agitated at varying intervals. They were then filtered via vacuum filtration using Whatman Filter Paper no. 41. Subsequently, the samples were placed in a rotary evaporator at 40 °C until the ethanol completely evaporated. Lastly, the extracts were subjected to a flame test to verify the absence of ethanol in the samples.

Collection and Acclimatization of Test Organisms. Twenty (20) third to early fourth instar mosquito larvae were used for both the preliminary and final testing. The first and second instars of the larvae were not utilized as they are considered too fragile to handle.

The *Ae. aegypti* larvae used in the study were bred and cultured by the Department of Science and Technology-Industrial Technology Development Institute (DOST-ITDI) Entomology Section Insectary according to the standard procedures and general guidelines set by World Health Organization (WHO).

Preparation of Test Set-ups. Larval populations containing 20 organisms in each 100 mL glass beakers with 50 mL dechlorinated water were established. Relatively smaller and moribund larvae were replaced.

Preparation of Treatments. As specified in the Guidelines for Laboratory and Field Testing of Mosquito Larvicides of WHO, the quantity of the stock solution was obtained by diluting 1.5 grams of each of the *A. heterophyllus* extracts, namely: pure rags crude extract, pure rind crude extract, and the 50:50 combination, with 1.5 mL 95% ethanol and 13.5 mL water to achieve 100000 ppm or 10% w/v crude extract-ethanol solution [14]. The stock solutions were placed in 140 mL beakers. Shaking and stirring of the solutions were done to dissolve the extract with the solvent.

Abate® 1SG mosquito larvicide and 1% ethanol in dechlorinated water were used as positive and negative controls, respectively. These were then applied to the mosquito larvae set-ups.

Larvicidal Bioassay. The WHO standard protocol for testing the mortality of mosquito larvicides was followed. Two (2) preliminary experiments were conducted to establish the range of lethal concentrations that would be effective in killing 10% to 90% of the larval population. Each preliminary test contained five (5) test concentrations with three (3) replicates each. The final test concentrations were obtained on the second preliminary test, ranging from 500–2500 ppm. Six (6) replicates were carried out for each concentration. A water depth between 5–10 cm was maintained to prevent undue mortality when soaked in deeper levels [14,15]. Mortality data was recorded after 24 and 48 hours of exposure for each test set-up. The mortality rates were calculated using the formula below:

$$Mortality\ rate = \frac{Total\ number\ of\ dead\ larvae}{Initial\ number\ of\ larvae\ present} \times 100\%$$

Larvae that fail to display any immediate activity when probed or prompted were identified as dead or moribund [14].

Qualitative Phytochemical Analysis. Two hundred grams (200 g) of oven-dried *A. heterophyllus* rags and rind samples were sent to DOST-ITDI. The presence and abundance of the phytochemical components, specifically alkaloids, flavonoids, glycosides, saponins, sterols, tannins, and triterpenes were determined and assessed.

Data Analysis. Data from all replicates of each treatment were pooled for linear regression probit analysis using Microsoft® Excel® for Microsoft 365 MSO (16.0.13929.20360) 64-bit. The lethal concentrations to kill 50% and 90% of the larval

population, also known as LC50 and LC90 values, were determined by plotting the data points in a spreadsheet. The concentrations were then converted into logarithmic functions whereas the mean percentage of larval mortality adopted the corresponding probit values. A one-way Analysis of Variance (ANOVA) test was conducted at $\alpha = 0.05$ to statistically compare the treatments.

Waste Disposal. No chemical substances were disposed of down the drains. The containers with chemical wastes were placed in the chemical waste disposal box in the Biology Laboratory 2 of PSHS-WVC.

Stock solutions used in the larvicidal bioassay were disposed of in a separate container specifically for chemical waste while dead larvae were placed in biohazard containers. The standard procedures of the institution were followed. Beakers after testing were treated and sterilized with hot water.

Safety Procedure. The chemical and waste management were done according to the WHO Laboratory Safety Manual 4th Edition [16]. All laboratory chemicals and chemical wastes were treated with caution and exposure was minimized by observing laboratory safety measures such as wearing personal protective equipment (PPE) and conducting activities under the supervision of laboratory personnel. Chemical wastes were stored in properly-labeled closed containers. Extracts were properly stored in a 15 mL amber glass bottle.

Results and Discussion. - This study aimed to evaluate the larvicidal efficacy of the individual and combined crude extracts of *A. heterophyllus* rags and *A. heterophyllus* rind against third to early fourth instar *Ae. aegypti* larvae. This was done through a larvicidal bioassay. The data were collected after 48 hours for comparison and analysis.

Figure 1 shows the larvicidal activity of the three treatments against third to early fourth instar *Ae. aegypti* larvae by larvicidal bioassay. The three crude extracts showed significant toxicity based on the mean (%) mortality of the *Ae. aegypti* larvae. The mean (%) mortality of the three extracts increases as the concentration of treatments increases.

Two thousand five hundred (2500) ppm of *A. heterophyllus* rind extract has the highest mean (%) mortality. Five hundred (500) ppm of crude extracts of *A. heterophyllus* rags and of the combined *A. heterophyllus* rags and rind exhibited no larval death.

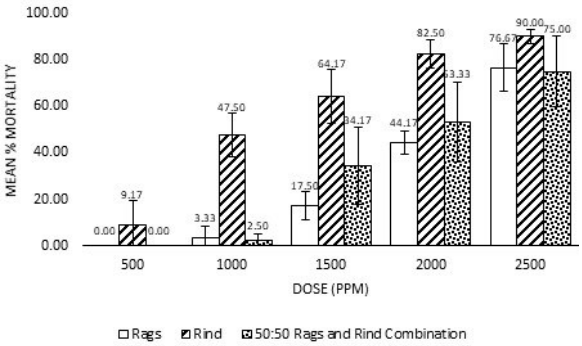

Figure 1. Larvicidal activity of the rind crude extract, rags crude extract, and 50:50 combination of rags and rind crude extract of *A. heterophyllus* against third and early fourth instar *Ae. aegypti* larvae after 48 hours.

Figure 2 shows the larvicidal activity of the positive control (Abate® 1SG larvicide) against third to early fourth instar *Ae. aegypti* larvae. The mortality of *Ae. aegypti* larvae was observed in all its concentrations with 0.3 ppm having the lowest mean (%) mortality at 10.00%, and 1.2 ppm having the highest at 96.67%. There was no larval mortality observed in the negative control treatment, 1% ethanol-dechlorinated water. The data show that all three crude extracts can be used as a larvicide. However, these are not as effective as the commercially available larvicide which is the positive control. Moreover, the results of the one-way ANOVA test showed that no significant difference exists between the groups determined by ($F(2,12) = 1.282$, $p = 0.3129$) at $\alpha = 0.05$. Thus, all extracts are equally effective.

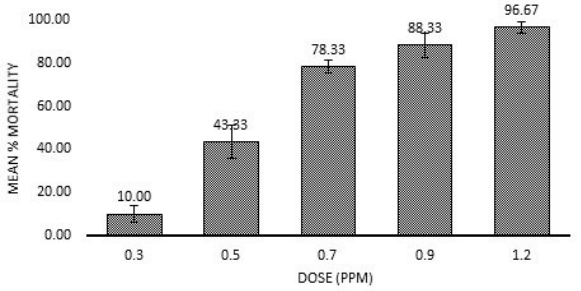

Figure 2. Larvicidal activity of the positive control, Abate® 1SG larvicide, against third to early fourth instar *Ae. aegypti* larvae after 48 hours.

Figure 3 shows the lethal concentrations of *A. heterophyllus* rags crude extract, *A. heterophyllu*s rind crude extract, and combined *A. heterophyllus* rags and rind crude extract against third to early fourth instar *Ae. aegypti* larvae after 48 hours of exposure.

The lowest LC50 and LC90 values were obtained from *A. heterophyllus* rind crude extract. The LC50 of *A. heterophyllus* rind crude extract was obtained at 1136 ppm while the LC90 was obtained at 2500 ppm. It was followed by combined *A. heterophyllus* rags and rind crude extract with LC50 and LC90 values of 1903 ppm and 3041 ppm, respectively. *A. heterophyllus* rags crude extract had its LC50 at 2012 ppm and LC90 at 3041 ppm.

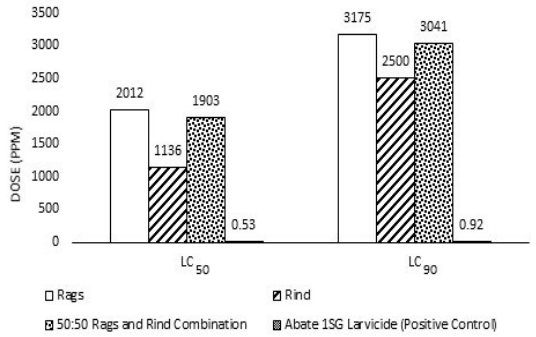

Figure 3. Lethal concentrations of different treatments against third to early fourth instar *Ae. aegypti* larvae after 48 hours of exposure period.

A. heterophyllus rind crude extract was the most effective larvicide among the three crude extracts for it has the lowest LC50 and LC90 values. The effectiveness of *A. heterophyllus* rind crude extract as a larvicide may be attributed to the abundance of known phytochemicals that are found in other plant-based larvicides in it.

A study conducted by Nair and Kavrekar [17] using the leaves of similar plant species was conducted and the results are more effective in terms of the LC50 and LC90. The LC50 and LC90 values of the treatment in the study are between 400 ppm and 600 ppm, and between 800 ppm and 900 ppm, respectively. The values mentioned are lower than the LC50 and LC90 values of the three treatments in this study [17]. Another study conducted by Pineda-Cortel et al. [18] made use of *Artocarpus blancoi* in different fractions and reported incomparable results with the result of the current study. Furthermore, the results of previous studies are more effective than the treatments used in this study.

The combination of crude extracts may exhibit synergistic or antagonistic effects. The combined extract used in this study, however, is only limited to one concentration which is 50:50. Other ratios were not studied in this study. Therefore, the best ratio to obtain a result that is more effective, in terms of the lethal concentration, than the individual extracts was not determined. The relationship of two crude extracts is synergistic when the quotient of the LC50 of the individual crude extract and of the combined plant crude extracts, also known as the synergistic factor, is greater than 1 [19]. The synergistic activity increases with the synergistic factor. In this study, the synergistic factor between the crude extracts of *A. heterophyllus* rags and the combined *A. heterophyllus* rags and rind crude extract is 1.057. On the other hand, the synergistic factor between the crude extracts of *A. heterophyllus* rind and the combined *A. heterophyllus* rags and rind is 0.597. This means that the crude extracts of *A. heterophyllus* rags and *A. heterophyllus* rind have an antagonistic relationship. This result is similar to the study of Grande et al. [20] where the combined extracts did not have an overall synergistic larvicidal effect against *Ae. aegypti* larvae. The LC50 and LC90 values of the combined extracts fell under the LC50 and LC90 values of the individual extracts. Based on the study, the failure of the combined extracts to have a synergistic effect on each other was due to the possible unforeseen chemical reactions between the phytochemicals that the individual extracts contain. However, this result differs in study of Yuan et al. [19] where the individual extracts exhibited a synergistic activity because the combined extracts were found to be a more effective larvicide than the individual extracts.

Table 1 shows the results of the qualitative phytochemical analysis of *A. heterophyllus* rags and rind. The results showed that *A. heterophyllus* rags crude extract does not contain sterols, flavonoids, and alkaloids. However, the rags extract has traces of saponins and glycosides, a moderate amount of tannins, and an abundance of triterpenes. The results also showed that *A. heterophyllus* rind crude extract does not contain sterols and alkaloids. Despite this, the rind extract contains traces of flavonoids and glycosides, and an abundance of triterpenes, saponins, and tannins.

Table 1. Qualitative phytochemical analysis of *A. heterophyllus* rags and *A. heterophyllus* rind samples.

Phytochemical	*A. heterophyllus* rind	*A. heterophyllus* rags
Sterols	(-)	(-)
Triterpenes	(+++)	(+++)
Flavonoids	(+)	(-)
Alkaloids	(-)	(-)
Saponins	(+++)	(+)
Glycosides	(+)	(+)
Tannins	(+++)	(++)

Traces (+), Moderate (++), Abundant (+++), Absent (-)

Saponins are known to decrease the digestive enzyme activity of mosquito larvae [21] and attack the cuticle membrane of the larvae [22]. Moreover, flavonoids attack the nerves and respiratory system of mosquito larvae [21]. Lastly, tannins form complexes with the digestive enzymes in the gut of insects which reduce the digestion efficiency and inhibit the growth of insects [22]. Previous studies have concluded that the abundance of saponins and tannins in plant extracts is responsible for the larvicidal activity of the plant extract [18,23,24].

In this study, the positive larvicidal activity exhibited by the three crude extracts was attributed to the presence of phytochemicals. Similar to previous studies, saponins, flavonoids, and tannins disrupted the normal body functions of larvae. The abundance of saponins and tannins in *A. heterophyllus* rind crude extract made it more effective than the other two crude extracts having a lesser amount of the mentioned phytochemicals present. Also, flavonoids are present in *A. heterophyllus* rind crude extract but not in *A. heterophyllus* rags crude extract. This is also a factor as to why *A. heterophyllus* rind crude extract is more effective as larvicide at a lower concentration than *A. heterophyllus* rags crude extract. Furthermore, the disruption of the normal body functions of the larvae decreased the health of the larvae and eventually caused the mortality of the larvae.

Limitations. The qualitative phytochemical test of DOST-ITDI only included a predetermined list of phytochemical components that were to be assessed in the plant samples. Thus, limiting the assessment to seven (7) components. The presence nor abundance

of other phytochemicals was not confirmed through the said test.

Conclusion. - The current study found *A. heterophyllus* rags, *A. heterophyllus* rind, and combinations of *A. heterophyllus* rags and rind crude extract as equally effective larvicides against third to early fourth instar *Ae. aegypti* larvae. The individual *A. heterophyllus* rind crude extract is the most efficient among the three treatments because it requires the least amount of concentrations to result in 50% and 90% mortality rates in the larval population. Phytochemicals were also found to be present in *A. heterophyllus* rags and rind, with the rind containing more phytochemicals. This is the reason why *A. heterophyllus* rind is more effective than *A. heterophyllus* rags. Therefore, the crude extracts of *A. heterophyllus* rags, *A. heterophyllus* rind, and a combination of *A. heterophyllus* rags and rind can be used as an alternative to synthetic larvicides.

Recommendations. - The researchers recommend that more replicates of each concentration for each treatment are to be used so as to eliminate outliers in the results. Other vector species may also be utilized as test organisms and various parts of the plant such as the leaves, bark, and seeds may be maximized for future studies involving a similar research design. The incorporation of essential oils in the treatments may also be considered. Furthermore, this study serves as a basis for future analyses on the active compounds present in *A. heterophyllus* rind and rags. Thus, it is recommended that an in-depth approach be conducted to further explore and identify the phytochemical components present in *A. heterophyllus*.

Acknowledgment - The researchers would like to extend their utmost gratitude to Mrs. Alicia Garbo and the personnel of the DOST-ITDI Standards and Testing Division for their close supervision. The knowledge imparted to and time allotted for the researchers are very much appreciated. They would also like to thank the vendors in Calle Real, Iloilo for entertaining and providing the needs of the researchers.

References

[1] Brown JE, Evans BR, Zheng W, Obas V, Barrera-Martinez L, Egizi A, Zhao H, Caccone A, Powell JR. 2014. Human impacts have shaped historical and recent evolution in *Aedes aegypti*, the dengue and yellow fever mosquito. Evolution. 68(2): 514–525. doi: 10.1111/evo.12281.

[2] Bhatt S, Gething PW, Brady OJ, Messina JP, Farlow AW, Moyes CL, et al. 2013. The global distribution and burden of dengue. Nature. 496(7446): 504–507. doi: 10.1038/nature12060.

[3] Bäck AT, Lundkvist A. 2013. Dengue viruses - an overview. Infection Ecology & Epidemiology 3:1, 19839. doi: 10.3402/iee.v3i0.19839.

[4] Hayes JB, Laws ER. 1991. Handbook of pesticide toxicology. San Diego: Academic Press.

[5] Prahbu K, Murugan K, Nareshkumar A, Ramasubramanian N, Bragadeeswaran S. 2011. Larvicidal and repellent potential of *Moringa oleifera* against malarial vector, *Anopheles stephensi* Liston (Insecta: Diptera: Culicidae). Asian Pac J Trop Biomed 1(2): 124–129. doi: 10.1016/S2221-1691(11)60009-9.

[6] Upadhyay RK. 2016. Botanicals; Its Safe Use in Pest Control and Environmental Management. Intern J Zool Invest. 2(1): 58–102.

[7] Elevitch CR, Manner HI. 2006. *Artocarpus heterophyllus* (jackfruit), verI.IV. In: Elevitch CR. (ed.). Species Profiles for Pacific Island Agroforestry. Permanent Agriculture Resources (PAR), Holualoa, Hawai'i. Available from: http://bit.ly/agroforestryorg.

[8] Silva JHV, Filho J, Ribeiro M, Silva EL. 2007. Effect of the addition of jackfruit (*Artocarpus heterophyllus* Lam.) seeds bran in dietary on the egg production, yolk pigmentation and dropping humidity in Japanese quais. Ciência Agrotécnica. 31: 523–530. doi: 10.1590/S1413-70542007000200037.

[9] Subburamu K, Singaravelu M, Nazar A, Irulappan I. 1992. A Study on the Utilization of Jackfruit Waste. Short Communication Bioresource Technology. 40: 85-86.

[10] Begum R, Aziz MG, Uddin MB, Yusof YA. 2014. Characterization of Jackfruit (*Artocarpus heterophyllus*) Waste Pectin as Influenced by Various Extraction Conditions. Agriculture and Agricultural Science Procedia. 2: 244–251. doi: 10.1016/j.aaspro.2014.11.035.

[11] Gupta D, Mann S, Sood A, Gupta RK. 2011. Phytochemical, nutritional and antioxidant activity evaluation of seeds of jackfruit (*Artocarpus heterophyllus*). International Journal of Pharma and Bio Sciences. 2(4): 333–343.

[12] Shanmugapriya K, Saravana S, Payal H, Mohamed P, Binnie W. 2011. Antioxidant activity, total phenolic and flavonoid contents of *Artocarpus heterophyllus* and *Manilkara zapota* seeds and its reduction potential. International Int J Pharm Pharm Sci. 3(5): 256–260.

[13] Abu Bakar MF, Abdul Karim F, Perisamy E. 2015. Comparison of phytochemicals and antioxidant properties of different fruit parts of selected Artocarpus species from Sabah, Malaysia. Sains Malaysiana. 44(3): 355–363. doi: 10.17576/jsm-2015-4403-06.

[14] [WHO] World Health Organization. 2005. Guidelines for laboratory and field testing of mosquito larvicides. Document WHO/CDS/CSR/LYO/2004.11. Geneva: World Health Organization.

[15] [WHO] World Health Organization. 2004. Laboratory safety manual. Document WHO/CDS/WHOPES/GCDPP/13. Geneva: World Health Organization.

[16] Pineda-Cortel MRB, Cabantog RJR, Caasi PM, Ching CAD, Perez JBS, Godisan PGM, Latorre CMG, Lucero DR, Salonga RB. 2019. Larvicidal and ovicidal activities of *Artocarpus blancoi* extracts against *Aedes aegypti*. Pharmaceutical Biology, *57*(1): 120–124. doi: 10.1080/13880209.2018.1561727.

[17] Nair S, Kavrekar V. 2017. In Vitro screening of larvicidal and insecticidal activity of methanolic extracts of Artocarpus heterophyllus, *Artocarpus altilis* and Piper betle. IJEAB. 2(1): 281–288. doi: 10.22161/ijeab/2.1.37.

[18] Pineda-Cortel MR, Cabantog RJ, Caasi P, Ching CA, Perez JB, Godisan PG, Latorre CM, Lucero D, Salonga R. 2019. Larvicidal and ovicidal activities of *Artocarpus blancoi* extracts against Aedes aegypti. *57*(1): 120–124. doi: 10.1080/13880209.2018.1561727.

[19] Yuan Y, Li L, Zhao J, Chen M. 2020. Effect of Tannic Acid on Nutrition and Activities of Detoxification Enzymes and Acetylcholinesterase of the Fall Webworm (Lepidoptera: Arctiidae). Journal of Insect Science. 20(1): 1–7. doi: 10.1093/jisesa/ieaa001.

[20] Grande RM, Balmaceda MD, Tanena MT, Mediodia H. 2019. Larvicidal activity of individual and combined ethanolic extracts of *Annona muricata* (Soursop) seed and Piper betle (Betel) leaf against *Aedes aegypti*. Publiscience 2(1): 73–76.

[21] Koneri R, Pantororing HH. 2016. Assay of Mahogani (*Swietenia macrophylla*) seed extract on Larvae of *Aedes aegypti* as Dengue Hemorrhagic fever vector. Jurnal MKMI. 12(4): 216–233.

[22] Jawale C. 2014. Larvicidal activity of some saponin containing plants against the dengue vector *Aedes aegypti*. DAMA International. 3(1): 1–11.

[23] Adewole A, Oderinde A, Bankole O, Farapusi F, Oyede RT. 2013. Larvicidal activities of three plant extracts of common wireweed *(Sida acuta*), Catnip (*Nepeta cataria*) and Neem (*Azadirachta indica*) against the larva of mosquito (*Anopheles gambiae*). Academia Journal of Medicinal Plants, 1(2): 37–40. doi: 10.15413/ajmp.2012.0106.

[24] Khanna VG, Kannabiran K. 2007. Larvicidal effect of *Hemidesmus indicus*, *Gymnema sylvestre*, and *Eclipta prostrata* against *Culex quinquefasciatus* mosquito larvae. Afr. J. Biotechnol. 6(3): 307–311. eISSN: 1684-5315.

[25] Carigaba MA, Leonida MA, Masculino CJ, Mediodia CJ, Garbo, AG. 2020. Larvicidal activity of *Citrofortunella microcarpa* (calamansi) peel essential oil against third and early fourth instar *Aedes aegypti*. Publiscience. 3(1): 37–41.

Publiscience Vol. 4 Issue 1

Reduction of acrolein concentrations in palm cooking oil emissions through the addition of *Muntingia calabura* (aratiles) leaf extract to inhibit lipid peroxidation

AMOS NATHAN B. TUANGCO[1], FRANCINE T. TARRAZONA[1], MARIA ZYKA J. YAMOG[1], ARIS C. LARRODER[1], and JADE G. PAHILA[2]

[1]*Philippine Science High School Western Visayas Campus - Department of Science and Technology (DOST-PSHSWVC), Brgy. Bito-on, Jaro, Iloilo City 5000, Philippines*
[2]*Food Science Laboratory, Regional Research Center, University of the Philippines Visayas, Miagao, Iloilo, Philippines*

Article Info

Submitted: Apr 19, 2021
Approved: Jun 24, 2021
Published: Aug 30, 2021

Keywords:
cooking oil fumes
acrolein
natural antioxidants
induction time
oxidative stability

Abstract

Inhaling acrolein, an aldehyde present in cooking oil fumes, is detrimental to human health. Fatty acids in oils can undergo the degradation process of oxidation, which produces acrolein and other volatile aldehydes. To prevent such degradation, plant-based antioxidants could be added to the oil. This study aimed to measure and compare acrolein concentrations in emissions of palm oil with varying concentrations (w/w) of *Muntingia calabura* ethanol leaf extract. Four set-ups were subjected to volatilization and dissolution through Rancimat analysis. Volatile oxidation products from the Rancimat were analyzed for acrolein through high-performance liquid chromatography. Results showed that acrolein concentrations decreased as the concentration of the leaf extract in the oil treatment increased. Thus, the addition of *M. calabura* leaf extract to palm oil has the potential of controlling oxidation during cooking by reducing acrolein emissions; safer kinds of cooking oil could be formulated with the preference of incorporating natural antioxidants.

Introduction. - Inhaled fumes from degrading cooking oil is a major matter of concern worldwide [1,2] due to their detrimental effects on the health of people staying indoors [2,3,4], particularly in the Philippines [5]. Mitigating the effects of indoor air pollution from oil-based cooking is important as people spend more than 90% of their time indoors [6,7,8], especially during the COVID-19 pandemic [9]. Meanwhile, among the air pollutants, aldehydes and polycyclic aromatic hydrocarbons are found to be the major products of oil degradation [3] and the most harmful [10,11,12].

As cooking oil is heated beyond its threshold smoke point, fatty acids present in oil oxidize rapidly to form aldehydes and free radicals [12]. However, the smoke point of the oil is not a reliable basis of aldehyde formation, as the formation of volatile organic compounds occurs before the temperature of the oil reaches the smoke point [13]. Oxidative stability is the better indicator of oil performance [13] since it is measured in terms of the time it takes for oils to start generating volatile secondary reaction products (induction time) before the temperature reaches the smoke point [14]. In addition, the rate of production of aldehydes is inversely related to the oxidative stability [12,15] of the cooking oil and directly related to cooking temperatures [3], fatty acid content [16], and atmospheric oxygen [17]. Hence, in this study, the relationship between oxidative stability and the amount of aldehydes emitted by the treated palm cooking oil samples was investigated.

Most of the studies conducted on cooking oil have focused on the improvement of its oxidative stability [15,18], but there has been none in reducing the harmful constituents found in cooking oil fumes. In relation to aldehyde formation, studies have postulated a possible association between the addition of natural antioxidants to cooking oil and the amount of aldehydes released by cooking oil when heated [12,18]. This is because the production of aldehydes can be inhibited through the use of antioxidants by bonding towards the singlet oxygen in the reaction intermediate as fatty acids degrade, as established by the same studies. The cooking oil emissions will be analyzed for acrolein, the simplest unsaturated aldehyde and the most abundantly produced by palm oil and soybean oil [12]. With this, it is necessary to examine the correlation between the addition of natural antioxidants and acrolein emissions.

Among various methods to inhibit oxidation, the use of antioxidants is most effective, convenient, and economical [19]. Between the natural and the synthetic antioxidants, the former are safer for

How to cite this article:
CSE: Tuangco ANB, Tarrazona FT, Yamog MZJ, Larroder AC, Pahila JG. 2021. Reduction of acrolein concentrations in palm cooking oil emissions through the addition of *Muntingia calabura* (aratiles) leaf extract to inhibit lipid peroxidation. Publiscience. 4(1): 20–25.
APA: Tuangco, A.N.B., Tarrazona, F.T., Yamog, M.Z.J., Larroder, A.C., & Pahila J.G. (2021). Reduction of acrolein concentrations in palm cooking oil emissions through the addition of *Muntingia calabura* (aratiles) leaf extract to inhibit lipid peroxidation. *Publiscience*, *4*(1), 20–25.

For supplementary data, contact: publiscience@wvc.pshs.edu.ph.

consumption due to toxicity problems associated with synthetic antioxidants [20]. Several studies investigated the effects of incorporating plant-based extracts, such as that from *Eucalyptus globulus* leaves, *Cinnamomum zeylanicum* bark, and *Sesamum indicum* coat, on the oxidative stability of cooking oil, resulting in longer induction times [15,18,20]. *Muntingia calabura* (aratiles) is one of the top five Philippine fruits to contain high antioxidant activity alongside *Diospyros blancoi* (velvet apple), *Tamarindus indica* (tamarind), *Sandoricum koetjape* (lolly fruit), and *Annona squamosa* (sugar apple) [22,23], making its extract a highly suitable additive, especially its leaves where the highest antioxidative activity can be found [24]. It is hypothesized that if *M. calabura* leaf extract is added to palm cooking oil (PCO), then its acrolein emissions will be reduced as an effect of the increase in its oxidative stability.

To address the issue of aldehyde emissions, this study aimed to measure and compare the acrolein concentrations in cooking oil fumes from palm oil with varying percent mass of *M. calabura* leaf extract. This study specifically aimed to:

(i) Determine the radical scavenging activity (RSA) and total phenolic content (TPC) of the *M. calabura* leaf extract through 2,2-diphenyl-1-picrylhydrazyl (DPPH) UV-visible radical scavenging assay;

(ii) Measure the induction time and antioxidative activity index (AAI) of the set-ups through Rancimat analysis;

(iii) Quantify the aldehyde concentrations derived from the fumes of the set-ups through high-performance liquid chromatography (HPLC);

(iv) Determine if there are significant differences among the induction times of the set-ups; and

(v) Determine if there are significant differences among the aldehyde concentrations from the fumes of the set-ups.

Methods. - The methods of this experimental study are composed of: (1) leaf harvesting and extraction, (2) DPPH assay, (3) treatment of oil samples, (4) Rancimat analysis, and (5) HPLC analysis. Four set-ups were prepared, with one set-up as the negative control and the other three as treatments.

Leaf Harvesting and Extraction. *M. calabura* leaves were washed and air-dried for one day, processed into smaller chunks, then transferred into a reagent bottle with 99% ethanol, following a 1:20 leaf to solvent ratio (w/v). The bottles were stored in a cool area for five days. Subsequently, the solution underwent vacuum filtration and rotary evaporation (60 °C heating bath temperature, 90 rpm, 5 hours). Lastly, the solution was reconstituted and air-dried in an exhaust for 3 days.

DPPH Assay. The RSA and TPC of the *M. calabura* leaf extracts were calculated through DPPH radical scavenging assay. Gallic acid was used as a standard to calculate the TPC. An extract-ethanol solution series (40, 80, 120, 160, 200 ppm) and a gallic acid solution (40 ppm) were prepared. Four milliliters (4 mL) of 0.1 mM DPPH-ethanol solution was added to 1 mL of each solution. All solutions were wrapped with aluminum foil and stored for 30 minutes in a cool dark area before the analysis. Absorbance values of the extracts and gallic acid were measured at a wavelength of 508.40 nm using a UV-vis spectrophotometer (Shimadzu UV-1800).

Treatment of Oil Samples. Four set-ups consisting of PCO samples with 0, 0.1%, 0.3%, and 0.5% mass of *M. calabura* leaf extract were prepared to achieve a total of 25 g. The maximum treatment concentration of 0.5% was based on the study of Mohamed et al. [25], which considered the limitations in the amount of additives safe for consumption. Oil samples were agitated for 5 minutes in an up-and-down motion before the analysis.

Rancimat Analysis. The Rancimat (Metrohm 892 Professional Rancimat) was set to a temperature of 150 °C and heated until it was stable to prevent temperature fluctuation. The gas flow of oxygen was set at the default setting of 20.0 L/hr while 60 mL of pure water (Merck, Elix Type II) was poured into each measuring vessel. The reaction vessels containing 3 g of the samples were heated in their respective heating blocks until the last sample had reached the stop criteria of 400 µS/cm conductivity. After 5 hours of heating, the resulting water samples were collected for further analysis of aldehydes. A total of 4 replicates were performed.

HPLC Analysis. Acrolein concentrations in the samples obtained from Rancimat analysis were determined through HPLC analysis (Shimadzu Prominence LC-20A UFLC Stack HPLC System), equipped with a UV-vis detector and a C8 150 x 4.6 mm 5µm column kept at 25 °C in the column oven. The analysis was carried out using an isocratic mode of elution using vacuum filtered distilled water as a mobile phase at a 2.0 mL/min flow rate. HPLC-grade acrolein (CPI International) standard solution (3, 6, 9, 12, and 15 ppm) was used to establish the calibration curve for quantification. The filtered (0.45 µm) samples were individually kept in a glass vial filled up to 2 mL volume, while 20 µL aliquots per sample were collected by the autosampler for analysis. A total of 4 replicates for each treatment were performed.

Computation of Parameters. The absorbance values obtained from the UV-vis spectrophotometer were used to calculate the RSA of the extract and gallic acid using Equation 1.

$$(1) \quad \%\ Inhibition = \frac{\lambda_{blank} - \lambda_{sample}}{\lambda_{blank}} \times 100\%$$

where λ_{blank} is the wavelength of the DPPH solution at maximum absorbance, and λ_{sample} is the wavelength of the DPPH-extract solution.

The TPC of the extract was calculated from the RSA of both gallic acid and the extract as shown in Equation 2.

$$(2) \quad TPC\ (\text{mg GAE/g}) = \frac{R_E \times 100}{R_G \times M_E}$$

where R_E is the RSA of the extract, R_G is the RSA of gallic acid, and M_E is the mass of extract used to calculate R_E.

Lastly, the AAI of the extract was calculated using Equation 3 [14].

$$(3)\quad AAI = \frac{I_{treatment}}{I_{control}}$$

where $I_{treatment}$ is the induction time of the treatment group and $I_{control}$ is the induction time of the control group.

Data Analysis. One-way analysis of variance (ANOVA) at α=0.05 was performed to determine if a significant difference exists between the percent mass extract in oil and the induction time among the four set-ups, as well as between the percent mass extract in oil and the acrolein concentration in its emissions. Pairwise comparisons using t-tests were then conducted to calculate the *p*-values between set-ups. All statistical analyses were performed using R software (RStudio®, v1.2.5033).

Safety Procedure. The samples and solutions were prepared under a fume hood. Personal protective equipment was worn at all times whenever handling reagents, samples, glassware, and equipment. Adherence to the respective safety data sheet of the chemicals was also observed. The use of equipment was done with proper protocol and training. Chemical and biological waste were placed in their respective waste containers to prevent further chemical reactions.

Results and Discussion. - After the DPPH assay was performed, the RSA was calculated, followed by the TPC. Through Rancimat analysis, the induction times of the samples were measured, and the AAI was determined. The water samples used from the Rancimat analysis were then analyzed for acrolein using the HPLC.

RSA and TPC. The RSA and TPC of the extracts were calculated based on the absorbance values obtained through UV-vis spectrophotometry. The RSA of extracts from *M. calabura* at different concentrations is shown in Table 1.

Table 1. Summary of radical scavenging activity (RSA), and total phenolic content (TPC) of increasing concentrations of leaf extract to DPPH solution. Data used to calculate for RSA and TPC are expressed in average by the UV-vis spectrophotometer.

Concentration (ppm)	RSA (%)	TPC (mg GAE/g)
40-Gallic Acid	94.24	N/A
40	54.59	57.92
80	56.63	60.09
120	60.47	64.16
160	63.47	67.35
200	66.59	69.38

RSA determines how likely the antioxidants present in *M. calabura* prevent the release of free radicals. DPPH is a purple-colored solution that gradually changes to a yellowish solution depending on the presence of antioxidants or antioxidative activity [25]. The absorbance of the gallic acid-DPPH aliquot at 40 ppm was measured to obtain the TPC in terms of mg GAE/g. In DPPH assays with gallic acid as the standard, a TPC value greater than 10 mg GAE/g is considered to have a high antioxidative capability [27]. *M. calabura* leaves are abundant in flavones, isoflavones, and polyphenols, which explain the high values for the TPC [28].

Induction time and AAI. The induction times of the samples were obtained through Rancimat analysis, while the AAI values of the samples were calculated based on the induction times. The induction time of cooking oil is one way to determine oxidative stability. The longer the induction time, the more stable the cooking oil is. The time indicates when the oil starts to break down at a certain temperature, in this case at 150 °C. The AAI explains the relative antioxidative activity between the control and the treated samples; the higher the index, the higher the antioxidant activity of the oil compared to the other [14].

Among the four set-ups, the set-up with 0.5% mass of extract shows the highest induction time and antioxidative index. Both induction time and AAI increased as the percent mass of extract added to PCO increased (0<0.1%<0.3%<0.5%). Meanwhile, the acrolein concentration decreased (0.5%<0.3%<0.1%<0) as shown in Table 2.

Table 2. Summary of mean values for induction time (IT), antioxidative activity index (AAI), and acrolein concentration (AC) of palm cooking oil with increasing percent mass of leaf extract. Data are expressed in terms of mean ± standard deviation (n = 4).

Extract (% Mass)	IT (h)	AAI	AC (ppm)
0	2.30 ± 0.20	1.00 ± 0.00	9.747 ± 0.67
0.1	2.51 ± 0.05	1.10 ± 0.09	8.120 ± 0.22
0.3	2.66 ± 0.06	1.16 ± 0.10	6.914 ± 0.48
0.5	2.78 ± 0.08	1.22 ± 0.08	5.262 ± 0.99

Each treatment group is significantly different (p<0.05) from the control group, which indicates that there is an increase in the oxidative stability of PCO as the mass percent composition of *M. calabura* leaf extract is increased. However, no significant difference (p>0.05) can be found from the pairwise comparisons of the 0.1% and 0.3% set-ups, and the 0.3% and 0.5% set-ups, as reflected in Figure 3.

Acrolein concentrations. To quantify the acrolein concentrations, HPLC analysis was performed on the water samples used for the Rancimat analysis. The acrolein concentrations from cooking oil fumes were observed to decrease as the concentration of extract is increased, as indicated in Table 2. Each pair of set-ups was also significantly different (p<0.05) from one another, as shown by Figure 3. Furthermore, an increase in the percent mass of extract by increments of 0.2% significantly decreased the acrolein

concentrations in the fumes of the oil, unlike the results obtained for induction time.

The approach of analyzing acrolein in PCO fumes through the use of the Rancimat is a novel method that utilizes the concept of polarity and solubility. The volatile oxidation products generated due to the lipid oxidation are directed by the air stream to the Rancimat vessels containing pure water [29]. Since acrolein and water are both polar, acrolein dissolves in water.

Fullana et al. [30] have investigated the level of aldehydes emitted at different times at 180 °C and 240 °C but were unable to analyze acrolein. Aside from their study, no studies have analyzed the aldehyde concentrations in fumes in cooking oil with antioxidant additives but such analysis was recommended [12,18].

The results of Endo et al. [31] show that acrolein in cooking oil is not formed from glycerol backbones in triacylglycerol but from methyl linolenate and methyl linoleate derived from polyunsaturated fatty acids, such as α-linolenic and linoleic acids, produced at high levels during heating. Thus, cooking with vegetable oils at high temperatures is not advisable as it induces the formation of acrolein. Furthermore, Da Silva and Pereira [12] formulated a reaction mechanism on how unsaturated fatty acids degrade to acrolein which provides several unstable singlet oxygens in intermediate reactions accompanied by the production of free radicals along the way. In the nucleophilic attack, antioxidants bind to singlet oxygen molecules to prevent the reduction of carboxylic acids to aldehydes. These antioxidants also bind to the free radicals produced due to oxidation, as shown in Figure 2 [12].

Comparing the values, it can be inferred that the induction time of oil is directly proportional to the antioxidant activity of the oil and inversely proportional to its acrolein emissions. This confirms the proposed association between the amount of natural antioxidants and the aldehyde emissions of the oil [12,18].

The basis for the oxidative stability of cooking oil majorly depends on its polyunsaturated fatty acid composition [32]. Hence, aside from the addition of antioxidants in cooking oil, the mixing of polyunsaturated fatty acid-rich oil with monounsaturated fatty acid-rich oil can be done to increase its oxidative stability [33]. The fatty acid composition of the oil is also the basis in determining the nature of volatile aldehyde formation [30,33]. The four parameters, namely fatty acid composition, antioxidant concentration, induction time, and volatile aldehyde concentration, are likely interrelated and can be the subject of further studies.

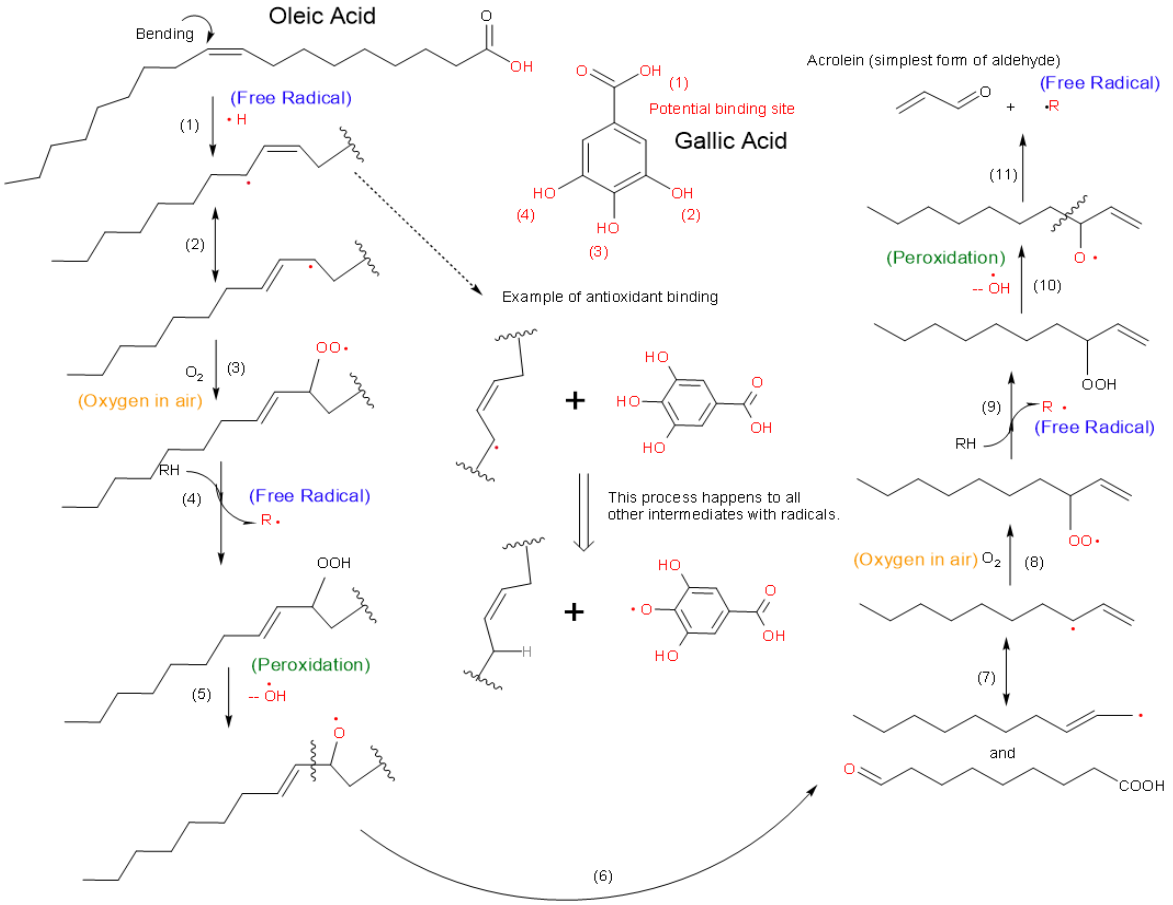

Figure 2. Reaction mechanism of the degradation of oleic acid—a monounsaturated fatty acid in palm cooking oil—into acrolein and the interaction of an antioxidant, gallic acid, in the prevention of such reaction [12].

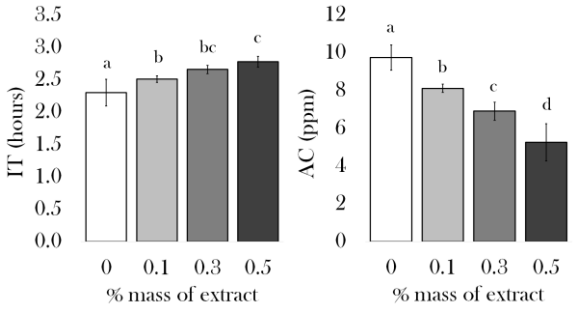

Figure 3. Induction time (IT) and acrolein concentrations (AC) in the fumes of palm cooking oil with varying % mass of *M. calabura* ethanol leaf extract. Data are presented as mean ± standard deviation (n=4). Values with different superscript letters represent significant differences among set-ups (p<0.05).

Limitations. The results of this study partially support the claims in the literature that the addition of antioxidants contributes to the reduction of aldehydes present in cooking oil fumes. However, the researchers were not able to identify specific antioxidants present in the extract. Second, the extract was not freeze-dried to maximize solubility in PCO. Third, the cooking oil used was already incorporated with butylated hydroxytoluene, a synthetic antioxidant. Fourth, other aldehydes aside from acrolein were not analyzed.

Conclusion. - Antioxidant capacity to reduce aldehyde emissions of palm cooking oil was investigated. Before treatment of the oil, it has been verified that *M. calabura* leaves contain high antioxidative activity, total phenolic content, and antioxidative activity index. Induction times of the treated oil samples increased, implying that oxidative stability increased. Hence, the addition of natural antioxidants, specifically *M. calabura* leaf extract, to palm cooking oil increases oxidative stability of the oil and reduces the aldehyde concentrations in palm cooking oil fumes. Significant differences were observed between the induction times of all pairs of set-ups except for the 0.1% and 0.3% pair and the 0.3% and 0.5% pair. Meanwhile, significant differences were observed between the acrolein concentrations of all pairs of set-ups (0 & 0.1%, 0 & 0.3%, 0 & 0.5%, 0.1% & 0.3%, 0.1% & 0.5%, and 0.3% & 0.5%). Lastly, this study can serve as a basis for the establishment of the correlation between the addition of antioxidants in cooking oil and its emission of aldehydes as fumes.

Recommendations. - It is recommended that similar studies are done with the use of gas chromatography-mass spectrometry which is more suited for volatile analytes. Other cooking oils, aldehydes, and sources of natural antioxidants should also be analyzed to compare the power and versatility of the natural antioxidants. Another recommendation is to test the treatments at varying higher temperatures and heating duration. Sensory analysis of the treated oil is also encouraged. Moreover, it is recommended to analyze the fatty acid composition and aldehyde concentrations of oil subjected to high heating temperatures to determine if the results are consistent with the aldehyde emissions. Lastly, antioxidant profiling and the determination of antioxidant binding ability with acrolein could be performed.

Acknowledgment. - The authors would like to extend their gratitude to the Department of Environment and Natural Resources (Region VI) for verifying the species of the plant samples used in the study. Their gratitude is also extended to the Food Science Laboratory of the University of the Philippines Visayas - Regional Research Center for allowing them to perform the Rancimat analysis.

References

[1] Harrison MR, Hester RE, editors. 2019. Indoor air pollution. [Internet]. The Royal Society of Chemistry; [cited 2020 Jan 27]. Available from: https://rsc.li/2lYHDjH.

[2] Chen HC, Wu CF, Chong IW, Wu MT. 2018. Exposure to cooking oil fumes and chronic bronchitis in nonsmoking women aged 40 years and over: a health-care based study. BMC Public Health. 18(246): 1–11. doi: 10.1186/s12889-018-5146-x.

[3] Katragadda HR, Fullana A, Sidhu S, Carbonell-Barrachina AA. 2010. Emissions of volatile aldehydes from heated cooking oils. Food Chem. 120: 59–65. doi: 10.1016/j.foodchem.2009.09.070.

[4] Neghab M, Delikhoon M, Baghani AN, Hassanzadeh J. 2017. Exposure to cooking fumes and acute reversible decrement in lung capacity. Int J Occup Env Med. 8(4):207–216. doi: 10.15171/ijoem.2017.1100.

[5] WHO (World Health Organization). 2018. [Cited 9 September 2019]. Available from https://bit.ly/3ekZASi.

[6] EPA (Environmental Protection Agency). 2019. [Cited 27 January 2020]. Available from https://bit.ly/2SrEuZT.

[7] Rivas I, Fussell J, Kelly F, Querol X. 2019. Indoor Sources of Air Pollutants. Issues Environ Sci Technol. 48: 1–15. doi: 10.1039/9781788016179-00001.

[8] Tham KW. 2016. Indoor air quality and its effects on humans — A review of challenges and developments in the last 30 years. Energy Buildings. 130: 637–650. doi: 10.1016/j.enbuild.2016.08.071.

[9] Haddad M. c2020. Coronavirus: How much more time are people spending at home? [Internet]. Aljazeera Media Network. [cited 2020 December 9]. Available from: https://bit.ly/3h6LHcb.

[10] Ghobadi S, Akhlaghi M, Shams S, Mazloomi SM. 2018. Acid and peroxide values and total polar compounds of frying oils in fast food restaurants of Shiraz, Southern Iran. Int J Nutr Sci. 3(1): 25–30.

[11] Lu F, Shen B, Yuan P, Li S, Sun Y, Mei X. 2019. The emission of PM2.5 in the respiratory zone from Chinese family cooking and its health effects.

Sci Total Env. 654: 671–677. doi: 10.1016/j.scitotenv.2018.10.397.

[12] Da Silva TO, Pereira PA. 2008. Influence of time, surface-to-volume ratio, and heating process (continuous or intermittent) on the emission rates of selected carbonyl compounds during thermal oxidation of palm and soybean oils. J Agric Food Chem. 56(9): 3129–3135. Doi: 10.1021/jf0734525.

[13] Guillaume C, De Alzaa F, Ravetti L. 2018. Evaluation of chemical and physical changes in different commercial oils during heating. Acta Scientific Nutritional Health. 2: 2–11.

[14] Metrohm. 2012. Oxidation stability of oils and fats – Rancimat method. Available from: https://bit.ly/3eYtMBU.

[15] Ali S, Chatha SAS, Ali Q, Hussain AI, Hussain SM, Perveen R. 2016. Oxidative stability of cooking oil blend stabilized with leaf extract of *Eucalyptus citriodora*. Int J Food Prop. 19(7): 1556–1565. doi: 10.1080/10942912.2015.1047514.

[16] Chowdhury K, Banu L, Khan S, Latif A. 2008. Studies on the fatty acid composition of edible oil. Bangladesh J Sci Ind Res. 42(3): 311–316. doi: 10.3329/bjsir.v42i3.669.

[17] Fujisaki M, Endo Y, Fujimoto K. 2002. Retardation of volatile aldehyde formation in the exhaust of frying oil by heating under low oxygen atmospheres. J Amer Oil Chem Soc. 79(9): 909–914. doi: 10.1007/s11746-002-0578-3.

[18] Shahid MZ, Saima H, Yasmin A, Nadeem MT, Imran M, Afzaal M. 2018. Antioxidant capacity of cinnamon extract for palm oil stability. Lipids Health Dis. 17(1): 1–8. doi: 10.1186/s12944-018-0756-y.

[19] Shahidi F, Zhong Y. 2010. Lipid oxidation and improving the oxidative stability. Chem Soc Rev. 39(11): 4067–4079. doi: 10.1039/B922183M.

[20] Taghvaei M, Jafari SM. 2015. Application and stability of natural antioxidants in edible oils in order to substitute synthetic additives. J Food Sci Technol. 52(3): 1272-1282. doi: 10.1007/s13197-013-1080-1.

[21] El-Roby AM, Hammad KSM, Galal SM. 2020. Enhancing oxidative stability of sunflower oil with sesame (*Sesamum indicum*) coat ultrasonic extract rich in polyphenols. J Food Process Preserv. e14564. doi: 10.1111/jfpp.14564.

[22] Recuenco MC, Lacsamana MS, Hurtada WA, Sabularse VC. 2016. Total phenolic and total flavonoid contents of selected fruits in the Philippines. Phil Journal Sci. 145(3): 275–281. doi: 10.1100/2012/728613.

[23] Singh A, Gupta R, Pandey R. 2017. Exogenous application of rutin and gallic acid regulate antioxidants and alleviate reactive oxygen generation in *Oryza sativa L*. Physiol Mol Biol Plants. 23(2): 301–309. doi: 10.1007/s12298-017-0430-2.

[24] Y MAK, Mundasada SC, Ramadas D. 2015. Antioxidative activity: root, leaves and fruits aqueous extracts of *Muntingia calabura*. JIPBS. 2(4): 363–368.

[25] Mohamed S, Mohd NF, inventors; University Putra Malaysia, Selangor, assignee. 2013. Cooking oil composition with additives to reduce oil adsorption. United States Patent Application No. 8.425,969 B2.

[26] Kedare SB, Singh RP. 2011. Genesis and development of DPPH method of antioxidant assay. J Food Sci Technol. 48(4): 412–422. doi: 10.1007/s13197-011-0251-1.

[27] Mahmood ND, Nasir NLM, Rofiee MS, Tohid SFM, Ching SM, Teh LK, Salleh MZ, Zakaria ZA. 2014. *Muntingia calabura*: a review of its traditional uses, chemical properties, and pharmacological observations. Pharm Biol. 52(12): 1598–1623. doi: 10.3109/13880209.2014.908397.

[28] Haerani A, Chaerunisa AY, Subarnas A. 2019. Antioxidant Activities of *Muntingia calabura*, *Syzygium cumini*, *Ocimum basilicum*, and *Eleutherine bulbosa* using DPPH Method. Indonesian Journal of Pharmaceutics. 1(2): 50–54. doi: 10.24198/idjp.v1i2.21531.

[29] Tinello F. Lante A, Bernardi M, Cappiello F, Galgano F, Caruso MC, Favati F. 2018. Comparison of OXITEST and RANCIMAT methods to evaluate the oxidative stability in frying oils. Eur Food Res Technol. 244(4): 747–755. doi: 10.1007/s00217-017-2995-y.

[30] Fullana A, Carbonell-Barrachina AA, Sidhu S. 2004. Comparison of volatile aldehydes present in the cooking fumes of extra virgin olive, olive, and canola oils. J Agric Food Chem. 52(16): 5207–5214. doi: 10.1021/jf035241f.

[31] Endo Y, Hayashi C, Yamanaka, T, Takayose K, Yamaoka M, Tsuno T, Nakajima S. 2013. Linolenic acid as the main source of acrolein formed during heating of vegetable oils. Journal of the American Oil Chemists' Society. 90(7): 959–964. doi: 10.1007/s11746-013-2242-z.

[32] Bhatnagar AS, Prasanth Kumar PK, Hemavathy J, Gopala Krishna AG. 2009. Fatty acid composition, oxidative stability, and radical scavenging activity of vegetable oil blends with coconut oil. J Am Oil Chem Soc. 86(10): 991–999. doi: 10.1007/s11746-009-1435-y.

[33] Maszewska M, Florowska A, Dłużewska E, Wroniak M, Marciniak-Lukasiak K, Zbikowska A. 2018. Oxidative stability of selected edible oils. Molecules. 23(1746): 1–12. doi: 10.3390/molecules23071746.

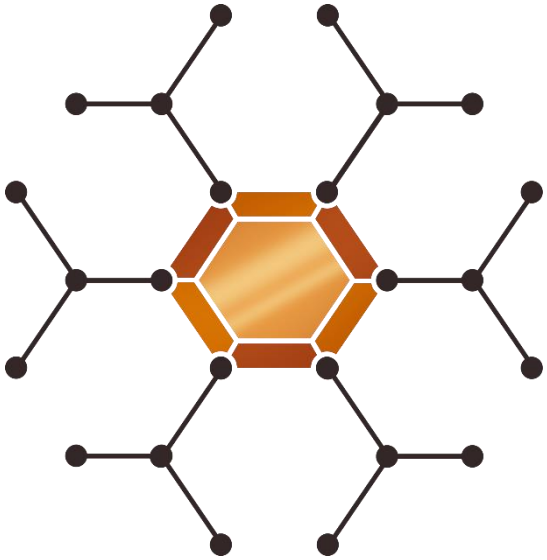

CLUSTER TWO

MATERIAL SCIENCE AND TECHNOLOGY

The connected structure surrounding the gemstone represents the promising applications--similar to the potential of graphene--of using existing material, then designing and discovering new compositions and structures, physically and chemically. Meanwhile, the orange color is representative of attraction. In this case, attraction may be used to represent the chemical bonds that can be referred down to the molecular level.

These studies fall under the Industry, Energy, and Emerging Technology (IEET) Research Development Agenda and its aims of developing competitive industries and increased focus on research in order to maximize usage of existing resources.

BASED ON: Harmonized National Research and Development Agenda (HNRDA)

Comparison in yield of the microwave-assisted method and conventional method in *Zea mays* var. *ceratina* (glutinous corn) cobs cellulose fiber extraction

CAROLYN GRACE C. SACATE, HENDRIK LORENZ B. ALABATA, JASON SANTINO T. ADVINCULA, and XAVIER ROMY O. BRAÑA

Philippine Science High School Western Visayas Campus - Department of Science and Technology (DOST-PSHSWVC), Brgy. Bito-on, Jaro, Iloilo City 5000, Philippines

Article Info

Submitted: May 07, 2021
Approved: Jul 13, 2021
Published: Aug 30, 2021

Keywords:
microwave-assisted
extraction
cellulose
yield
Zea mays var. *ceratina*

Abstract

Cellulose is a biopolymer that is abundant in nature, often extracted from raw materials via the conventional method. However, a new method of fiber extraction called the microwave-assisted method is said to be cost and energy-efficient. In this study, cellulose fibers were extracted from *Zea mays* var. *ceratina* cobs via microwave-assisted method (MAM) and conventional method (CM), wherein the yield means of the two methods were determined and statistically compared. *Z. mays* cob powder was subjected to 8% (w/v) NaOH for the alkalization process, 5% (w/w) H_2O_2 for the acid hydrolysis, and heated using a microwave oven and hot plate for MAM and CM, respectively. The results showed that the MAM and CM yielded 72.7% and 44.6% cellulose fibers, respectively. Statistical analysis via Mann-Whitney U test showed that there is an observed trend towards MAM yielding a higher percentage of crude cellulose in contrast to CM.

Introduction. - Cellulose is a biopolymer that is abundant in nature, renewable, and biodegradable, making it a potential industrial material [1]. Synthesized cellulose fibers are utilized in various applications such as in textiles, paper, packaging, building materials, and synthetic fibers [2].

For the past several years, climate change and the additional problems involving agricultural waste urge industries to utilize natural sources instead of synthetic materials. According to Zafar [3], the Philippines is an agricultural country that consists of a land area 30 million hectares wide, wherein 47% of which is utilized in the agricultural sector. Due to this, agricultural residues are also abundant which are common sources of renewable materials and most of them are considered as waste materials. Cobs are by-products derived from *Zea mays*, more commonly known as corn plants. In 2020, the Philippine corn production was about 8.12 million metric tons [4]. Subsequently, the corn cob waste by-product had an estimated technical volume of about 1.95 million metric tons, with most of it being discarded or burnt [5]. This resulted in environmental damages such as global warming due to greenhouse gas emissions (e.g. carbon dioxide, methane) [6,7]. Corn cobs, however, have the potential to become a cheap and abundant raw material for cellulose extraction, as corn cobs are primarily composed of cellulose, hemicellulose, and lignin [2]. The cobs typically have a cellulose fiber content of around 40–44% [8].

Cellulose extraction is the process of isolating cellulose from raw materials or natural fibers. It generally involves the use of alkalis or bisulphites for the treatment of the fibers to isolate lignin and obtain the hemicellulose. There are three primary methods used in extracting cellulose: alkaline treatment, bleaching, and acid hydrolysis [9]. Moreover, cellulose can be extracted using different kinds of methods such as the conventional and microwave-assisted. Every procedure has different pros and cons associated with the yield and properties of the cellulose [10].

The conventional method typically involves the use of instruments that heat the walls of reactants through conduction or convection [11]. Most studies use the conventional method for extracting cellulose fiber because it is simple, effective, and has a high fiber yield [12,13]. However, the process is often slow since it requires high external temperatures to generate the required heat. Furthermore, the rate of the heat flow into the body of the material from the surface limits the process time. Moreover, the heat is also uneven since some parts such as the surface, edges, and corners tend to be hotter in contrast to the interior of the material [11].

Contrasting this, a new method of fiber extraction, called the microwave-assisted method, reportedly yields analytes with higher purity compared to the conventional method [11].

How to cite this article:
CSE: Sacate CGC, Alabata HLB, Advincula JST, Braña XRO. 2021. Comparison in yield of the microwave-assisted method and conventional method in *Zea mays* var. *ceratina* (glutinous corn) cob cellulose fiber extraction. Publiscience. 4(1): 27–31.
APA: Sacate C.G.C, Alabata H.L.B., Advincula J.S.T, & Braña X.R.O. (2021). Comparison in yield of the microwave-assisted method and conventional method in *Zea mays* var. *ceratina* (glutinous corn) cob cellulose fiber extraction. *Publiscience*, *4*(1), 27–31.

For supplementary data, contact: publiscience@wvc.pshs.edu.ph.

Microwave heating is an alternative method in extracting bio-based materials due to its capability to accelerate chemical processes. As compared to the conventional method, microwave-assisted method is more rapid and volumetric due to the direct interaction between the material subjected and the heat generated by the applied electromagnetic field. Additionally, it is highly selective, uniform, and utilizes less amount of energy for the pretreatment of bioproducts [2].

With the above information in mind, cellulose from glutinous corn cobs was extracted using the microwave-assisted and conventional methods. The resulting yield obtained from both methods were compared and analyzed using Mann-Whitney U test to determine if a significant difference exists in terms of yield. Microwave-assisted mechanism can be implemented in the production of cellulose obtained from corn cobs, specifically *Zea mays* var. *ceratina,* to address problems such as expensive cost and longer duration of the extraction process, as well as the lack of investigation regarding the comparison of yields between the microwave-assisted and conventional methods.

This research aimed to compare the yields of the microwave-assisted method and conventional method in extracting cellulose fibers from *Zea mays* var. *ceratina* cobs. Specifically, it aimed to:

(i) measure the percent yield of the extracted cellulose fibers from corn (*Z. mays* var. *ceratina*) cobs via microwave-assisted chemical extraction method;

(ii) measure the percent yield of the extracted cellulose fibers from corn (*Z. mays* var. *ceratina*) cobs via conventional method;

(iii) determine a significant difference among yield means of crude cellulose extracted via microwave-assisted and conventional methods, respectively, using Mann-Whitney U test, and;

(iv) qualitatively assess the presence of cellulose in the extracted analytes through the development of a purplish hue upon addition of the Schultze's reagent.

Methods. - This study is descriptive in nature. *Z. mays* cobs cellulose fibers were extracted using two extraction methods: microwave-assisted method (MAM) and conventional method (CM). Cellulose fiber extraction is mainly composed of two main processes: alkalization and acid hydrolysis. Ground corn cob powder was subjected to alkalization using sodium hydroxide (NaOH), then followed by acid hydrolysis using hydrogen peroxide (H_2O_2). Three replicates per setup were extracted and percentage yield means were calculated. Extraction processes were then followed by the determination of whether the analyte contains cellulose or not using Schultze's reagent. A purplish color upon contact would then signify the presence of cellulose. In determining whether the percentage yield means are significantly different from each other, the non-parametric statistical analysis tool Mann-Whitney U test was used.

Zea mays Cobs Acquisition, Authentication and Storage. Glutinous corn cobs (*Z. mays* var. *ceratina*) were purchased and collected from a local corn vendor located in Q. Abeto St., Mandurriao, Iloilo City. Corn variety was authenticated by the Department of Agriculture - Iloilo Research Outreach in Sta. Barbara, Iloilo, to which an official certification was issued.

Acquired corn cobs were washed prior to sun-drying. This is to ensure the safety of the researchers and the residents of the household wherein the study was conducted in. The obtained corn cobs were sundried outdoors for 48 hours to remove moisture. The cobs were also turned every six (6) hours to ensure that every part was evenly dried. The corn cobs were stored in an airtight container and kept in a place away from direct sunlight at room temperature to prevent dry matter loss during nighttimes, prior to usage [14].

Zea mays Cob Preparation. Corn cobs were pulverized into fine powder using a blender (Moulinex Turbo Blender). The powder was then sieved using a fine mesh sieve (pore size: 841 µm). Larger particles were reground using a mortar and pestle to enable passage through the sieve. The powder used for all treatments was a mixture of all grounded cobs. Powdered samples were dried in an oven (La Germania SL6031-21) at 135 °C until a constant weight was achieved. Constant weight was determined through the continuous drying and hourly weighing of samples until two consecutive weighings did not differ by more than 0.5 mg per gram of the sample initially taken [15]. Prior to the hourly weighing of heated samples, samples were cooled to room temperature. Ten (10) grams of *Zea mays* var. *ceratina* powder from each replicate were then placed inside airtight containers. They were then stored at room temperature until further use.

Cellulose Extraction via Microwave-assisted Method. Microwave heating was conducted in a 2450 MHz microwave oven (Hanabishi HMO-17M-3), wherein the power per microwave-assisted heating was set to 500W, three (3) minutes per replicate [2,16].

The corn cob powder samples underwent alkalization using NaOH as the alkaline treatment, wherein ten (10) grams of the corn cob powder was added into 150 mL 4% (w/v) NaOH, then subjected to microwave heating with the specified settings. The acquired corn cob pulp was washed with distilled water until neutral pH (around 6.5–8) was acquired, measured using pH test strips [16,17]. After the alkalization process, acid hydrolysis was performed. Here, the alkalized corn pulp was bleached in 50 mL 5% (w/w) H_2O_2 solution. The pulp was then subjected to microwave heating following the same settings stated above. Extracted cellulose fibers were then rewashed until neutral pH was acquired. To rid the analyte of water, it was dried using the oven until a constant weight was achieved [2,18]. Three (3) replicates were used in this step.

Cellulose Extraction via Conventional Method. Corn cob powder was subjected to alkalization then

heated using a hot plate equipped with a temperature reader (Biobase MS7-NS50-Pro), wherein the beaker with the alkaline treatment was placed on the hot plate set at 100 °C for four (4) hours with constant stirring. After washing until neutral pH was acquired, the pulp was then submerged and hydrolyzed in the H_2O_2 solution. Extracted cellulose fibers were then subjected once more to washing until neutral pH was acquired. To rid the analyte of water, the analyte was dried using the oven until a constant weight was achieved [18]. Three (3) replicates were used in this step.

Qualitative Determination of Presence of Cellulose using Schultze's Reagent. Extracted cellulose fibers were assessed qualitatively using Schultze's reagent to determine the presence of cellulose in the extracted analyte. In preparing the reagent, twenty (20) grams of zinc chloride ($ZnCl_2$) was dissolved in 9.5 mL warm distilled water then cooled. On a separate beaker, 0.5 g iodine and 1 g potassium iodide were dissolved in 20 mL deionized water, wherein 1.5 mL of this solution was added to the zinc chloride solution until a persistent precipitate of iodine formed. Direct contact of the Schultze's reagent to cellulose fibers would yield a purplish color [19,20].

Computation of Percentage Yield. In the computation of percentage yield, the following formula was used:

$$\%yield = \frac{acquired\ dry\ mass\ of\ cellulose\ fibers\ (g)}{dry\ mass\ of\ raw\ material\ used\ (g)} \times 100$$

The mean percent cellulose fiber yields were then calculated. The calculated mean—one for each method—served as the overall percentage of cellulose fiber yield.

Data Analysis. Mann-Whitney U test was utilized in determining whether the percentage yield means are significantly different from each other, wherein in this process, the equation function of Microsoft® Excel® for Microsoft 365 MSO (16.0.13929.20360) 64-bit. The data would be then deemed significantly different if $p<0.05$ [21].

Safety Procedure. A Materials Safety Data Sheet (MSDS) was secured and provided beforehand wherein hazards regarding the conduct of this study were determined. Mitigation of these hazards were subsequently observed and implemented. Laboratory protective gear consisting of laboratory gowns, gloves, and masks were worn at all times during the conduct of the study.

Results and Discussion. - Crude cellulose fibers were extracted from *Zea mays* var. *ceratina* cobs via MAM and CM. Schultze's agent was then added to the extracted analyte to determine the presence of cellulose. The resulting purple hue signified that the extracted analyte contains cellulose. This is shown in Figure 1. However, a greenish hue was also observed, signifying the presence of non-cellulosic material such as lignin.

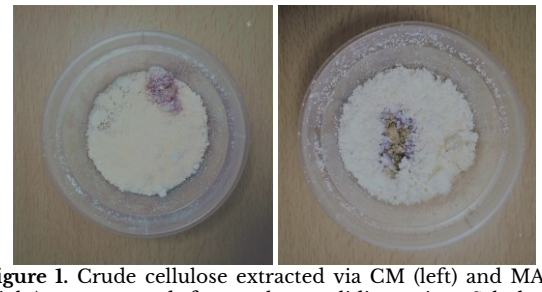

Figure 1. Crude cellulose extracted via CM (left) and MAM (right) were tested for analyte validity using Schultze's reagent, to which the purplish color indicated the presence of cellulose.

Furthermore, the crude cellulose extracted via MAM are higher in contrast to the ones extracted via CM, as shown in Table 1. Additionally, replicate yields and means per setup along with their respective standard deviations are presented in Figure 2.

Table 1. The table below shows the percentage yield means and medians per setup.

Setup	Yield mean (%)	Yield median (%)
MAM	72.7	72.0
CM	44.6	42.0

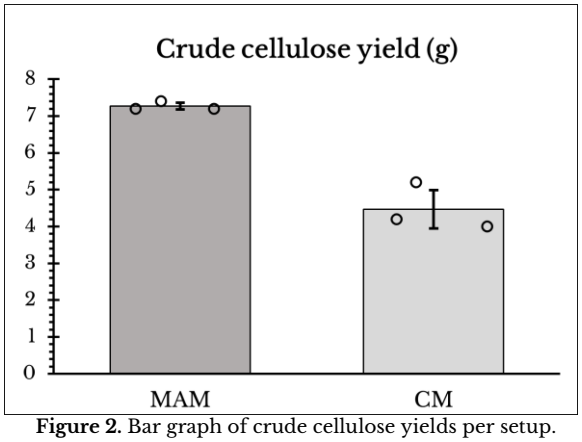

Figure 2. Bar graph of crude cellulose yields per setup.

The higher crude cellulose yield through MAM extraction may be attributed to the uniformity of heat generated by the emitted low-frequency radiation of the microwave [17]. Reactants and solvents are heated rather than the container itself as the radiation passes through the walls of the container, exciting the polar molecules within the substance being heated. Heat is generated through the movement of these polar molecules. This leads to less by-products and decomposition products which enabled the increase of the yield percentage [17,22].

In contrast, heating using CM is prone to temperature gradient which results in overheating and eventually product decomposition leading to a lower yield percentage [22]. The 2015 study of Garadimani et al. [23], which used the conventional method of extraction, found that the extraction of *Z. mays* cobs cellulose fibers yielded a mean of 41.5% of cellulose. In terms of yield, this is close to the findings of the current study using the same method.

Calculations showed that the p-value of the data acquired from both extraction methods is 0.049535. Though less than the significance level of 0.05, a clear significant difference is not apparent; therefore, the p-value only signifies a trend towards MAM extracting a higher amount of crude cellulose in contrast to CM.

Limitations. Due to time and resource constraints, this study only compared the methods based on only one parameter. This is due to the lack of equipment as the study was conducted during a pandemic.

Conclusion. - Findings show that the MAM and CM were able to extract 72.7% and 44.6% of crude cellulose, respectively. The purple hue that developed upon the addition of Schultze's reagent signifies the presence of cellulose. However, the development of a greenish hue signifies the presence of non-cellulosic material within the extracted analytes. Through statistical analysis, it was determined that there is an observed trend towards the microwave-assisted method yielding a higher percentage of *Zea mays* var. *ceratina* crude cellulose in contrast to the conventional method.

Recommendations. - Future related studies are recommended to include more parameters such as thermal stability, morphology, and crystallinity for comparison of MAM and CM [2]. Moreover, in contrast to the Schultze's reagent, the usage of the Van Soest Analysis would provide a quantitative result with regards to analyte purity [24,25]. Furthermore, future studies are recommended to explore more on the non-thermal effects of microwave heating as well as the effects of microwave heating modes (e.g. intermittent, continuous) in biopolymer extraction from raw materials.

Acknowledgment. - Gratitude is extended to Ms. Ma. Carmen Primitiva B. Malaga of the Department of Agriculture-Iloilo ROS for authenticating the corn cob samples, and to Mrs. Corazon Jotas for supplying the cobs.

References

[1] Saragih SW, Wirjosentono B, Eddyanto, Meliana Y. 2019. Extraction and Characterization of Cellulose from Abaca Pseudo Stem (Musa textile). J Phys Conf Ser. 1232:012018. doi: 10.1088/1742-6596/1232/1/012018.

[2] Li M, Cheng YL, Fu N, Li D, Adhikari B, Chen XD. 2014. Isolation and characterization of corncob cellulose fibers using microwave-assisted chemical treatments. Int J Food Eng. 10(3): 427–436. doi: 10.1515/ijfe-2014-0052.

[3] Zafar S. 2020 Jul 23. Agricultural wastes in the Philippines. Bioenergyconsult.com. [accessed 2020 Oct 24]. Available from: https://bit.ly/3ftZloE.

[4] Philippine Statistics Authority. 2021. Palay and Corn Production Survey. [accessed 2021 Mar 13]. Available from: https://bit.ly/3fSScwR.

[5] Caparino, O. A., PhD. 2018 Feb 22. Status of Agricultural Waste and Utilization in the Philippines. [accessed 2020 Nov 26]. Available from: https://bit.ly/3yNvdfl.

[6] Berber-Villamar NK, Netzahuatl-Muñoz AR, Morales-Barrera L, Chávez-Camarillo GM, Flores-Ortiz CM, Cristiani-Urbina E. 2018. Corncob as an effective, eco-friendly, and economic biosorbent for removing the azo dye Direct Yellow 27 from aqueous solutions. PLoS One. 13(4): e0196428. doi:10.1371/journal.pone.0196428.

[7] Romasanta RR, Sander BO, Gaihre YK, Alberto MC, Gummert M, Quilty J, Nguyen VH, Castalone AG, Balingbing C, Sandro J, et al. 2017. How does burning of rice straw affectCH_2 and N_2Oemissions? A comparative experiment of different on-field straw management practices. Agric Ecosyst Environ. 239:143–153. doi: 10.1016/j.agee.2016.12.042.

[8] Wang Y, Hu Y, Qi P, Guo L. 2019. A new approach for economical pretreatment of corncobs. Applied Sciences (Basel, Switzerland), 9(3), 504. doi: 10.3390/app9030504.

[9] Johar N, Ahmad I, Dufresne A. 2012. Extraction, preparation and characterization of cellulose fibres and nanocrystals from rice husk. Ind. Crops Prod. 37: 93–99. doi: 10.1016/j.indcrop.2011.12.016.

[10] Moran JI, Alvarez VA, Cyras VP, Vasquez A. 2007. Extraction of cellulose and preparation of nanocellulose from sisal fibers. Cellulose. 15: 149–159. doi: 10.1007/s10570-007-9145-9.

[11] Zhu YJ, Chen F. 2014. Microwave-assisted preparation of inorganic nanostructures in liquid phase. Chem. Rev. 114(12): 6462–6555. doi: 10.1021/cr400366s.

[12] Yilmaz ND. 2013. Effect of chemical extraction parameters on corn husk fiber characteristics. Indian J Fibre Text Res. 38: 29–34. Available from: https://bit.ly/3fveupO.

[13] Naili, H., Jelidi, A., Limam, O., Khiari, R. 2017. Extraction process optimization of Juncus plant fibers for its use in a green composite. Ind Crops Prod. 107: 172–183. doi: 10.1016/j.indcrop.2017.05.006.

[14] Del Campo BG, Brumm TJ, Bern CJ, Nyendu GC. 2014. Corn Cob Dry Matter Loss in Storage as Affected by Temperature and Moisture Content. Agricultural and Biosystems Engineering Publications. 57(2): 573–578. doi: 10.13031/trans.57.10426.

[15] General Notices and Requirements: Applying to Standards, Tests, Assays, and Other Specifications of the United States Pharmacopeia. 2013 Feb 1. [accessed 2020 Nov 22]. Available from: https://bit.ly/3i03wu3.

[16] Camani PH, Anholon BF, Toder RR, Rosa DS. 2020. Microwave-assisted pretreatment of eucalyptus waste to obtain cellulose fibers. Cellulose. 27(7): 3591–3609. doi: 10.1007/s10570-020-03019-7.

[17] Izgi AA, Kocak ED, Sahinbaskan BY. 2018. Microwave Assisted Surface Treatment of Okra Fibers. IOP Conf Ser Mater Sci Eng. 460 012042. doi: 10.1088/1757-899X/460/1/012042.

[18] Hernando, K., Abayon, M., Sitjar, J., Aguirre, M., Catolico, J. 2019. Characterization of the Physical Properties of Bacillus thuringiensis Corn husk Fibers through Alkalization. Publiscience. 1(1): 2–7. Available from: https://bit.ly/2SzEs2b.

[19] Elfick, J. 2020 May 15. *School Science Lessons - Appendix B*. [accessed 2020 Oct 22]. Available from: https://bit.ly/2TpXEQt.

[20] Jenkin, A., Jenkin, D. 2012. *Sugar, starch or cellulose? What sort of carbohydrates do plants make?* [accessed 2020 Oct 22]. Available from: https://bit.ly/3vveMSR.

[21] Zach. 2020 Mar 24. How to perform a Mann-Whitney U test in Excel. Statology.org. [accessed 2020 Dec 5]. Available from: https://bit.ly/3uuRKKH.

[22] Lidstrom P, Tierney J, Wathey B, Westman J. 2001. Microwave assisted organic synthesis - a review. *Tetrahedron. 57*(45): 9225–9283. doi: 10.1016/S0040-4020(01)00906-1.

[23] Garadimani KR, Raju GU, Kodancha KG. 2015. Study on Mechanical Properties of Corn Cob Particle and E-Glass Fiber Reinforced Hybrid Polymer Composites. Am J Mater Sci. 5(3C): 86–91. doi: 10.5923/c.materials.201502.18.

[24] Holtzapple MT. 2003. CELLULOSE. *Encyclopedia of Food Sciences and Nutrition.* 998–1007. doi:10.1016/b0-12-227055-x/00185-1.

[25] Wichern M, Gehring T, Lübken M. 2018. Modeling of biological systems in wastewater treatment. In: Reference Module in Earth Systems and Environmental Sciences. Elsevier. doi: 10.1016/B978-0-12-409548-9.10944-3.

Publiscience Vol. 4 Issue 1

Development of a reduced nanoporous graphene oxide membrane synthesized from *Oryza sativa* husk using the Tour method for the reduction of salt ions

VENN DEO JUSTIN E. ALBALADEJO[1], RAYMOND T. BORRES[1], ZEDDREX N. NAVARRA[1], ARIS C. LARRODER[1], and MARK V. ROSALES[2]

[1]*Philippine Science High School Western Visayas Campus - Department of Science and Technology (DOST-PSHSWVC), Brgy. Bito-on, Jaro, Iloilo City 5000, Philippines*
[2]*Metrology Laboratory, Regional Standards, and Testing Laboratories, Lapaz, Iloilo City 5000, Department of Science and Technology, Philippines*

Article Info

Submitted: Apr 19, 2021
Approved: Jun 24, 2021
Published: Aug 30, 2021

Keywords:
graphene oxide
nanoporous membrane
Tour method
Oryza sativa
desalination

Abstract

Membrane desalination is limited by issues of high costs and energy consumption. Moreover, high-quality membranes require high carbon content sources such as biowastes, among others. One example of biowastes commonly found in the Philippines are *Oryza sativa* (rice) husks. Thus, this study aimed to determine the feasibility of developing a reduced nanoporous graphene oxide (rNPGO) membrane synthesized from *Oryza sativa* husks using the Tour method for membrane desalination. To assess the membrane, a salt solution (1% w/v) was prepared and subjected to membrane desalination. After three readings, the recorded mean salt rejection rate of the membrane was 6.55%. The results indicate a significant difference between the salinity content before and after desalination. Therefore, rNPGO synthesized from *O. sativa* husks using the Tour method can be used for the reduction of salt ions.

Introduction. - Membrane desalination is a process that removes salt ions from saltwater with the use of membranes [1,2,3]. Recent developments in the field of membrane desalination have led it to become one of the primary solutions to address saltwater intrusion [1,3]. Saltwater intrusion is a form of groundwater contamination wherein saltwater intrudes into freshwater sources, making it unsuitable for human consumption. By removing the salt ions in the water, membrane desalination provides the possibility of expanding the water supply by supplementing it with water from oceans and brackish waters [4].

However, the current leading technologies for membrane desalination are limited in part due to high costs and energy consumption [2]. One of the causes of the elevated operating costs is the presence of membrane fouling, which is the degradation of the membrane due to the deposition of permeate molecules on the surface [5]. This leads to the deterioration of permeate flux, frequent chemical cleaning, and replacement of the membrane, contributing to a shorter membrane lifespan [6,7].

In a study conducted by Wang et al. [7], graphene-based membranes can withstand membrane fouling. Graphene is an ultra-thin carbon film that contains a honeycomb lattice structure which gives it a large surface area and excellent conductivity [8]. Additionally, graphene-based membranes can withstand membrane fouling due to their hydrophilic nature as well as their strong adsorption capacity and large surface area [9].

Moreover, the introduction of nanopores to graphene-based membranes causes an increase in permeate flux while maintaining a relatively high salt rejection rate [4,10,11]. Additionally, graphene-based nanoporous membranes are commonly utilized in membrane desalination because of their attractive properties to salt ions [11], and effective nanopore filtration [12]. The attractive properties of graphene-based nanoporous membranes to salt ions derive from the Gibbs-Donnan effect wherein negatively charged membranes such as graphene-based nanoporous membranes attract positively charged molecules such as sodium ions. Furthermore, due to the size difference between nanopores and salt ions, salt ions are unable to pass through nanopores that are under a certain size [13].

Since nanoporous graphene oxide (NPGO) membranes are chemically unstable due to the presence of oxygen-containing functional groups, they must be stabilized through thermal reduction. Thermal reduction is a controlled approach to removing the oxygen-containing functional groups

How to cite this article:
CSE: Alabaldejo VDJE, Borres RT, Navarra ZN, Larroder AC, Rosales MV. 2021. Development of a reduced nanoporous graphene oxide membrane synthesized from Oryza sativa husk using the Tour method for the reduction of salt ions. Publiscience. 4(1): 32–37.
APA: Alabaldejo, V.D.J.E., Borres, R.T., Navarra, Z.N., Larroder, A.C., & Rosales, M.V. (2021). Development of a reduced nanoporous graphene oxide membrane synthesized from Oryza sativa husk using the Tour method for the reduction of salt ions. *Publiscience*, *4*(1), 32–37.

For supplementary data, contact: publiscience@wvc.pshs.edu.ph.

in the NPGO membranes, which increases membrane permeability, uniformity, and stability [13].

When synthesizing a graphene oxide (GO) membrane, the quality of the resulting membrane is dependent on the quality of the graphite used in its synthesis. Hence, in order to obtain high-quality membranes, high carbon content sources are necessary. One example of sources with high carbon content are biomasses such as rice husks, among others [7,14,15]. In the study conducted by Supriyanto et al. [16], promising results were obtained for the synthesis of GO from graphite that had been obtained from *O. sativa* (rice) husk.

The two main methods used for the synthesis of GO are the Tour method and Hummer's method. However, in the study of Habte and Ayele [17], the Tour method was shown to have a clear advantage in the synthesis of GO in comparison to the Hummer's method. This is because the oxidation degree of the synthesized GO was found to be better when the Tour method is used. The higher oxidation degree implies that the attractive filtration property of the membrane was stronger and therefore increased the salt rejection rate of the membrane. Additionally, the presence of health risks and hazards when synthesizing the GO was reduced when the Tour method is utilized because it minimizes the fumes released during the process in contrast with Hummer's Method.

Therefore, the study aimed to explore the feasibility of developing a reduced nanoporous graphene oxide membrane (rNPGO) synthesized from rice husk using the Tour method to reduce salt ions. It specifically aimed to:

(i) synthesize graphite from *O. sativa* husk;

(ii) synthesize graphene oxide from graphite using the Tour method;

(iii) etch nanopores in the graphene oxide powder;

(iv) prepare and reduce the NPGO membrane; and

(v) assess the salinity level of the water samples pre and post-desalination using the rNPGO membrane.

Methods. - *Oryza sativa* husks were gathered from the Department of Agriculture - Western Visayas Agricultural Research Center and synthesized into graphite. The graphite was then synthesized into graphene oxide using the Tour method. Subsequently, nanopores were etched into the graphene oxide. After the preparation of the membrane, a salt solution was prepared and measured based on its salinity content. It was then filtered using the membrane and the salinity content of the permeate was measured.

Synthesis of Graphite. The synthesis of graphite was needed to make a graphene oxide membrane. The graphite powder for this research was derived from *O. sativa* husks. The rice husks (500 g) were washed with distilled water and subjected to oven-drying for 24 hours in different batches at 50°C. The material produced was then ground and screened using a sieve mesh size 60 (0.250 mm). A hundred grams of the rice husk residue was placed in a furnace at 1000 °C for 2 hours, under 1 atm. To obtain graphite, silica was removed from the furnaced rice husk using 4 M sodium hydroxide (NaOH) that was pre-diluted in a volumetric flask. This was done by dissolving 10 g of the furnaced rice husk in 30 mL of 4 M NaOH in a flask which was then heated and stirred for 3 hours. The solution was then vacuum-filtered and oven-dried for 3 hours at 50 °C. The resulting graphite underwent a confirmatory test using the Fourier-Transform Infrared Radiation - Attenuated Total Reflectance (FTIR-ATR) to confirm if the synthesized material is indeed graphite by comparing it with the FTIR-ATR spectroscopy results of related literature.

Synthesis of Graphene Oxide using the Tour Method. Ninety milliliters (90 mL) of concentrated 98% sulfuric acid (H_2SO_4) was mixed in a glass beaker with 10 mL of concentrated 85% phosphoric acid (H_3PO_4). The mixture was poured into a beaker with a mixture of 0.5 g of graphite powder and 4.5 g of potassium permanganate ($KMnO_4$), heated at 50 °C using a water bath, and stirred for 12 hours. The mixture was then cooled at room temperature and 250 mL distilled water was added. Ten milliliters (10 mL) of 30% hydrogen peroxide (H_2O_2) was added to reduce the manganese ions present. The resulting solution was filtered using a 45 microns filter paper. The produced graphite oxide filter cake was washed using a 5% hydrochloric acid (HCl) (aq) in a centrifuge at 4000 rpm for 4 hours. The GO was then manually stirred with distilled water at 60 °C for 12 hours in a water bath [17]. The solution was vacuum-filtered and oven-dried to produce GO powder which was tested using the FTIR-ATR to confirm if the synthesized material is indeed GO.

Etching of GO. Thirty milligrams (30 mg) of GO powder was redispersed into 90 mL of 30% hydrogen peroxide and placed in an ultrasonic bath treatment for 20 minutes to ensure a good dispersion. After 20 minutes, the solution was heated up to 70 °C in a water bath and was refluxed in a reflux set-up for 10 hours. The mixture was purified in a permeable plastic bag with deionized water for 3 days to obtain a stable NPGO solution. The NPGO was diluted to 50 mg/L using deionized water for membrane preparation.

Preparation of NPGO membrane. An NPGO membrane was prepared using vacuum filtration. The NPGO solution was filtered by using a filter paper with a pore size of 45 microns to remove the moisture. The filtered NPGO sheet was poured from the Buchner flask to the beaker, vacuum-filtered, and dried in an oven at 60 °C for 12 hours. Then, it was thermally reduced in an oven at 150 °C at 1 atm for 1.5 hours to maximize salt rejection to synthesize an rNPGO membrane. The surface and cross-sectional morphology of the rNPGO membrane was characterized using Scanning Electron Microscopy (SEM). The membrane was captured and the pores in

the resulting image were measured using the 2D image of the result from the SEM Imaging.

Assessment of salinity content. To measure and evaluate the efficiency of the rNPGO membrane, an assessment of the salinity level of water samples was conducted. A salt solution was prepared using one gram of analytical reagent grade sodium chloride (NaCl) to make a 1% NaCl solution. Prior to testing the membrane, a control made of a blank filter paper was utilized. The salt solution was poured on top of the filter paper until the funnel was full. The permeate was then placed in a 250 mL beaker for salinity content testing. A conductivity meter, pre-calibrated by dipping it in a container filled with distilled water, was used by dipping it in the solution until the value stabilized after three minutes. For the final testing, the same method was then utilized for the rNPGO membrane.

The salt rejection of the membrane was analyzed using the salinity content of both the feed and the permeate. After all the data were plotted, data analysis was using the formula for salt rejection.

$$R_{salt\%} = \left(1 - \frac{C_p}{C_f}\right) * 100\%$$

Where:
$R_{salt\%}$ = percent of salt rejection
C_p = concentration of the permeate
C_f = concentration of the feed

Data Analysis. The results were analyzed using t-test for dependent samples using RStudio (version 1.3.1093.0, free license) to observe any significant difference between the salinity content before and after desalination. The salt rejection was analyzed among the three replicates. This was to ensure that the efficiency of the membrane was not reduced by washing it with deionized water.

Safety Procedures. During the conduct of the data gathering process, the wearing of the proper personal protective equipment such as gloves, masks, and goggles was observed. The methods were conducted alongside the supervision of experts. A wash bottle was utilized in cleaning the glassware and the contaminants in the conductivity meter to ensure accurate readings. Furthermore, the safety data sheet of each chemical and equipment was strictly followed. Additionally, when performing methods with the use of chemicals, a fume hood was utilized to avoid the inhalation of fumes. Lastly, for the disposal of chemicals, each chemical was disposed of according to the safety data sheet and in accordance with the disposal protocol of the laboratory.

Results and Discussion. - This study aimed to explore the feasibility of developing an rNPGO membrane synthesized from *O. sativa* husk using the Tour method to reduce salt ions. This was done through membrane assessment by analyzing its pore size, membrane thickness, and salt rejection rate.

The graphite powder synthesized from rice husk was analyzed using the FTIR-ATR analysis with three replicates. The mean result of the FTIR-ATR analysis of the graphite powder, colored in red, was compared with the FTIR-ATR results of the graphite powder in the study of Wenxuan et al. [18], colored in black (Figure 1). Since a graphite library was unavailable in the FTIR-ATR used, the graphs were superimposed and the peaks were compared. The peaks of both graphs are similar, which peaks at around 624.38/cm, 790.75/cm, and 1066.50/cm.

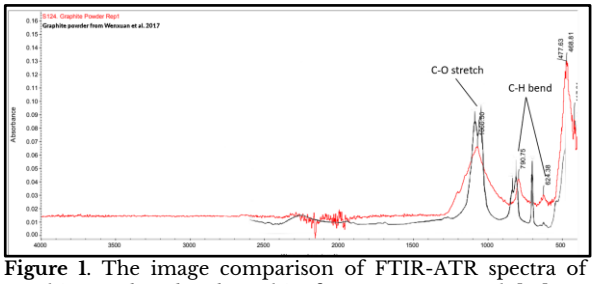

Figure 1. The image comparison of FTIR-ATR spectra of graphite produced and graphite from Wenxuan et al. [18].

The graphene oxide powder synthesized using the Tour method was analyzed using the FTIR-ATR analysis with three replicates. The mean result of the FTIR-ATR analysis of the graphene oxide powder, colored in red, was compared to the FTIR-ATR results of the graphene oxide powder in the study of Çiplak et al. [19] colored in blue (Figure 2). The peaks of both graphs which peaks at around 791.67/cm and 1070.04/cm are similar.

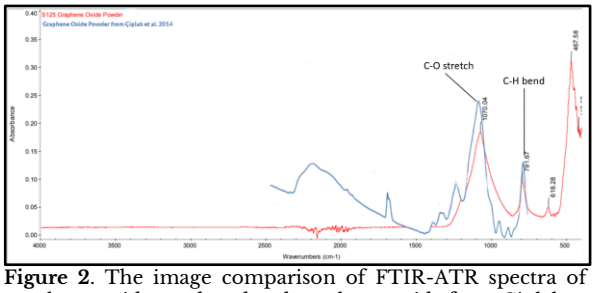

Figure 2. The image comparison of FTIR-ATR spectra of graphene oxide produced and graphene oxide from Çiplak et al. [19].

Using an SEM, the rNPGO was analyzed for its pore size and thickness. The nanopore sizes were measured from three different locations and different magnifications respectively on the rNPGO membrane. This was done so that the pores are visible with the use of the instrument. The statistical mean pore sizes of the three replicates are 555.4 nm, 615.1 nm, 837.9 nm respectively. Moreover, the pores have varying sizes that range from 286.0 nm to as large as 1920.0 nm (Table 1).

Table 1. Statistical parameters of rNPGO membrane pore sizes based on the 3 locations with 3 magnifications (8500x, 5000x, 3000x).

Parameters	Replicate at 8500x (nm)	Replicate at 5000x (nm)	Replicate at 3000x (nm)
Statistical Mean	555.4	615.1	837.9
Standard Deviation	323.9	372.7	413.6

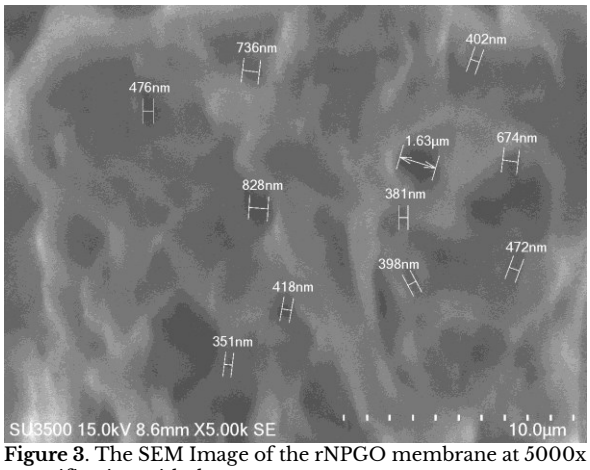

Figure 3. The SEM Image of the rNPGO membrane at 5000x magnification with the pore measurements.

The thicknesses of the rNPGO membrane were measured from three different locations and different magnifications respectively. This was done so that the rNPGO membrane was visible enough to measure its thickness with the use of the instrument. The mean thickness, as well as the standard deviation from the three replicates, varies as shown (Table 2). The statistical means of the three replicates are 37.33 µm, 33.19 µm, and 45.43 µm, respectively. Additionally, the thickness of the membrane varies from a range of 27.0 µm to 53.6 µm.

Table 2. The statistical parameters of nanoporous graphene oxide membrane thickness based on the 3 locations with 3 magnifications (420x, 370x, 250x).

Parameters	Replicate at 420x (µm)	Replicate at 370x (µm)	Replicate at 250x (µm)
Statistical Mean	37.73	33.19	45.43
Standard Deviation	3.66	4.98	4.75

The mean salinity content of the prepared salt solution was measured using a conductivity meter (PS-2230 Advanced Water Quality Sensor). The salinity content of both pre-desalination and post-desalination were further analyzed using the Salt Rejection Rate formula. Additionally, the statistical mean and standard deviation were calculated (Table 3).

Table 3. The statistical parameters of pre-desalination and post-desalination salinity content of the water samples.

Replicates	Pre-Desal-ination Salinity Content (%)	Post-Desal-ination Salinity Content (%)	Salt Rejection Rate (%)
1	1.04479815	0.96423745	7.710647267
2	1.04164610	0.98627760	5.315480949
3	1.03442845	0.96588000	6.626698057
Statistical mean	1.04029090	0.97213168	6.551938501
Standard deviation	0.00434051	0.01002512	0.979288738

The FTIR-ATR spectra results showed that the graphite powder produced is similar to the graphite produced in the study of Wenxuan et al. [18], thus, it is feasible to synthesize graphite powder from *O. sativa* husks. The graphs of the FTIR-ATR spectra can be presented in two ways, wavelength vs. transmittance and wavelength vs absorbance. In the study of Wenxuan et al. [18], they utilized wavelength vs transmittance which in turn caused the graph to be reflected based on Beer-Lambert's Law as stated in the study of Mayerhöfer et al. [20].

To determine the feasibility of synthesizing graphite powder from *O. sativa* husk, the reflected graph was compared to the study of Wenxuan et al. [18] based on its fingerprint region. With this, it reflected the result of the study of Supriyanto et al. [16] wherein they also utilized *O. sativa* husk to synthesize graphite.

The FTIR-ATR spectra results showed that the graphene oxide powder produced is similar to the graphite produced in the study of Çiplak et al. [19]. Thus, it is feasible to synthesize graphene oxide powder from graphite using the Tour method. In the study of Çiplak et al. [19], they also utilized the wavelength vs transmittance which in turn caused the graph to be reflected based on Beer-Lambert's Law as stated in the study of Mayerhöfer et al. [20]. To determine the feasibility of synthesizing graphene oxide powder from *O. sativa* husk, the reflected graph was compared to the study of Çiplak et al. [19] based on its functional groups. The graph of the graphene oxide produced has two visible peaks within the fingerprint region of the spectra. By comparing the graphs in this region, it could help indicate if the product is similar to another.

The results obtained from the SEM showed that the graphene oxide membrane produced pore sizes ranging from as small as 286 nm to as large as 1920 nm. Although these are hundreds of nm in diameter, these could not be considered nanopores. This is probably because the nanopores could not be seen by the instrument used since the sample was not sputter-coated beforehand.

The rNPGO membrane was subjected to an SEM imaging analysis at 15 kV settings so that the membrane will not burn. The morphology was analyzed and the measured pores vary in size with a standard deviation of 323.9 nm, 372.7 nm, and 413.6 nm. The deviation between the pore sizes may also be due to the dispersion of the hydrogen peroxide with the graphene oxide powder in a plastic sheet instead of a cellulose dialysis bag as well as the placement of the bag during the stabilization phase [13]. To visualize the pore sizes smaller than 200 nm in size the membrane could have been sputter-coated with gold or analyzed using Atomic Force Microscopy.

Additionally, the results for the SEM imaging of the thickness of the membrane showed that a membrane was prepared onto the filter paper. The thickness of the membrane ranges from 27.0 μm to 53.6 μm which shows the uneven distribution of the membrane probably due to the process of uneven vacuum filtration of the NPGO solution. In addition, this assumption is also reflected by the standard deviation of the membrane thickness which are 3.66 μm, 4.98 μm, and 4.75 μm.

Furthermore, membrane desalination using rNPGO synthesized from *O. sativa* husk has resulted in a mean salt rejection rate of 6.55% and a significant difference between the pre-desalination and post-desalination salinity content. This was done through a t-test for dependent samples (α=0.05) and a p-value of 0.011. This shows that the rNPGO membrane developed and synthesized from *O. sativa* husks using the Tour method was capable of reducing salt ions.

The filtration of salt ions can potentially prove that the pore size of the graphene oxide can be considered as nanopores since it was able to reduce the salt ions in the water sample. This is because the attractive properties of graphene-based nanoporous membranes to salt ions are derived from the Gibbs-Donnan effect wherein negatively charged membranes such as graphene-based nanoporous membranes attract positively charged molecules such as salt ions. Furthermore, it can potentially prove that the pore size is nanoporous due to the size difference between nanopores and salt ions. Salt ions are unable to pass through nanopores that are under a certain size since salt ions have a size that is considered nanoparticles. This was reflected in the results when the NPGO membrane was tested for its salt rejection rate and permeate flux and compared with the results of a graphene oxide membrane [13].

Limitations. The FTIR-ATR results did not directly indicate that the sample is graphite due to the graphite library unavailability for the FTIR-ATR utilized. Additionally, the *O. sativa* husks did not undergo vacuum furnacing, one of the ideal methods for synthesizing graphite from biomass. Lastly, the removal of silica was not conducted using hydrofluoric acid (HF), which is better for removing silica than NaOH in terms of purity.

Conclusion. In this study, the feasibility of developing a rNPGO synthesized from *O. sativa* husk using the Tour method was explored. The FTIR-ATR results of both the graphite powder and graphene oxide powder indicated the feasibility of synthesizing graphene oxide powder using the Tour method from the graphite powder synthesized from rice husk. The membrane produced contained pores etched in the graphene oxide powder. Moreover, there is a significant difference in the salinity content of the pre-desalination and post-desalination water samples after undergoing desalination using the nanoporous graphene oxide membrane. Thus, a nanoporous graphene oxide membrane was developed and synthesized from *O. sativa* husk using the Tour method.

Recommendations. - The sample could be placed in a polyethersulfone filter and sputter-coated to better visualize the nanopores of the graphene oxide using an SEM. Atomic Force Microscopy could also be utilized for better magnification in the sample. Additionally, the salt load capacity of the membrane could be assessed by desalinating the sample multiple times. This study can be a step further towards the right direction for exploring new avenues for the use of biowastes such as *O. sativa* husk that is abundant in the Philippines. However, there is still a lot of room for improvement in the desalination aspect of a reduced nanoporous graphene oxide (rNPGO) membrane derived from *O. sativa* husk before it can be used as a solution to the saltwater intrusion in coastal areas in the Philippines.

Acknowledgment. - The researchers would like to extend their gratitude to NEDA Region VI for helping in the conceptualization of the research problem, Mr. Roxzien Sesbreño for facilitating their data gathering at DOST-VI, and Mrs. Jessebel V. Gadot for facilitating the data gathering at UPV-RRC.

References

[1] Abd-Elhamid HF, Javadi AA. 2011. A Cost-Effective Method to Control Seawater Intrusion in Coastal Aquifers. Water Resources Management. 25(11): 2755–2780. doi: 10.1007/s11269-011-9837-7.

[2] Shaffer DL, Yip NY, Gilron J, Elimelech M. 2012. Seawater desalination for agriculture by integrated forward and reverse osmosis: Improved product water quality for potentially less energy. Journal of Membrane Science. 415-416: 1–8. doi: 10.1016/j.memsci.2012.05.016.

[3] Mehdizadeh S, Badaruddin S, Khatibi S. 2019. Abstraction, desalination and recharge method to control seawater intrusion into unconfined coastal aquifers. Global Journal of Environmental Science and Management. 5(1): 107–118.

[4] Cohen-Tanugi D, Mcgovern RK, Dave SH, Lienhard JH, Grossman JC. 2014. Quantifying the potential of ultra-permeable membranes for water desalination. Energy Environ. Sci. 7(3): 1134–1141. doi: 10.1039/c3ee43221.

[5] Li H, Chen V. 2010. Membrane Fouling and Cleaning in Food and Bioprocessing. Membrane Technology. 213–254. doi: 10.1016/b978-1-85617-632-3.00010-0.

[6] Goh P, Lau W, Othman M, Ismail A. 2018. Membrane fouling in desalination and its

mitigation strategies. Desalination. 425: 130–155. doi: 10.1016/j.desal.2017.10.018.

[7] Wang X, Lu Z, Jia L, Chen J. 2016. Physical properties and pyrolysis characteristics of rice husks in different atmosphere. Results in Physics. 6: 866–868. doi: 10.1016/j.rinp.2016.09.011. [8] Pareek A, Venkata Mohan S. 2019. Graphene and Its Applications in Microbial Electrochemical Technology. Microbial Electrochemical Technology. 75–97. doi: 10.1016/b978-0-444-64052-9.00004-2.

[9] Hu M, Zheng S, Mi B. 2016. Organic Fouling of Graphene Oxide Membranes and Its Implications for Membrane Fouling Control in Engineered Osmosis. Environmental Science & Technology. 50(2):685–693. doi: 10.1021/acs.est.5b03916.

[10] Cohen-Tanugi D, Grossman JC. 2012. Water Desalination across Nanoporous Graphene. Nano Letters. 12(7): 3602–3608.

[11] Yang Y, Yang X, Liang L, Gao Y, Cheng H, Li X, Zou M, Ma R, Yuan Q, Duan X. 2019. Large-area graphene-nanomesh/carbon-nanotube hybrid membranes for ionic and molecular nanofiltration. Science. 364(6445): 1057–1062.

[12] Abraham J, Vasu KS, Williams CD, Gopinadhan K, Su Y, Cherian CT, Carbone P. 2017. Tunable sieving of ions using graphene oxide membranes. Nature nanotechnology. 12(6): 546.

[13] Li Y, Zhao W, Weyland M, Yuan S, Xia Y, Liu H, Jian M, Yang J, Easton CD, Selomulya C, et al. 2019. Thermally Reduced Nanoporous Graphene Oxide Membrane for Desalination. 53(14): 8314–8323.

[14] Lori J, Lawal A, Ekanem E. 2007. Proximate and Ultimate Analyses of Bagasse, Sorghum and Millet Straws as Precursors for Active Carbons. Journal of Applied Sciences. 7(21): 3249–3255. doi: 10.3923/jas.2007.3249.3255.

[15] Othman N, Hussin MH, Shuib RK, Sulaiman N. 2018. Comparison characteristic between milled coconut shell activated carbon powder and carbon black: Physical, chemical and morphological properties. 1985 (2018).

[16] Supriyanto G, Rukman NK, Nisa AK, Jannatin M, Piere B, Abdullah, Fahmi MZ, Kusuma HS 2018. Graphene Oxide from Indonesian Biomass: Synthesis and Characterization. BioResources. 13(3): 4832–4840.

[17] Habte AT, Ayele DW. 2019. Synthesis and Characterization of Reduced Graphene Oxide (rGO) Started from Graphene Oxide (GO) Using the Tour Method with Different Parameters. Advances in Materials Science and Engineering. 2019: 1–9.

[18] Wenxuan Z, Zhanpeng L, Jing X, Feng L, Wenzhi H, Guangming L, Juwen H. 2017. Frontiers of Environmental Science & Engineering. Preparing graphene from anode graphite of spent lithium-ion batteries. 11(5): 6.

[19] Çiplak, Z, Yildiz N, Çalimli A. 2014. Investigation of graphene/Ag nanocomposites synthesis parameters for two different synthesis methods. Fullerenes, Nanotubes, and Carbon Nanostructures. 23(4): 361–370.

[20] Mayerhöfer TG, Mutschke H, Popp J. 2016. Employing Theories Far beyond Their Limits-The Case of the (Boguer-) Beer-Lambert Law. ChemPhysChem. 17(13): 1948–1955.

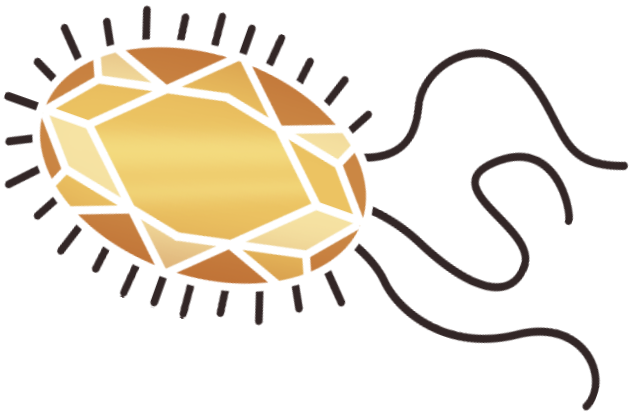

CLUSTER THREE

MICROBIOLOGY AND BIOCHEMISTRY

Yellow is associated with both caution and sickness, commonly linked with the advent of antibiotic-resistant pathogens. The gem depicts a quintessential microbe for this reason. However, the brighter shades of yellow are associated with hope and positivity. The following research studies, tackling the above-mentioned issues and other related topics through various means both in the laboratory and virtually, hope to emulate and be symbols of such positive traits.

The microbiology studies fall under the scope of the Health Research and Development Agenda, primarily due to their potential contributions to drug discovery and antibacterial research in the face of pressures of current health problems and drug-resistant bacteria. The biochemistry studies fall under the scope of the Health Research and Development Agenda and the Aquatic, Agriculture, and Natural Resources (AANR) Research and Development Agenda as they provide substantial findings which contribute to knowledge-gathering in their respective fields and form bases for future practical applications.

BASED ON: Harmonized National Research and Development Agenda (HNRDA)

Formulation and evaluation of antibacterial gel incorporated with *Stachytarpheta jamaicensis* crude ethanolic leaf extract against *Staphylococcus aureus*

JAN JOSEPH JACELA, ALTHEA VENICE M. RELLO, NUJAEL IRISH C. BERMUDO, and RAMON ANGELO N. SINCO

Philippine Science High School Western Visayas Campus - Department of Science and Technology (DOST-PSHSWVC), Brgy. Bito-on, Jaro, Iloilo City 5000, Philippines

Article Info

Submitted: May 06, 2021
Approved: Aug 09, 2021
Published: Aug 30, 2021

Keywords:
Stachytarpheta jamaicensis
Staphylococcus aureus
plant extract
antibacterial gel
agar well diffusion method

Abstract

Stachytarpheta jamaicensis (sentimento) is utilized by locals from Maasin, Iloilo as an open wound poultice for its antibacterial properties. This study aimed to formulate and evaluate an antibacterial gel incorporated with *S. jamaicensis* leaf extract against *Staphylococcus aureus*. The gel's antibacterial activity was compared to that of a negative control (gel base) and a positive control (hand sanitizer) using the agar well diffusion method. The gel was found to be stable in all physicochemical parameters evaluated (pH, viscosity, spreadability, centrifugation, and mechanical vibration) except for viscosity. The hand sanitizer exhibited the highest zone of inhibition (6.17 ± 0.29 mm) followed by the gel (4.67 ± 0.29 mm). Although not comparable to the positive control, the gel exhibited antibacterial activity. Thus, the drug delivery system effectively delivered the extract's active ingredient. However, it can not be used as a hand sanitizer with its current extract concentration.

Introduction. - Plant species traditionally used as an alternative medicine to address various illnesses and diseases have been widely investigated through phytochemical screenings. Those proven to contain phytochemical constituents whose functions coincide with their intended use are then subjected to antibacterial and anti-inflammatory tests, among others [1]. Once their efficacy has been tested in the laboratories, they can now be incorporated into medicinal preparations such as syrups, tablets, capsules, and topical formulations for mass production and commercial sale [1].

One such plant is the *Stachytarpheta jamaicensis*, locally known as kandikandilaan or sentimento, a flowering plant that belongs to the family of *Verbenaceae*. This plant can be found thriving in the tropical forests of the Americas, and the subtropical forests of Asia and Africa. It has numerous medicinal benefits in infectious and chronic health systems [2]. In the Philippines, there is an abundance of *S. jamaicensis* where locals use its leaves as a poultice in treating open wounds, for it is known to have antibacterial properties [3,4].

Since Abadilla et al. [5] have already developed an ointment using *S. jamaicensis* leaf extracts, this study formulated and evaluated a gel. Gel formulations are generally preferred over other topical semisolid preparations because they stay longer on the skin, have a higher viscosity, are more bioadhesive, and cause less irritation [6]. In addition, gel formulations are moisturizing, water-dependent, have a smooth application, and release active ingredients more effectively [6,7].

According to Taylor and Unakal [8], *Staphylococcus aureus* is a common bacteria usually found in the skin of most healthy humans, since *S. aureus* is one of the standard components of the human's environment and normal flora. According to the study of Jacopin et al. [9], a significant number of community-acquired and hospital-acquired diseases are triggered by commensal bacteria such as *Escherichia coli*, *Staphylococcus aureus*, or *Streptococcus pneumoniae* which can also be opportunistic pathogens.

With this, an antibacterial gel incorporated with *S. jamaicensis* crude ethanolic leaf extract was formulated and evaluated. If proven effective, the antibacterial gel may be commercialized to produce a sanitizer affordable for the masses and address the necessity of discovering new drug delivery systems for herbal medicine.

Thus, the study aimed to formulate and evaluate an antibacterial gel incorporated with *Stachytarpheta jamaicensis* (sentimento) crude ethanolic leaf extract against *Staphylococcus aureus.* The specific objectives of this study were to:

(i) Formulate an antibacterial gel incorporated with *S. jamaicensis* crude ethanolic leaf extract against *S. aureus*;

How to cite this article:
CSE: Jacela JJ, Rello AV, Bermudo NI. 2021. Formulation and evaluation of antibacterial gel incorporated with *Stachytarpheta jamaicensis* (sentimento) crude ethanolic leaf extract against *Staphylococcus aureus*. Publiscience. 4(1): 39–44.
APA: Jacela, J.J., Rello, A.V., & Bermudo N.I. (2021). Formulation and evaluation of antibacterial gel incorporated with *Stachytarpheta jamaicensis* (sentimento) crude ethanolic leaf extract against *Staphylococcus aureus*. *Publiscience*, *4*(1), 39–44.

For supplementary data, contact: publiscience@wvc.pshs.edu.ph.

(ii) Evaluate and compare the results of the physicochemical tests of the formulated gel before and after accelerated stability testing;

(iii) Evaluate the antibacterial activity of the formulated gel against *S. aureus* by measuring its zone of inhibition using the agar well diffusion method; and

(iv) Determine if there is a significant difference between the antibacterial activity of the formulated gel with the gel base without the extract as the negative control and a commercially available hand sanitizer as the positive control.

Methods. - The methodology is divided into four (4) parts: extraction, gel formulation, physicochemical evaluation, and antibacterial evaluation. The formulated gel's physicochemical properties and antibacterial activity against *Staphylococcus aureus* alongside the gel base (negative control) and a commercially available sanitizer (positive control) were evaluated.

Collection and Identification of Samples. A random sampling method was employed in the leaf collection in a lot located at Brgy. Daja, Maasin, Iloilo, at 10°53'45.3"N, 122°24'43.5"E on November 27, 2020. A 36-sq. meter (6 m by 6 m) main plot was established that was further divided into 36 1-square meter subplots with dimensions of 1 m by 1 m. Each subplot was labeled with numbers from 1 to 36, and 9 subplots were randomly chosen as sampling sites. Sentimento plants with green leaves and bright even colors were uprooted and then verified as *S. jamaicensis* by the Department of Agriculture in Sta. Barbara, Iloilo.

Extract Acquisition. The collected *S. jamaicensis* leaves were washed under running tap water and rinsed with distilled water. The leaves were oven-dried for 48 hours [4], pulverized using a blender, and sifted with sieves mesh numbers 5 and 10 [10]. Fifty (50) grams of the leaf powder was mixed with 500 mL of 70% ethanol [11,12] and was sonicated using an ultrasonic cleaner (42 kHz, 135 W; Branson Ultrasonic Corporation, USA) for 60 minutes. The mixture was filtered twice [4] using a vacuum pump and was subjected to a rotary evaporator (Biobase IKA RV8-S099) at 40 °C with 150 revolutions per minute (rpm) for 10 hours [13]. The aqueous extract with a concentration of 100 mg/mL was then used for the antibacterial gel formulation for better solubility with the gel base.

Antibacterial Gel Formulation. To formulate the gel, propylene glycol, an antifreeze and anti-melting preservative, was added to enhance its stability [14]. Glycerin was also added to help the gel stay on the skin for a prolonged period [15]. Five (5) grams of carbomer 934 (1%), 35 mL of propylene glycol (7%), and 35 mL of glycerin (7%) were dispersed using a hot plate with a magnetic stirrer in 410 mL of distilled water. The mixture was allowed to rest for 60 minutes for the carbomer to hydrate and swell [16].

The initial mixture was neutralized with 2 mL of triethanolamine to attain the desired pH of 8.0 [16]. Forty (40) milliliters of the formulation was then set aside in a beaker at room temperature until use, while 460 mL was incorporated with the leaf extract. Five (5) mL of the leaf extract [4] was diluted with 5 mL of polysorbate 20, which also improves the gel's stability [17]. The leaf extract and polysorbate 20 mixture was then added to the carbomer mixture. The final concentration of the extract in the carbomer mixture was 106 mg/mL.

Physicochemical Evaluation of Gel. The tests suggested by the Food and Drug Administration (FDA), the United States Pharmacopeia (USP), and the Brazilian Health Surveillance Agency (ANVISA) were conducted with the formulated antibacterial gel [18].

pH. The pH of the formulated antibacterial gel was measured using a digital pH meter. The electrode was dipped into the antibacterial gel and left for 10 minutes at room temperature before pH reading [19,20]. The measurement was carried out in triplicates and the average of the three readings was recorded to ensure accuracy.

Viscosity. The viscosity of the antibacterial gel was determined using a viscometer at 25 °C with a spindle speed of 12 rpm [21]. The measurement was carried out in triplicates and the average of the three readings was recorded to ensure accuracy.

Spreadability. The parallel-plate method was used to measure the spreadability of the formulated gel [22]. Spreadability was calculated using the formula:

$$S = \frac{M \cdot L}{T}$$

Where:
S = Spreadability (g · cm/s)
M = Weight (g) tied to the upper slide
L = Length (cm) moved by the glass slide
T = Time (s) it took to separate the upper and lower slides

The measurement was carried out in triplicates and the average of the three readings was recorded to ensure accuracy.

Centrifugation Test. Five (5) grams of the antibacterial gel were subjected to a centrifuge at a cycle of 3000 rpm for 30 minutes at room temperature [23] to observe the occurrence phase separation.

Mechanical Vibration Test. Five (5) grams of the antibacterial gel were transferred to a test tube and subjected to a vortex shaker for 10 seconds to observe the occurrence of phase separation [24].

Stability Test. The formulated antibacterial gel underwent a hot and cold temperature cycling adopted from Krongrawa et al. [22]. It was placed alternately at 4 ± 1 °C and 45 ± 1 °C for 24 hours each for 6 cycles. The pH, viscosity, and spreadability were measured, and centrifugation and vibration testing were conducted in the post-stability test antibacterial gel.

Antibacterial Evaluation of Gel. Samples obtained from the *S. aureus* Tryptic Soy Broth (TSB) subculture from the Philippine Biobank Facility in University of the Philippines Los Baños were inoculated to the surface of the Mannitol Salt Agar (MSA) using the quadrant streaking method. The plate was then incubated for 24 hours at 35 °C. Large, bright yellow, and opaque isolated colonies of *S. aureus* were inoculated to 15 mL of TSB and incubated [23]. Tryptic Soy Broth (TSB) was then added to reduce and achieve the turbidity of 0.5 McFarland standard [23].

Using a sterile blue micropipette tip, three Mueller Hinton Agar (MHA) plates were each punctured to create three uniformly sized wells. Pure colonies of *S. aureus* from the TSB were then inoculated and swabbed to the three MHA plates [23]. Treatments were then dispensed using a micropipette into the wells according to their labels with a uniform amount of 1 mL. The plates were then incubated for 24 hours at 37 °C [23]. The antibacterial activity of the formulated gel, gel base without leaf extract (negative control), and a commercially available hand sanitizer (positive control) were evaluated by measuring the zone of inhibition [23].

Data Analysis. For calculations, p-values were calculated using R (v4.04, GNU GPL v2). Paired t-test was then performed to determine if there is a significant difference between the mean pH, viscosity, and spreadability of the formulated gel obtained before and after accelerated stability testing. One-way ANOVA test with the statistical significance set at 5% was then used to determine if there is a significant difference between the antibacterial activity of the gel base, formulated gel, and commercially available hand sanitizer against *S. aureus* based on their generated zones of inhibition, and post-hoc analysis was evaluated using Tukey HSD test.

Safety Procedure. Proper protective equipment was worn throughout the conduct of the data gathering to avoid sample and bacterial contamination. Working areas were disinfected with 70% ethanol. All chemical wastes were handled according to their respective safety data sheet, placed inside empty water bottles, and were disposed of by the personnel of the school. Biological materials such as cultures and contaminated glassware were autoclaved before disposal.

Results and Discussion. - The data from the agar well diffusion assay were statistically analyzed using one-way ANOVA to determine if there is a significant difference between the zones of inhibition generated. Paired t-test was used to determine if there is a significant difference among the pH, viscosity, and spreadability values acquired.

Physicochemical Evaluation. For the physicochemical evaluation, three parameters, namely the pH, viscosity, and spreadability of the gel, were assessed. Each parameter was then statistically analyzed through paired t-tests set at 0.05 alpha with n=3 trials. With this, the p-values of the pH, viscosity, and spreadability are 0.11, 5.17 x 10^{-2}, and 0.23, respectively. The paired t-test showed that there is no significant difference in the formulated gel before and after accelerated stability testing (AST) in terms of pH and spreadability, indicating stability and good quality of the formulated gel in these parameters. Meanwhile, a significant difference in the viscosity of the formulated gel was established before and after stability testing, indicating that the formulated gel is not of good quality in terms of this parameter. No phase separation was observed in the formulated gel following the centrifugation and mechanical vibration tests before and after stability testing, indicating stability and retained homogeneity of the formulated gel.

The formulated gel is slightly runny, immediately dries after spreading on the skin, has a chartreuse color, and has a smooth and somewhat heavy feel. The chartreuse color of the gel is due to the dark green color of the extract used.

Stability studies on pharmaceutical gels are done to determine if a formulation stored in a specific container is capable of retaining its physical, chemical, and microbiological properties, as well as evaluate the effect of the environmental factors on the formulation [24].

Topical treatments usually have an acidic pH, since an acidic environment improves the release of oxygen in wounded or affected tissues, hence aiding in the healing of the wounds [25]. The formulated gel had an acidic pH due to its main component being carbomer, which is an acid-based polymer [26]. Although the pH of the formulated gel is slightly lower than that of the skin which is 4.1 to 5.8 [27], it was not acidic enough to cause skin irritation, therefore safe to use [28].

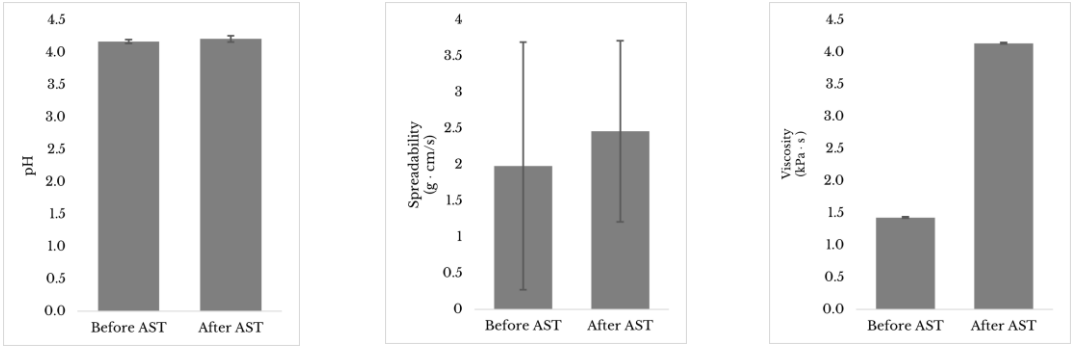

Figure 1. Results of the physicochemical evaluation. Data are expressed in terms of mean ± standard deviation.

Viscosity is important in evaluating a gel formulation because it affects the spreadability and release of the active ingredient. Spreadability aids the ability of the gel to be uniformly applied to the skin [16]. The spreadability of the formulated gel before stability testing was low therefore not ideal [29,30]. The low pH attained by the formulated gel caused a decrease in its viscosity [30]. The viscosity of a gel is highest at its gelling point [32], which in the case of the gelling agent used, carbomer, is 8 [16]. With this, it could be inferred that the low pH of the gel affected its viscosity. The decrease in viscosity then caused an increase in the gel's spreadability [16]. The formulated gel is therefore favorable for wound healing in terms of its pH [28]. However, the formulated gel still requires a lower viscosity and, consequently, a higher spreadability in order to improve in these parameters [16,29,30].

Antibacterial Evaluation. The One-way ANOVA test conducted on the results of the agar well diffusion assay showed that there is a significant difference between the formulated gel and the positive control. It is significantly different in favor of the positive control (refer to Figure 2).

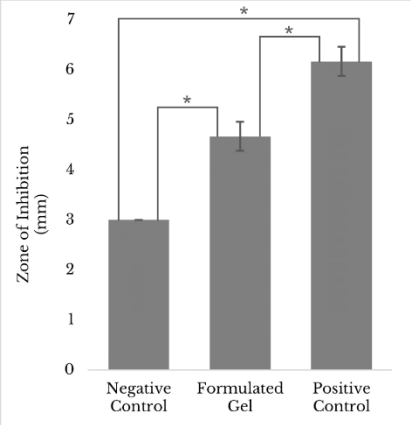

Figure 2. Results of the antibacterial evaluation. Data are expressed in terms of mean ± standard deviation.

A higher concentration of the extract may have achieved the same effectivity as the commercially available hand sanitizer which corresponds to the findings of Ruma and Zipagang [33], which states that higher concentration extract results in better effectivity in bacterial growth inhibition.

Although the formulated gel is effective as an antibacterial gel, it still has areas of improvement and the findings of this study may be different to future research. Therefore it is prescribed that more studies be conducted that would improve the formulated gel's antibacterial activity and physicochemical properties.

This indicates that the positive control is a more effective antibacterial formulation in comparison to the formulated gel. The commercially available hand sanitizer used for the positive control is alcohol-based therefore is more effective compared to the formulated gel which is water-based. This difference in formulation provides the commercially available hand sanitizer with more efficacy attributed to its alcohol content. The formulated gel is not as effective as the commercially available hand sanitizer because of the concentration of the crude ethanolic leaf extract of *S. jamaicensis*, which was based on the minimum inhibitory concentration (MIC) test of Idu et al. conducted in 2007 [4].

Limitations. The data gathering was conducted for two months. Within those two months, the period between the acquisition of the extract and gel formulation was a month. Hence, the quality of the extract may also have been compromised, particularly the antibacterial activity. Despite the setback, the findings of this research may help future studies in improving the formulation and discover the most effective concentration for antibacterial inhibition. Furthermore, the commercially available hand sanitizer used as a positive control has a different formulation as to that of the formulated gel, which may have affected its diffusion to the agar in the antibacterial evaluation.

Conclusion. - The formulated gel with *S. jamaicensis* crude ethanolic leaf extract has antibacterial activity against *S. aureus*. However, due to it having a significantly smaller zone of inhibition, it is not comparable to that of the commercially available sanitizer.

Table 1. Zones of inhibition generated on the MHA plates after incubation.

	Replicate No. 1	Replicate No. 2	Replicate No. 3
MHA Plates	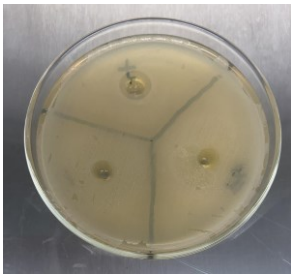	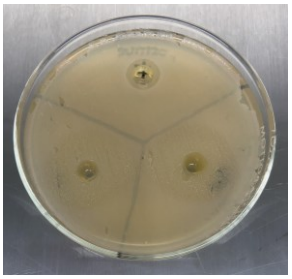	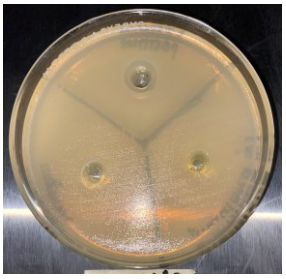

Recommendation. - To further improve the results of the study, it is recommended to perform the MIC test before proceeding with gel formulation since the literature where the MIC was based may be outdated. It is also recommended to use a higher concentration of *S. jamaicensis* extract or incorporate the extract of another plant that exhibits antibacterial properties to investigate synergistic effects to attain a higher antibacterial activity. Isolation of known phytochemicals associated with the antibacterial activity of *S. jamaicensis*, such as tannins and saponins [33], can be done to further improve its bactericidal effect. With this, it is recommended that the positive control would be the gel base incorporated with a known antibiotic with the same concentration as the extract. Furthermore, it is recommended to perform a microbial load count on the gel to determine its degree of microbial contamination. It is also recommended to use a paddle attachment in formulating the gel base in addition to the overhead stirrer to thoroughly mix the gel and reduce the formation of bubbles. Moreover, it is recommended to measure the physicochemical properties in regular intervals during AST to be able to plot a trend line that monitors the state of the gel throughout the stability testing. Lastly, it is recommended to perform the accelerated stability testing for a longer period to identify the limit of the gel and to determine its expiration date.

Acknowledgment. - The researchers would like to express their gratitude to Mrs. Zenith Villorente, Ms. Brienz Athena Suaberon, and Mr. Kent Orven Gabayeron, the professionals at Pharma GalenX Innovations Inc., for assisting them with their data gathering, specifically on the proper use of the equipment utilized for the gel formulation and physicochemical evaluation. Their guidance made a significant contribution to the success of this study.

References

[1] Bhalodia N, Shukla V. 2011. Antibacterial and antifungal activities from leaf extracts of *Cassia fistula* l.: An ethnomedicinal plant. J Adv Pharm Technol Res. 2(2): 104. doi: 10.4103/2231-4040.82956.

[2] Naik ND, Suresh B, Priyanka MP, Geethanjali B, Yamini K, Malothu R. 2012. Formulation and evaluation of herbal ointment consisting *Sida spinosa* leaves extracts. Pharm Biol. 2(2): 40–42.

[3] Ololade ZS, Ogunmola OO, Kuyooro SE, Abiona OO. 2017. *Stachytarpheta jamaicensis* leaf extract: chemical composition, antioxidant, anti-arthritic, anti-inflammatory and bactericidal potentials. Int J Sci. 6(4): 119–125.

[4] Idu M, Omogbai EKI, Aghimien GE, Amaechina F, Timothy O, Omonigho SE. 2007. Preliminary phytochemistry, antibacterial properties and acute toxicity of *Stachytarpheta jamaicensis* (L.) Vahl. Leaves. Trends Med Res. 2: 193–198. doi: 10.1155/2016/7842340.

[5] Abadilla SC, Bonete TM, Carinugan RJ. 2009. Wound healing and antibacterial property of vervain ointment from *Stachytarpheta jamaicensis* (L) Vahl (*Verbanaceae*). University of the Philippines Manila. Available from: https://bit.ly/3bk5Ic3.

[6] Loganathan VM, Animaran S, Jaswanth A, Sulaiman A, Sivaprasadha RMV, Senthil KB, Rajaseskaran A. 2001. The effects of polymers and permeation enhancers on releases of flurbiprofen from gel formulations. Indian J Pharm Sci. 63(3): 200–204.

[7] Chang RK, Raw A, Lionberger R, Yu L. 2012. Generic Development of Topical Dermatologic Products: Formulation Development, Process Development, and Testing of Topical Dermatologic Products. AAPS J. 15(1): 41–52. doi: 10.1208/s12248-012-9411-0.

[8] Taylor TA, Unakal CG. 2020. *Staphylococcus aureus*. StatPearls Publishing LLC.

[9] Jacopin E, Lehtinen S, Débarre F, Blanquart, F. 2020. Factors favouring the evolution of multidrug resistance in bacteria. J R Soc Interface. 17(168): 20200105. doi: 10.1098/rsif.2020.0105.

[10] Deli M, Ndjantou EB, Ngatchic-Metsagang JT, Petit J, Njintang-Yanou N, Scher J. 2019. Successive grinding and sieving as a new tool to fractionate polyphenols and antioxidants of plants powders: Application to *Boscia senegalensis* seeds, *Dichrostachys glomerata* fruits, and *Hibiscus sabdariffa* calyx powders. Food Sci Nutr. 7(5): 1795–1806. doi: 10.1002/fsn3.1022.

[11] Rozianoor M, Nadia K, Nurdiana S. 2014. *Stachytarpheta jamaicensis* ethanolic leaf extract as wound healer on alloxan-induced diabetic sprague dawley rats. Indian J Biotechnol. 9: 460–466. doi: 10.1155/2016/7842340.

[12] Balamurugan V, Sheerin F, Velurajan S. 2019. A guide to phytochemical analysis. Int J Adv Res Innov Ideas Educ. 5: 236–245.

[13] Yen MP, Tang G. 2019. JoVE Science Education [Internet]. Massachusetts: J Vis Exp. Available from: https://bit.ly/2IAOFqr.

[14] Aiyalu R, Govindarjan A, Ramasamy A. 2016. Formulation and evaluation of topical herbal gel for the treatment of arthritis in animal model. Braz J Pharm Sci. 52(3): 493–507.

[15] Dashnau JL, Nucci NV, Sharp KA, Vanderkooi JM. 2006. Hydrogen Bonding and the Cryoprotective Properties of Glycerol/Water Mixtures. J Phys Chem B. 110(27): 13670.

[16] Dantas MGB, Reis SAGB, Damasceno CMD, Rolim LA, Rolim-Neto PJ, Carvalho FO, Almeida JRGS. 2016. Development and evaluation of stability of a gel formulation containing the Monoterpene Borneol. Sci World J. 2016: 1–4.

[17] Ross ARS. 2005. Application of surface activity in therapeutics. Surface Activity in Drug Action. 233–293.

[18] Food and Drug Administration (FDA). 2014. Minimum number of sample units required for each test analysis. Alabang, Muntinlupa City, Philippines.

[19] Queiroz MBR., Marcelino NB, Ribeiro MV, Espindola LS, Cunha F, Silva MV. 2009. Development of gel with *Matricaria recutita* L. extract for topic application and evaluation of physical-chemical stability and toxicity. Lat Am J Pharm. 28(4): 574–579.

[20] Viswanad V, Jayakar B, Thomas L, Aleykutty N, Zacharia S. 2012. Development and evaluation of antimicrobial herbal formulations containing the methanolic extract of *Samadera indica* for skin diseases. J Adv Pharm Technol. 3(2): 106. doi: 10.4103/2231-4040.97285.

[21] Nayak SH, Nakhat PD, Yeole PG. 2005. Development and evaluation of cosmeceutical hair styling gels of ketoconazole. Indian J Pharm Sci. 52: 231–33.

[22] Krongrawa W, Limmatvapirat S, Pongnimitprasert N, Meetam P, Limmatvapirat C. 2018. Formulation and evaluation of gels containing coconut kernel extract for topical application. Asian J Pharm Sci. doi: 10.1016/j.ajps.2018.01.005.

[23] Tendencia EA. 2004. Disk diffusion method. In Laboratory manual of standardized methods for antimicrobial sensitivity tests for bacteria isolated from aquatic animals and environment (pp. 13–29). Tigbauan, Iloilo, Philippines: Aquaculture Department, Southeast Asian Fisheries Development Center.

[24] Bajaj S, Singla D, Sakhuja N. 2012. Stability testing of pharmaceutical products. J Appl Pharm Sci. 2:. 129–138. doi: 10.7324/JAPS.2012.2322.

[25] Hunt TK, Beckert S. 2005. Therapeutical and practical aspects of oxygen in wound healing. In: Lee B (ed) The Wound Management Manual. McGraw-Hill Medical, New York.

[26] Caluya ED. 2017. Wound healing potential of the crude leaf extract of *Stachytarpheta jamaicensis* Linn. Vahl (Kandikandilaan) on induced wounds in rats. 5(1). 375-381.

[27] Proksch E. 2018. pH in nature, humans and skin. J Dermatol. 45(9): 1044–1052. doi: 10.1111/1346-8138.14489.

[28] Lambers H, Piessens S, Bloem A, Pronk H, Finkel P. 2006. Natural skin surface pH is on average below 5, which is beneficial for its resident flora. Int J Cosmet Sci. 28(5): 359–370.

[29] Singh VK, Singh PK, Sharma PK, Srivastava PK, Mishra A. 2013. Formulation and evaluation of topical gel of acelofenac containing piparine. Indo Am J Pharm. 2013: 3(7).

[30] Shukr MA, Metwally GF. 2013. Evaluation of Topical Gel Bases Formulated with Various Essential Oils for Antibacterial Activity against Methicillin Resistant *Staphylococcus aureus*. Trop J Pharm Res. 12(6): 877–884.

[31] Mahalingam R, Li X, Jasti BR. 2008. Semisolid dosages: ointments, creams, and gels. Pharmaceutical Manufacturing Handbook, 267–312.

[32] Maslii Y, Ruban O, Kasparaviciene G, Kalveniene Z, Materiienko A, Ivanauskas L, Mazurkeviciute A, Kopustinskiene DM, Bernatoniene J. 2020. The Influence of pH Values on the Rheological, Textural and Release Properties of Carbomer Polacril® 40P-Based Dental Gel Formulation with Plant-Derived and Synthetic Active Components. Molecules (Basel, Switzerland). 25(21): 5018. doi: 10.3390/molecules25215018.

[33] Ruma OC, Zipagang TB. 2015. Determination of secondary metabolites and antibacterial property of extract from the leaves of *Stachytarpheta jamaicensis* (L.) Vahl. J Med Plants Stud. 3(4): 79–81.

Molecular docking of selected phytochemicals from malunggay (*Moringa oleifera*) against the chromosomal trehalose-6-phosphate phosphatase (PDB ID: 6CJ0) enzyme of *Pseudomonas aeruginosa*

ROANNE G. AZUR, RAPHAEL FRANCIS E. DEQUILLA, JOHANNA MARIE G. GAVAN, and FERNANDO CHRISTIAN G. JOLITO III

Philippine Science High School Western Visayas Campus - Department of Science and Technology (DOST-PSHSWVC), Brgy. Bito-on, Jaro, Iloilo City 5000, Philippines

Article Info

Submitted: May 13, 2021
Approved: Jun 29, 2021
Published: Aug 20, 2021

Keywords:
molecular docking
Pseudomonas aeruginosa
trehalose-6-phosphate phosphatase
phytochemicals
inhibitor

Abstract

The trehalose-6-phosphate phosphatase (TPP) enzyme, a common enzyme that is important for organism survival under stress, is utilized by some strains of *Pseudomonas aeruginosa*. Its presence in such pathogens but absence in hosts such as humans makes it a viable anti-pathogenic target. As for potential inhibitors, phytochemicals are known to possess medicinal properties and offer holistic drug action. Using molecular docking, the study screened selected phytochemicals from *Moringa oleifera* against the TPP enzyme of *P. aeruginosa*. The 13 initial phytochemicals were tested for drug-likeness using the Lipinski test, of which 11 passed and were used in the docking procedure done in AutoDock Vina. Analysis of the generated docks has shown that seven phytochemicals bind in close proximity to the active site, two bound elsewhere on the surface of the TPP enzyme, and one has both attributes. The docked phytochemicals were determined to act as either possible competitive or noncompetitive inhibitors.

Introduction. - The efficacy of antibiotics is at risk due to rapidly emerging resistant bacteria [1]. Antibiotic resistance in clinically relevant microorganisms such as *Pseudomonas aeruginosa* has been associated with an increase in hospitalization and mortality rates [2]. Antibiotic resistance is observed in microorganisms that develop the ability to survive medicine targeted against it [3]. Multidrug resistance patterns in both Gram-positive and Gram-negative bacteria are difficult to treat, if not untreatable. The increasing numbers of bacterial strains acquiring resistance to a wide range of antibiotics in recent decades is also alarming [4].

Trehalose is a disaccharide that plays an important role in the survival of some pathogens. Recent studies have highlighted its role in desiccation resistance, osmoprotection, and resistance to heat or cold [5,6,7]. One of the most studied pathways of trehalose synthesis in bacteria is the trehalose-6-phosphate phosphatase (TPP) pathway due to its conserved biosynthesis route [8]. The TPP enzyme is a member of the haloacid dehydrogenase (HAD) superfamily, a group of enzymes that facilitates the hydrolysis of a diverse range of organic phosphate substrates [9].

P. aeruginosa, a Gram-negative, opportunistic pathogen, is known to infect many organisms, including humans [10]. Surveys of genomic databases have shown that *P. aeruginosa* strains possess two different TPP coding genes which are chromosomal and extrachromosomal [11]. Trehalose can be utilized by *P. aeruginosa* as a carbon and energy source for its growth and survival [12]. An increasing number of occurrences of drug-resistant *P. aeruginosa* strains have been observed in recent years [12]; a solution to this problem must be urgently identified.

Studies have shown the potential of phytochemicals in antibiotic resistance research [13]. Phytochemicals are known to affect specific molecular targets both directly and indirectly through affecting metabolic pathways as stabilized conjugates [14]. They are also known to have a wide range of medicinal properties and offer holistic drug action against pathogens without having many side effects [15].

One important factor to consider in the invention of new drugs is the risk that such drugs would target additional or multiple receptors [16]. According to the study of Umesh et al. [13], the TPP enzyme could become a viable anti-pathogenic target due to its important role in pathogen stress tolerance while being completely absent in animal hosts. However, there has only been limited research done utilizing the chromosomal TPP enzyme of *P. aeruginosa* as an

How to cite this article:
CSE: Azur RG, Dequilla RFE, Gavan JMG, Jolito FCC III. 2021. Molecular docking of selected phytochemicals from malunggay (*Moringa oleifera*) against the chromosomal trehalose-6-phosphate phosphatase (TPP) enzyme of *Pseudomonas aeruginosa*. Publiscience. 4(1): 45–50.
APA: Azur, R.G., Dequilla, R.F.E., Gavan, J.M.G., & Jolito, F.C.C. III. 2021. Molecular docking of selected phytochemicals from malunggay (*Moringa oleifera*) against the chromosomal trehalose-6-phosphate phosphatase (TPP) enzyme of *Pseudomonas aeruginosa*. *Publiscience*, *4*(1), 45–50.

For supplementary data, contact: publiscience@wvc.pshs.edu.ph.

anti-pathogenic target.

In recent years, the incorporation of computer-based methods in medicinal chemistry has brought with it advantages in rational drug design [17]. Methods such as molecular docking are now available for the *in silico* study of biological systems and drug discovery [17].

The present study proposed to virtually screen the selected phytochemicals from *Moringa oleifera* against the chromosomal trehalose-6-phosphate phosphatase (TPP) enzyme of *P. aeruginosa*. Phytochemicals from *M. oleifera* were used as they were the most abundant types of phytochemical [18], and others have already been used in previous molecular docking studies [19]. Specifically, the study aimed to:

(i) evaluate the drug-likeness of the phytochemicals using the Lipinski rule through SwissADME;

(ii) identify the predicted binding sites of the selected phytochemicals to the TPP enzyme of *P. aeruginosa* through AutoDock Vina;

(iii) predict the interactions between the TPP enzyme and each phytochemical through LigPlot+; and

(iv) provide proof-of-concept for the mechanism of binding between each phytochemical and the TPP enzyme.

Methods. - A preliminary Lipinski test was conducted to test the drug-likeness of 13 selected phytochemicals from *M. oleifera*. The phytochemicals which passed the test were then subjected to molecular docking with the chromosomal TPP enzyme of *P. aeruginosa* using AutoDock Vina [20]. Data analysis on the predicted binding sites and interactions was done using LigPlot+ [21], PyMOL [22], and UCSF Chimera [23]. The phytochemicals' potential to be possible inhibitors of the TPP enzyme was contextualized using existing literature.

Selection of Phytochemicals. Thirteen phytochemicals involved in the studies of Lin et al. [18] and Zainab et al. [19] from *M. oleifera* were selected to be docked with the TPP enzyme. These phytochemicals and their respective PubChem Compound ID numbers are: (1) alpha-carotene (4369188), (2) anthraquinone (6780), (3) apigenin (439726), (4) excoecariatoxin (5281400), (5) flavylium (145858), (6) hemlock tannin (15559687), (7) isorhamnetin (5281654), (8) kaempferol (5280863), (9) laurifolin (102301875), (10) phenolic steroid (439726), (11) quercetin (5280343), (12) serpentine (73391), and (13) sitogluside (5742590). The three-dimensional structures of trehalose-6-phosphate (T6P)-substrate (positive control), carbon tetrachloride (negative control), and the phytochemicals in structured data format (SDF) were retrieved from the National Center for Biotechnology Information (NCBI) PubChem.

Lipinski Test for Drug-likeness. To evaluate and assess compounds during drug discovery and optimization, the Lipinski rule of five is used [24]. The phytochemicals were evaluated for their drug-likeness using the Lipinski rule by uploading their SDF files to SwissADME, a web-based application [25]. The phytochemicals that passed the rule with one or no violations were the only ligands to be tested with TPP.

Preparation of Molecular Models. The three-dimensional structure of TPP (PDB ID: 6CJ0) in PDB format was retrieved from Protein Data Bank (PDB). The natural ligands (CO_3 and Mg^{+2}) of the TPP enzyme were deleted using UCSF Chimera before the file was saved in PDB format. This file was then opened in AutoDock Tools to remove water molecules to avoid distortion in the search for possible binding sites [26]. Afterward, polar hydrogen atoms were added to establish the hydrogen bonds that may be involved in the binding of the protein and ligand. The whole macromolecule was enclosed by the grid box. The offset numbers and the number of points in the x, y, and z dimensions were noted down to define the search space for ligand binding in AutoDock Vina . The TPP was saved as a PDBQT file. Moreover, the SDF files of each phytochemical were converted in PDB format using UCSF Chimera. The substrate and each phytochemical were then opened in AutoDock Tools to detect its root to assign rotatable torsion angles of the ligand. After that, the controls and each phytochemical were saved as a PDBQT file.

Molecular Docking Proper. The config file was written in Python programming language. The input placed were the receptor (TPP enzyme) and the ligand (phytochemicals and controls). The filenames of the output of AutoDock Vina in PDBQT and TXT format were then stated. After, the offset values and grid box size were also stated. The exhaustiveness was then set to 24. The MS/DOS command prompt was opened to run AutoDock Vina. The directory was changed to the file path of the folder where the PDBQT and config files were saved. To dock the ligand and the receptor, the file path of the .exe file of AutoDock Vina was pasted on the command prompt. This was then followed by two dashes and the word 'config' and its TXT file extension.

Data Analysis. AutoDock Vina automatically generates the top nine conformations per ligand. Each conformation of the docked ligand and receptor was individually saved as a PDB file using PyMOL The PDB files of the conformations were analyzed using UCSF Chimera and LigPlot+. LigPlot+ was utilized to analyze the two-dimensional (2D) structure of the conformations and to generate schematic 2D diagrams of ligand-protein interactions. The amino acids involved in hydrogen bonding and hydrophobic interactions were noted down and verified using UCSF Chimera, which was also used to generate three-dimensional (3D) structures of the conformations.

Safety Procedure. Since the study was done *in silico*, the researchers took frequent breaks and practiced the 20-20-20 rule; every 20 minutes, watch an object 20 feet away for 20 seconds. This was done to ensure that the researcher's eyes were not strained from long exposure to digital screens during the data gathering procedure.

Results and Discussion. - The study aimed to virtually screen the selected phytochemicals from *M. oleifera* against the chromosomal trehalose-6-phosphate phosphatase (TPP) enzyme of *P. aeruginosa*. The 13 selected phytochemicals were subjected to the Lipinski rule. Those that passed were docked with the TPP enzyme using AutoDock Vina. Each generated conformation was then analyzed using UCSF Chimera and LigPlot+.

Lipinski Drug-likeness Test. According to the Lipinski rule, the requirements for a compound to be considered drug-like state that an orally active drug must not violate more than one of the following criteria: the molecular weight should not exceed 500 grams/mole, the MlogP [27] should not exceed 4.15, there must not be more than five hydrogen bond donors, and there must not be more than ten hydrogen bond acceptors [28]. The 13 phytochemicals were subjected to Lipinski drug-likeness test using SwissADME. Among the 13 phytochemicals, 11 passed the Lipinski drug-likeness test. These can be referred to in Table 1.

Table 1. Drug-likeness of selected *M. oleifera* phytochemicals based on Lipinski rule.

a	*b*	*c*	*d*	*e*	*f*
Alpha-carotene*	536.87	12.46	0	0	2
Anthraquinone	208.21	1.86	0	2	0
Apigenin	270.24	0.52	5	3	0
Excoecariatoxin	528.63	1.47	3	8	1
Flavylium	207.25	3.28	0	1	0
Hemlock tannin*	578.52	-0.26	10	12	3
Isorhamnetin	316.26	-0.31	4	7	0
Kaempferol	286.24	-0.03	4	6	0
Laurifolin	356.37	1.09	3	6	0
Phenolic steroid	256.38	4.46	1	1	1
Quercetin	302.24	-0.56	5	7	0
Serpentine	349.40	2.21	0	4	0
Sitogluside	576.85	3.96	4	6	1

a Phytochemical; *b* Molecular weight (g/mol); *c* MlogP; *d* No. of hydrogen bond donors; *e* No. of hydrogen bond acceptors; *f* No. of violations; *Phytochemicals that did not pass the Lipinski test.

Alpha-carotene and hemlock tannin did not meet two and three out of four criteria, respectively; they were not included in the list of phytochemicals that were used in the molecular docking process.

Analysis of Predicted Binding Sites and Interactions. After generating the top nine conformations in AutoDock Vina, the top two poses of each docked ligand (phytochemical or control) were selected to be analyzed further. For ligands which are bound restrictively to one chain, the two poses correspond to the top-ranked conformations for Chain A and Chain B, respectively. For ligands that interacted with both chains, the first and second-ranked conformations were selected.

The chromosomal TPP enzyme of *P. aeruginosa* is a member of the haloacid dehydrogenase (HAD) superfamily [11], which comprises enzymes such as phosphatases, ATPases, phosphomutases, phosphonatases, and dehalogenases [29]. TPP possesses a core phosphatase domain with α/β-hydrolase fold, which is common among the hydrolase family, as well as a cap domain [30]. While the fold of the core domain, which functions as base and side walls of the active site, is well conserved among the HAD superfamily, the cap domain, which functions as the cover, can vary in size and structure [30]. Through comparisons to other bacterial TPPs, the structure of the TPP enzyme from *P. aeruginosa* is also revealed to have four HAD conserved motifs located in the core domain [11].

The study found that all of the top predicted conformations of the docked phytochemicals interacted with amino acid residues located in the core domain. The top predicted conformations (for both chain A and B) of seven phytochemicals were in close proximity to the active site of the TPP enzyme; this is because they bound to one or more motifs within the core domain [11]. The exception is the top predicted conformation of sitogluside in chain A since it is bound near the β12 sheet. The other two phytochemicals (flavylium and serpentine) that did not bind near the active site were also bound to amino acid residue/s near the β12 sheet, the hydrophobic interface that links the two monomers.

The active site of an enzyme is defined as the region that binds the substrate (a ligand that becomes the starting material of an enzymatic reaction) and converts it into a product [31]. It is formed by amino acid residues; the properties and spatial arrangement of these determine which molecules can bind to and become substrates for the enzyme. The forces which bind the substrate are multiple weak forces such as hydrogen bonds, hydrophobic interactions, electrostatic interactions, and van der Waals bonds [31]. This study only observed the hydrogen and hydrophobic bonds that each phytochemical had with the TPP enzyme.

The phytochemicals anthraquinone, apigenin, isorhamnetin, kaempferol, laurifolin, phenolic steroid, and quercetin may be possible competitive inhibitors since these phytochemicals bind in close proximity to the active site of the TPP enzyme – all of these phytochemicals bound to one or more motifs – through steric hindrance. Steric hindrance prevents the further interaction of the natural substrate to the receptor when a competitive inhibitor is bound to the active site [32]. This effect of steric hindrance implies that if the phytochemicals bound to the active site of the TPP enzyme, T6P (the natural substrate) could not be catalyzed by the TPP enzyme into trehalose.

As for flavylium and serpentine, they could be considered as allosteric modulators or possible noncompetitive inhibitors due to their binding site being quite different from the active site. Allosteric

modulators bind elsewhere on the protein surface other than the active site and induce an allosteric conformational change of the active site of the receptor by shifting the free energy landscape [33,34] However, while noncompetitive inhibitors may or may not affect the structure of the protein, it is less certain what effect they may have on the binding affinity of the natural substrate since noncompetitive inhibitors do not compete with the substrate for active site binding [35].

As for sitogluside, its different conformation in each chain may suggest that it may possibly act as an allosteric modulator (in the case of Chain A) or a competitive inhibitor (in the case of Chain B). This is illustrated in Figures 1 and 2.

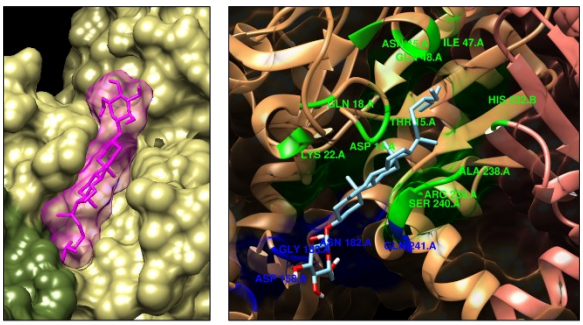

Figure 1. *(a)* Third-ranked predicted binding site of sitogluside in the TPP enzyme; *(b)* Top predicted binding site of sitogluside in chain A of the TPP enzyme with corresponding amino acid residues with *(green)* hydrogen bonds or *(blue)* hydrophobic bonds.

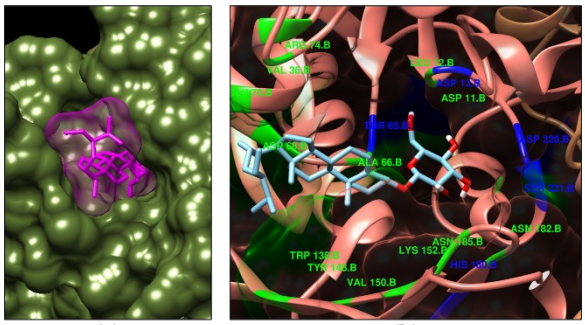

Figure 2. *(a)* Top-ranked predicted binding site of sitogluside in the TPP enzyme; *(b)* Top predicted binding site of sitogluside in chain B of the TPP enzyme with corresponding amino acid residues with *(green)* hydrogen bonds or *(blue)* hydrophobic bonds.

Inhibiting the T6P-substrate from binding to the active site would eventually lead to its accumulation. The intracellular accumulation of T6P is toxic to host organisms [36]. Previous studies determined that T6P accumulation can be lethal to *Caenorhabditis elegans* and *Mycobacterium tuberculosis* [36,37]. This adverse effect is due to the inhibition of metabolic enzymes such as phosphotransferases caused by sugar-phosphatases acting as antimetabolites [38]. The effects of the accumulation of T6P in *P. aeruginosa* are still unknown. However, the widespread toxicity of T6P and the presence of a glycolytic enzyme - known to be inhibited by T6P in other organisms - in *P. aeruginosa* all suggest that T6P accumulation may have adverse effects on the bacteria [11].

Antibacterial Properties of Phytochemicals. Several of the phytochemicals are already known to exhibit antibacterial properties against bacteria. Likewise, *M. oleifera* is also known to exhibit antibacterial properties against both Gram-positive and Gram-negative bacteria [39]. As for the phytochemicals, four of the seven possible competitive inhibitors are known to exhibit antibacterial activity against *P. aeruginosa* [40,41,42,43]. There is a lack of studies on the antibacterial activity of isorhamnetin, and the noncompetitive inhibitors flavylium and serpentine, against *P. aeruginosa*. Sitogluside exhibited low activity against *P. aeruginosa* in a study testing the antibacterial activity of daucosterol isolated from the roots of *Cissus populnea* [44].

Limitations. The study was not able to analyze the top rankings of excoecariatoxin since the generated conformation files could not be opened in LigPlot+ for further data analysis. This affected the third objective because the study was not able to predict the interactions between the TPP enzyme and the excoecariatoxin.

Conclusion. - The study concluded that after virtually screening the selected phytochemicals *of M. oleifera* against the chromosomal trehalose-6-phosphate phosphatase (TPP) enzyme of *P. aeruginosa*, all of the 11 docked phytochemicals that were analyzed are either possible competitive inhibitors or allosteric modulators of the enzyme.

Recommendations. - The researchers would recommend the utilization of software programs which could process the docked excoecariatoxin conformations. *In situ* analysis via nuclear magnetic resonance spectroscopy is also encouraged to examine the possible allosteric sites. Isothermal titration calorimetry to confirm the intended binding target of the TPP enzyme and each phytochemical is also recommended.

Acknowledgement. - The authors would like to thank the SIDHI Mentorship community for providing the opportunity to hold consultations and provide insights regarding the study. The authors would also like to thank Mr. Jose Sandino Bandonil of Academia Sinica and of the SIDHI Mentorship community, and Mr. Romie Azur, Science Research Specialist II at the National Institute of Molecular Biology and Biotechnology of the University of the Philippines-Diliman, for their guidance in the data gathering and data analysis procedures.

References

[1] Ventola CL. 2015. The antibiotic resistance crisis. P.T. 40(4): 277-283. PMID: 25859123.

[2] Berendonk, TU, Manaia CM, Merlin C, Fatta-Kassinos D, Cytryn E, Walsh F, Bürgmann H, Sorum H, Norström M, Pons MN, and others. 2015. Tackling antibiotic resistance: the environmental framework. Nat Rev Microbiol. 13(2015): 310–317. doi: 10.1038/nrmicro3439.

[3] CDC. 2020. About antibiotic resistance. [Internet]. Centers for Disease Control and Prevention;

[cited 2021 Feb 27]. Available from: https://bit.ly/3eNL9F9.

[4] Lewis R. 1995. The rise of antibiotic-resistant infections. FDA. 1–7. PMID: 10145087.

[5] Iordachescu M, Imai R. 2011. Trehalose and abiotic stress in biological systems. In: Shanker A, Venkateswarlu B, editors. 2011. Abiotic stress in plants: mechanisms and adaptations. IntechOpen. doi: 10.5772/22208. Available from: https://bit.ly/2QMMxQr.

[6] Ash C. 2017. Trehalose confers superpowers. Science. 358(6869): 1398.5–1399. doi: 10.1126/science.358.6369.1398-e.

[7] Zeidler S, Hubloher J, Schabacker K, Lamosa P, Santos H, Müller V. 2017. Trehalose, a temperature- and salt-induced solute with implications in pathobiology of *Acinetobacter baumannii*. Environ Microbiol. 19(12): 5088–5099. doi: 10.1111/1462-2920.13987.

[8] Avonce N, Mendoza-Vargas A, Morett E, Iturriaga G. 2006. Insights on the evolution of trehalose biosynthesis. BMC Evol Biol. 6(109): 1–15. doi: 10.1186/1471-2148-6-109.

[9] Koonin EV, Tatsutov RL. 1994. Computer analysis of bacterial haloacid dehalogenases defines a large superfamily of hydrolases with diverse specificity: application of an iterative approach to database search. J Mol Biol. 244(1): 125–132. doi: 10.1006/jmbi.1994.1711.

[10] Sadikot RT, Blackwell TS, Christman JW, Prince AS. 2005. Pathogen-host interactions in *Pseudomonas aeruginosa* pneumonia. Am J Respir Crit Care Med. 171: 1209–1223. doi: 10.1164/rccm.200408-1044so.

[11] Cross M, Biberacher S, Park SY, Rajan S, Korhonen P, Gasser RB, Kim JS, Coster MJ, Hofmann A. 2018. Trehalose 6-phosphate phosphatases of *Pseudomonas aeruginosa*. FASEB J. 32(2018): 5470–5482. doi: 10.1096/fj.201800500R.

[12] Argüelles. 2000. Physiological roles of trehalose in bacteria and yeasts: a comparative analysis. Arch Microbiol. 174(4): 217–224. doi: 10.1007/s002030000192.

[13] Umesh HR, Ramesh KV, Devaraju KS. 2020. Molecular docking studies of phytochemicals against trehalose–6–phosphate phosphatases of pathogenic microbes. Beni-Suef Univ J Basic Appl Sci. 9(5): 1–14. doi: 10.1186/s43088-019-0028-6.

[14] Jagadeeshan S, Prasad MM, Nair SA. 2018. Role of deguelin in chemoresistance. In: Aggarwal B, Alok B. 2018. Role of Nutraceuticals in Cancer Chemosensitization, Volume 2. 287–296. doi: 10.1016/B978-0-12-812373-7.00014-0.

[15] Barbieri R, Coppo E, Marchese A, Daglia M, Sobarzo-Sánchez E, Nabavi SF, Nabavi SM. 2017. Phytochemicals for human disease: an update on plant-derived compounds antibacterial activity. Microbiol Res. 196: 44–68. doi: 10.1016/j.micres.2016.12.003.

[16] Dickson M, Gagnon JP. 2004. Key factors in the rising cost of new drug discovery and development. Nat Rev Drug Discov. 3(2004): 417–429. Available from: https://go.nature.com/3eaFCtv.

[13] Umesh HR, Ramesh KV, Devaraju KS. 2020. Molecular docking studies of phytochemicals against trehalose–6–phosphate phosphatases of pathogenic microbes. Beni-Suef Univ J Basic Appl Sci. 9(5): 1–14. doi: 10.1186/s43088-019-0028-6.

[17] Ramírez D. 2016. Computational methods applied to rational drug design. Open J Med Chem. 10(1): 7–20. doi:10.2174/1874104501610010000.

[18] Lin M, Zhang J, Chen X. 2018. Bioactive flavonoids in *Moringa oleifera* and their health-promoting properties. J Funct Foods. 47(2018): 469–479. doi: 10.1016/j.jff.2018.06.011.

[19] Zainab B, Ayaz Z, Alwahibi MS, Khan S, Rizwana H, Soliman DW, Alawaad A, Abbasi AM. 2020. *In-silico* elucidation of *Moringa oleifera* phytochemicals against diabetes mellitus. Saudi J Biol Sci. 27(9): 2299–2307. doi: 10.1016/j.sjbs.2020.04.002.

[20] Trott O, Olson AJ. 2010. AutoDock Vina: improving the speed and accuracy of docking with a new scoring function, efficient optimization and multithreading. J Comput Chem. 31(2010): 455-461. doi:10.1002%2Fjcc.21334.

[21] Laskowski RA, Swindells MB (2011). LigPlot+: multiple ligand-protein interaction diagrams for drug discovery. J Chem Inf Model., 51, 2778-2786. doi:10.1021/ci200227u.

[22] The PyMOL Molecular Graphics System, Version 1.2r3pre, Schrödinger, LLC. https://pymol.org/2/.

[23] Pettersen EF, Goddard TD, Huang CC, Couch GS, Greenblatt DM, Meng EC, Ferrin TE. 2004. UCSF Chimera--a visualization system for exploratory research and analysis. J Comput Chem. 25(13): 1605-1612. doi:10.1002/jcc.20084.

[24] Pollastri MP. 2010. Overview on the rule of five. Curr Protoc Pharmacol. 49(1): 9.12.1–9.12.8. doi: 10.1002/0471141755.ph0912s49.

[25] Daina A, Michielin O, Zoete V. 2017. SwissADME: a free web tool to evaluate pharmacokinetics, drug-likeness and medicinal chemistry friendliness of small molecules. Sci Rep. 7(1): 1-13. doi:10.1038/srep42717.

[26] Forli S, Huey R, Pique ME, Sanner MF, Goodsell DS, Olson AJ. 2016. Computational protein–

ligand docking and virtual drug screening with the AutoDock suite. Nature Protocols. 11(5): 905–919. doi: 10.1038/nprot.2016.051.

[27] Moriguchi I, Hirono S, Nakagome I, Hirano H. 1994. Comparison of reliability of log P values for drugs calculated by several methods. Chem Pharm Bull. 42(4): 976–978. doi: 10.1248/cpb.42.976.

[28] Lipinski CA, Lombardo F, Dominy BW, Feeney PJ. 2001. Experimental and computational approaches to estimate solubility and permeability in drug discovery and development settings. Adv Drug Deliv. 46(1–3): 3–26. doi: 10.1016/s0169-409x(00)00129-0.

[29] Burroughs AM, Allen KN, Dunaway-Mariano D, Aravind L. 2006. Evolutionary genomics of the HAD superfamily: understanding the structural adaptations and catalytic diversity in a superfamily of phosphoesterases and allied enzymes. J Mol Biol. 361(5):1003–1034. doi: 10.1016/j.jmb.2006.06.049.

[30] Rao KN, Kumaran D, Seetharaman J, Bonanno JB, Burley SK, Swaminathan S. 2006. Crystal structure of trehalose-6-phosphate phosphatase– related protein: biochemical and biological implications. Protein Sci. 15(2006): 735–1744. doi: 10.1110/ps.062096606.

[31] Aryal S. 2018. Enzymes – properties, classification and significance. [Internet]. Microbenotes; [cited 2021 April 21]. Available from: https://bit.ly/3vuU31h.

[32] Kenakin T. 2016. Allosterism in drug discovery. Chapter 2. Identifying and quantifying allosteric drug function. eISBN:978-1-78262-927-6. doi: 10.1039/9781782629276-00024.

[33] Wood MR, Hopkins CR, Brogan JT, Conn PJ, Lindsley CW. "Molecular switches" on mGluR allosteric ligands that modulate modes of pharmacology. Biochemistry 2011; 50: 2403–10. doi: 10.1021/bi200129s.

[34] Nussinov R. 2012. The different ways through which specificity works in orthosteric and allosteric drugs. Curr Pharm Des. 18(9): 1311–1316. doi: 10.2174/138161212799436377.

[35] Delaune KP, Alsayouri K. 2020. Physiology, noncompetitive inhibitor. StatPearls. [accessed 2021 April 26]. Available from: https://bit.ly/3vuU6Kv.

[36] Kormish JD, McGhee JD. 2005. The *C. elegans* lethal gut-obstructed gob-1 gene is trehalose6-phosphate phosphatase. Dev Biol. 287(1): 35–47. doi: 10.1016/j.ydbio.2005.08.027.

[37] Korte J, Alber M, Trujillo CM, Syson K, Koliwer-Brandl H, Deenen R, Kohrer K, DeJesus MA, Hartman T, Jacobs WR Jr., and others. (2016) Trehalose-6-phosphate-mediated toxicity determines essentiality of OtsB2 in *Mycobacterium tuberculosis* in vitro and in mice. PloS Pathog. 12: e1006043. doi: 10.1371/journal.ppat.1006043.

[38] Liu C, Dunaway-Mariano D, Mariano PS. 2017. Rational design of first eneration inhibitors for trehalose 6-phosphate phosphatases. Tetrahedon. 73(2017): 1324–1330. doi: 10.1016/j.tet.2017.01.041.

[39] Rahman MM, Sheikh MMI, Sharmin SA, Islam MS, Rahman MA, Rahman MM, Alam MF. 2009. Antibacterial ability of leaf juice and extracts of *Moringa oleifera* Lam. against some human pathogenic bacteria. CMU J Nat Sci. 8(2): 219–227. [accessed 2021 Jan 29]. Available from: https://bit.ly/2PDvsb9.

[40] Lenta BN, Weniger B, Antheaume C, Noungoue DT, Ngouela S, Assob JCN, VonthronSenecheau C, Fokou PA, Devkota KP, Tsamo E, and others. 2007. Anthraquinones from the stem bark of *Stereospermum zenkeri* with antimicrobial activity. Phytochemistry. 68(11):1595–1599. doi: 10.1016/j.phytochem.2007.03.037.

[41] Nayaka HB, Londonkar RL, Umesh MK, Tukappa A. 2014. Antibacterial attributes of apigenin, isolated from *Portulaca oleracea* L. Int J Bacteriol. 2014. doi:10.1155/2014/175851. [accessed 2021 Jan 23]. Available from: https://bit.ly/2QKmwBr.

[42] Ha LK, Kong HJ, Cho YL, Gue JC, Sang KS, Hwang JS, Chung P. 2012. Antimicrobial and anti-wrinkle effect of kaempferol and kaempferol rhamnosides isolated from *Hibiscus cannabinus* L. The Korean Journal of Medicinal Crop Science. doi:10.7783/KJMCS.2012.20.6.454. [accessed 2021 Jan 23]. Available from: https://bit.ly/3396uU4.

[43] Ouyang J, Sun F, Feng W, Sun Y, Qiu X, Xiong L, Liu Y, Chen Y. 2016. Quercetin is an effective inhibitor of quorum sensing, biofilm formation and virulence factors in *Pseudomonas aeruginosa*. J Appl Microbiol. 120(2016): 966–974. doi: 10.1111/jam.13073.

[44] Nyemb JN, Djankou MT, Talla E, Tchinda AT, Ngoudjou DT, Iqbal J, Mbafor JT. 2018. Antimicrobial, α-Glucosidase and alkaline phosphatase inhibitory activities of bergenin, the major constituent of *Cissus populnea* roots. Med Chem. 08(02). doi:10.4172/2161-0444.1000492. [accessed 2021 Jan 24]. Available from: https://bit.ly/3hsY02S.

CLUSTER FOUR

AGRICULTURE

The earthly green is the color most associated with nature and its bounties. This is also where the leaf-inspired gems take their inspiration from. The toils of agriculture have long reaped results, from milestones in harvesting and food production to significant developments in procedure and emerging technologies. It is through research and scientific breakthroughs that the agricultural sector is overcoming the challenges facing it. These research studies sought to analyze, determine, and test various methods that can provide increased insight into agricultural research and development.

These studies also fall under the Aquatic, Agriculture, and Natural Resources (AANR) Research and Development Agenda. They are in line with the goal of developing improved and sustainable agricultural management.

BASED ON: Harmonized National Research and Development Agenda (HNRDA)

Publiscience Vol. 4 Issue 1

The effect of humic acid and inorganic fertilizer application on the growth and yield of *Ipomoea reptans* Poir. (kangkong)

JOHN ONEIL M. ALCOBILLA, NADINE T. BAUTISTA, JAY VANERI T. PORRAS, and JULNAFE B. LIBO-ON

Philippine Science High School Western Visayas Campus - Department of Science and Technology (DOST-PSHSWVC), Brgy. Bito-on, Jaro, Iloilo City 5000, Philippines

Article Info

Submitted: May 11, 2021
Approved: Aug 08, 2021
Published: Aug 30, 2021

Keywords:
Ipomoea reptans
urea
humic acid
plant growth and yield
randomized complete block design

Abstract

Humic acid (HA), a plant growth stimulator, has not yet established its credibility despite being utilized for several decades in agriculture. Therefore, this study determined the effect of HA and its combined effect with inorganic fertilizer on the growth and yield of *I. reptans*. In each of the two sites, four plots replicated thrice were constructed with three treatment groups - T0B (HA only), T1 (inorganic fertilizer only), and T2 (HA + inorganic fertilizer) - and one control group (T0A, soil only). The plant height and stem diameter of ten randomly chosen plants were measured every 7 days for 21 days while the crop yield was determined 35 days after sowing. From the analysis, significant differences were found in only one of the two sites. Results showed that the treatment with HA only was significantly higher in plant height and crop yield. Data from this study contributes to the current knowledge of crop production for local farmers and the agricultural community.

Introduction. - Agriculture is an essential part of the Philippine economy as it involves 22.9% of Filipino workers and contributes about 9.2% of the gross domestic product as of 2019. However, there is a decrease in crop production of 0.7% in 2018 and 1.0% in 2019 compared to the years preceding them [1]. To address this, researchers have studied the many factors affecting plant growth and productivity, mainly the effects of nutrient composition [2]. Different fertilizers with varying concentrations of nutrients, mainly nitrogen, phosphorus, and potassium, supply plants with the nutrients necessary for their growth. In addition, the increasing amounts of fertilizer increase plant growth, and there are optimal concentrations of these nutrients for optimizing the growth of certain plants [3]. Aside from these nutrients, plant growth simulators such as humic substances have been studied on their positive effects on plant growth and yield.

Humic substances (HSs) are the brown to black, fully decomposed remains of plant or animal organic matter that compose about 80% of organic matter in dark soils [4]. These substances arise from the physical, chemical, and microbiological transformation of biomolecules, and can be divided into three components: fulvic acids (FAs), humic acids (HAs), and humin [5]. Due to their molecular structure, HSs provide numerous benefits to crop production as they help break up clay and compacted soils, assist in transferring micronutrients from the soil to the plant, enhance water retention, increase seed germination rates and penetration, and stimulate the development of microflora populations in soils [6].

Humic substances have been established to also facilitate plant growth and yield as they increase nutrient availability and improve the physical structure of the soil [7, 8]. These substances also have a role in plant metabolism as they contain growth-triggering hormones such as auxin and gibberellins [9]. These hormones promote cell elongation which mainly affects plant height and the development of plant roots [10]. Furthermore, HA has been shown to increase macronutrient and micronutrient uptake of plants [11].

In the Philippines, one of the commonly-used agricultural plants is upland kangkong, also known as *Ipomoea reptans*, which is one of the most cultivated leafy vegetables in Southeast Asia [12]. Although being primarily used for human consumption, *I. reptans* is also considered a common medicinal plant in some Southeast Asian countries, having purgative, anti-inflammatory, hypolipidemic, antidiabetic, diuretic, antiepileptic, and antimicrobial properties [13]. However, in the Philippines, the growth and yield potential of *I. reptans* has not yet been fully exploited due to the inadequate use of inputs and lack of information on its production [14], which includes the utilization of humic substances among others. Given these conditions, it is necessary to utilize HA in fertilizers and determine whether it improves the growth of *I. reptans*. It is hypothesized that combining HA with fertilizers will improve *I. reptans* growth and yield as HA increases nutrient uptake and photosynthesis and respiration rates of plants [8].

This study focused on the effect of HA and its combined effect with inorganic fertilizer on the

How to cite this article:
CSE: Alcobilla JOM, Bautista NT, Porras JVT, Libo-on JB. 2021. The effect of humic acid and inorganic fertilizer application on the growth and yield of *Ipomoea reptans* Poir. (kangkong). Publiscience. 4(1): 52–57.
APA: Alcobilla, J. O. M. , Bautista N. T., Porras J. V. T., & Libo-on J. B. (2021). The effect of humic acid and inorganic fertilizer application on the growth and yield of *Ipomoea reptans* Poir. (kangkong). *Publiscience*, *4*(1), 52–57.

For supplementary data, contact: publiscience@wvc.pshs.edu.ph.

growth and yield of *I. reptans*. Data from this research can be used to establish the credibility of HA utilization in agriculture, and contribute to the knowledge of the production of *I. reptans* species for local farmers.

This research aims to determine the effect of HA and additionally its combined effect with inorganic fertilizer on the growth and yield of *I. reptans*. Specifically, it aimed to:

(i) measure the plant height (cm), stem diameter (cm), and yield (kg/ha) of *I. reptans*. treated without HA (control; T0A), with HA alone (T0B), without HA but with inorganic fertilizer (T1), and treated with combined HA and inorganic fertilizer (T2);

(ii) determine whether using HA improves growth and yield of *I. reptans* by comparing the means of each parameter per treatment group using One-Way ANOVA;

(iii) determine which among the treatment groups is best used for *I. reptans*. production.

Methods. - The methodology is divided into six (6) parts: plot preparation and seed sowing, randomization, watering and monitoring, treatment application, measuring of parameters, and statistical analysis.

Research sites. The two (2) set-ups were done in Barangay Buray, Oton, Iloilo (10° 42' 12" N 122° 28' 6" E) which has soil classified in the Santa Rita soil series [15] and Barangay Balabag, Malay, Aklan (11° 58' 0" N 121° 55' 39" E) using the same soil series. The locations were chosen due to their proximity to the residences of the researchers for easy monitoring. The data was gathered for 35 days. The research conducted in Oton lasted from January 12, 2021, to February 16, 2021, while the one conducted in Malay lasted from January 19, 2021, to February 25, 2021.

Plot Preparation and Seed Sowing. A plot had dimensions of 30 cm by 40 cm. Before sowing the seeds, the soil was tilled up to 15 cm deep while it was moist. Six (6) planting holes were placed in each plot with three (3) seeds in each planting hole, 1-centimeter deep into the soil [12], which amounted to a total of 18 seeds per unit plot. Commercially available *I. reptans* seeds were used.

Randomization. The replicates and plots were laid out in a randomized complete block design. Each replicate was randomized separately (RCBD) [16, 17]. The 18 plants in each plot were labeled from 1 to 18 respectively. A random number generator from 1 to 18 was used to generate 10 random numbers in each plot to determine which plants were measured. The same selected plants that were measured remained constant throughout the weekly data gathering process.

Watering and Monitoring. The treatment plots were monitored daily. They were watered once at 17:00 with a volume of 500 mL of tap water per plot [18]. The plants were not watered if the surface of the soil is moist to the touch and the soil was also weeded when necessary. A screen was also constructed to protect the plants from any damage from pests.

Treatment Application. Two (2) set-ups were made simultaneously, each having three (3) treatment groups and one (1) control group. The treatments evaluated are as follows — T0B: soil applied with HA; T1: inorganic fertilizer + soil; T2: inorganic fertilizer + HA +soil. On the other hand, the control group that was evaluated was T0A: soil only. For the inorganic fertilizer, 250 kg/ha of urea fertilizer (46% N) was applied 7, 14, 21, and 28 DAS [19]. Five hundred (500) mL of 0.1% (1 g/L) solution of HA was applied in the plot every 14 days [20]. POWHUMUS® WSG 85 was used for the HA, derived as potassium humate, manufactured by HuminTech and contains 68-73% total humic acids [20]. The instructions indicated on the product packaging were the basis for the concentrations used in the study. Ramgo Plant Nutrition: Urea Fertilizer by Ramgo International Corporation was used for the inorganic fertilizer.

Measuring of parameters. The plant height and stem diameter were measured every seven (7) days starting at 14 DAS until 35 DAS and were recorded in centimeters (cm). The plant height was measured in cm from the ground level to the tip of the highest growing point using a ruler with ± 0.1 cm accuracy [21]. On the other hand, the stem diameter was measured in cm at the ground level at the base of the plant using a Vernier caliper with ± 0.05 cm accuracy [21]. The crop yield was determined by measuring the fresh weight in grams (g) using a top-loading balance with an accuracy of ±0.01g. The measured weight was then used in the formula below to determine the crop yield in kilograms per hectare (kg/ha) [22].

$$crop\ yield\ (\frac{kg}{ha}) = \frac{yield/plot\ (in\ g)\ \times\ 10^8 cm^2}{1200\ cm^2\ \times\ 1000}$$

Statistical analysis. The raw data collected was subjected to analysis using One-way Analysis of Variance (ANOVA) at 95% confidence level (α=0.05) using Microsoft Excel 365. It was done on groups of the same time point. The Least Significant Difference post-hoc analysis was then made to determine which groups exist a significant difference.

Safety Procedure. The wearing of proper gardening attire was observed during the conduct of the study. The chemicals used were also stored and sealed properly in a glass bottle and a copy of the chemical's MSDS was also kept at all times.

Results and Discussion. - Means of the gathered data were statistically analyzed using one-way ANOVA, and subjected to the Least Significant Difference (LSD) test as post-hoc analysis.

Kangkong in Oton site vs in Malay site. Significant differences were found in the three parameters—plant height, stem diameter, and crop yield—specifically at 28 and 35 DAS at the Oton site. However, no significant differences ($p \leq 0.05$) among treatments were found in all three parameters within five weeks of cultivation at the Malay site.

The varied set of data gathered from the Malay site may be attributed to the different microclimate parameters present in the areas during the duration of the experiment [23]. Considering that the two sites belong to two different climate types classified by PAGASA, this seems to be the case.

With this, the results that will be presented in this study are purely from the Oton site.

Plant height. Results showed that the plant height means of the treatments at 28 and 35 days after sowing (DAS) are significantly different ($p \leq 0.05$).

As seen in Figure 1, at 28 DAS, the mean plant height of the *I. reptans* treated with 0.1% HA (T0B = 23.40 cm) was significantly higher than those of other treatments – T0A (19.82 cm), T1 (19.69 cm), and T2 (18.38 cm). At 35 DAS, the mean plant height of the *I. reptans* treated with 0.1% HA (T0B = 38.24 cm) was also significantly higher than those of other treatments – T0A (30.73 cm), T1 (28.94 cm), and T2 (31.28 cm).

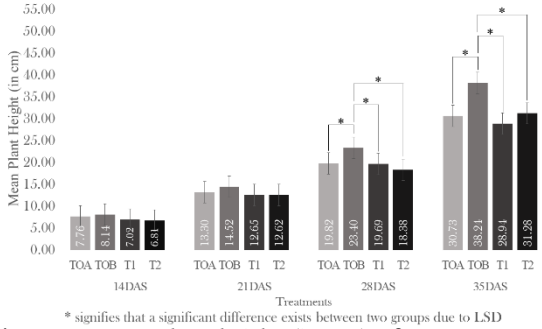

Figure 1. Mean plant height (in cm) of *I. reptans* under different treatments in the Oton site.

This indicates that there was a rise in nitrogen uptake [24]. Nitrogen boosts the growth of plants by stimulating height growth [25]. This may also be attributed to the hormones found in humic substances like auxins and gibberellins, as well as compounds such as amino acids, indole acetic acid, etc. [9][26]. The activation of auxin caused by the HA can induce cell elongation [10][27]. Cell elongation is an obligatory component of plant growth as it refers to the irreversible, rapid, and manifold increase in cell size and volume. It occurs in axial organs, such as stems and roots, wherein cells are elongated predominantly by cell wall growth on the cell lateral sides, resulting in the increase in plant height as plant morphogenesis depends on it [28].

Stem diameter. The One-way ANOVA showed that the stem diameter means of the different treatments were not significantly different ($p \leq 0.05$) as seen in Figure 2.

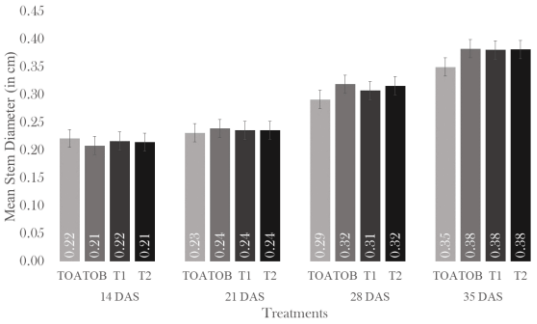

Figure 2. Mean stem diameter (in cm) of *I. reptans* under different treatments in the Oton site.

It can be speculated that there may be an insufficient concentration of Ca^{2+} ions in the soil that HA can keep in a dissolved state [29] and can be absorbed by the plant. This is because Ca^{2+} plays an important role in strengthening plant stems by forming bonds with pectin compounds in plants which are important for plant tissue rigidity and integrity resulting in thicker and stronger stems [30].

Another reason could be because of how cell elongation works which is facilitated by HA. Cell elongation is defined as cells expanding in one dimension to elongate cells and organs [31]. Since the auxins activated by HA induce cell elongation [10] rather than expansion (in all three dimensions), the stem diameter of the plants cannot significantly increase.

Crop yield. One-way ANOVA showed that the crop yield means (in kg/ha) of the different treatments are significantly different ($p \leq 0.05$).

The mean crop yield (kg/ha) of the *I. reptans* treated with 0.1% HA (T0B = 6738.90) was significantly higher ($p \leq 0.05$) than those of other treatments – T0A (4872.20 kg/ha), T1 (4711.10 kg/ha), and T2 (3616.67 kg/ha) (Figure 3). This indicates that the treatment with 0.1% HA (T0B) improves crop yield the most among other treatments.

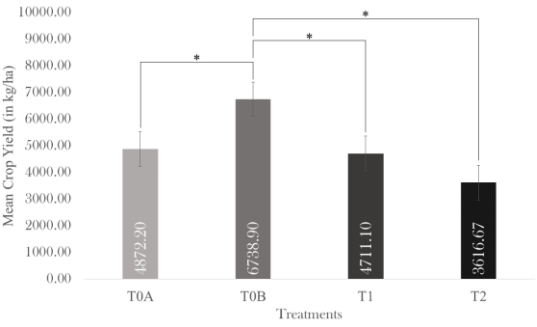

Figure 3. Mean crop yield (in kg/ha) of *I. reptans* under different treatments in the Oton site.

This increase in crop yield is attributed to the aforementioned growth-promoting hormones, auxins and gibberellins, which also play a role in the development of plant roots [32]. Increased vegetative growth and productivity are mainly due to the hormone-like activities of HA as it is involved in cell respiration, oxidative phosphorylation, protein synthesis, photosynthesis, antioxidants, and various enzymatic reactions [28]. The influence of HA is also

found in the development of plant roots, thus increasing plant production [24].

Optimal treatment for I. reptans growth and production. Among the four treatments, T0B (soil applied with 0.1% HA) was the best treatment for *I. reptans* growth and production. Despite not having a notable impact on stem diameter, the treatment yielded positive significant effects on plant height and crop yield. Given that these parameters indicate the quality of plant growth and production, it can be deduced that the sole application of HA is the best treatment for *I. reptans*.

This is in contrast however to the initial hypothesis based on the studies conducted by Sangeetha et al. [33] and Zhang et al. [9]. The positive effects of HA and the positive effects of urea separately may improve plant growth and yield when both substances are used in combination. To summarize, HA may contain auxin- and gibberellin-like substances or induce the activity of these to promote cell elongation of axial organs such as stems and roots. Urea provides nitrogen for the plant, as nitrogen boosts the growth of plants by stimulating height growth [34].

It is suspected that plant toxicity by NH_4^+ has occurred due to an increase in soil pH, which generally has adverse effects on higher plants physiologically [35]. The toxicity of NH_4^+ depends upon the substrate-solution concentration of NH_3, the un-ionized form of NH_4^+. Since NH_3 increases as pH increases, this makes NH_4^+ more toxic as the soil becomes more acidic]. Furthermore, a decrease in phosphorus (P) uptake and utilization as an effect of an increase in soil pH due to urea fertilization can also be the case. This has caused plants to use urea inefficiently. Phosphorus (P) deficiency reduces plant growth which is attributed to either decrease in photosynthesis or an increase in energy investment and negatively impacts crop yield and quality [35].

Limitations. The data gathering was conducted within 35 days in two sites with varying climate types and weather conditions, which affected the plant samples even with significant efforts to control the effect of these factors. Although *I. reptans* can already be harvested at this time, the difference in plant growth and yield among treatments can be seen more clearly within a longer timespan. Furthermore, due to the unavailability of laboratory equipment, other parameters such as nutrient uptake, soil moisture, and other soil parameters were not measured.

Despite this, the findings of this study may aid future research in improving the growth and production methods of agricultural crops and in establishing the credibility of humic substances in agriculture.

Conclusion. - Significant differences were found between groups in only one site at 95% confidence level in mean plant height both at 28 and 35 DAS, and mean crop yield. Meanwhile, no significant differences were found in stem diameter means at all seven-day intervals. Post-hoc analysis using Fisher's LSD test showed significant differences between T0A and T0B, T1 and T0B, and T2 and T0B but none in other pairs of treatments in terms of plant height and crop yield. Thus, the sole application of HA produced *I. reptans* with the tallest plant height and largest crop yield among the treatments used.

Recommendations. - Results in this study can be improved by replicating in an enclosed space more suitable for plant growth to avoid the effects of weather conditions and to prevent infiltration and infestation of pests. Other treatments can be utilized such as other types and levels of fertilizers and HA, and the use of other humic substances such as naturally extracted HA or substances. It is also recommended to conduct the study with a larger plant population and sample size for better representation. Certain parameters such as the number of leaves and branches, nutrient uptake, and soil parameters can be evaluated and measured. These parameters help determine their overall effect on plant growth and measure the growth of the plant itself. Replication of these types of studies on other plant species may be done. The use of HA in agriculture is recommended as it has positive results on crop growth and yield.

Acknowledgment. - The researchers would like to extend their gratitude to agro centers and hardware stores in Iloilo City and Malay, Philippines, for providing them with the necessary materials. They also thank Ceres Liner for transporting materials between the two sites.

References

[1] [PSA] Philippine Statistics Authority. 2020. 2020 Selected statistics on agriculture. Philippines: Philippine Statistics Authority. p. 1–5. ISSN-2012-0362.

[2] Liliane TN, Charles MS. 2020. Factors Affecting Yield of Crops. In: Khan A, editor. Agronomy: Climate Change & Food Security. London (UK): IntechOpen. [cited 2020 Oct 23]. Available from http://bit.ly/lilianecharles 2020.

[3] Purbajanti ED, Slamet W, Fuskhah E. 2019. Effects of organic and inorganic fertilizers on growth, activity of nitrate reductase, and chlorophyll contents of peanuts (Arachis hypogaea L.). In IOP Conference Series: Earth and Environmental Science (Vol. 250, No. 1, p. 012048). IOP Publishing.

[4] Mayhew L. 2004. Humic substances in biological agriculture. Rev ACRES. 34(1–2): 80–88.

[5] Peña-Méndez EM, Havel J, Patočka J. 2005. Humic substances-compounds of still unknown structure: applications in agriculture, industry, environment, and biomedicine. J Appl Biomed. 3(1): 13–24.

[6] Senesi N, Miano TM, Provenzano MR, Brunetti G. 1991. Characterization, differentiation, and classification of humic substances by fluorescence spectroscopy. Soil Sci. 152(4): 259–271.

[7] Mora V, Bacaicoa E, Zamarreno AM, Aguirre E, Garnica M, Fuentes M, García-Mina JM. 2010. Action of humic acid on promotion of cucumber shoot growth involves nitrate-related changes associated with the root-to-shoot distribution of cytokinins, polyamines, and mineral nutrients. J Plant Physiol. 167(8): 633–642.

[8] Zhang L, Zhou JUN, Zhao YG, Zhai Y, Wang KAI, Alva AK, Paramasivam S. 2013. Optimal combination of chemical compound fertilizer and humic acid to improve soil and leaf properties, yield, and quality of apple (Malus domestica) in the loess plateau of China. Pak J Bot. 45(4): 1315–1320.

[9] Tan KH. 2003. Principles of Soil Chemistry. New York (US): Marcel Dekker Inc.

[10] Farabee MJ. 2007. Plant Hormones, Nutrition and Transport [Internet]. Avondale (AZ): Estrella Community College; [cited 23 Nov 2020]. Available from: http://bit.ly/farabee2007.

[11] Nikbakht A, Kafi M, Babalar M, Xia YP, Luo A, Etemadi NA. 2008. Effect of humic acid on plant growth, nutrient uptake, and postharvest life of gerbera. J Plant Nutr. 31(12): 2155–2167.

[12] Palada MC, Chang LC. 2003. Suggested cultural practices for kangkong (No. OTHER). AVRDC-The World Vegetable Center.

[13] Manvar MN. 2011. Pharmacognostical investigations on Ipomoea aquatica Forsk. Int J Pharm Sci Res. 2(11): 2812.

[14] Susila AD, Prasetyo T, Palada MC. 2008. Optimum fertilizer rate for kangkong (Ipomoea reptans L.) production in ultisol Jasinga.

[15] Status of Digital Soil Mapping in BSWM. 2015. Quezon City (PH). Bureau of Soil and Water Management; [cited 2020 Oct 9]. Available from: http://bit.ly/BSWM2015.

[16] Jayaraman K. 1999. A Statistical Manual for Forestry Research. Bangkok (TH): Forestry and Agriculture Organization of the United Nations [cited 2020 Oct 23].

[17] Grant T. 2019. Randomized Complete Block Design. Columbus (OH): Plant Breeding and Genomics; [cited 2020 Oct 23]. Available from: http://bit.ly/grantt2019.

[18] Luyen LT, Preston TR. 2004. Effect of level of urea fertilizer on biomass production of water spinach (Ipomoea aquatica) grown in soil and in water. Livestock Research for Rural Development. [cited 2020 Nov 10] 16(81). Available from: http://bit.ly/luyenpreston 2004.

[19] Sophia K, Preston TR. 2001. Comparison of biodigester effluent and urea as fertilizer for water spinach vegetable. Livestock Research for Rural Development. [cited 2020 Nov 10] 13(59). Available from http://bit.ly/sophia preston2001.

[20] PowHumus® WSG 85. [date unknown]. Grevenbroich (DE): Humintech; [cited 2020 Oct 22]. http://bit.ly/powhumusagnosto.

[21] Ibrahim MH, Rahman NYA, Zain NAM. 2018. Effect of nitrogen rates on growth and quality of water spinach (Ipomea aquatica). Annu Res Rev Biol. 1–12.

[22] Technical guidelines for measuring crop yields in field crops. 2004. Bajo (BT): Agricultural Research and Development Center Bajo Wangdue Phodrang; [cited 2020 Oct 11]. Available from: http://bit.ly/rcbajo2004.

{23] Rahman S. 2002. Performance of summer vegetables under reduced light condition as agroforestry systems [thesis]. [Dhaka, Bangladesh]: Sher-e-Bangla Agricultural University. Chapter 4.2.3. Kangkong; p. 40–43. Available from: http://bit.ly/rahman2002.

[24] Suwardi, Cholili SN, Anwar S. 2019. Application of humic substances with zeolite as carrier to increase the production of water spinach (Ipomoea reptans Poir.). IOP Conf Ser: Earth Environ Sci. 393 (2019): 1–9.

[25] Leiwakabessy FM, Wahjudin UM, Suwarno. 2003. Kesuburan Tanah. Bogor (ID): IPB.

[26] Gardiner DT, Miller RW. 2004. Soil in Our Environment, 10th ed. New Jersey (US): Pearson Education.

[27] Mora V, Baigorri R, Bacaicoa E, Zammareño AM, Garcia-Mina JM. 2012. The humic acid-induced changes in the root concentration of nitric oxide, IAA, and ethylene do not explain the changes in root architecture caused by humic acid in cucumber. Environ Exp Bot. 76: 2432. doi: 10.1016/j.envexpbot.2011.10.001.

[28] Obroucheva NV. 2008. Cell elongation as an inseparable component of growth in terrestrial plants. Russ J Dev Biol. 39(1): 13–24.

[29] Rahmandhias DT and Rachmawati D. 2020. The Effect of Humic Acid on Productivity and Nitrogen Uptake in Kangkong (Ipomoea reptans Poir.). JIPI. 25 (2): 316–322. doi: 10.18343/jipi.25.2.316.

[30] Demarty M, Morvan C, Thellier M. 1984. Calcium and the cell wall. Plant Cell Environ. 7(6): 441–448.

[31] Oh MH, Honey SH, Tax FE. 2020. The control of cell expansion, cell division, and vascular development by brassinosteroids: A historical perspective. Int J Mol Sci. 21(5): 1–15. doi: 10.3390/ijms21051743.

[32] Trevisan S, Francioso O, Quaggioti S, Nardi S. 2010. Humic substances biological activity at

the plant soil interface. Plant Sign Behav. 5(6): 635–643.

[33] Sangeetha M, Singaram P. 2007. Effect of lignite humic acid and inorganic fertilizers on growth and yield of onion. Asian J Soil Sci. 2(1): 108-110.

[34] Witte, CP. 2011. Urea metabolism in plants [Abstract]. Plant Sci. 180(3): 431-438. doi: 10.1016/j.plantsci.2010.11.010.

[35] Goyal SS, Huffaker RC. 1984. Nitrogen toxicity in plants. Nitrogen in crop production. 97-118.

Publiscience Vol. 4 Issue 1

Effects of hydropriming on the germination of *Oryza sativa* L. NSIC Rc 216 (rice) under sodium chloride (NaCl) stress

C-SAR MART P. AGUIRRE, JOECILE FAITH C. MONANA, and MICHAEL PATRICK M. PADERNAL

Philippine Science High School Western Visayas Campus - Department of Science and Technology (DOST-PSHSWVC), Brgy. Bito-on, Jaro, Iloilo City 5000, Philippines

Article Info

Submitted: May 11, 2021
Approved: Jun 23, 2021
Published: Aug 30, 2021

Keywords:
Oryza sativa L.
hydropriming
seedling vigor index
sodium chloride
salt stress

Abstract

Elevated salt concentration can be toxic to plant development. Hydropriming can overcome this by increasing the seeds' stress tolerance. This study determined the effects of hydropriming on the germination of *Oryza sativa* L. var. NSIC Rc 216, a widely used rice variety in the Philippines, subjected to sodium chloride stress. Seeds were hydroprimed for 12, 24, or 48 hours with unprimed rice seeds as control. Seeds were then allowed to germinate for seven days and germination parameters were recorded. Significant differences were recorded with the germination energy percentage (GEP) and speed of germination means (SG). The 48-hour treatment had significantly higher GEP and SG means when compared to the control set-up; however, no significant differences were recorded with the final germination percentage (FGP) and seedling vigor index (SVI). In conclusion, hydropriming had effects on the germination rate of rice under salt stress but not with its overall germination performance.

Introduction. - Rice (*Oryza sativa* L.) is an important staple food crop in the world and in the Philippines, feeding half of the human population [1].

However one of the major problems of the agriculture industry is soil salinity. It affects the plant at almost all of its growth stages and impacts the germination and growth of plants [2]. Highly saline environments can decrease the osmotic potential of soil and make it toxic to seedlings [3]. The growth of rice, in particular, can be negatively affected by increased salt concentration that leads to the reduction of several germination parameters such as its final germination percentage (FGP), germination energy percentage (GEP), and speed of germination (SG) [4].

Hydropriming has been recommended to address the effects of soil salinity [5,6,7]. It is a simple method that only requires distilled water as the priming medium for the seeds before sowing [8]. This process enables the seeds to imbibe water which facilitates the emergence of the seeds' radicle [9,10]. With this, it has the potential to upregulate the tolerance of plants from abiotic stresses by enhancing seed germination, seedling growth, and development [7,10].

Although there have been few studies on the effect of hydropriming on the germination of *O. sativa* L, under salt stress [11, 12, 13], there is limited research on its effect on the variety NSIC Rc 216 subjected to elevated salinity levels.

NSIC Rc 216 rice variety has a wide adaptation under different stresses presented by varying climates across the country thus making it one of the most popular rice varieties in the Philippines [14]. Although it is considered versatile, it was classified as salt-sensitive by Imai and Sevilla [15] which may lead to poor germination and plant growth that can cause yield losses during harvest if subjected to salt stress during germination [4].

This study tested the efficacy of hydropriming in counteracting salt stress in *O. sativa* L., variety NSIC Rc 216, helping determine how generalizable is hydropriming's pro-germination effects to other rice varieties.

More specifically, it aimed to:

(i) determine and calculate the number of seedlings per day, the height of seedlings, and the seed germination parameters: final germination percentage (FGP), germination energy percentage (GEP), speed of germination (SG), and seedling vigor index (SVI);

(ii) determine the effects of different hydropriming durations (12 hours, 24 hours, and 48 hours) on the calculated germination parameters of *Oryza sativa* L. variety NSIC Rc 216 under saline stress; and

(iii) compare and determine if there is a significant difference among the treatments using one-way analysis of variance (ANOVA) and

How to cite this article:
CSE: Aguirre CM, Montana JF, Padernal MP. 2021. Effects of hydropriming on the germination of *Oryza sativa* L. NSIC Rc 216 (rice) under NaCl (sodium chloride) stress. Publiscience. 4(1): 58–62.
APA: Aguirre C.M., Monana, J.F., & Padernal, M.P. (2021). Effects of hydropriming on the germination of *Oryza sativ*a L. NSIC Rc 216 (rice) under NaCl (sodium chloride) stress. *Publiscience, 4*(1), 58–62.

For supplementary data, contact: publiscience@wvc.pshs.edu.ph.

Least Significant Difference (LSD) post-hoc analysis using Rstudio and R programming language.

Methods. - Rice seeds were hydroprimed at varying durations (12, 24, or 48 hours) following a completely randomized design (CRD), with unprimed rice seeds as control, as seen in Table 1. They were subsequently air-dried for three (3) hours, then they were allowed to germinate in the prepared germination media and chamber. After seven (7) days, all the germination parameters were measured and recorded. Statistical analysis was then performed.

Table 1. The different hydropriming duration, replicates, and corresponding labels of the different set-ups used.

Hydropriming duration (hours)	No. of seeds per replicate	Replicates
12	50	3
24	50	3
48	50	3
0 (Control)	50	3

Seed authentication, storage, and selection. Rice variety NSIC Rc 216 was acquired from the local farmers at Oluangan, Leon, Iloilo, and authenticated with the help of the Department of Agriculture at Leon, Iloilo.

They were then stored in an airtight container at room temperature until use. The seeds were tested for moisture content to ensure seed viability. Seeds that had moisture content of 14% or less were considered viable, while the rest were discarded.

Seed hydropriming. Fifty (50) seeds per replicate per treatment were selected. They were hydroprimed for 0 (control), 12, 24, and 48 hours using distilled water (Absolute Pure Distilled Drinking Water) with a ratio of 5 mL of water for every 12 rice seeds. The seeds were then air-dried for 3 hours and stored in growing media for germination.

Growing media. A total of 12 Petri dishes, with three (3) layers of filter paper each, were used as growing media. They were kept sealed during the experiment to prevent moisture loss.

Saline stress simulation. To induce salt stress, a 0.15 M saline solution was prepared using a technical grade sodium chloride (NaCl) and distilled water. Ten (10) mL of the prepared solution was then administered evenly to each replicate of each treatment after the hydroprimed and control seeds were sowed on the growing media.

According to Chunthaburee et al. [16], a 0.15 M salt concentration generally induces hyperosmotic stress to rice seeds through ion imbalance.

Growth period and conditions. The Petri dishes were then stored in a germination chamber with LED tubes at a 12-hour light and 12-hour dark photoperiodic cycle with the light intensity maintained at 4000 lux during the light cycle [17]. The seeds were then allowed to germinate for seven (7) days.

Data collection and calculation. Germinated seeds were counted every 24 hours at 6:00 AM, following the procedure by the International Research Institute (IRRI) where both plumule and radicle must be present [18]. After the germination period, 15 sprouted seedlings with the longest lengths (root+shoot) per replicate per set-up were selected and their lengths were recorded. The final germination percentage (FGP), speed of germination (SG), germination energy percentage (GEP), and seedling vigor index (SVI) were then calculated using the following equations [4, 19]:

$$FGP = \frac{No.of\ germinated\ seeds\ on\ the\ 7th\ day}{Number} \times 100$$

$$SG = \frac{No.of\ ger.seeds}{Days\ of\ first\ count} + \cdots + \frac{No.of\ ger.seeds}{Days\ of\ last\ count}$$

$$GEP\ = \frac{No.of\ seeds\ germinated\ on\ the\ fourth\ day}{Total\ number\ of\ seeds} x\ 100$$

$$SVI = FGP \times seedling\ length\ (root + shoot)$$

Statistical analysis. One-way analysis of variance (ANOVA) was conducted for each calculated parameter of all treatments with a confidence interval of 95% (α=0.05). Least Significant Difference (LSD) post-hoc analysis was then performed using Rstudio (version 1.4.1106, Open Source License).

Safety procedure. The safety data sheet (SDS) for NaCl was secured and the hazards of handling were considered beforehand. NaCl was disposed of in chemical waste containers while the discarded seeds were segregated properly. Proper protective equipment was worn at all times while performing all experimental procedures. All the procedures were done at home to prevent COVID-19 infection.

Results and Discussion. - The study aimed to determine the effects of hydropriming on the germination of *O. sativa* L. var. NSIC Rc 216 under NaCl stress.

After seven days, a germination lag was observed with the control setup for two (2) days and both 12 and 24-hour setup for one (1) day. No germination lag has been observed with the seeds hydroprimed for 48 hours.

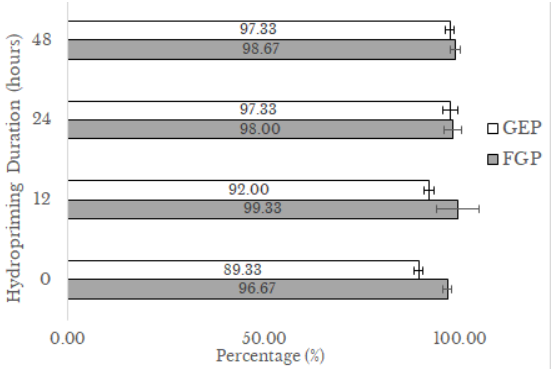

Figure 1. The calculated Final Germination Percentage (FGP) and Germination Energy Percentage (GEP) for all the experimental set-ups.

Final Germination Percentage and Germination Energy Percentage. The highest FGP mean was recorded with the 12 hours of hydropriming of rice, as seen in Figure 1; however, this was not significant when compared to other treatments. The highest recorded GEP mean, on the other hand, was with 24 and 48 hours of hydropriming, both having the same value of 97.33% and were significantly different when compared to the rest of the set-ups with a p-value of 0.03.

The values of both parameters (FGP and GEP) may indicate that hydropriming affects the germination of rice seeds at the earlier stages. This was suggested by the significantly different values for GEP which was a parameter calculated using the data on the 4th day.

With that, seeds germinated faster when hydroprimed at longer durations; however, after some time, seeds hydroprimed at shorter durations germinated as well. This may have caused the FGP values, which was a parameter calculated on the 7th day, to be non-significant.

This is in accordance with the results of Prasad [20] in which GEP also increased with longer durations of hydropriming, with the highest GEP mean recorded with 28 hours of hydropriming. This effect was attributed to the different biological mechanisms triggered by hydropriming, such as the release of enzymes that produce soluble food nutrients for the seeds. This may have enabled the seeds to germinate upon sowing [20].

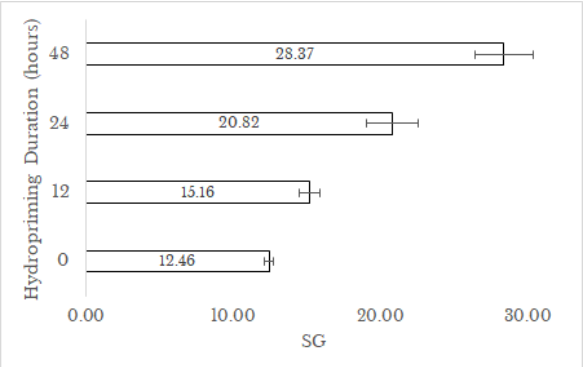

Figure 2. The calculated Speed of Germination (SG) for all the experimental set-ups.

Speed of Germination. The highest SG mean was recorded with the 48-hour hydroprimed seeds, as seen in Figure 2. The SG also increased with longer durations of treatment. This may be caused by the jumpstart in germination through a series of biological and physiological processes such as the acceleration of the emergence phase and multiplication of radicle cells [11, 21, 22]. In the study of Amooaghie [23], it was stated that the early germination stage of plants was "from sowing to seedling emergence" in which they are most vulnerable to external conditions such as salt stress. Hydropriming speeds up the germination process through stimulatory effects through cell division mediation and thus limits the exposure of the seeds to the stressful conditions presented by the environment [11, 24]. This was also in line with the findings of Kaya et al. [9] in which hydropriming of *Helianthus annuus* L. seeds resulted in the acceleration of germination even in low osmotic potential (i.e. salt stress).

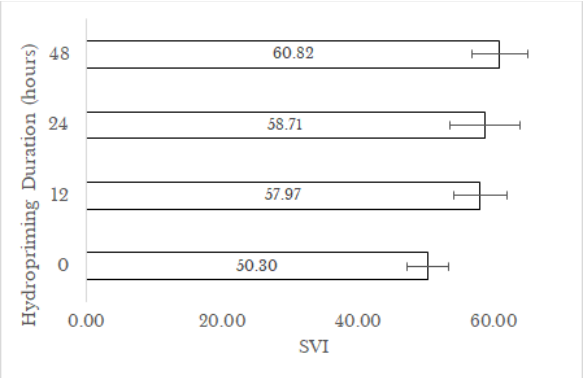

Figure 3. The calculated Seedling Vigor Index (SVI) for all the experimental set-ups.

Seedling Vigor Index. The highest SVI was recorded with 48-hour hydroprimed seeds, as seen in Figure 3. The seedling vigor index increased with the increasing duration of hydropriming; however, it was determined that these values are not significant with a p-value of 0.06. Similar to the FGP, the SVI was not affected probably because the parameter was recorded over a longer period and hydropriming may have only affected the earlier germination stages of rice seeds [24].

The study of Elyasirad et al. [25] had contrasting findings to these results. The study observed that hydropriming *Ferula assa-foetida* has a significant effect on the germination parameters of the seeds, including the SVI [25].

This may be explained by the positive effects of saline content observed by previous studies. An example of this is with Lutts et al. [13] which found out that increased NaCl concentration of up to 50 mM, caused proline accumulation of rice seedlings. This proline accumulation may be responsible for improving the germination of rice seeds by counteracting the effects of salinity by ion detoxification. This protects the plant at the cellular level from osmotic imbalance presented by the saline content of the environment [26]. This may have happened to the unprimed seeds that caused the ger-

mination performance in this setup to be comparable to the performance of 48-hour hydroprimed seeds, as evaluated by the SVI.

Limitations. Due to time constraints, this study only observed the effects of hydropriming on limited parameters and only one salinity level has been used. The entire experiment has been done at home which may have affected the overall results of this study specifically with the unavoidable external factors such as humidity, light from other sources within the study site, and resident presence.

Conclusion. - Hydropriming was concluded to only have effects on the early days of rice seed germination, primarily affecting the germination rate but not with the overall germination performance while the rice seeds were being subjected to saline stress. Hydropriming may also be used to accelerate germination of *O. sativa* L.in saline conditions.

Recommendations. - It is highly encouraged to use other Philippine rice varieties to further assess the effects of hydropriming on their germination while being subjected under saline stress. A larger scale of this experiment with a longer duration of observation is also recommended. The replication of the experiment in laboratory and field conditions may also be considered to minimize or completely eliminate the effects of external conditions that can affect the study.

Acknowledgments. - The researchers would like to thank the Department of Agriculture of Leon, Iloilo for assisting the authentication of the rice variety and for sharing their knowledge on the study, and the local farmers of Oluangan Leon, Iloilo for providing the rice seeds. They would also like to thank Ma'am Ramona Miral, for her help with the statistical analysis of the data.

References

[1] Portilla JC, Pagaduan JMR. 2015. Status of other staple crops as substitute to rice: an assessment in Isabela and Quirino [Philippines]. Philipp J Crop Sci. 39(1): 132–133.

[2] Franco AJ, Esteban C, Rodriguez C. 1993. Effects of salinity on various growth stages of muskmelon cv. Revigal. Int J Hortic Sci. 68(6): 899–904.

[3] Kozlowski TT, Pallardy SG. 1996. Growth Control in Woody Plants. San Diego (CA). Academic Press.

[4] Hakim AM, Juraimi SA, Begum M, Hanafi MM, Ismail MR, Selamat A. 2010. Effect of salt stress on germination and early seedling growth of rice (*Oryza sativa* L.). Af J Biotechnol. 9(13): 1911–1918.

[5] Damalas A, Koutroubas S, Fotiadis S. 2019. Hydro-priming effects on seed germination and field performance of Faba bean in spring sowing. Agriculture. 9(9): 201.

[6] Taylor AG. 2003. SEED DEVELOPMENT | seed treatments. In: Encyclopedia of Applied Plant Sciences. Elsevier. 1291–1298.

[7] Farahani HA, Maroufi K. 2011. Effect of hydropriming on seedling vigour in basil (*Ocimum basilicum* L.) under salinity conditions. Adv Environ Biol. 828–834.

[8] Khalid MF, Hussain S, Anjum MA, Ejaz S, Ahmad M, Jan M, Zafar S, Zakir I, Ali MA, Ahmad N, et al. 2019. Hydropriming for Plant Growth and Stress Tolerance. In: Priming and Pretreatment of Seeds and Seedlings. Singapore: Springer Singapore. 373–384.

[9] Kaya MD, Okçu G, Atak M, Çikili Y, Kolsarici Ö. 2006. Seed treatments to overcome salt and drought stress during germination in sunflower (*Helianthus annuus* L.). Eur J Agron. 24(4): 291–295.

[10] Jayesh V, Meeta J. 2015. Influence of halopriming and hydropriming on seed germination and growth characteristics of *Zea mays* L. cv. GSF-2 under salt stress. Res J Chem Environ. 19(1): 10.

[11] Ibrahim N, Bhadmus Z, Singh A. 2013. Hydro-Priming and Re-Drying Effects on Germination, Emergence, and Growth of Upland Rice (*Oryza sativa* L.). Nig J Basic Appl Sci. 2013: 21(2).

[12] Koirala N, Poudel D, Bohara GP, Ghimire NP, Devkota AR. 2019. Effect of seed priming on germination, emergence, and seedling growth of spring rice (*Oryza sativa* L.) cv. Hardinath-1. Azarian J Agric. 6(1): 7–12.

[13] Lutts S, Majerus V, Kinet JM. 1999. NaCl effects on proline metabolism in rice (*Oryza sativa*) seedlings. Physiol Plant. 105(3): 450–458.

[14] Laborte A, Paguirigan N, Moya P, Nelson A, Sparks, Gregorio G. 2015. Farmers' preference for rice traits: Insights from farm surveys in Central Luzon, Philippines, 1966-2012. PLOS ONE. 10(8):e0136562.

[15] Imai T, Sevilla L. 2012. Screening for salt stress tolerance in different varieties of *Oryza sativa L.* [dissertation]. University of the Philippines Manila. Accessed from: DSpace Repository.

[16] Chunthaburee S, Sanitchon J, Pattanagul W, Theerakulpisut P. 2014. Alleviation of salt stress in seedlings of black glutinous rice by seed priming with spermidine and gibberellic acid. Not Bot Horti Agrobot Cluj Napoca. 42(2):405-413.

[17] Anuradha S, Rao SSR. 2003. Application of brassinosteroids to rice seeds (*Oryza sativ*a L.) reduced the impact of salt stress on growth, prevented photosynthetic pigment loss, and increased nitrate reductase activity. Plant Growth Regul. 40(1): 29–32.

[18] Crop and Environmental Sciences Division (CESD). 2013. Seed Quality Testing Manual. Int Rice Res Ins*t.* 1(1): 1-23

[19] Vashisth A, Nagarajan S. Effect on germination and early growth characteristics in sunflower (Helianthus annuus) seeds exposed to static magnetic field. J Plant Physiol. 167(2):149–156.

[20] Prasad S. 2012. Effect of hydro-priming duration on germination and seedling vigour of rice (*Oryza sativa* L.) cv. J Crop Weed, 8(1):65–71.

[21] Dastanpoor N, Fahimi H, Shariati M, Davazdahemami S, Hashemi SMM. 2013. Effects of hydropriming on seed germination and seedling growth in sage (*Salvia officinalis* L.). Af J Biotechnol. 12(11): 1223–1228.

[22] Mcdonald M. Seed deterioration: Physiology, repair and assessment. 1999. Seed Sci and Technology 27: 177–237.

[23] Amooaghaie R, 2011. The effect of hydro and osmopriming on alfalfa seed germination and antioxidant defenses under salt stress. Af J Biotechnol. 10(33): 6269–6275.

[24] Freeman CE. 1973. Germination responses of a Texas population of ocotillo (*Fouquieria splendens* Engelm.) to constant temperature, water stress, pH and salinity. American midland Naturalist. 252–256.

[25] Elyasirad S, Mousavi SG, Sanjari, G. 2006. Effects of priming and salt stress on seed germination and emergence characteristics of asafetida (*Freula assa foetida*): A laboratory and glasshouse trial. ARPN J Agric Biol Sci. 12(4): 150–160.

[26] Singh M, Singh AK, Nehal N, Sharma N. 2018. Effect of proline on germination and seedling growth of rice (*Oryza sativa* L.) under salt stress. Pharmacogn Phytochem. 7(1): 2449–2452.

Effects of powdered chicken eggshells as a soil amendment on the vegetative growth of *Vigna radiata*

JOHAR H. RACHO and VIRNA JANE M. NAVARRO

Philippine Science High School Western Visayas Campus - Department of Science and Technology (DOST-PSHSWVC), Brgy. Bito-on, Jaro, Iloilo City 5000, Philippines

Article Info

Submitted: May 07, 2021
Approved: Jul 12, 2021
Published: Aug 30, 2021

Keywords:
powdered eggshells
calcium
vegetative growth
Vigna radiata
soil amendment

Abstract

The continuous and excessive generation of eggshells as agricultural and industrial waste results in various environmental problems. However, recent studies have shown that eggshells contain essential compounds that promote plant growth and soil condition. Thus, this study aimed to determine the effects of powdered chicken eggshells (PCES) on the vegetative growth of *Vigna radiata*. Chicken eggshells were air-dried, crushed, and powdered. The plants were then grown on PCES-soil compositions of 0%, 10%, and 15% (w/w). The stalk and root length were statistically compared between treatments using one-way ANOVA and post-hoc Tukey-Kramer test. The results indicate that a significant difference existed for both mean plant length scores between plants grown on untreated soil and PCES-treated soil; PCES was found to improve the vegetative growth of *V. radiata*. However, adverse effects were observed at 15% PCES due to excessive calcium uptake. Hence, quantifying the amount threshold of PCES is necessary.

Introduction. - Food industries continuously produce excessive amounts of waste, making it increasingly crucial to formulate solutions to solve this problem. Eggs are one of the products with extensive production quantities under the industry [1]. Hence, considerable amounts of eggshells are being discarded every day, resulting in various environmental issues such as increased waste in landfill sites and pollution [2]. According to the Food and Agriculture Organization of the United Nations (FAO) [3], the world egg production in 2019 was recorded to be about 83.5 million tonnes. In addition, eggshells constitute about 11% of the total egg weight. Thus, the waste generated can be estimated to be about 9.2 million tonnes per year, globally [1].

An eggshell is composed of 94% calcium carbonate, 1% calcium phosphate, 1% magnesium carbonate, and 4% organic substances [4]. Hence, eggshells are known to contain substantial amounts of calcium, and due to this, they can be utilized for the improvement of plant growth [5,6]. A study conducted by Gaonkar and Chakraborty [7] reported that powdered eggshells increase the pH and calcium content of the soil. Furthermore, the study indicated that chicken eggshells contain larger quantities of calcium carbonate than duck eggshells. Additionally, Ok et al. [8] and Soares et al. [9] reported the successful immobilization of heavy metals such as cadmium, lead, and zinc in contaminated soils through treatment with eggshells. Moreover, a study conducted by Wijaya and Teo [5] reported that eggshells significantly improved the height of *Ocimum basilicum* (sweet basil), which is associated with its calcium content.

These findings are mainly associated with the composition of eggshells as previously mentioned. Furthermore, it must be noted that calcium, an essential mineral for plant growth, is the main constituent sought after eggshells in the study [5,11]. Additionally, the mechanism of entry of this mineral cation to plant cells is via passing through Ca^{2+}-permeable ion channels situated in the plasma membrane [10]. This separates the other components of calcium salts such as the carbonate group for the case of calcium carbonate [11].

The aforementioned information and findings highlight the practical application of eggshells in utilizing their properties to strengthen waste management and agricultural production. Hence, its application as a soil amendment to increase the calcium content of the soil will be beneficial to developing countries. Furthermore, this is in line with the promotion of zero hunger, economic growth, and responsible consumption and production, which are some of the Sustainable Development Goals (SDGs) being targeted by the United Nations (UN) [12].

Vigna radiata (mung beans or "monggo") is one of the major crops in the Philippines, commonly used in various local dishes. It is an annual, erect or semi-erect legume that is usually cultivated for its seeds or sprouts across Asia [13]. Additionally, it is one of the cheapest protein sources in the Filipino diet as it is easily cultivated [14]. Furthermore, according to the Philippine Statistics Authority (PSA) [15], a production of about 23.8 thousand tonnes of the legume was observed within the second quarter of 2020. Although it shares a considerable fraction of the Philippine agriculture, the effects of eggshells on the vegetative

How to cite this article:
CSE: Racho JH, Navarro VJM. 2021. Effects of powdered chicken eggshells as a soil amendment on the vegetative growth of *Vigna radiata*. Publiscience. 4(1): 63–66.
APA: Racho, J.H., & Navarro, V.J.M. (2021). Effects of powdered chicken eggshells as a soil amendment on the vegetative growth of *Vigna radiata*. *Publiscience*, *4*(1), 63–66.

For supplementary data, contact: publiscience@wvc.pshs.edu.ph.

growth of *V. radiata* are yet to be explored. Since it can be easily cultivated, it can serve as a model plant to determine the effects of calcium derived from chicken eggshells towards vegetative growth in general, which is a key factor that determines whether or not a plant proceeds to the reproductive stage [14].

To address this gap, the study investigated the effects of powdered chicken eggshells (PCES) on the vegetative growth of *V. radiata*. Specifically, it aimed to:

(i) measure the stalk length of *V. radiata* grown on PCES-soil compositions of 0%, 10%, and 15% (w/w) at 10, 20, and 30 days after planting;

(ii) measure the root length of *V. radiata* grown on PCES-soil compositions of 0%, 10%, and 15% (w/w) at 30 days after planting; and

(iii) determine if a significant difference exists among the mean values for stalk length and root length of *V. radiata* between treatments.

Methods. - Chicken eggshells were air-dried, crushed, and powdered. Then, the acquired PCES were mixed with 400 g of soil at 0%, 10%, and 15% (w/w). *V. radiata* seeds were planted at the PCES-soil compositions and received 50 mL of distilled water every day. The stalk length was measured at 10, 20, and 30 days after planting, and the root length was measured at 30 days after planting.

Preparation of PCES. Chicken eggshells were collected and air-dried for two weeks. The dried eggshells were then crushed and powdered using an electric grinder (Nima Japan 150 W NM-8300). Subsequently, the PCES was acquired from the resulting solid through a sieve (pore size: 0.16 cm).

Formulation of PCES-soil compositions. The soil compositions were prepared at the following PCES percentages: 0%, 10%, and 15% (w/w). Six pots were allotted for each treatment. For each pot, about 400 g of dry loam soil was homogenized with a mass of PCES corresponding to its assigned treatment.

Growing of V. radiata plants. Five *V. radiata* seeds were planted in each pot and about 50 mL of distilled water was allocated to each pot per day. Moreover, the blocking of the pots was randomized every day.

Measurement of morphological lengths. After 10 and 20 days, the stalk length of the plants was measured using Measure © 2020 Apple Inc. (precision: ±1 cm). After 30 days, both the stalk length and root length of the plants were measured using a vernier caliper (precision: ±0.005 cm).

Data Analysis. One-way analysis of variance (ANOVA) test was conducted to determine significant differences at the morphological lengths between treatments, and a post-hoc Tukey-Kramer test was conducted to determine which treatments significantly differed from each other. The tests were conducted at an alpha level of 0.05 (α=0.05) using the Analysis Toolpak add-in of Microsoft® Excel® for Microsoft 365 MSO (16.0.13901.20436) 64-bit.

Safety Procedure. During the conduct of the study, the use of appropriate personal protective equipment (PPE) was observed. Electricity-powered and hazardous equipment were properly handled according to their safety precautions. Lastly, all organic and inorganic waste were disposed of accordingly.

Results and Discussion. - In this study, a significant difference exists between the total means of the morphological lengths of the plants grown on 0% PCES and PCES-treated soil (10% and 15% PCES) at all intervals. Additionally, there was no significant difference between the stalk length of the plants grown on 10% and 15% PCES at all intervals, but interestingly, a significant difference exists between their root lengths. Simply put, the addition of PCES as a soil amendment significantly improved the vegetative growth of *Vigna radiata* (Figures 1 and 2).

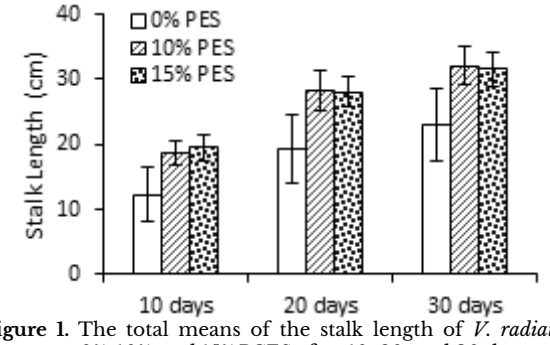

Figure 1. The total means of the stalk length of *V. radiata* grown on 0%, 10%, and 15% PCES after 10, 20, and 30 days.

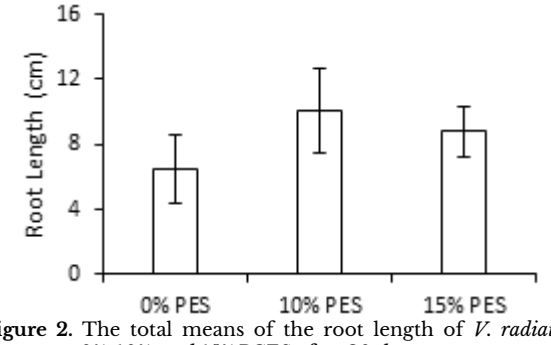

Figure 2. The total means of the root length of *V. radiata* grown on 0%, 10%, and 15% PCES after 30 days.

These findings are mainly associated with the calcium content of eggshells [1,4], where the mineral plays a key role in several physiological processes in plants [5,11]. Furthermore, similar studies conducted by Wijaya and Teo [5] and Gaonkar and Chakraborty [7] reported similar findings as well.

Contrastingly, adverse effects were observed on the plants grown on 15% PCES. As previously mentioned, a significant difference exists between the root lengths of the plants grown on 10% and 15% PCES; it was presented in Figure 2 that this was in favor of the prior treatment. Furthermore, chlorosis was observed on the leaves of the plants grown on 15% PCES. It is known that excessive calcium uptake may lead to disturbances in the ion balance, resulting in an antagonistic effect towards other minerals, such as iron, potassium, and magnesium [11,16]. This results in mineral deficiency, mainly indicated by chlorosis—the decreased green pigmentation in

interveinal areas but an increased pigmentation in the veins of the leaves [11,16,17]. In this study, plants grown on 15% PCES had their third and succeeding trifoliates afflicted with chlorosis. Simply put, the younger leaves were afflicted, which was also observed in previous studies that investigated iron and potassium deficiency [11,17] (Figure 3).

Figure 3. The leaves of a *V. radiata* plant grown on 15% PCES afflicted with chlorosis.

As previously mentioned, the occurrence of chlorosis in the plants may be due to the excessive amount of calcium present in the soil composition. Consequently, this results in the deficiency of essential plant growth minerals, such as iron, potassium, and magnesium, due to the induction of an ion imbalance associated with the antagonistic relationship between calcium and the aforementioned cation minerals [11,16,17]. Moreover, a study conducted by Giel and Bojarczuk [11] reported that other than the induction of mineral deficiencies, the addition of calcium salts such as calcium carbonate increases the total nonstructural carbohydrates (TNC) in the roots and leaves of plants. This limits the utilization of photosynthetic products and subsequently causes growth inhibition. Furthermore, this may be attributed to the observed significant difference between the root length of the plants grown on 10% and 15% PCES.

In summary, PCES significantly improved the vegetative growth of *V. radiata* in terms of the morphological lengths measured. However, excessive calcium uptake may have occurred at the plants grown on 15% PCES, which resulted in chlorosis. Furthermore, it is critical to note that calcium uptake was not quantified in this study. The occurrence of chlorosis has been associated with excessive calcium uptake since it is the major component of the PCES—the variable that was varied among treatments. In addition, there is existing literature that correlates mineral deficiencies to interveinal chlorosis, and only the plants grown on 15% PCES were afflicted with chlorosis despite the randomization of the blocking of the pots on a daily basis and the homogenization of the soil compositions.

Limitations. Only two parameters were evaluated to observe vegetative growth, namely, stalk and root length, since the plants were observed for only 30 days due to time constraints. Furthermore, no tests or analyses were done regarding soil parameters, calcium uptake, mineral and TNC content, and chlorosis due to the unavailability of equipment since the study was conducted during a pandemic.

Conclusion. - Powdered chicken eggshells significantly improved the vegetative growth of the *V. radiata* plants. However, excessive amounts induced adverse effects on the plants.

Recommendations. - It is recommended to observe the plants until the reproductive stage to quantify other morphological structures. Furthermore, the analysis of variables correlated with excessive calcium uptake such as mineral and TNC content is advised to quantify the influence of excess calcium. This is to determine which mineral deficiency occurred due to their identical visual indicator—chlorosis. Regarding this, reflectance spectroscopy is suggested to quantify the occurrence of chlorosis. Lastly, it is advised to determine the amount threshold of PCES with regards to the adverse effects and the ideal PCES supplementation for the best mean scores.

Acknowledgment. - The authors would like to extend their gratitude to Mrs. Ma. Romy Alexis C. Consulta for the validation of the statistical tests used in the study.

References

[1] Oliveira DA, Benelli P, Amate ER. 2013. A literature review on adding value to solid residues: egg shells. Journal of Cleaner Production. 46(2013): 42–47. doi: 10.1016/j.jclepro.2012.09.045.

[2] Francis AA, Abdel Rahman MK. 2016. The environmental sustainability of calcined calcium phosphates production from the milling of eggshell wastes and phosphoric acid. Journal of Cleaner Production. 137(2016): 1432–1438. doi: 10.1016/j.jclepro.2016.08.029.

[3] Food and Agriculture Organization of the United Nations. 2021. FAOSTAT Database. World: FAO. https://bit.ly/2VoBGy9.

[4] Murakami FS, Rodrigues PO, de Campos CMT, Silva MAS. 2007. Physicochemical study of CaCO3 from egg shells. Ciência e Tecnologia de Alimentos. 27(3): 658–662. doi: 10.1590/S0101-20612007000300035.

[5] Wijaya VT, Teo SS. 2019. Evaluation of eggshell as an organic fertilizer on sweet basil. International Journal of Sustainable Agricultural Research. 6(2): 79–86. doi: 10.18488/journal.70.2019.62.79.86.

[6] Khairnar MD, Nair SS. 2019. Study on eggshell and fruit peels as a fertilizer. International Conference on Sustainable Development. Novateur Publications. 14–15 February. ISBN No. 987-93-87901-05-6.

[7] Gaonkar M, Chakraborty AP. 2016. Application of Eggshell as Fertilizer and Calcium Supplement Tablet. International Journal of Innovative Research in Science, Engineering, and Technology. 5(3): 3520–3525. doi: 10.15680/IJIRSET.2016.0503183.

[8] Ok YS, Lee SS, Jeon WT, Oh SE, Usman ARA, Moon DH. 2011. Application of eggshell waste for the immobilization of cadmium and lead in a contaminated soil. Environmental Geochemistry and Health. 33(2011): 31–39. doi: 10.1007/s10653-010-9362-2.

[9] Soares MAR, Quina MJ, Ferreira RMQ. 2015. Immobilisation of lead and zinc in contaminated soil using compost derived from industrial eggshell. Journal of Environmental Management. 164(2015): 137–145. doi: 10.1016/j.jenvman.2015.08.042.

[10] White PJ, Broadley MR. 2003. Calcium in Plants. Annals of Botany. 92(4): 487–511. doi: 10.1093/aob/mcg164.

[11] Giel P, Bojarczuk K. 2010. Effects of high concentrations of calcium salts in the substrate and its pH on the growth of selected rhododendron cultivars. Acta Societatis Botanicorum Ploniae. 80(2): 105–114. doi: 10.5586/ASBP.2011.021.

[12] [UN] United Nations. 2020 September 19. Sustainable Development Goals [Internet] [cited 2020 October 22]. Available from: https://bit.ly/3941J2y.

[13] Huezé V, Tran G, Bastianelli D, Lebas F. 2015. Mung bean (*Vigna radiata*). Feedipedia, a programme by INRA, CIRAD, AFZ and FAO. http://www.feedipedia.org/node/235 Last updated on July 3, 2015.

[14] Balinado LO, Manzano RME, Ate CN, Fernandez M, Chan MA. 2019. Early Vegetative Growth Responses of *Vigna radiata* L. (Mungbean) cv NSIC Mg 17 to Boron Toxicity. Journal of Nature Studies. 18(1): 11–21.

[15] PSA. 2020. Major Vegetables and Rootcrops Quarterly Bulletin. 14(2): ISSN 2094-618x. https://bit.ly/35TOmjs.

[16] Samborska IA, Kalaji HM, Sieczko L, Goltsev V, Borucki W, Jajoo A. 2018. Structural and functional disorder in the photosynthetic apparatus of radish plants under magnesium deficiency. Functional Plant Biology. 45(2018): 668–679. doi: 10.1071/FP17241.

[17] Rustioni L, Grossi D, Brancadoro L, Failla O. 2018. Iron, magnesium, nitrogen, and potassium deficiency symptom discrimination by reflectance spectroscopy in grapevine leaves. Scientia Horticulturae. 241(2018): 152–159. doi: 10.1016/J.SCIENTA.2018.06.097.

Comparison of the percent adsorption of raw corn husk and raw rice husk for bunker fuel

YURI V. ESCARILLA, BHEA ELAINE P. MALLARE, JULIA DUANE J. SELIBIO, and ZENNIFER L. OBERIO

Philippine Science High School Western Visayas Campus - Department of Science and Technology (DOST-PSHSWVC), Brgy. Bito-on, Jaro, Iloilo City 5000, Philippines

Article Info

Submitted: May 06, 2021
Approved: Jun 16, 2021
Published: Aug 30, 2021

Keywords:
adsorption
rice husks
corn husks
bunker fuel
oil spill

Abstract

Oil spills are detrimental to the environment and its inhabitants. In this study, raw corn husks (RCH) and raw rice husks (RRH) were used as sorbents for bunker fuel. Adsorption tests were performed by subjecting the sorbents in bunker fuel. The mean percent adsorption of RCH, RRH, and sorbent pad were 10.1%, 3.75%, and 56.8%, respectively. It was found that RCH exhibited a significantly higher mean percent adsorption than RRH which was most likely due to its relatively higher cellulose content. Additionally, sorbent pad exhibited a significantly higher mean percent adsorption than the husks possibly due to its higher saturation point. Although the adsorption percentages of RCH and RRH were significantly less than that of sorbent pads, their ability to adsorb made them viable sorbents for bunker fuel removal, and when compared, RCH would be the better sorbent over RRH.

Introduction. - Oil spill incidents pose a serious threat to the marine environment. These spills may be caused by accidents involving oil tankers and pipes, natural disasters, and runoffs [1]. Spills including crude oil from tankers, refined petroleum products, and heavy fuels such as bunker fuel are a major environmental concern. This is because most components of the oil-like polycyclic aromatic hydrocarbons (PAHs) are toxic to both aquatic and terrestrial organisms, and induce irreversible effects to the environment [2,3]. Bunker C fuel (No. 6 oil), which powers marine vessels, is the most common in these incidents [4]. Bunker fuel evaporates in small percentages and presents a higher viscosity relative to the other oil types [5].

Adsorption is an economically advantageous and eco-friendly approach in remediating oil spill incidents. It is a process wherein oil particles are attracted to the surface of the sorbent. The process relies on the adhesion of the oil particles to the sorbent surface and cohesive properties of oil which allow greater amounts of oil to be retained by the sorbent [8].

Studies have investigated the adsorption capabilities of different agricultural wastes on crude oil [1,7,9]. The use of rice husks and corn husks as sorbents for oil spill remediation removes environmental pollutants while minimizing the negative impacts of burning and disposal of agricultural by-products [10]. It was concluded in the study of Razavi et al. [7] that the oil adsorption capacity of raw rice husk on crude oil was independent of pH. They added that the particle size of the sorbent and viscosity of the oil would significantly affect the adsorption capacity wherein directly proportional relationships would be observed between the adsorptive capability and the two parameters. Biological structures were also found to affect adsorption capacity [11,12]. Furthermore, previous studies have utilized pre-treated husks in removing environmental pollutants such as dyes, heavy metals, and certain organic compounds [1,9]. However, it should be noted that these pre-treatment steps may be time-consuming and costly [10]. Thus, the use of husks in their raw state would be highly advantageous, especially in emergency oil spill situations.

Previous studies have found that cellulose content is higher in raw corn husk (RCH) than in raw rice husk (RRH) [13,14,15,16,17]. It was also observed that when the cellulose content was increased, the adsorption capacity of husks also increased [11,12]. Therefore, it is hypothesized that RCH will exhibit a significantly higher fuel percent adsorption compared to RRH.

This study aimed to determine and compare the percent adsorption of RRH, RCH, and sorbent pads for bunker fuel. It specifically aimed to:

(i) determine the weight of the sorbents before and after adsorption; and

(ii) calculate and compare the percent adsorption of the three sorbents.

Methods. - The corn husks and rice husks were washed, sun-dried, ground, sifted, wrapped in polypropylene fabric, and then submerged in pure

How to cite this article:
CSE: Escarilla YV, Mallare BEP, Selibio JDJ, Oberio ZL. 2021. Comparison of the percent adsorption of raw corn husk and raw rice husk for bunker fuel. Publiscience. 4(1): 67–70.
APA: Escarilla, Y.V., Mallare, B.E.P., Selibio, J.D.J., & Oberio, Z.L. (2021). Comparison of the percent adsorption of raw corn husk and raw rice husk for bunker fuel. *Publiscience, 4*(1), 67–70.

For supplementary data, contact: publiscience@wvc.pshs.edu.ph.

bunker fuel. Commercially available polypropylene sorbent pads, also wrapped in polypropylene fabric, were used as a positive control. The samples were allowed to drain before weighing to determine the percent adsorption of the three sorbents (RRH, RCH, and sorbent pads). The mean percent adsorption of the three sorbents were then determined and compared using One-Way Analysis of Variance (ANOVA). Ten samples were conducted per sorbent.

Materials. RCH and RRH were gathered from San Joaquin, Iloilo, and Roxas City, Capiz, respectively, while sorbent pads were obtained from the Philippine Coast Guard Station in Bo. Obrero, Iloilo City. Bunker fuel was procured from the Iloilo City Public Safety and Transportation Management Office.

Preparation. RCH and RRH were washed, sun-dried, subjected to grinding, then sifted using a 2 mm sieve. Ground husks then underwent the coning and quartering method thrice for randomization. Five grams of each sorbent was wrapped in polypropylene fabric. Polypropylene fabric was used as a container for easy retrieval of the ground sorbents after submersion in bunker fuel.

Adsorption. Wrapped RCH was soaked in 80.0 g of bunker fuel for 3 hours and was allowed to drip until the point when no further dripping was observed. Finally, the resulting sorbent was weighed using a calibrated digital weighing scale. Similar procedures were followed for the RRH and sorbent pads. Ten samples were tested for each sorbent. To control the effect of the polypropylene fabric on fuel sorption, three samples of empty polypropylene pouches of the same dimensions as those used in wrapping the sorbents were subjected into the fuel under the same experimental conditions. Their weights were then taken, and averaged. The calculated average weight of 10.62 grams was subtracted from the weights of the sorbents wrapped in polypropylene fabric with adsorbed fuel.

Data Analysis. The percent adsorption for each sorbent was calculated using the following formula adapted from the study of Razavi et al. [1]:

$$\%\ Adsorption = \left(\frac{S_t - S_0}{W_{fuel}}\right) \times 100$$

Where:
S_t = the weight (in grams) of the sorbent after adsorption
S_o = the weight (in grams) of the sorbent before adsorption
W_{fuel} = the weight of the fuel before adsorption in grams.

Statistical Analysis. One-way ANOVA was conducted to compare the three mean percent adsorption using Microsoft Excel 2016 with Real Statistics Resource Pack software (Release 7.2) and QI Macros statistical process control (SPC) software package plugin, version 2021.01. The level of significance was at 0.05. The Levene's test was used for the homogeneity of variances and the Tukey test for post-hoc analysis. Both were executed using the same program. To check for normality, the Shapiro-Wilk test was conducted using the software JASP 0.14.1.

Safety Procedure. Excess bunker fuel and used sorbents were stored in a closed container and were handed over to the community waste disposal team.

Results and Discussion. - Table 1 shows the average weights (in grams) of each sorbent before and after fuel adsorption.

Table 1. Mean and standard deviation of the weights before and after fuel adsorption (in grams) of RCH, RRH, and sorbent pad.

Sorbent	Before Adsorption (g)	After Adsorption (g)
RCH	5.00	13.2 ± 1.89
RRH	5.00	8.00 ± 0.78
Sorbent Pad	5.00	50.4 ± 1.74

Figure 1 shows the respective mean percent adsorption of the three sorbents for bunker fuel.

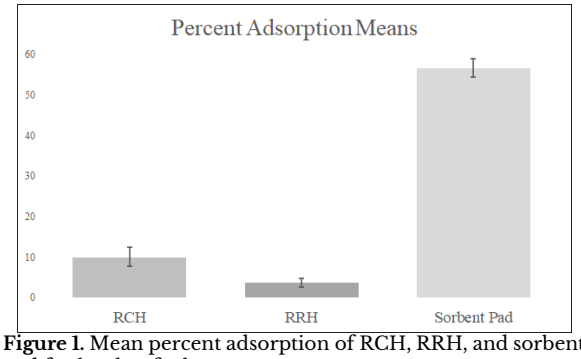

Figure 1. Mean percent adsorption of RCH, RRH, and sorbent pad for bunker fuel.

RCH yielded a mean percent adsorption of 10.1 ± 2.40. The RRH on the other hand had mean adsorption of 3.75% ± 1.03. Finally, for the sorbent pad, the mean adsorption was 56.8% ± 2.29.

Using the Shapiro-Wilk test, data was confirmed to have a normal distribution. Additionally, there was a statistically significant difference between groups as determined by one-way ANOVA ($F(2,27) = 2090.11$, $p = .000$). Data was found to satisfy the assumption of homogeneity of variances through Levene's test ($p = 0.093 > 0.05$). Tukey post hoc test revealed that RCH (10.13% ± 2.40%, $p = .000$) exhibited a significantly higher mean percent adsorption than RRH (3.75% ± 1.03%, $p = .000$), and sorbent pad (56.77% ± 2.29%, $p = .000$) exhibited a significantly higher mean percent adsorption than RCH.

The significantly higher percent adsorption of RCH over RRH could be attributed to the cellulose content of the sorbents. The cellulose content in RCH is generally greater than that in RRH [13, 14, 15, 16, 17], where the mentioned studies only featured either of the husks. In addition to this, characterization studies using the Technical Association of Pulp and Paper Industry (TAPPI) method of identifying the chemical composition of husks revealed that cellulose in corn husks reached 31-39% while only a maximum of 31%

was present in rice husks [18, 19]. Cellulose was found to play a key role in maintaining the mesopore structure of activated carbon as a sorbent [11]. Mesopores function in accelerating diffusion into micropores and increasing the equilibrium coverage of the micropore surface which contains adsorptive sites wherein the inner layers possess higher adsorption energies [12].

According to the International Tanker Owners Pollution Federation Limited (ITOPF) [8], sorbent materials for oil spills should attract oil to their surface or incorporate the oil in the material itself. RCH and RRH exhibited mean percent adsorption of 10.19% ± 2.40 and 3.76% ± 1.02, respectively. The exhibited percent adsorption, although low, can qualify RCH and RRH as sorbent materials. In addition, there is no basis for comparison for the RRH results since the methods used in this study were not similar to other related studies. With this, due to the husks' biodegradability, high supply, simple preparation, low cost, but low adsorption capacity, RCH and RRH could be potential sorbents only for emergency bunker fuel spill situations, in cases when the commercially used sorbent pads are unavailable.

It was also found that the sorbent pad exhibited a significantly higher percent adsorption compared to the other two organic sorbents. This was concurrent with the information that polypropylene sorbent pads can recover up to 20% more oil than natural organic sorbents [17]. Although natural-based materials are inexpensive, abundant, and environmentally friendly, their relatively lower oleophilic property makes their adsorption capacity inferior to some synthetic materials which are engineered for the sole purpose of adsorbing fuels [18, 19]. Furthermore, the difference in the packing of the sorbent pad and the husks may have affected the surface area of each sorbent, which is another factor that influences adsorption [8]. Since the sorbent pads were laid in sheets, they may have had greater surface area than the ground husks, therefore yielding a significantly greater percent adsorption

In conducting the experiments, the sorbent pad was first tested to identify the ideal contact time and bunker fuel dosage, which is the least possible amount of fuel and time for the sorbent pad to be completely soaked. The contact time should ensure the sorbent has reached its maximum saturation [23]. It was found out that five grams of sorbent pad were completely saturated when immersed in 80 grams of bunker fuel at the 3-hour mark. A contact time of three hours, bunker fuel dosage of 80 grams, and initial sorbent weight of five grams were uniformly followed for the final data gathering for all three sorbents.

The dripping time after adsorption used for the final data gathering was 15 minutes which was observed during the preliminary data gathering to be the point of no dripping. Dripping time should reach the point of no dripping to ensure that the fuel loosely held by the sorbent is lost to report an accurate adsorption capacity [23]. This can also be backed by the study of Said et al. [24] which also utilized the same length of fuel dripping.

To avoid the interference of the possible fuel adsorption of the polypropylene fabric that was used to wrap the sorbents, its mean fuel adsorption was also separately measured thrice following the same contact and dripping times as the final data gathering. The mean fuel adsorption of the polypropylene fabric was then subtracted from the total weight of the sorbent after the fuel adsorption in calculating for the percent adsorption of the final data.

Limitations. Due to the lack of resources, mathematical models were not used in presenting the results. In addition, there was no basis for comparison for the RRH results since the methods used in this study were not similar to other related studies. Lastly, due to the unavailability of the necessary equipment, the uniformity of the packing of the sorbents in the polypropylene fabric was not followed wherein the husks were in powder form while the sorbent pads were laid in sheets when subjected to bunker fuel.

Conclusion. - The adsorption percentages of RCH and RRH were significantly less than that of sorbent pads, and when compared, RCH would be the better sorbent over RRH. Despite the limited inclusion of adsorption parameters, this study showed a simple preliminary measure of screening oil adsorption capacities of ground sorbents for possible usage in oil spills.

Recommendations. - It is recommended that future studies conduct adsorption isotherm modelling to investigate the interaction mechanism between the adsorbent and the adsorbate. Furthermore, future studies can also test different physical modifications such as size and surface area variations to RCH and RRH and determine any significant differences with respect to their adsorption capacities. In addition, it is recommended that the size and morphology of the tested sorbents be characterized by electron microscopy techniques and their chemical composition by spectroscopic techniques like infrared spectroscopy. It is also recommended that when comparing different sorbents, the packing should be uniform for all tested sorbents. Lastly, it is recommended to test the adsorption capacities of RCH and RRH on other oil pollutants in an oil/water mixture.

Acknowledgment. - The researchers would like to extend their gratitude to Mr. Jeck Conlu of the Iloilo City Public Safety Transportation Management Office and Mr. Edgar Boado of the Philippine Coast Guard - Western Visayas for their help in the procurement of materials.

References

[1] Razavi Z, Mirghaffari N, Rezaei B. 2014. Performance comparison of raw and thermal modified rice husk for decontamination of oil polluted water. Clean (Weinh). 43(2): 182–190.

[2] Briggs IL, Briggs BC. 2018. The political ecology of oil and gas activities in the Nigerian aquatic ecosystem. Cambridge (MA): Academic Press. Petroleum industry activities and human health; p. 143–147.

[3] Gammoun A, Tahiri S, Albizane A, Azzi M, De la Guardia M. 2007. Decontamination of water polluted with oil through the use of

tanned solid wastes. Environ Eng Sci. 6(5): 553–559.

[4] Schnurr REJ, Walker TR. 2019. Reference module in earth systems and environmental sciences. Elsevier. Marine Transportation and Energy Use.

[5] Fingas M. 2017. Oil spill science and technology. Houston (TX): Gulf Publishing Company. Introduction to spill modeling; p. 419–453.

[6] Tsamo C, Kidwang GD, Dahaina DC. 2020. Removal of Rhodamine B from aqueous solution using silica extracted from rice husk. SN Appl Sci. 2(2): 256–268.

[7] Razavi Z, Mirghaffari N, Rezaei B. 2013. Adsorption of crude and engine oils from water using raw rice husk. Water Sci Technol. 69(5): 947–952.

[8] ITOPF. 2012. Use of sorbent materials in oil spill response. Canterbury: Impact PR and Design Limited (UK). Report No.: 8.

[9] Husseien M, Amer AA, El-Maghraby A, Hamedallah N. 2009. A comprehensive characterization of corn stalk and study of carbonized corn stalk in dye and gas oil sorption. J Anal Appl Pyrolysis. 86(2009): 360–363.

[10] Ahmaruzzaman M, Gupta VK. 2011. Rice husk and its ash as low-cost adsorbents in water and wastewater treatment. Ind Eng Chem Res. 50: 13589–13613

[11] Xue Y, Du C, Wu Z, Zhang L. 2018. Relationship of cellulose and lignin contents in biomass to the structure and RB-19 adsorption behavior of activated carbon. New J Chem. 42(20): 16493-16502.

[12] Hsieh CT, Teng H. 2000. Influence of mesopore volume and adsorbate size on adsorption capacities of activated carbons in aqueous solutions. Carbon. 38(6): 863–869.

[13] Rahman IA, Ismail J, Osman H. 1997. Effect of nitric acid digestion on organic materials and silica in rice husk. J Mater Chem. 7(8): 1505–1509.

[14] Jantip S, Suwanruji P. 2011. Preparation and properties of microcrystalline cellulose from corn residues. Adv Mat Res. 332-334. 1781–1784.

[15] Ibrahim MIJ, Sapuan SM, Zainudin ES, Zuhri MYM. 2019. Extraction, chemical composition, and characterization of potential lignocellulosic biomasses and polymers from corn plant parts. BioResources. 14(3): 6485–6500.

[16] Chabannes, Bénézet JC, Clerc L. 2014. Use of raw rice husk as natural aggregate in a lightweight insulating concrete: An innovative application. Constr Build Mater. 70: 428–438.

[17] Aremu MO, Aperolola SO, Dabonyan OO. 2015. Suitability of Nigerian corn husk and plantain stalk for pulp and paper production. Eur. Sci. 11(30): 146–152.

[18] Johar N, Dufresne A. 2012. Extraction, preparation and characterization of cellulose fibres and nanocrystals from rice husk. Ind Crops Prod. 37(1): 93–99.

[19] Mendes CA, Adnet FA, Leite MCA, Furtado CR, De Sousa AM. 2015. Chemical, physical, mechanical, thermal, and morphological characterization of corn husk residue. Cellulose Chem Technol. 49 (9–10): 727–735.

[20] Fingas M. 2011. Oil spill science and technology. Houston (TX): Gulf Publishing Company. Introduction to spill modeling; p. 303–337.

[21] Chol HM, Cloud RM. 1992. Natural sorbents in oil spill cleanup. Environ Sci Technol. 26: 772–776.

[22] Zamparas M, Tzivras D, Dracopoulos V, Ioannides T. 2020. Application of sorbents for oil spill cleanup focusing on natural-based modified materials: a review. Molecules. 25(4522): 1–22.

[23] Bazargan A, Tan J, McKay G. 2015. Standardization of oil sorbent performance testing. J Test Eval. 43(6): 1271–8.

[24] Said AA-EA, Ludwick AG, Aglan HA. 2009. Usefulness of raw bagasse for oil absorption: a comparison of raw and acylated bagasse and their components. Bioresour Technol. 100(6): 2219–2222.

CLUSTER FIVE

AQUACULTURE

The gem is depicted as a blue-colored aquatic animal that represents aquatic life, both as an important part of the environment and as an important resource. Blue is also commonly associated with water, our planet's most precious resource and a major part of life and our ecosystem. As such, it is important to maintain our aquatic resources and find solutions to the existing problems that aquaculture faces. These research studies aim to address such problems and provide an avenue of locally-based research in aquaculture-centered fields of science.

These studies also fall under the Aquatic, Agriculture, and Natural Resources (AANR) Research and Development Agenda. They are in line with the priorities and agendas set for aquaculture research moving forward.

BASED ON: Harmonized National Research and Development Agenda (HNRDA)

Publiscience Vol. 4 Issue 1

Sodium lactate as a potential preservative to green mussel meat

CHARMY JAMME A. AMPORDAN, HERA ELOISA B. REGULACION, and JULNAFE B. LIBO-ON

Philippine Science High School Western Visayas Campus - Department of Science and Technology (DOST-PSHSWVC), Brgy. Bito-on, Jaro, Iloilo City 5000, Philippines

Article Info

Submitted: May 11, 2021
Approved: Jul 12, 2021
Published: Aug 30, 2021

Keywords:
green mussels
Perna viridis
preservation
shelf life
sodium lactate

Abstract

The short shelf life of green mussels could limit its consumption and wider distribution to the market and thus, proper storage of this product is necessary. In this study, the effects of different concentrations (1%, 2%, 3%, and 4%) of sodium lactate on the preservation of green mussels during chilled storage of nine days were determined. Changes in pH and weight loss of the mussel meat were recorded every three days. Results showed that the pH values of the treated samples are around the neutral pH (6.7 to 7.1) and are significantly higher than the untreated samples throughout the duration of storage. No significant difference was observed in the weight loss between the control and treatment groups. Thus, the results of the parameters showed that sodium lactate has the potential to be utilized as a preservative agent for meat.

Introduction. - Green mussel (*Perna viridis*) is a type of shellfish that is commonly sold in local markets. This bivalve is widely consumed, especially by people living in coastal areas, as a cheap protein source [1]. However, the process of transporting these products from mussel farms to different markets is too laborious due to the small amount of meat produced per kilogram of the green mussels. Consequently, the immediate consumption or proper storage of this product is necessary since it could only be stored for two (2) days at ambient temperature [2]. The process of product deterioration occurs due to the growth of bacteria in the product over time [3]. The development of a processing method is important for extending the shelf life of mussels [4] since this could ensure that the product is still safe for consumption after a period of time.

Various methods on the preservation of green mussel meat, including pre-treatment with organic acids and modified atmosphere packaging, have already been studied. Organic acids are commonly used in food preservation since they have the ability to inhibit the growth of microorganisms, and they also occur naturally in food (i.e. lactic acid from corn and citric acid from oranges) [5]. Preservation occurs when the molecules of these acids dissociate inside bacterial cells due to low pH, resulting in the release of toxic charged anions and protons that inhibit the metabolic reactions of the bacteria [6,7]. Organic salts of these acids, such as sodium acetate, sodium lactate, and sodium citrate, are also used for food preservation.

Sodium lactate is the organic salt of lactic acid that is generally produced from natural lactic acid that is reacted with sodium hydroxide [8], and is reported to be a very prominent flavor enhancer with few negative effects [9]. The addition of this organic salt to meat products delays the development of sour and off-flavors by binding to free radicals in the meat to prevent lipid oxidation [9].

One of the qualities that are analyzed in food preservation is weight loss. This property is an important indicator because it is attributed to the loss of water in the meat [10]. High water retention in food may serve as a nutrient and contribute to the microbial proliferation in the product [4]. Sodium lactate is known for its ability to improve the moisture retention of materials [11]. The addition of sodium lactate to meat products has shown improvement in the cooking yield of the meat due to its humectant properties that contribute to the water-holding capacity of the product [12]. There are three proposed mechanisms by which sodium lactate can have an antimicrobial effect: (1) It has the ability to lower the water activity of the meat and thereby slowing the bacterial growth; (2) Sodium lactate passes through the cell membrane and lowers intracellular pH; and (3) It affects the cellular metabolism by inhibiting ATP^2 generation [13]. The lactic acid portion of sodium lactate and the sodium ion has antimicrobial effects, which slows down the normal metabolic process that generates energy in the cell [13].

Additionally, pH values are usually measured as a quality indicator for seafood products. The ideal pH of green mussels ranges from 6.00-6.85 [14].

How to cite this article:
CSE: Ampordan CJ, and Regulacion HE. 2021. The Use of Different Sodium Lactate Concentrations as a Potential Preservative to Green Mussel Meat. Publiscience. 4(1): 72–76.
APA: Ampordan C.J., & Regulacion H.E. (2021). The Use of Different Sodium Lactate Concentrations as a Potential Preservative to Green Mussel Meat. *Publiscience*, *4*(1), 72–76.

For supplementary data, contact: publiscience@wvc.pshs.edu.ph.

According to Miller (2010) [13], sodium lactate addition is associated with increasing the meat pH, increasing the water-holding capacity, and reducing cook losses which results in the increase in the tenderness of meat. Sodium lactate has been proven to be an effective additive in preserving seafood products such as refrigerated sliced salmon [15], and refrigerated rainbow trout [16]. It is also hypothesized that sodium lactate has the ability to preserve green mussel meat. Therefore in this study, sodium lactate was utilized as an additive for the preservation of green mussel meat.

This study aims to determine the effects of different concentrations of sodium lactate on the preservation of green mussel meat during chilled storage. Specifically, this study aims to:

(i) measure the weight loss of the green mussel meat after treatment with different concentrations (1%, 2%, 3%, 4%) of sodium lactate and without treatment for 9 days.

(ii) determine the change in pH of the green mussel meat after treatment with different concentrations (1%, 2%, 3%, 4%) of sodium lactate and without treatment for 9 days

Methods. - The methods for the conduct of this study were designed to be doable at home. Two parameters were analyzed, namely the change in pH and weight loss. Each member of the work unit prepared a set-up of the experiment. However, the same materials were utilized for the conduct of the experiment. The experiment performed was the same for both set-ups. Green mussels were obtained from a mussel farm in Dangula-an, Anilao, Iloilo. Aqueous solutions of sodium lactate with different concentrations (1%, 2%, 3%, 4%) were prepared for the treatment of the shucked mussel meat.

The study was conducted for 9 days, and analyses of weight loss and pH were performed every 3 days during the duration of the study. Samples were stored in a storage condition of 3 ± 1°C [4].

Sample collection. Samples of green mussels were collected in Dangula-an, Anilao, Iloilo. An icebox filled with seawater was used to store the mussels. The samples were then transported back to Iloilo City, with the duration of the travel being approximately one hour from the collection site.

Sample preparation. Upon arrival, the mussels were shucked, washed with distilled water, and drained. Mussels having a foul odor or open shells were removed. A total of 2 kg of mussel meat was obtained. The mussels were divided into five (5) groups: (a) 1% sodium lactate, (b) 2% sodium lactate, (c) 3% sodium lactate, (d) 4% sodium lactate, and (e) negative control, which are the samples without treatment. Sodium lactate (USP grade) was purchased online through the website of Dalkem Corporation. The formula $C_1V_1 = C_2V_2$ was used to calculate the different concentrations of sodium lactate. The concentrations 1%, 2%, 3%, and 4% were obtained by diluting 60% sodium lactate solution with distilled water. The solutions were stored in clean, plastic bottles. The calculations were as follows:

Calculation for 1%:

$$C_1V_1 = C_2V_2$$
$$60\% \cdot V_1 = 1\% \cdot 1000\,mL\ water$$
$$V_1 = 16.67\,mL$$

Calculation for 2%:

$$C_1V_1 = C_2V_2$$
$$60\% \cdot V_1 = 2\% \cdot 1000\,mL\ water$$
$$V_1 = 33.33\,mL$$

Calculation for 3%:

$$C_1V_1 = C_2V_2$$
$$60\% \cdot V_1 = 3\% \cdot 1000\,mL\ water$$
$$V_1 = 50.00\,mL$$

Calculation for 4%:

$$C_1V_1 = C_2V_2$$
$$60\% \cdot V_1 = 4\% \cdot 1000\,mL\ water$$
$$V_1 = 66.67\,mL$$

For the sample storage, 20 plastic resealable bags were utilized. A different bag for each treatment was used for every sampling interval. The ratio of the weight of the mussels to the solution is 1:2. Each pack of samples contains 100 g of green mussel meat. The samples were treated with 200 ml sodium lactate solution. The solutions were then poured into the resealable plastic bags according to the labels. The samples were stored inside the refrigerator for nine (9) days with a storage condition of 3 ± 1°C [4]. A thermometer was utilized in order to monitor the temperature inside the refrigerator.

pH determination. The pH of the control and treated samples was measured using a pen-type pH meter (Milwaukee, PH600AQ Digital pH Pen). This device was calibrated by measuring the pH of distilled water in every sampling interval before analysis. The pH of each group was determined by following the standard method of measuring the pH of solid-liquid mixtures. The samples were drained using a strainer to separate the mussel meat from the solution. The liquid solution was transferred to a beaker, and then its pH value was measured. Then, the mussels were blended into a homogenous paste and the pH measurement was taken. After that, the liquid solution and paste were combined, and pH was measured. The measurements were done in triplicates.

Weight loss. For the weight loss determination, the samples were weighed before and after storage. An analytical balance (Shimadzu, BL3200H) was utilized to determine the weight of the samples. This analysis was done in triplicates for every sampling interval. Percentage of weight loss was determined using the formula [17]:

$$Weight\ loss\ (\%) = \frac{initial\ weight - final\ weight}{initial\ weight} \times 100$$

Data Analysis. The data gathered was analyzed using One-way ANOVA, and post-hoc analysis was evaluated using Duncan's multiple range test. Differences between the means of the control and treated samples were examined with the level of significance set at $\alpha < 0.05$. This analysis was performed through the SPSS software.

Safety Procedure. The use of safety equipment such as laboratory gowns, gloves, and surgical masks was observed at every sampling interval. Different types of waste were segregated into different bins, and liquid wastes were collected in empty plastic bottles.

Results and Discussion. - The study aimed to determine the effects of different concentrations of sodium lactate on the preservation of green mussel meat. To this end, the pH change and weight loss of treated and untreated samples were monitored for 9 days.

Weight loss analysis. Weight loss is attributed to the loss of water in meat products [4]. High water retention is linked to the deterioration of meat since it might serve as a nutrient, which contributes to the microbial proliferation in food products [18]. However, the ability of a product to retain water is also integral to its quality in terms of juiciness and tenderness [19].

All samples showed a decrease in weight at the end of the storage. Results of the statistical analysis showed no significant difference in the weight loss between the control and treatment groups (Figure 1). This indicates that adding sodium lactate has no significant effect on the water retention of the mussel meat. The ability of myofibrillar proteins and myofibrils to entrap water is directly affected by pH and ionic strength [20]. This may explain the absence of significant difference in the weight loss between the treated and untreated samples since the pH values recorded are near neutral.

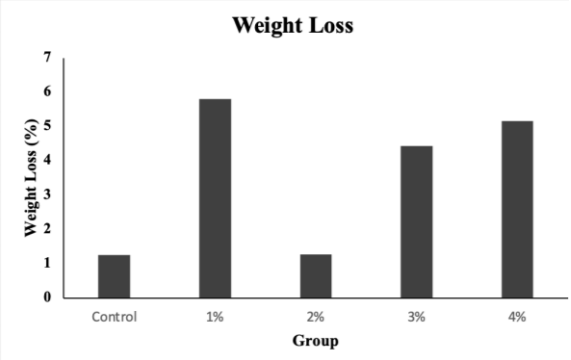

Figure 1. Percent weight loss of treated (1%, 2%, 3%, or 4% sodium lactate) and untreated samples after treatment (n=3). No significant difference observed between the treated samples and control.

In the second set-up, the analysis also showed no significant difference between the weight of the control and the treated samples. The mussels had high water retention since the weight loss percentage was low. Sodium lactate exhibits high water holding capacity which may explain the low weight loss of the samples [21].

Changes in pH. One of the physical qualities that are frequently analyzed for food quality control is pH value [4]. This factor is examined along with the Total Volatile Basic Nitrogen (TVB-N), Trimethylamine Nitrogen (TMA-N), and Thiobarbituric acid reactive substances (TBARS) for seafood quality assessment [22]. It indicates the degradation of muscle components and post-mortem change of glycogen to lactic acid during long storage [23].

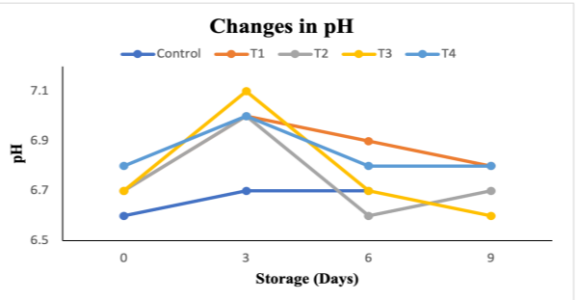

Figure 2. The trend of change in pH of the homogenized mussel meat observed per treatment throughout the nine-day period (n=3).

It is observed that all groups have yielded a pH value that is near neutral. The pH values of the mussel meat for the last day of storage were lower compared to the initial pH values. Figure 2 shows the trend of the pH change per group throughout the storage period. Based on the initial pH values of the treated and untreated samples, an increase in the pH of the treated samples could be observed on the third day of storage. After this, the pH value of the samples eventually decreased in the succeeding days except for treatment 4, where an increase in pH was observed on the final day of storage. Slight changes in the pH value upon addition of sodium lactate were also observed in other studies on meat products such as ground beef [24], cig kofte [25], poultry sausage [26], and sliced salmon [14]. Sallam and Samejima [24] indicated that sodium lactate has the ability to stabilize the pH of most meat products during storage. The recorded pH of the treated samples in this study verified an almost constant pH since all treatment groups have maintained pH values that are near neutral (6.7-7.1) throughout the duration of storage. The results of this analysis contradict the data reported in the study conducted by Eckert et al. [27], and Tan and Shelef [28], where it was stated that sodium lactate had no significant effects on the initial pH of ground meat products.

After the 9-day period, One-way ANOVA showed that the green mussels treated with sodium lactate have pH values significantly higher than the control group which indicates that there is a significant difference between the groups of samples. However, no significant difference was found to exist between the treatment groups, which implies that these four (4) treatments are not significantly different in terms of their effect on the pH of green mussel meat during chilled storage. This further indicates that 1% sodium lactate is enough to significantly increase the pH value of green mussels during storage. Having a pH value near neutral indicates that the green mussels are still safe for consumption. A decline in pH values could be due to factors such as post-mortem changes, muscle component degradation, and the fermentative conversion of glycogen [18,29]. It could also be attributed to increasing microbial count, which could be considered as the deterioration stage of the product [30]. A pH value of 5.9 for mussels is an indicator of deterioration according to Hardey [31].

However, no significant difference has been found between the control and treated groups during

the second set-up. The result may have been affected due to an error in data gathering during the first sampling interval. The pH was not correctly measured because the mussels were not blended and there was no separate measurement for the liquid part. Throughout the storage, the pH of the control has declined. This was also observed in the study conducted by Arcales and Nacional (2019) [21] that showed that the control samples had a near-neutral pH value at the start of the study and had decreased during storage.

The results of the analysis conducted on the weight loss and pH in the untreated and treated samples showed that the effect of adding sodium lactate is only evident on the change in pH and not on the percent (%) weight loss. An increase in the pH value of the samples was only observed on the third day of sampling. Based on these data alone, it could be inferred that the addition of 1% sodium lactate is already sufficient in increasing the pH level of green mussel meat that makes it suitable for consumption after longer storage. Although the pH value of the control group is significantly lower, it still falls in the range of suitable pH values for green mussels. Therefore, the data collected in this study only shows that sodium lactate has the potential to be used as a preservative agent as evidenced by its ability to increase the pH value of green mussel meat. Further analysis on the microbial proliferation and chemical reactions taking place in green mussel meat treated with sodium lactate shall be made to further determine the effectiveness of sodium lactate as a preservative for green mussels.

Limitations. A power outage occurred during the storage which lasted for 10-15 minutes (during the first set-up) and 30 minutes (during the second set-up). This circumstance may have affected the storage condition of the samples. Slight differences in the draining time of the samples may have affected the recorded weight of the samples in every sampling interval.

Conclusion. - The results obtained from each parameter showed that there is a significant difference in the pH between the treated and untreated samples. However, no significant difference was observed in the weight loss of the control and treatment groups. These results indicate that sodium lactate has the potential to be used as a preservative to green mussel meat. However, further analysis on the microbial proliferation and chemical reaction taking place in the mussel meat must be performed to determine the effectiveness of sodium lactate as a preservative and to further prove this claim.

Recommendations. - A study analyzing the bacterial load and chemical reactions taking place in green mussel meat after subjecting to sodium lactate preservation must be conducted to determine the quality of green mussel meat after the addition of the organic salt. Other recommendations include the setting of a specific duration for the draining time and provision of a backup power source in case of power outages. The addition of parameters to be analyzed such as TVB-N and TMA-N determination and sensorial evaluation is also recommended. Another recommendation is the addition of a positive control group such as using other organic substances such as sodium acetate, lactic acid, and sodium citrate, which already have established concentrations for green mussel meat preservation, in order to have a comparison for the efficacy of the organic salt that is utilized in the study.

Acknowledgment. - The researchers would like to express their utmost gratitude to Mr. Nestor Julleza for helping secure and obtain the green mussels that were utilized in this study. They would also like to extend their gratitude to Mrs. Rubylie Magaso for providing the laboratory materials that were utilized for the experiment.

References

[1] Azanza MP, Azanza R. Ventura S. 2005. Heat Shocking of Philippine Green Mussels, *Perna viridis*. Int. J. of Food Sci. and Tech. 40: 689-694.

[2] Batista I, Mendes R. 2012. Processing molluscs, shellfish and cephalopods. In: Second International Congress on Seafood Technology on Sustainable, Innovative and Healthy Seafood. p. 85–107.

[3] Masniyom P, Benjama O. 2007. Effect of lactic, acetic and citric acids on quality changes of refrigerated green mussel, *Perna viridis* (Linnaeus, 1758). Sci. Technol. 29(4): 1123–1134.

[4] Arcales JAA, Nacional LM. 2018. Effect of Lactic and Citric Acid Pretreatment on Quality Changes of Green Mussel (*Perna viridis*) During Chilled Storage. Curr. Res. Nutr. Food Sci.ch in Nutrition and Food Science Journal. 6(3): 862–872. doi:10.12944/crnfsj.6.3.29.

[5] Nakai SA, Siebert KJ. 2003. Validation of bacterial growth inhibition models based on molecular properties of organic acids. Int. J. Food Microbiol. 86(3): 249–255. doi:10.1016/s0168-1605(02)00551-2.

[6] Booth IR, Gould RG. 1989. The preservation of foods by low pH. In: Mechanisms of action of food preservation procedures. London, United Kingdom: Elsevier Applied Science, Elsevier Science Publishers Ltd. p. 119–160.

[7] Russell J. 1992. Another explanation for the toxicity of fermentation acids at low pH: anion accumulation versus uncoupling. J. Appl. Bacteriol. 73(5): 363–370. doi:10.1111/j.1365-2672.1992.tb04990.x.

[8] Houtsma, P. C. 1996. The antimicrobial activity of Sodium Lactate. Department of Food Science of the Agricultural University in Wageningen and at the Department of Microbiology of the University of Groningen in Haren.

[9] Organic Materials Review Institute. 2015. Lactic Acid, Sodium Lactate, and Potassium Lactate Handling/Processing. Available from: https://www.ams.usda.gov/sites/default/files/media/Lactic%20Acid%20TR%202015.pdf.

[10] Hadawey A, Tassou SA, Chaer I, Sundararajan R. 2017. Unwrapped food product display shelf-life assessment. Energy Procedia. 123: 62–69.

[11] Onoda H., Haruki M. 2015. Effect of mechanical treatment on the powder properties of zinc phosphate white pigments. J. Adv. Ceram. 4(4): 312–317. doi:10.1007/s40145-015-0167-8.

[12] McClure, B.N. 2009. The Effect of Lactate on Nitrite in a Cured Meat System. Graduate Thesis, Iowa State University.

[13] Miller, R. 2010. Functionality of Non-Meat Ingredients Used In Enhanced Pork. Extension.Org. https://bit.ly/3smGT6h.

[14] pH values of foods and food products. Arrow Scientific. [accessed 2020 Oct 12]. http://www.arrowscientific.com.au/index.php?option=com_content&view=article&id=61%3Aph-values-of-foods-and-food-products.

[15] Sallam KI. 2007. Antimicrobial and antioxidant effects of sodium acetate, sodium lactate, and sodium citrate in refrigerated sliced salmon. Food Control. 18(5): 566–575. doi:10.1016/j.foodcont.2006.02.002.

[16] Haghparast S., Kashiri H., Shabanpour B., Pahlavani M.H. 2009. Antioxidant properties of sodium acetate, sodium citrate and sodium lactate on lipid oxidation in rainbow trout (Onchorhynchus mykiss) sticks during refrigerated storage (4°C). Iran. J. Fish. Sci. 9(1) 73-86.

[17] [FAO] Food and Agriculture Organization of the United Nations. Proximate Analyses. Nutrition of Fish and Crustaceans a Laboratory Manual. [accessed 2020 Jan 31]. http://www.fao.org/3/AB479E/AB479E03.htm#ch3.1.

[18] Sengor G., Kalafatoglu H. and Gun H. 2004. The Determination of Microbial Flora, Water Activity and Chemical Analyses in Smoked, Canned Mussel (*Mytilus galloprovincialis, L.*). Turkish J. Vet. Anim. Sci. 28: 793–797.

[19] Brewer M.S. 2014. Chemical And Physical Characteristics Of Meat | Water-Holding Capacity. Encyclopedia of Meat Sciences (Second Edition). pp. 274–282. https://doi.org/10.1016/B978-0-12-384731-7.00247-6.

[20] Goncalves A., Ribeiro J. 2008. Do Phosphate Improve the Seafood Quality: Reality and Legislation. Pan-Am. J. Aquat. Sci. 3(3): 237–247.

[21] Arcales JAA, Nacional LM. 2019. Quality Changes of Chilled Green Mussel (*Perna viridis*) Pre-Treated with Organic Acids and Sodium Tripolyphosphate. Curr. Res. Nutr. Food Sci.ch in Nutrition and Food Science Journal. 7(3):894–904. doi:10.12944/crnfsj.7.3.28.

[22] Terzi G., Gucukoglu A., Cadirci O., Kevenk T., Alisarli M. 2012. Effects of chitosan and lactic acid immersion on the mussel's quality changes during the refrigerated storage. Kafkas Univ Vet Fak Derg. pp. 1–8.

[23] Songsaeng S., Sophanodora P., Kaewsrithong J., Oshima T. 2010. Quality changes in oyster (*Crassotreabelcheri*) during frozen storage as affected by freezing and antioxidant. Food Chem. 123: 286–290.

[24] Sallam KI., Samejima K. 2004. Microbiological and chemical quality of ground beef treated with sodium lactate and sodium chloride during refrigerated storage. LWT. 37(8): 865–871. doi: 10.1016/j.lwt.2004.04.003.

[25] Bingol, E. B., Colak, H., Cetin, O., & Hampikyan, H. 2012. Effects of Sodium Lactate on the Shelf Life and Sensory Characteristics of Cig Kofte - A Turkish Traditional Raw Meatball. J. Food Process. Preserv. 38(3): 1024–1036.

[26] Radziejewska RC., Pikul J. 2003. Sodium Lactate Addition on the Quality and Shelf Life of Refrigerated Sliced Poultry Sausage Packaged in Air or Nitrogen Atmosphere. J. Food Prot.. 67(3): 601–606.

[27] Eckert L.A., Maca J.V., Miller R.K. Acuff G.R. 1997. Sensory, microbial and chemical characteristics of fresh aerobically stored ground beef containing sodium lactate and sodium propionate. J. Food Sci. 62: 429–433.

[28] Tan W., Shelef L.A. 2002. Effects of sodium chloride and lactates on chemical and microbiological changes refrigerated and frozen fresh ground pork. Meat Sci. 62: 27–32.

[29] Cao R., Xue C., Liu Q. 2009. Changes in Microbial Flora of Pacific Oyster (*Crassotrea gigas*) During Refrigerated Storage and its Shelf-life Extension by Chitosan. Int. J. Food Microbiol. 131: 272–276.

[30] Lima M., Melo M., Monteiro A. 2013. Evaluation of the Processing of *Perna perna* mussels: The Influence of Water Quality Involved in the Cooling Operations in the Physico-Chemical and Microbiological Characteristic of the Product. J. Sci. Food Agric. 93: 3322–3329.

[31] Hardey D. 1991. Handling, Processing and Marketing Scallop Farming. Fishing News Books, Osney Meat, Oxford, pp. 168–180.

DNA barcoding of freshwater gastropods found in the upstream of Jalaur River in Barangay Garangan, Calinog, Central Philippines

DANIELLE THERESE F. CASTILLO, FRELEAN FAITH M. ENGALLADO, AIRAH CLARISSE G. HABUYO, CATHERINE JOY A. MEDIODIA, and ANDREA LUCYLE M. BELA-ONG

Philippine Science High School Western Visayas Campus - Department of Science and Technology (DOST-PSHSWVC), Brgy. Bito-on, Jaro, Iloilo City 5000, Philippines

Article Info

Submitted: Apr 19, 2021
Approved: Jul 05, 2021
Published: Aug 30, 2021

Keywords:
DNA
DNA barcoding
COI gene
freshwater gastropods
Jalaur River

Abstract

Multiple species of gastropods can be found in the Jalaur River which encompasses almost the entire province of Iloilo. However, the identification of these species can be challenging with their complex morphology. DNA barcoding using the cytochrome oxidase I (COI) gene was performed to accurately identify and classify the organisms of Class Gastropoda. Through phylogenetic analysis, one sample was identified to be *Pomacea canaliculata* while the remaining four samples remained unidentified due to unrepresented taxa in the GenBank. This shows a lack of available information about the organisms found in the Jalaur River as nucleotide sequences of these species have not been provided to public databases. With this, further research must be done to know more about the species found in Jalaur River and their conservation status. It is recommended to maintain the storage condition of samples to prevent DNA degradation. PCR conditions should also be adjusted to achieve optimal results.

Introduction. - Systematics and taxonomies are the basis of all biology as it ensures the quality of life of future generations [1]. However, there are still a vast number of unknown species that have not yet been identified. Studies suggest that the Earth is home to about 8.7 million species [2]; meanwhile, only 14% had been identified as of 2011 [3]. The Philippines is home to about 22,000 mollusks species [4]. Gastropods, in particular, have a wide range of habitats and are prone to evolve as they are sensitive to slight changes in the environment [5]. In addition to this, gastropods have one of the highest numbers of documented extinctions among the major taxonomic groups in the world making its identification necessary [6].

Moreover, gastropods are also ecologically important as some of their species can be used as indicators to assess the condition of the aquatic habitat along with the quality of any water impoundments [7]. Gastropods may also serve as pests to agriculture with the potential to invade and alter the ecosystem [8]. Additionally, some gastropods species may be intermediate hosts of infections despite being a source of food for fishes, birds, and humans [7,9]. Despite this, the understanding of its systematics is still incomplete [10] and the phylogenetics among its family is largely unresolved [11].

Studies had been done assessing freshwater gastropods in the Philippines which was identified as *P. canaliculata*, *V. costata*, *L. natalensis*, *M. tuberculata*, *M. turricula*, *T. granifera*, *G. ladacensis*, *L. accuminata*, *L. caperata*, and Planorbis sp. [7, 12];. Alcala et al. [13] were also able to taxonomically identify *N. polita, T. granifera, P. porcellana, T. scabra, P. canaliculata, L. scabra, C. cucullate, C. manillensis, C. plicata,* and Ostrea sp. in Jalaur River. Despite their findings, morphological identification may not always be accurate due to the existence of cryptic species having similar morphology but different DNA sequences [14, 15].

To address this, past research recommends the use of DNA barcoding as an effective tool to authenticate and accurately identify organisms [14, 15]. DNA barcoding is a process that involves sequencing a short fragment of the COI gene taken from the unidentified organisms and comparing their DNA barcodes to existing sequences [16]. It can reveal possible misidentified organisms, discover overlooked species, and identify new or evolved species promptly and accurately as complete data can be collected from a single specimen irrespective of its morphological features or its stage in life [1, 17]. The DNA barcodes can be used to generate a phylogenetic tree for the evaluation of each organism, along with the phylogeny, diversity, and relationship among the organisms. With the data,

How to cite this article:
CSE: Castillo DTF, Engallado FFM, Habuyo ACG, Mediodia CJA, Bela-ong ALM. 2021. DNA barcoding of freshwater gastropods found in the upstream of Jalaur River in Barangay Garangan, Calinog, Central Philippines. Publiscience. 4(1): 77–81.
APA: Castillo D.T.F., Engallado F.F.D., Habuyo A.C.G., Mediodia C.J.A., & Bela-ong A.L.M. (2021). DNA barcoding of freshwater gastropods found in the upstream of Jalaur River in Barangay Garangan, Calinog, Central Philippines. *Publiscience*, *4*(1), 77–81.

For supplementary data, contact: publiscience@wvc.pshs.edu.ph.

actions can be taken for an organism's conservation and management [18]. The significance of DNA barcoding makes it a prominent research topic as it can authenticate the organisms to assess their safety, conserve genetics, and detect possible invasive alien species [14].

The Jalaur River encompasses almost the entire Iloilo with its upstream located at Barangay Garangan, Calinog, Iloilo. Previous studies mentioned that freshwater gastropods, specifically stream snails, are known to exhibit upstream migration in temperate and tropical regions [19,20]. Additionally, this area is also home to the Panay Bukidnon indigenous people thus with the identity of the freshwater gastropods, awareness will be given to the locals regarding the availability of certain gastropods in their area. Monitoring and assessment of the species could also be done along with its conservation and management. Additionally, the result of this research can be used as a baseline for further taxonomic research.

This study aimed to identify selected freshwater gastropods in the Jalaur River located in Barangay Garangan, Calinog, Iloilo, Philippines by analyzing gene sequences to establish their relationship and conservation status. Specifically, this study aimed to:

(i) identify selected species of freshwater gastropods collected from Jalaur River in Barangay Garangan, Calinog, Iloilo using phylogenetic analysis;

(ii) determine the relationship among the collected gastropod species by interpreting the phylogenetic tree; and

(iii) query the conservation status of each identified gastropod species on the International Union for Conservation of Nature (IUCN) Red List Index.

Methods. - This research is a descriptive study on the phylogenetics of freshwater gastropods. The methodology includes sample collection, DNA extraction, DNA amplification, agarose gel electrophoresis, DNA sequencing and alignment, species identification, and phylogenetic analysis.

Sample Collection and Preparation. To collect samples, a permit was requested from the National Commission on Indigenous Peoples (NCIP) since the sampling site is part of the Panay-Bukidnon's ancestral domain. Freshwater gastropods in shallow waters were collected through handpicking [7]. A total of 11 samples were collected from upstream of the Jalaur River in Barangay Garangan, Calinog, Iloilo, Philippines with the geographic coordinate 11°11'29" N 122°27'13" E at 367.0 meters of elevation using opportunistic sampling with the help of the indigenous people.

The collected samples were then stored in separate airtight bags labeled according to their vernacular names that were provided by the indigenous people and were placed in a cooler for transportation. The samples' foot muscle was then extracted and cut into small pieces then submerged in 70% ethanol to prevent the degradation of DNA [20].

DNA Extraction. DNA extraction was performed following the standard protocol for animal tissue according to the NucleoSpin Tissue Genomic DNA Purification User Manual. It was then tested in the Thermo Scientific™ Multiskan™ GO to check the quality of the extracted DNA.

DNA Amplification. DNA amplification was done through polymerase chain reaction (PCR). The universal primers for the amplification of the (COI) gene, LCO1490 (*5′* -GGT CAA CAA ATC ATA AAG ATA TTG G-3′) and HCO2198 (*5′* -TAA ACT TCA GGG TGA CCA AAA AAT CA-3′) were used [21]. The PCR was performed following the thermal regime: 3 min at 94 ℃, then 25 cycles of 20 sec at 94 ℃, 30 sec at 50 ℃, and 1 min at 72 ℃, followed by extension for *5* min at 72 ℃ set for seashells at the West Visayas State University laboratory.

Agarose Gel Electrophoresis. The amplified DNA was subjected to gel electrophoresis using 1% agarose gel and stained with Invitrogen 10X BlueJuice to check the integrity of the samples. The result was then viewed under the UV transilluminator.

DNA Sequencing and Alignment. The PCR products were sent to Macrogen Inc., Seoul, South Korea for sequencing. The sequences were then assembled using their forward and reverse sequences with DNABaser.

Species Identification. Each assembled DNA was queried using Basic Local Alignment Search Tool (BLAST) to compare the sequences to the available sequences in GenBank. The species with the lowest E-value and the highest bit score was determined for each sample. From the family, sequences of multiple species were downloaded to be included in the phylogenetic tree.

Phylogenetic Analysis. Using MEGA X, the sequences were aligned using ClustalW. This software also generated the best model for DNA substitution to be the Tamura 3-parameter model. Then a Neighbor-Joining tree from 1000 replicates was constructed using the maximum likelihood statistical method. Clades with bootstrap values higher than 70 were considered well-supported [22]. These were used as the basis to verify the identity of the sample. After verifying each sample's species, it was queried in the IUCN Red List Index for the conservation status.

Safety Procedure. Proper protective equipment was utilized at all times. Lab gowns and nitrile gloves were used during DNA extraction, DNA amplification, and gel electrophoresis to avoid exposure to hazardous chemicals. After the collection of DNA, the waste materials and the samples were autoclaved and disposed of properly as medical/biohazard waste.

Results and Discussion. - Freshwater gastropods in the upstream of Jalaur River were identified through DNA barcoding. The process includes sample collection, DNA extraction, DNA amplification, agarose gel electrophoresis, DNA sequencing and alignment, species identification, and phylogenetic analysis. From the 11 samples that were collected, only *5* were successfully barcoded due to possible DNA degradation and non-optimal conditions set for the

PCR amplification. Furthermore, only one of the five was identified to its species-level namely *Pomacea canaliculata* while the other 4 barcoded samples remained unidentified due to unrepresented taxa.

The initial identification was done based on their vernacular names. After obtaining the assembled DNA, initial species identification was performed using BLAST to classify them into specific species. The program presents the e-value and bit score of the top matches for each sequence. The e-value shows the statistical significance of a match while the bit score gives an indication of the quality of the alignment [22]. A low E-value and bit score higher than 950 are suggested for assigning species identity; thus, the sequence with the lowest E-value and the highest bit score was chosen as the BLAST identification [23]. These identifications are summarized in Table 1.

Table 1. The barcoded samples are presented with their corresponding vernacular name and BLAST Identification with the lowest E-value and the highest bit score.

Sample	Vernacular Name	BLAST Identification	E-value	Bit Score
A1	Awis	*Stenomelania* sp.	0	1158
A2	Awis	*Stenomelania* sp.	0	1122
K2	Kuol	*Pomacea canaliculata*	0	1179
TG	Tamburuko (gurob-gurob)	*Tarebia granifera*	0	1210
TM1	Tamburuko (mugot)	*Stenomelania denisoniensis*	0	1031

While BLAST was able to identify the samples with E-value = 0 and bit score > 1000, the study conducted by Ross et al. [24] raises major concerns as many taxa are unrepresented. In addition to this, it cannot give accurate identification of species because top hits are often not the closest phylogenetic relatives of the organisms [24, 25]. In a study by Hillis and Bull [26], clades having bootstrap values ≥70 correspond to a ≥95% probability of it being real. Thus, to verify the initial identity of each sample, phylogenetic analysis was performed where clades with bootstrap values of seventy (70) or higher were considered well-supported to be of the same species after undergoing one thousand (1000) replicates. Figure 1 shows the bootstrap consensus tree of the five (5) samples along with representative sequences from the family of their BLAST identities with the outgroup *Paludomus siamensis*.

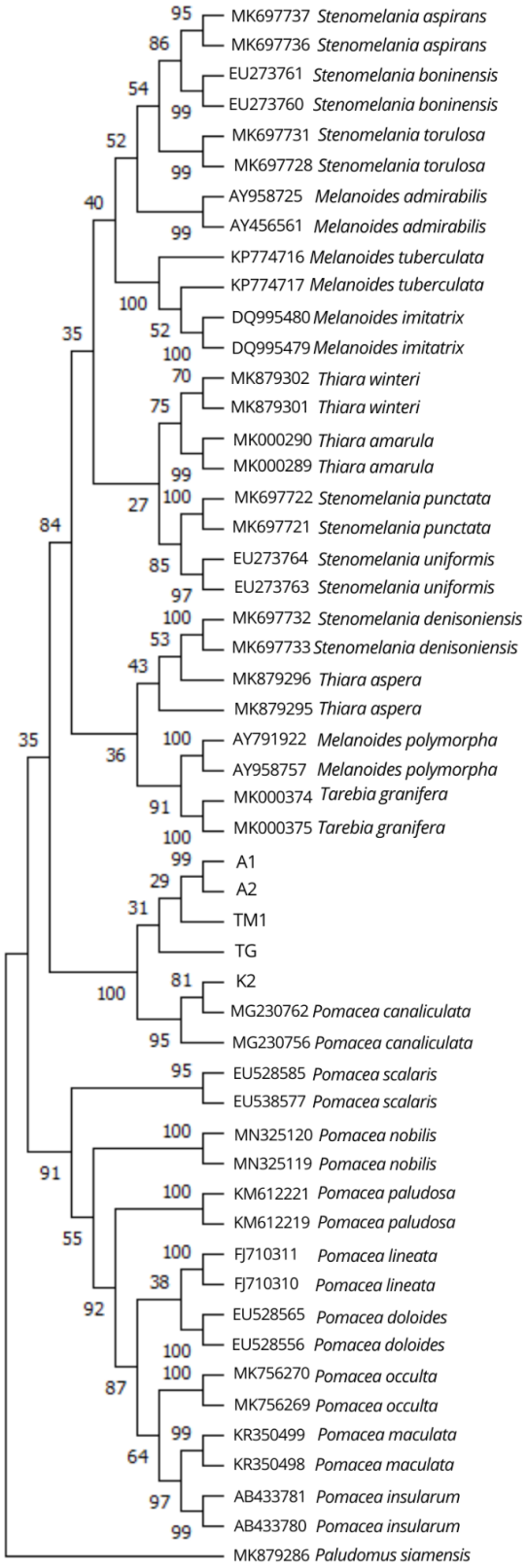

Figure 1. Bootstrap consensus tree of the samples is shown along with representative sequences from the family of their BLAST identification with *Paludomus siamensis* as the outgroup.

The phylogenetic tree shows that K2 can be identified to be *Pomacea canaliculata* with a bootstrap value of 81. This is the same species of gastropods that was identified by Alcala et al. [13] in the same river in

2010. Aside from this, it was also found in other parts of the Philippines such as Bukidnon and Agusan del Sur [7,12].

The identified species for K2 was queried in the IUCN Red List of Threatened Species for the identification of their conservation status. *Pomacea canaliculata* is categorized as Least Concern. Though it is not a focus of species conservation, its management is still necessary as it can serve as pests to rice crops [27].

Additionally, *Pomacea canaliculat*a was found to be an invasive species in the Global Invasive Species Database (GISD) [28]. With its ability to adapt to harsh environmental conditions along with its high reproductive rate, it can colonize and invade natural habitats [27, 29] which results in alterations in the ecosystem [8].

The remaining four samples belong to the same clade. It can be interpreted that A1 and A2 that have the same vernacular name, "Awis", are of the same species based on the phylogenetic analysis having a bootstrap value of 99. Collectively, the samples were more closely related to each other than their BLAST identification. This may be due to more common ancestors shared by the samples. The inaccuracy of the BLAST identification can be attributed to unrepresented taxa in the GenBank [24]. This shows a lack of available information about the organisms found in the Jalaur River as nucleotide sequences of these species have not been provided to public databases.

Limitations. The study barcoded less than the actual number of samples collected due to possible degradation of DNA and non-optimal conditions during the DNA amplification. Moreover, some samples were unrepresented species of gastropods in the GenBank, thus out of the five barcoded samples, only one organism was identified.

Conclusion. - In conclusion, "Kuol", identified to be *Pomacea canaliculata* or Golden Apple Snail, can be found in the Jalaur River along with four other unidentified gastropods. The identified species was not found to be a focus of species conservation since it is under the Least Concern categorization; however, its management is necessary as it is an invasive species and pests to rice crops. Aside from the Jalaur River in Iloilo, *Pomacea canaliculata* was also found in other areas in the Philippines. The four other organisms were not identified due to the limited sequences recorded in GenBank or the possibility of evolution.

Recommendations. - Further research must be done to identify the gastropods found in Jalaur River for their proper management. It is also recommended to perform all procedures in one laboratory with complete equipment for DNA barcoding to maintain a constant storage temperature of -20 ℃ and prevent DNA degradation [30]. More time should also be dedicated in the study to allow adjustments in PCR conditions to achieve optimal results which may vary depending on the organism being amplified.

Acknowledgment. - The researchers would like to express their gratitude to Sir Stephen Sabinay of West Visayas State University for helping with the data collection, Sir Chris Apurillo of Philippine Science High School-Eastern Visayas Campus for helping the researchers in analyzing the data, the local government unit of Calinog, Iloilo for assisting during the sample collection, and the Panay-Bukidnon tribe for allowing and helping the researchers in collecting samples.

References

[1] Ali MA, Gyulai G, Hidvegi N. 2014. The changing epitome of species identification – DNA barcoding. Saudi J. Biolog. Sci. 21: 204–231.

[2] Mora C, Tittensor DP, Adl S, Simpson AGB, Worm B. 2011. How many species are there on earth and in the ocean? PLoS Biology. 9 (8): e1001127.

[3] Watson T. 2011. 86 percent of earth's species still unknown? National Geographic News. [accessed 26 November 2020] https://on.natgeo.com/32fPnQ5.

[4] Ramos DAE, Batomalaque GA, Anticamara JA. 2018. Current status of Philippine mollusk museum collections and research, and their implications on Biodiversity Science and Conversion. Philippine Journal of Science. 147(1): 123–163.

[5] Pan H, Zhu X. 2008. Gastropods. The Jehol Fossils. 36–39. doi: 10.1016/b978-012374173-8.50004-1.

[6] Lydeard C, Cowie RH, Ponder WF, Bogan AE, Bouchet P, Clark SA, Cummings KS, Terrence JF, Gargominy O, Herbert DG, et al. 2004. The global decline of nonmarine mollusks. BioScience. 54(4): 321–330.

[7] Cuardo JT. 2015. Preliminary assessment of freshwater gastropods in the selected rivers in Esperanza, Agusan del Sur, Philippines. The Journal of Zoology Studies. 2(4): 13–20.

[8] Maheshini DB, Hirimuthugoda GN, Shalika S. 2017. A short survey of pest gastropods and their potential threats to local agriculture in the Kandy District.

[9] Brown DS. 1994 Freshwater Snails of Africa and Their Medical Importance, 2nd edn. Taylor & Francis, London.

[10] Strong E, Olivier G, Ponder W, Bouchet, P. 2007. Global diversity of gastropods (Gastropoda; Mollusca) in freshwater. Hydrobiologia. 595: 149–166. 10.1007/s10750-007-9012-6.

[11] Uribe JE, Zardoya R, Puillandre N. 2018. Phylogenetic relationships of the Conoidean snails (Gastropoda: Caenogastropoda) based on mitochondrial genomes. Molecular Phylogenetics and Evolution. 127: 898–906.

[12] Galan GL, Ediza MM, Servasques MS, Porquis HC. 2015. Diversity of Gastropods in the Selected Rivers and Lakes in Bukidnon. International

Journal of Environmental Science and Development. 6(8): 615–619.

[13] Alcala E, Bucol A, Averia L, and Dusaran R. 2010. A Study on the Invertebrate and Vertebrate Biodiversity of the Jalaur River System of Iloilo, Panay, Philippines. Silliman Journal. 51(1): 191–224.

[14] Trivedi S, Aloufi AA, Ansari AA, Ghosh SK. 2016. Role of DNA barcoding in marine biodiversity assessment and conservation: An update. Saudi J. Biolog. Sci. 23(2): 161–171.

[15] Palasio RGS, Guimaraes MCDA, Ohlweiler FP, Tuan R. 2017. Molecular and morphological identification of Biomphalaria species from the state of São Paulo, Brazil. ZooKeys. 668:11-32.

[16] Wilson JJ, Sing KW, Jarutas N. 2019. DNA barcoding: bioinformatics workflows for beginners. Reference Module in Life Sciences. 3: 985-995.beginners. Reference Module in Life Sciences. 3: 985-995.

[17] Puillandre N, Strong EE, Bouchet P. 2009. Identifying gastropod spawn from DNA barcodes: possible but not yet practicable. Mol. Ecol. Resour. 9: 1311–1321. doi: 10.1111/j.1755-0998.2009.02576.

[18] Areño APD, Cambel LEJ, Hilapad MS, Bela-ong ALM, Castillo RVF, Valdez Jr MB. 2019. DNA barcoding of molluscs (Bivalvia) in selected sites in Capiz, Philippines. Publiscience. 2(1): 143–148.

[19] Kappes H, Haase P. 2012. Slow, but steady: dispersal of freshwater molluscs. Aquatic Sciences. 74(1): 1–14. doi: 10.1007/s00027-011-0187-6.

[20] Huryn AD, Denny MW. 2003. A biomechanical hypothesis explaining upstream movements by the freshwater snail *Elimia*. Functional Ecology. 11(4): 472–483.

[21] Folmer O, Black MB, Wr H, Lutz R, Vrijenhoek R. 1994. DNA primers for amplification of mitochondrial cytochrome c oxidase subunit I from diverse metazoan invertebrates. Molecular marine biology and biotechnology. 3(5): 294–9.

[22] Madden T. 2003. The NCBI Handbook. Biolateral Pty. Ltd. Chapter 16. The BLAST sequence analysis tool; p.1-15.

[23] Kyle CJ, Wilson CC. 2007. Mitochondrial DNA identification of game and harvested freshwater fish species. Forensic Science International. 166(1): 68–76. doi: 10.1016/j.forsciint.2006.03.025.

[24] Ross HA, Murugan S, Li WLS. 2008. Testing the reliability of genetic methods of species identification via simulation. Syst. Biol. 57(2): 216–230.

[25] Koski LB, Golding GB. 2001. The closest BLAST hit is often not the nearest neighbor. J Mol Evol. 52(6):540–542. doi: 10.1007/s002390010184. PMID: 11443357.

[26] Hillis DM, Bull JJ. 1993. An empirical test of bootstrapping as a method for assessing confidence in phylogenetic analysis. Systematic Biology. 42(2): 182–192.

[27] Joshi RC. 2007 Problems with the Management of the Golden Apple Snail Pomacea canaliculata: an Important Exotic Pest of Rice in Asia. In: Vreysen M.J.B., Robinson A.S., Hendrichs J. (eds) Area-Wide Control of Insect Pests. Springer, Dordrecht. https://doi.org/10.1007/978-1-4020-6059-5_24.

[28] Global Invasive Species Database. 2021. [cited 2021 June 30]. Available from https://bit.ly/374v8Yh.

[29] Halwart M. 1994. Fish as biocontrol agents in rice: the potential of common carp *Cyprinus carpio* (L.) and Nile tilapia *Oreochromis niloticus* (L.). Tropical Agroecology: 8.

[30] Velusamy R, Singh BP, Raina OK. 2004. Detection of *Fasciola gigantica* infection in snails by polymerase reaction. Veterinary Parasitology. 120 (1-2): 85–90. doi: 10.1016/j.vetpar.2003.11.009.

Publiscience Vol. 4 Issue 1

Effect of different irradiance levels on the growth of the cyanobacterium *Lyngbya majuscula*

ANDREA ROSE V. FRANCO, FRANCIZ LOVELY L. TIANIA, and ANDREA LUCYLE M. BELA-ONG

Philippine Science High School Western Visayas Campus - Department of Science and Technology (DOST-PSHSWVC), Brgy. Bito-on, Jaro, Iloilo City 5000, Philippines

Article Info

Submitted: Apr 07, 2021
Approved: Jun 13, 2021
Published: Aug 30, 2021

Keywords:
Lyngbya majuscula
cyanobacteria
irradiance
specific growth rate
algal growth

Abstract

Lyngbya majuscula is a prolific producer of secondary metabolites that are used in the pharmaceutical industry. As a photosynthetic organism, the effect of irradiance on its cultivation was studied to maximize algal growth for mass production. The cyanobacterium was subjected to different irradiances of 20, 45, 110, 180, and 320 µmol photons $m^{-2}s^{-1}$ to determine its specific growth rate (SGR) in each treatment. Results showed the highest SGR under 20 and 45 µmol photons $m^{-2}s^{-1}$ during the exponential phase, showing a significant difference ($p < 0.05$) among all other treatments. Minimal growth rates were obtained under 110, 180, and 320 µmol photons $m^{-2}s^{-1}$ and results showed that the SGRs under these treatments have no significant difference ($p > 0.05$) with the negative control; however, color changes were observed at these irradiances. These showed that *L. majuscula* prefers lower irradiances to maximize its growth, while higher irradiances are unideal.

Introduction. - *Lyngbya majuscula* is a filamentous marine alga that is a prolific producer of 196 novel and diverse secondary metabolites, whose genus is responsible for over 40% of all marine cyanobacterial secondary metabolites (1,2,3). These metabolites are carotenoids, proteins, and vitamins which are beneficial in the pharmaceutical industry and food technology for their antioxidative and antimicrobial properties [4].

Several factors can be modified to optimize the growth and secondary metabolite production of cyanobacteria. For instance, Burja et al. [2] investigated the effect of culture vessel configuration, growth conditions, and media composition and determined that culture conditions have the greatest effect on secondary metabolite production. One important culture condition [3,5,6] that can be modified is light availability. Studies [7,8] reported that algal growth is better under continuous lighting since growth is directly proportional to the length of the light exposure.

Although most studies investigate the relationship of light received by the algae to its growth, little research has been done regarding the optimization of the yield under continuous light exposure. There are claims that *L. majuscula* would yield highest growth under various light–dark cycles and among different levels of irradiation from ranges of 20 µmol photons $m^{-2}s^{-1}$ to 120 µmol photons $m^{-2}s^{-1}$ [3,9,10].

Previous research would suggest that the optimum growth of the algae *L. majuscula,* would be sustained under higher light intensities within the ranges of 180 µmol photons $m^{-2}s^{-1}$ to 320 µmol photons $m^{-2}s^{-1}$. This is due to the property of *L. majuscula* being a surface cyanobacterium; hence, it readily produces more carotenoids as a mechanism against photoinhibition [9]. However, Loogman [10] also observed general cyanobacterial death at 320 µmol photons $m^{-2}s^{-1}$. Low light irradiances have also been claimed as the optimum irradiance for other *Lyngbya* species such as *Lyngbya kuetzingii* and *Lyngbya stagnina,* where the irradiance values found were 20 µmol photons $m^{-2}s^{-1}$ and 45 µmol photons $m^{-2}s^{-1}$, respectively [11,12].

Realizing the need to optimize the growth of the algae for future use in the pharmaceutical industry, *L. majuscula* was chosen to be subjected to stress or bioprocess intensification through light irradiance. Mass cultivation of the algae was targeted because most drug candidates do not reach the pharmaceutical market due to the low availability or small yield of bioactive compounds [13].

This study aimed to determine at which irradiance between 20, 45, 110, 180, and 320 µmol photons $m^{-2}s^{-1}$ the algal growth of *Lyngbya majuscula* is at a maximum. Specifically, it aimed to:

(i) assess changes in the color, pH, and temperature of *L. majuscula* during each treatment;

(ii) analyze the trend of algal growth in terms of dry weight and specific growth rate (SGR); and

How to cite this article:
CSE: Franco ARV, Tiania FLL, Bela-ong ALM. 2021. Effect of different irradiance levels on the growth of the cyanobacterium *Lyngbya majuscula*. Publiscience. 4(1): 82–86.
APA: Franco, A.R.V., Tiania, F.L.L., & Bela-ong, A.L.M. (2021) Effect of different irradiance levels on the growth of the cyanobacterium *Lyngbya majuscula*. *Publiscience*, *4*(1), 82–86.

For supplementary data, contact: publiscience@wvc.pshs.edu.ph.

(iii) determine the highest specific growth rate by comparing the SGR values during each treatment using Planned Comparisons after One-Way Analysis of Variance (ANOVA)

Methods. - The methods were divided into 5 steps: (1) preparation of the alga, (2) culture of the alga in different irradiance levels, (3) determination of dry weight using gravimetry, (4) computation of specific growth rate, and (5) analysis of data.

Sample Collection. *L. majuscula* was purchased from the Southeast Asian Fisheries Development Center/Aquaculture Department (SEAFDEC/AQD) in Tigbauan, Iloilo. Samples were washed to remove residues and were subjected to a scale-up of 2 L after purification based on the standard protocol from the Handbook of Phycological methods [14].

Culture Set-up. Twenty-four (24) containers were each filled with 5 L algal cultures composed of 500 mL alga mixed with 4500 mL Ozonated Seawater-Conwy solution [15]. Five (5) lightboxes (92 cm x 31 cm x 66.5 cm) were made to contain four replicate containers each. The lightboxes had different irradiance levels: 20, 45, 110, 180, and 320 µmol photons $m^{-2}s^{-1}$, which were achieved using LED lamps (1 lamp = 2000 lumens). For the negative control, four replicate containers were not exposed to light.

The setup was irradiated for 24h throughout the 8-day culture. Irradiance was measured using a photometer (resolution: 0.1 µmol photons $m^{-2}s^{-1}$ in the range 0 - 1999 µmol photons $m^{-2}s^{-1}$), and one-point continuous aeration, pre-filtered (5 µm), was supplied by centralized pumps in the laboratory. The temperature and pH of the alga were recorded everyday using a temp/pH meter (resolution: 0.01 pH at range: 0.00 to 14.00 pH and 0.1°C at range: 0.0 to 100.0°C). The color of the alga in each treatment was also monitored everyday.

Algal Dry Weight. The biomass of *L majuscula* was measured in terms of dry weight using the Gravimetric method. The standard protocol set by the American Public Health Association (APHA) was followed [16]. One hundred (100) mL of the sample from each treatment replicate was vacuum filtered in pre-tared GF/F glass microfiber filters (0.7 µm pore size). Twenty (20) mL ammonium formate (Sigma Aldrich, 1M concentration with purity >99.0%) was then added to remove salt residues from the sample. The filter papers with alga residue were then oven-dried (Precision Scientific) at 60 °C for 2 hours, desiccated for 30 minutes, and then weighed using an analytical balance. This process was repeated until the net weight of the alga was obtained, with a difference of ± 0.0002 when weighed. Dry weight was calculated using the formula:

$$Dry\ Weight\ = \frac{W_1 - W_2}{mL},$$

Equation 1. Formula for Dry Weight

where W_1 = weight of the filter paper with the dried residue of the sample in mg, W_2 = tare weight of the filter paper in mg, and mL = volume of the sample.

Specific Growth Rate. Specific growth rate was calculated after obtaining the dry weight of the alga to determine the rate of algal biomass increase per day. It was computed using the formula [17]:

$$Specific\ Growth\ Rate\ (SGR) = \frac{ln\ (W_f) - ln(W_i)}{t}\ x\ 100,$$

Equation 2. Formula for Specific Growth Rate

where W_f = final weight in mg, W_i =initial weight in mg, and t = days of culture.

Data Analysis. Qualitative data were in the form of pictures of the treatment replicates each day. Quantitative data were in the form of algal dry weight (mg/mL), specific growth rate (d^{-1}), temperature (°C), and pH, where the mean and standard deviation in each treatment were computed. One-Way ANOVA with Planned Comparisons at 95% Confidence Interval was used to analyze the significant difference between samples. Tests of normality and homogeneity were also conducted to determine the conditions for the conduct of Planned Comparisons as post-hoc analysis.

Results and Discussion. - *Lyngbya majuscula* is a marine cyanobacterium that forms dense mats near the surface of the water, and its growth is dependent on numerous factors, with one of these being light availability [3,5,6]. The growth of the cyanobacterium in 8 days of culture was observed in different irradiances of 20, 45, 110, 180, and 320 µmol photons $m^{-2}s^{-1}$ using LED lamps.

The exponential phase of the alga was first identified before being subjected to the different irradiances. This phase was chosen among all other phases of the cyanobacterial growth due to the rapid and frequent cell division that contributed to the maximum growth rate of the alga. In addition, the higher growth rate or biomass production rate will result in faster production of metabolites which are usually produced in the late exponential phase [18,19]. The alga showed the highest growth during the 4th day of culture, showing that the exponential phase can be observed from Day 0 to Day 4. After the 4th day, disintegration of the alga was observed, indicating that it has entered the stationary phase, leading to the death phase. A similar study on the culture of *L. majuscula* conducted by Mandal et al. [20] also showed the decay of the alga after its exponential phase of 3-4 days.

Morphological Color Changes. Changes in the color of the alga were observed in the different treatments, which indicate the presence of photosynthetic pigments that contribute to the color of the alga such as chlorophyll *a*, phycobilin, and carotenoids (Table 1). At low irradiances, the alga produced a dark-red violet color, possibly due to high concentrations of the photosynthetic pigment, phycoerythrin. In contrast, at high irradiances, the alga exhibited a dull yellowish-brown color, possibly due to the decrease in the phycobilin accessory pigment and chlorophyll *a* levels, and an increase in the carotenoid production [21].

Table 1. The color variation of the algae on day 0, 4, and 8 with color observations below the pictures.

Day	Irradiance (μmol photons $m^{-2}s^{-1}$)					
	0	20	45	110	180	320
0	 Transparent	 Transparent	 Transparent	 Transparent	 Transparent	 Transparent
4	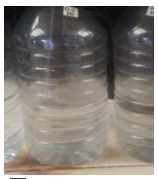 Transparent	 Dark-red	 Red	 Yellowish-brown	 Brown	 Light brown
8	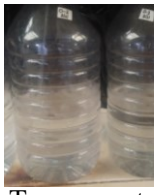 Transparent	 Dark-red	 Red	 Brown	 Brown	 Greenish-brown

The increase in the amount of carotenoids in the alga at high irradiances is necessary to protect cyanobacteria from photoinhibition. Carotenoids absorb excessive light energy that would damage the chlorophyll molecules. Excess absorption of irradiation of the cyanobacterium can lead to the formation of harmful reactive oxygen molecules through interaction with oxygen which would result in further damage of the photosystem II from photoinhibition [22]. These observations indicate that exposure to higher irradiances is closely linked to marked changes in the morphology of an alga.

A similar study by Mandal et al. [20] showed that *L. majuscula* under long exposure to high UV-B radiation formed yellowish sheaths. The alga under the negative control (0 μmol photons $m^{-2}s^{-1}$) experienced a color change from light red to transparent, showing no growth due to the inability of cyanobacterium to photosynthesize under the absence of light. These indicate that the alga exhibits color changes depending on the irradiance level.

Data Analysis. The dry weight and SGR of each of the treatments during the exponential phase were compared and analyzed. A significant difference existed among the groups at 95% confidence interval. After conducting Planned Comparisons, it was found that a significant difference exists between 20 μmol photons $m^{-2}s^{-1}$ and all other treatments, and 45 μmol photons $m^{-2}s^{-1}$ and all other treatments. However, no significant difference was found between the two treatments. Moreover, the treatments 110, 180, and 320 μmol photons $m^{-2}s^{-1}$ also showed no significant difference with each other and the negative control.

Table 2. The dry weight obtained at each irradiance level during the exponential phase.

Irradiance	Dry Weight (mg/mL)	
(μmol photons $m^{-2}s^{-1}$)	Day 0	Day 4
0	0.018 ± 0.005	0.024 ± 0.003[b]
20	0.018 ± 0.005	0.10 ± 0.04[a]
45	0.018 ± 0.005	0.08 ± 0.02[a]
110	0.018 ± 0.005	0.07 ± 0.04[b]
180	0.018 ± 0.005	0.04 ± 0.01[b]
320	0.018 ± 0.005	0.039 ± 0.003[b]

*where a and b indicate the groupings based on their significant differences.

Algal Dry Weight. Noticeable increase in average dry weight from Day 0 to Day 4 can be observed in each treatment as seen in Table 2. The highest biomass of *L. majuscula* during the exponential phase was observed under 20 μmol photons $m^{-2}s^{-1}$ among all treatments. The alga under 45 μmol photons $m^{-2}s^{-1}$ exhibited the second highest biomass. Previous studies have also identified both irradiance values as optimum algal growth values [6,22,23].

Specific Growth Rate. The alga under the treatment of 20 µmol photons $m^{-2}s^{-1}$ exhibited the highest SGR of 42.3 % d^{-1} during the exponential phase, while the alga under 45 µmol photons $m^{-2}s^{-1}$ exhibited the second highest SGR of 36.9% d^{-1} as shown in Figure 1. Minimal growth rate was also observed in treatments under 110, 180, and 320 µmol photons $m^{-2}s^{-1}$ (Figure 1).

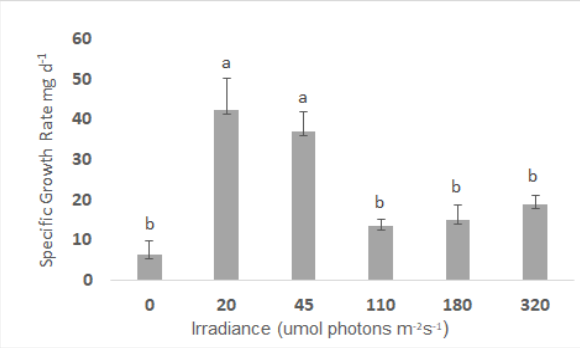

Figure 1. The Specific Growth Rate (SGR) of *L. majuscula* during the exponential phase (Day 0 to Day 4), where a and b indicate the groupings in which they are significantly different using Planned Comparisons after One-Way ANOVA ($p<0.05$).

pH and Temperature. Differences in irradiance caused small changes in the temperature and pH of each setup as shown in Figure 2.

As the irradiance increased, the temperature also increased. The excess energy formed from the reaction during the absorption of chlorophyll *a* photons is turned into heat; thus, the higher the irradiance, the more heat is transferred. According to Ras et al. [24], increasing temperature, above optimal conditions, in the outdoor production of algae may result in the decrease in the growth of the alga.

As shown in Figure 2, the pH in each setup was ≈ 8 which indicated growth and efficient CO_2 retention of the algae. A pH level closer to 8 corresponds to normal CO_2 concentration in a saltwater environment [25].

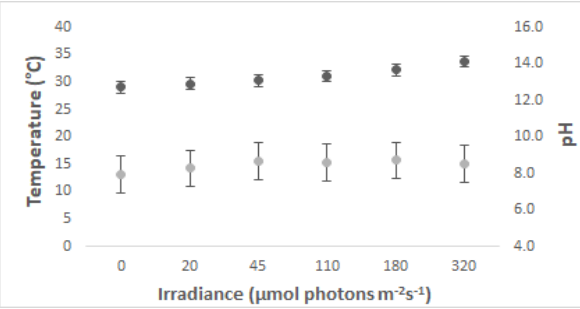

Figure 2. The average temperature and pH obtained in each treatment for 8 days of culture.

Effect of irradiance on growth. Individual dry weights and specific growth rates of the alga were significantly affected by the irradiance they were exposed to. For both 20 and 45 µmol photons $m^{-2}s^{-1}$, the alga exhibited higher dry weight and SGR values than the other treatments. This indicates that *L. majuscula* prefers low irradiances possibly because of the low maintenance rate of cyanobacteria - requiring only little energy to maintain their cell structure and function. Van Liere & Mur [9] compared the maintenance energy requirements in *Oscillatoria agardhii*, a cyanobacteria, with those of eukaryotes [22]. It was shown that maintenance requirements in cyanobacteria are much smaller than that of eukaryotes under limiting light. In addition, cyanobacteria at low irradiances have the capability to broaden the overall absorption band in order to balance the two antenna pigments responsible for their photosynthesis [6]. A study conducted by Yin et al. [26] on *Lyngbya wollei*, a close relative of *L. majuscula*, exhibited optimum growth at 22 µmol photons $m^{-2}s^{-1}$. Similarly, in a study conducted by Zhang et al. [12] on *Lyngbya kuetzingii,* the alga had its optimum growth under 20 µmol photons $m^{-2}s^{-1}$ while the study on *Lyngbya stagnina* by Jindal et al. [11] resulted in the highest exopolysaccharides and protein production under 45 µmol photons $m^{-2}s^{-1}$ in continuous light [11,12].

The minimal growth exhibited at irradiance levels of 110, 180, and 320 µmol photons $m^{-2}s^{-1}$ indicates that higher irradiances limit the growth of the alga. This is a minimizing response of the alga to the effects of photoinhibition caused by the excessive formation of Reactive Oxygen Species (ROS) [26]. Consequently, the results in the data analysis showed that the SGR values at high irradiances do not have a significant difference with each other and the negative control due to the cyanobacterium not being able to grow in the absence and at high light intensities.

Limitations. Due to time constraints, sampling was done only on days 0, 4, and 8; hence, daily growth rate of the alga was not assessed. No repetitions of the experiment were also made to further narrow down the irradiance values.

Conclusion. - *L. majuscula* exhibited maximum growth at 20 µmol photons $m^{-2}s^{-1}$ (29.7 °C, 8.28 pH) and 45 µmol photons $m^{-2}s^{-1}$ (30.25 °C, 8.67 pH). It can therefore be concluded that the species prefers low irradiance to maximize its growth. High irradiance, on the other hand, limits its growth.

Recommendations. - Information in this paper can be used as a basis for future studies in determining the irradiance that will result in the maximum growth of *L. majuscula*. The researchers recommend further studies between the irradiance levels of 20 µmol photons $m^{-2}s^{-1}$ and 45 µmol photons $m^{-2}s^{-1}$, with equal intervals, to exactly identify the most ideal irradiance level of maximum growth of the alga. Lastly, the researchers would also like to recommend daily sampling to determine the daily growth rate of the alga which is necessary to model a cyanobacterial growth curve.

Acknowledgment. - The researchers would like to thank Mrs. Annie Franco and Mrs. Ghing Gamuza of the Phycology Laboratory at SEAFDEC for their help and guidance during the conduct of the study, Dr. Iris Ann Borlongan of the University of the Philippines - Visayas for her comments and suggestions, and Mr. Vicente Balinas of the University of the Philippines - Visayas for his help in the statistical analysis.

References

[1] Marine Literature Database. [cited June 13, 2021]. Available from https://bit.ly/2V3XTS0.

[2] Engene N, Choi H, Esquenazi E, Rottacker E, Ellisman M, Dorrestein P, Gerwick W. 2011. Underestimated biodiversity as a major explanation for the perceived rich secondary metabolite capacity of the cyanobacterial genus *Lyngbya*. Environ. Microbiol. 13(6): 1601–1610.

[3] Burja AM, Abou-Mansour E, Banaigs B, Payri C, Burgess JG, Wright PC. 2002. Culture of the marine cyanobacterium, *Lyngbya majuscula* (Oscillatoriaceae), for bioprocess intensified production of cyclic and linear lipopeptides. J Microbiol Methods. 48(2-3): 207–219.

[4] Gupta RK, Pandey VD. Advances in applied phycology. Delhi: Daya Pub. House; 2007.

[5] Kumar M, Tripathi K, Srivastava A, Gour JK, Singh RK, TIlak R, Asthana RK. 2013. Cyanobacteria, *Lyngbya aestuarii* and *Aphanothece bullosa* as antifungal and antileishmanial drug resources. Asian Pac. J. Trop. Biomed. 3(6): 458–456.

[6] Watkinson A. 2000. Ecophysiology of the marine cyanobacterium, *Lyngbya majuscula* (Oscillatoriacea).

[7] Xu Y, Ibrahim IM, Harvey PJ. 2016. The influence of photoperiod and light intensity on the growth and photosynthesis of *Dunaliella salina* (chlorophyta) CCAP 19/30. Plant Physiol Biochem. 106: 305–315.

[8] Bouterfas R, Belkoura M, Dauta A. 2006. The effects of irradiance and photoperiod on the growth rate of three freshwater green algae isolated from a eutrophic lake. Limnetica. 25(3): 647–656.

[9] Van Liere L, Mur LR. 1979. Occurrence of *Oscillatoria agardhii* and some related species, a survey. Dev. Hydrobiol. 2: 67.

[10] Loogman J. 1982. Influence of photoperiodicity on algal growth kinetics. Thesis, University of Amsterdam.

[11] Jindal N, Singh DP, Khattar JS. 2013. Optimization, characterization, and flow properties of exopolysaccharides produced by the cyanobacterium *Lyngbya stagnina*. J. Basic. Microbiol. 53: 1–11.

[12] Zhang T, Lin L, Song L, Chen L. 2009. Effects of temperature and light on the growth and geosmin production of *Lyngbya kuetzingii* (Cyanophyta). J Appl Phycol. 21: 279–285.

[13] Kuhlmann J. 1999. Alternative strategies in drug development: clinical pharmacological aspects. Int J Clin Pharmacol Ther. 37(12): 573–583.

[14] Slein J. 1973. Handbook of phycological methods. Culture methods and growth measurements. *Cambridge University Press*, 448.

[15] Dela Pena M & Franco A. 2013. Culture of marine phytoplankton for aquaculture seed production. AEM55, SEAFDEC. ISSN 0115–5369.

[16] American Public Health Association. Standard methods for the examination of water and wastewater. 18th ed. Washington, DC: APHA.

[17] Luhan MRJ, Sollesta H. 2012. Growing the reproductive cells (carpospores) of the seaweed, *Kappaphycus striatum*, in the laboratory until outplanting in the field and maturation to tetrasporophyte. J Appl Phycol 22: 579–585.

[18] Flynn K. 2019. Enhancing microalgal production. European Union. https://bit.ly/3eOo6eg.

[19] Sanchez S and Demain A. 2011. 1.10 - Secondary metabolites. comprehensive biotechnology (Third Edition). Pergamon. 131–143.

[20] Mandal S, Rath J, Adhikary S. 2011. Adaptation strategies of the sheathed cyanobacterium *Lyngbya majuscula* to ultraviolet-B. J Photochem and Photobio. 102: 115–122.

[21] Ahern KS, Ahern CR, Savige GM, Udy, JW. 2007. Mapping the distribution, biomass and tissue nutrient levels of a marine benthic cyanobacteria bloom (*Lyngbya majuscula*). Marine and Freshwater research. 58: 883–904.

[22] Leitao E, Oxefelt F, Oliveira P, Moradas-Ferreria, Tamagini P. 2005. Analysis of the hupSL operon of the nonheterocystous cyanobacterium *Lyngbya majuscula* CCAP 144/6: regulation of the transcription and expression under a light-dark regimen. App Environ Microbiol. 71(8): 3567–4576.

[23] Lundgren P, Bauer K, Bergman B. 2003. Reevaluation of the nitrogen fixation behaviour in the marine non-heterocystous cyanobacterium *Lyngbya majuscula*. Journal of Phycology. 39

[24] Ras M, Steyer J, Bernard O. 2013. Temperature effect on microalgae: a crucial factor for outdoor production. Reviews in Environmental Science and Bio/Technology volume. 12: 152–164.

[25] Mangan N, Flamholz A, Hood R, Milo R, Savage D. 2016. pH determines the energetic efficiency of the cyanobacterial CO_2 concentrating mechanism. PNAS. 113 (36).

[26] Yin Q, Carmichael W, Evans W. 1997. Factors influencing growth and toxin production by cultures of the freshwater cyanobacterium *Lyngbya wollei* Farlow ex Gomont. Journal of Applied Phycology.

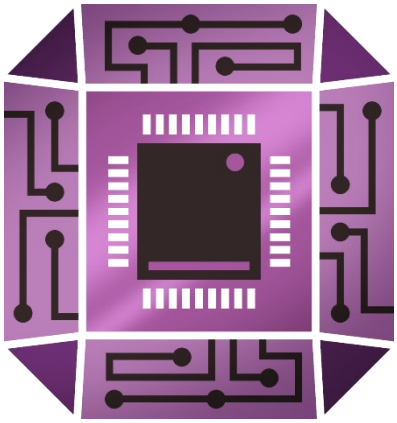

CLUSTER SIX

COMPUTER SCIENCE

The color violet is synonymous with power, and the gem design is inspired by printed circuit boards often found in electronic devices, wherein a microchip is integrated into the middle. Hence, the gem is representative of a computer, in that it requires a power source and circuitry to function. Through scientific analysis of data done mainly through the power of computers, studies under this cluster aim to derive information that transcends electronic applications.

These studies fall under the Industry, Energy, and Emerging Technology (IEET) Research Development Agenda, in line with goals to increase state-of-the-art information and communications technology (ICT) research and the utilization of computer-based systems in various industries and scientific fields.

BASED ON: Harmonized National Research and Development Agenda (HNRDA)

Publiscience Vol. 4 Issue 1

Developing a neural network that uses satellite imagery to estimate carbon dioxide emissions in the Philippines

EWEMIZ C. INSIGNE, KIRSTEN DIANNE G. DELMO, NICO ANDREI R. SERRATO, and GERALD U. SALAZAR

Philippine Science High School Western Visayas Campus - Department of Science and Technology (DOST-PSHSWVC), Brgy. Bito-on, Jaro, Iloilo City 5000, Philippines

Article Info

Submitted: May 14, 2021
Approved: Jul 21, 2021
Published: Aug 30, 2021

Keywords:
artificial intelligence
carbon dioxide
satellite imagery
neural network
data science

Abstract

In recent years, satellite imagery has become a popular subject of studies involving artificial intelligence. AI and satellite imagery were used together to estimate real-life variables in various fields, such as predicting poverty levels, detecting oil spills, and analyzing coal mine areas. With the rising importance of climate change, this study aimed to develop a convolutional neural network trained with daytime and nighttime data through a transfer learning approach to predict carbon dioxide emissions in the Philippines. The developed scripts were adapted and based on code from public GitHub repositories and existing research. The trained model was concluded to have high predictive power ($r^2 = 0.74$), and can be used as a starting point for more fully developed software and models that can serve as an alternative method of collecting CO_2 emissions data.

Introduction. - Data science uses statistics, artificial intelligence (AI), and available data from various sources to process into valuable information [1]. AI in data science looks for patterns, predicts outcomes, and offers evidence-based information using the data that it was given [2]. More and more AI-based tools and technologies are beginning to emerge as datasets begin to be more readily available online and in other publicly-available sources. A specific type of AI, the convolutional neural network (CNN), is mainly used for the analysis of images. It takes an input and extracts features from the image to be analyzed by neurons – an interconnected system of cells that takes input and multiplies it by a specific weight that constantly changes until the CNN can correctly predict an outcome.

Recent studies were able to use satellite imagery to predict poverty levels in an area [3,4,5]. Other studies utilized satellite imagery for purposes such as detecting oil spills, analyzing coal mine areas, and detecting clouds [6,7,8]. The effectiveness of combining satellite imagery and AI and show how it has many potential uses in various fields.

With the increase of CO_2 concentration in the atmosphere, the need for "the quantification of the spatial distribution of CO_2 in the atmosphere" was felt by researchers in the last decade [9]. The main focus of currently available literature on estimating CO_2 emissions focus on mathematical models that don't utilize AI. [9,10]. The correlation of nightlights and CO_2 emissions using satellite imagery has also been proven by studies, where highly-lit points were characterized to be highly urbanized and were seen to have high CO_2 emissions [9,11]. While using AI (specifically neural networks) to estimate CO_2 emissions is not an uncommon method [12], this study differs in that it develops a CNN that estimates CO_2 emissions in specific 1km x 1km areas within the Philippines, and utilizes a transfer learning approach. Transfer learning is a method that utilizes the learning extracted from one problem or variable (such as nightlights data) and uses it to make better predictions for related data.

The objective of this paper is to see how effective the use of AI with satellite imagery can be for the estimation of real-life variables, such as CO_2 emissions, in order to prove its versatility as a tool to be used in a wide range of applications in various fields. As a tool specifically used to estimate CO_2 emissions, it could serve as an alternative method of collecting such data. Thus, the goal of this study is to develop an AI—specifically a CNN—that uses satellite imagery to estimate CO_2 emissions in the Philippines. The specific objectives are enumerated below. They also serve as an outline for the succeeding Methods section.

(i) Design an algorithm for the CNN model;

(ii) Collect latest (at the time of development) satellite imagery and CO_2 emissions data;

(iii) Code the scripts for data preprocessing, CNN model training, and evaluating the model's estimations using Python 3.8;

(iv) Train the CNN using the collected data; and

How to cite this article:
CSE: Insigne EC, Delmo KDG, Serrato NAR, Salazar GU. 2021. Developing a neural network that uses satellite imagery to estimate carbon emissions in the Philippines. Publiscience. 4(1): 88–92.
APA: Insigne, E.C., Delmo, K.D.G., Serrato, N.A.R., & Salazar, G.U. (2021). Developing a neural network that uses satellite imagery to estimate carbon emissions in the Philippines. *Publiscience*, *4*(1), 88–92.

For supplementary data, contact: publiscience@wvc.pshs.edu.ph.

(v) Train a ridge regression model using the CNN's extracted features for evaluation and data visualization of results

Methods. - This study consisted of five phases: *Design*, *Data Collection* (for data pre-processing), *Development*, *Training*, and *Evaluation*. The *Design* phase was for the creation of the algorithm for the CNN model; *Data Collection* phase was for the collection of images and nightlight values for pre-processing used for training the developed program; *Development* phase was for the coding and debugging of the scripts; *Training* phase was for the tuning and fitting of the model, and; *Evaluation* was for the training of the ridge regression model for evaluation and data visualization of results.

Design phase. During the *Design* phase, a flowchart and the equivalent pseudocode of the program's process were made to be used as a basis for the creation of our actual program during the *Development* phase. The flowchart presented the various parts of the process in an human-readable format that can then be converted to code. This phase employed the use of open-source codes by Jean et al. [4] and Tingzon et al. [5] that were available on the authors' GitHub repositories.

Data Collection phase. In order to properly train the AI, certain data were gathered and pre-processed. This study used the Open-Data Inventory for Anthropogenic Carbon dioxide (ODIAC) of the National Institute for Environmental Studies (NIES) Japan for the year 2015 [13]. The data points for the Philippines were filtered out, as seen in Figure 1. Daytime satellite images were then collected through a script that downloads 1 km by 1 km Google Static Maps API images according to the given data points from the CO_2 emissions data. Nighttime lights data was collected from the Visible Infrared Imaging Radiometer Suite (VIIRS) Day/Night Band (DNB) data of the Earth Observation Group, Payne Institute for Public Policy [14].

Development phase. The method used in the developed scripts were adapted from the transfer learning approach used by Jean et al. [4] Daytime satellite image features were extracted by the CNN to estimate the CO_2 emission level in an area.

The scripts were developed based on the algorithm made in the design phase as well as open-source scripts and codes from similar studies publicly available on GitHub [15,16,17]. Python 3.8 was the primary programming language used for development, and the scripts were coded in JupyterLab 1.1.4 and JupyterNotebook 6.0.1.

The first three scripts were used for the pre-processing of data. The first script filtered out the CO_2 emission data points for the Philippines. The second script downloaded the daytime satellite images for each datapoint with a zoom level of 13, and the third script compiled the corresponding nighttime radiance for the coordinates of each CO_2 emission datapoint.

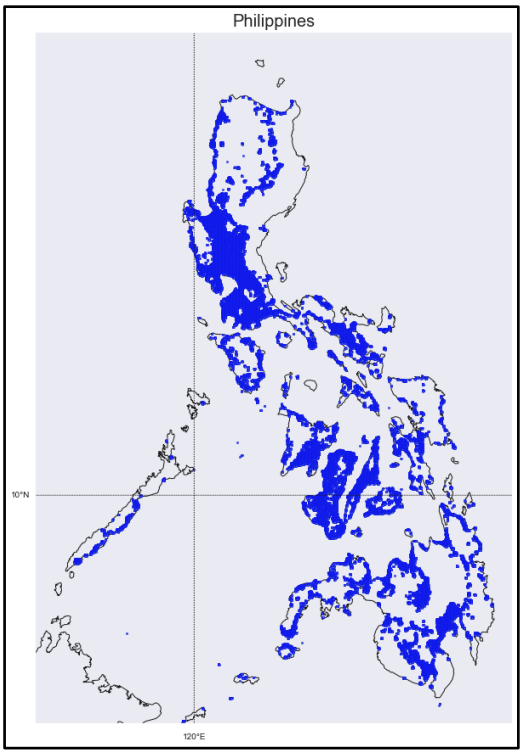

Figure 1. Philippine CO_2 emission data points. The data points for the Philippines were filtered out from the ODIAC dataset.

The first script also created a dataframe with the latitude and longitude values, the corresponding CO_2 emission. These values were then exported into a comma-separated values (.csv) file.

The second script downloads 400 px by 400 px Google Static Maps API images at a zoom level of 13 (corresponding to an estimated 1 km by 1 km area) for each data point. A total of 79942 unique images were downloaded.

The third script collected the corresponding nightlight radiance for each point in the dataset. The values were then appended to the data frame created in the first script.

The fourth script was for the training. In its initial stages, the dataset and the corresponding images were divided into two folders: 80% of the images were used for training and the remaining 20% were used for validation/testing of the model. Three nighttime light intensity classes were obtained by fitting a mixture of three Gaussian distributions to the relative frequencies of the nighttime light intensity values.

Training phase. The training phase aimed to train the CNN with images so that it could create its own model in order to analyze patterns and make accurate estimations close to the given CO_2 data.

In the first part of the training, we fine-tuned a pre-trained model, VGG F, to estimate nighttime light intensity at various locations given the corresponding daytime satellite images. This pre-trained model network is an eight-layer deep convolutional neural network (DCNN), which had been originally designed and trained for image classification on ImageNet [18].

The training method and code were heavily adapted from Mather's Predicting Poverty repository on GitHub [15] and the Pytorch CNN Training Method [19].

After training, the model was then tested by making estimations using the testing data set.

Evaluation phase. Once the CNN was trained, the extracted features were then used to train a ridge regression model. It specifically used k-fold cross-validation. Python was also used in data visualization, specifically for the creation of the graphs.

Data Analysis. For data visualization and analysis, this study used Python 3.8 and different libraries that were available and used for statistical calculations and data visualization such as NumPy, Pandas, Scikit-learn, and Matplotlib.

This analysis utilized a cross-validation technique, which is a data resampling method that assesses the generalization ability of a predictive model and prevents overfitting. The *k*-fold cross-validation technique is much less prone to selection bias compared to other cross-validation methods. In *k*-fold cross-validation, the process starts out by dividing the dataset into given k subsets and uses *k-1* subsets as the training sets while the remaining set serves as the testing set. This cross-validation method is then repeated *k* times, using different testing sets from the original *k* subsets each time. The *k* value for this study was *5*, similar to that of Jean et al. [4].

Safety Procedure. As this study focused on AI, all processes were done on a computer. There were no major ethical issues dealt with. The data used is publicly available and the source codes are open-access.

Results and Discussion. - The aim of this study is to develop a convolutional neural network to analyze CO_2 emissions in the Philippines using satellite imagery, and see how effective the use of AI with satellite imagery can be for the estimation of real-life variables (such as CO2 emissions). This was done by creating the algorithm for the program, collecting data that would be used for pre-processing and training, developing the scripts used for the program, and then evaluating and visualizing the results. The evaluation phase specifically employed k-fold cross validation, with various libraries in Python such as Matplotlib used for data visualization.

The current results, shown in Figure 2, showcase strong predictive power using the model trained on a dataset with 79942 data points. With a r^2 value of 0.74, this means that the trained model fits the data well, with 74% of the total variation being accounted for.

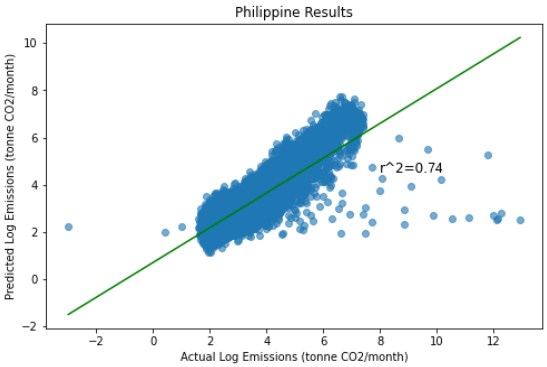

Figure 2. Philippine results. Predictions and reported r^2 value are from five-fold cross-validation. Green line shown is the line of best fit.

To assure the accuracy of this statistic, five random sampling trials were performed. Five thousand random points were selected from the data set and were processed through the final script to predict emissions. The summary of trials is presented in Table 1.

Table 1. Summary of five trials of 5000 randomly selected points.

Trial	R^2	Ridge Score (Validation)	Ridge Score (Training)
1	0.64	0.62	0.85
2	0.69	0.66	0.86
3	0.65	0.63	0.84
4	0.66	0.57	0.92
5	0.65	0.58	0.90
Ave	0.66	0.61	0.87

The average r^2 value of the five trials is 0.66, and the average ridge score for validation is 0.61. Compared to the final result's r^2 of 0.74 and ridge score for validation of 0.73, there is some difference. The small disparity can be explained by the fact that the trials only used 5000 data points, which affects the forward pass process within the predicting consumption script. Still, the results are notable as it shows that 5000 data points (6.7% of the original 79942) can already show high predictive power, explaining up to 69% of the variance.

The trials' ridge scores for training are much higher compared to their respective ridge scores for validation, which may show that there is some overfitting. In the final result, however, the difference between the training ridge score (0.78) and the validation ridge score (0.74) is much smaller, showing that a bigger dataset helps minimize overfitting.

The ODIAC dataset served as the proxy ground-truth data in this study but can also be used as a basis for a comparison of the model's performance. In a study by Chen et al. [20], the ODIAC dataset's predictions among 14 large cities were compared to emission inventory statistics. This revealed that in

some cities, especially in developing countries, the dataset overestimates. As Chen states, this overestimation could be due to the "poor correlation between nightlight intensity with human activity [...] in developing countries." This is similar to a problem Jean et al. [4] cites, in which areas with very low light levels (often in developing countries) often show little variation, leading to models incapable of distinguishing differences in economic activity. Jean et al. improved upon existing studies by using a transfer learning approach in their model, which allowed them to have better estimates in countries and areas with minimal nightlight data. This study applied a similar approach; it was based on the transfer learning approach by Jean et al., which utilized both daytime images and nighttime data to estimate CO_2 emissions, thus making predictions within the Philippines - especially in areas that are darker or with low luminosity values - more accurate.

Though the results cannot be directly compared, due to the models measuring different variables, a comparison may offer some valuable insight. It was found that the developed model of this study estimates CO_2 emissions better than how the models of Jean et al. ($r^2_{max} = 0.55$) and Tingzon et al. ($r^2 = 0.63$) predict economic status.

Limitations. One of the primary concerns in this study was the lack of "true" ground truth data. Directly-measured CO_2 emissions data in the Philippines could not be found available in any of the country's database agencies, despite many efforts. Because of this, the study decided to use the ODIAC dataset as a proxy for ground truth data, which, while still a valid substitute, may contain overestimations and underestimations in urban areas and rural areas respectively as it is based on space-based nighttime light data and individual power plant emission/location profiles.

Due to restraints in time and processing power, data points with no emissions (data points with a value of 0) were removed, which left the 79942 data points which were then used for the rest of the study. It is recommended that in future studies and developments, all data points, including those with 0-emission values, should be included.

A heatmap couldn't be done in this study due to the lack of time and experience on the part of the researchers.

Conclusion. - Through the development of the scripts, adapted from and based on the publicly available GitHub repositories of Jatin Mather (2016) and Jean et al. (2016), this study was able to conclude that the developed convolutional neural network model used to estimate CO2 emissions in the Philippines has strong predictive power. It improves upon ODIAC, an existing CO_2 dataset, by looking at both daytime and nighttime images and data through transfer learning. The developed scripts and CNN model can be used as a starting point for more fully developed software and models that can serve as an alternative method of collecting CO_2 emissions data.

Recommendations. - Though the scripts and algorithms may prove themselves to be valid processes with strong predictive power, concerns may arise if the dataset itself has some issues - such as overestimations and underestimations - similar to that of ODIAC. It is recommended that, if there is access to a cleaner dataset of direct measurements from the Philippines rather than estimations, future researchers may want to utilize that instead.

This model is limited to data in 2015. It is possible that this model could be used for more recent years, but further research is required in order to confirm so.

A direct comparison between the accuracy of the ODIAC dataset and the accuracy of the developed model (compared to existing emission inventories) through graphs or a heatmap may also give additional insights.

Acknowledgment. - The researchers would like to thank Mr. Neal Jean of Stanford University and Thinking Machines Data Science Inc. for their invaluable time, knowledge, and support that was extended to this study.

References

[1] Van der Aalst WP. 2018. Data Science in Action. In: Process Mining. Berlin: Springer Berlin. p. 3–23.

[2] Dinov I. 2019. Data Science and Predictive Analytics: Biomedical and Health Applications Using R. S.l.: Springer.

[3] Xie M, Jean N, Burke M, Lobell D, Ermon S. 2016. Transfer learning from deep features for remote sensing and poverty mapping. In: Schuurmans D, Wellman MP, editors. c2016. AAAI'16. Proceedings of the Thirtieth AAAI Conference on Artificial Intelligence; 2016 Feb 12-17; Phoenix, Arizona. Palo Alto (CA): AAAI Press. p. 3929–3935.

[4] Jean N, Burke M, Xie M, Davis WM, Lobell DB, Ermon S. 2016. Combining satellite imagery and machine learning to predict poverty. Science 353: 790–794.

[5] Tingzon I, Orden A, Sy S, Sekara V, Weber I, Fatehkia M, Herranz MG, Kim D. 2019. Mapping Poverty in the Philippines Using Machine Learning, Satellite Imagery, and Crowd-sourced Geospatial Information. International Conference on Machine Learning AI for Social Good Workshop.

[6] Zhi-Ming D, Li-Xia G, Jian-Kui Z, Xue-Bin Z. 2015. Oil-Spills Detection in Net-Sar Radar Images Using Support Vector Machine. The Open Automation and Control Systems Journal 7(1): 1958–1962.

[7] Demirel N, Emil MK, Duzgun HS. 2011. Surface coal mine area monitoring using multi-temporal high-resolution satellite imagery. International Journal of Coal Geology 86:3–11.

[8] Bai T, Li D, Sun K, Chen Y, Li W. 2016. Cloud Detection for High-Resolution Satellite Imagery Using Machine Learning and Multi-Feature Fusion. Remote Sensing 8: 715.

[9] Ghosh T, Elvidge CD, Sutton PC, Baugh KE, Ziskin D, Tuttle BT. 2010. Creating a Global Grid of Distributed Fossil Fuel CO2 Emissions from Nighttime Satellite Imagery. Energies 3: 1895–1913.

[10] Makido Y, Dhakal S, Yamagata Y. 2012. Relationship between urban form and CO2 emissions: Evidence from fifty Japanese cities. Urban Climate 2: 55–67.

[11] Rayner PJ, Raupach MR, Paget M, Peylin P, Koffi E. 2010. A new global gridded data set of CO2 emissions from fossil fuel combustion: Methodology and evaluation. Journal of Geophysical Research 115.

[12] Abdullah L, Mohd Pauzi H. 2015. METHODS IN FORECASTING CARBON DIOXIDE EMISSIONS: A DECADE REVIEW. Jurnal Teknologi 75.

[13] Tomohiro O, Shamil M. 2015. ODIAC Fossil Fuel CO2 Emissions Dataset (ODIAC v1.7). Center for Global Environmental Research, National Institute for Environmental Studies, Downloaded from https://bit.ly/2SPGE5O.

[14] Elvidge, Christopher D., Kimberly Baugh, Mikhail Zhizhin, Feng Chi Hsu, and Tilottama Ghosh. "VIIRS night-time lights." International Journal of Remote Sensing 38, no. 21 (2017): 5860–5879.

[15] Mather, J. 2019. Predicting poverty replication. https://bit.ly/34IeUmm

[16] Tingzon I, Orden A, Sy S, Sekara V, Weber I, Fatehkia M, Herranz M, Kim D. 2018. Mapping Poverty in the Philippines Using Machine Learning, Satellite Imagery, and Crowd-sourced Geospatial Information. https://bit.ly/3fNvSGp.

[17] Jean N, Burke M, Xie M, Davis WM, Lobell DB, Ermon S. 2016. Combining satellite imagery and machine learning to predict poverty. https://bit.ly/3vN79HL.

[18] Deng J, Dong W, Socher R, Li L-J, Li K, Fei-Fei L. 2009. ImageNet: A large-scale hierarchical image database. 2009 IEEE Conference on Computer Vision and Pattern Recognition.

[19] Paszke A, Gross S, Massa F, Lerer A, Bradbury J, Chanan G, Killeen T, Lin Z, Gimelshein N, Antiga L, Desmaison A. 2019. PyTorch: An Imperative Style, High-Performance Deep Learning Library. Advances in Neural Information Processing Systems 32 https://bit.ly/3gbmoUq.

[20] Chen J, Zhao F, Zeng N, Oda T. 2020. Comparing a global high-resolution downscaled fossil fuel CO2 emission dataset to local inventory-based estimates over 14 global cities. Carbon Balance and Management 15.

[21] Oxford University Press. 2020. Overfitting. In: Lexico. [accessed 2020 Dec 10]. https://bit.ly/3uH04Hb.

[22] Brownlee J. 2019. Overfitting and Underfitting With Machine Learning Algorithms. Machine Learning Mastery. [accessed 2020 Dec 10]. https://bit.ly/34Irm5K.

[23] Ying X. 2019. An Overview of Overfitting and its Solutions. Journal of Physics: Conference Series 1168: 022022.

Evaluating the ripening stages of *Musa acuminata* × *balbisiana* (Saba) using 2D-image analysis

ILYSSA MARIE D. MOSO, SEAN RAFAEL L. PUDA, PIA O. TIMAAN, and MARIA DEANNA B. JOLITO

Philippine Science High School Western Visayas Campus - Department of Science and Technology (DOST-PSHSWVC), Brgy. Bito-on, Jaro, Iloilo City 5000, Philippines

Article Info

Submitted: May 12, 2021
Approved: Aug 11, 2021
Published: Aug 30, 2021

Keywords:
banana
image analysis
Python
ripening stage
SVM

Abstract

Saba banana is one of the Philippines' main export products but has a fast ripening process which affects its quality and marketability. Most instruments utilized in measuring banana quality are destructive. However, few have used 2D-image analysis in assessing the ripeness of the banana. This paper presents the evaluation of the ripening stage of Saba banana using 2D-image analysis as an alternative, non-destructive method. The 120 banana images were pre-processed by obtaining the mask to remove the background, retaining only the region of interest, which was further converted into HSV and Grayscale. Ninety of the processed images were utilized as training data sets and the rest as testing data sets for the Support Vector Machine (SVM) where the overall agreement is 70%. The researchers recommend that future studies increase the texture features of the Gray Level Co-occurrence Matrix (GLCM) Analysis to improve the performance of the SVM.

Introduction. - Bananas are the top traded fruit worldwide, and it is one of the top fruit exports of the Philippines [1]. Therefore, it is important to ensure the quality (appearance, texture, flavor, and nutritive values) of the banana being exported and consumed locally because it affects their profitability [2].

There are four major cultivars of bananas in the Philippines and *Musa acuminata x balbisiana* (Saba) is one of the country's main products [22]. It is rich in vitamins and minerals and is also included in many Filipino dishes. *M. acuminata x balbisiana* is also used as a supplement or an alternative staple food from rice and corn in rural areas [3]. There was also a lack of research articles involving the analysis of the different ripening stages of this specific variety of banana using 2D image analysis. Bananas tend to be eaten at their mature stage which is why they are usually harvested at the mature green stage and remain without significant changes depending on the temperature, humidity, and age of the banana at the time of harvest. This is because the ripening process of bananas is irreversible once it starts because it brings about physical and chemical changes to the bananas [4]. It can be observed with the alterations in the fruit texture, the changes in the peel color (usually from green to yellow), the appearance of brown spots, and the synthesis of volatile components [5]. Bananas are known to have seven stages in the ripening process, as seen in Table 1, which are usually assessed through visual comparison of the colors of the peels [6]. As the banana ripens, its shape, size, color, and texture change which are observed by producers to decide when to harvest, transport, and sell the fruit [7]. The ability to identify maturity will help farmers optimize the harvesting phase [8].

Table 1. The stages of banana ripening based on peel color [6].

Ripening stage		Banana peel color
Unripe	**1**	Dark Green
	2	Light green, traces of yellow
Ripe	**3**	More green than yellow
	4	More yellow than green
	5	Green tip and yellow
	6	All yellow
Overripe	**7**	Yellow, flecked with brown

The usual methods for determining fruit quality involve destructive and time-consuming measures such as evaluation of dry matter content, total soluble solids content, sugar content, and juice acidity. Thus, non-destructive alternatives such as image analysis are encouraged [12]. As manual inspections tend to be tedious, subjective, and non-uniform, image analysis using different image processing techniques has been

How to cite this article:
CSE: Moso IMD, Puda SRL, Timaan PO. 2021. Evaluating the ripening stages of *Musa acuminata x balbisiana* (Saba) using 2-D image analysis. Publiscience. 4(1): 93–98.
APA: Moso, I.M.D., Puda, S.R.L., & Timaan, P.O. (2021). Evaluating the ripening stages of *Musa acuminata x balbisiana* (Saba) using 2-D image analysis. *Publiscience*, *4*(1), 93–98.

For supplementary data, contact: publiscience@wvc.pshs.edu.ph.

used to assess and evaluate the ripening process of bananas. Techniques such as the use of colorimeters [11], feature extraction and texture analysis [7], imaging and spectroscopy [12], color histogram [7], and many others have been used over the past few years. Many algorithms have also been utilized for the purpose of identifying the different ripening stages of bananas such as the use of the Gray Level Co-occurrence Matrix (GLCM) for processing; Support Vector Machine (SVM) and K-nearest Neighbor (KNN) for recognition [13]; Fuzzy Color Histogram (FCH) and Movement Imagination (MI) methods for feature extraction [14]; Artificial Neural Network (ANN) to increase quality detection [15], and many others have been proven to be effective and usable in real-life applications. There are also new and efficient techniques that are based on the Hue Saturation Value (HSV) colorspace, development of brown spots, and texture analysis of the banana. According to Tichkule and Gawali [20], non-destructive applications that can use texture analysis techniques on the products are good alternatives for effective food quality assessment because they contain information on the color and geometric structure of the fruit.

The results of this study will benefit researchers who aim to further enhance the use of 2D-image analysis as a non-destructive assessor of quality.

This study aimed to predict the ripening stages (unripe, ripe, and overripe) of *Musa acuminata x balbisiana* (Saba) using 2D-image analysis. Specifically, it aimed to:

(i) analyze the ripe, unripe, overripe stages of Saba banana by applying the Hue Saturation Value (HSV) and Grey-level Co-occurrence Matrix (GLCM) feature extraction techniques.

(ii) compare the HSV of the unripe, ripe, and overripe Saba bananas using histograms.

(iii) determine the different ripening stages of the bananas using the SVM.

Methods. - The Saba bananas were acquired from the local farmers in Leganes, Iloilo, Philippines. The samples were grouped into ripe, unripe, and overripe stages by. This research utilized 120 banana samples overall, 40 for each ripening stage. From each ripening stage, ten of the images were processed while the rest were used to train the SVM. The images were converted into binary images [7]. Next, the images underwent image segmentation which produced the original picture without the background [8]. For the feature extraction, the HSV color space was used to categorize each pixel based on its color and brightness and the GLCM was used in measuring the texture of the image. The final process utilized an SVM to differentiate the ripe, unripe, and overripe bananas [7].

Program Implementation. The Python programming language of version 3.7.10 was implemented through Google Colaboratory which was mounted onto specific Google Drive folders where the acquired images were uploaded.

Sample Collection. The Saba banana samples collected in Leganes, Iloilo were identified and grouped by a qualified banana farmer. Six hands of bananas which were classified as unripe, ripe, and overripe were collected. Unripe bananas are green (stage 1 - stage 2), ripe bananas are usually yellow (stage 5 - stage 6) and overripe bananas are yellow with brown spots (stage 7) [8]. Forty (40) individual bananas were chosen from each ripening stage having 120 samples in total.

Image Acquisition. Images of the samples were acquired inside an enclosed black cardboard box by taking photos using a mobile phone model Vivo 1806 with a 9.8MP camera which was attached to a phone stand 19 cm above the surface of the black cloth. The picture was taken in a room with a temperature of 302°C [17] and with one major source of white light being an LED ring light [12]. Overall, 120 pictures were taken and transferred from the mobile phone to a Google Drive folder in JPEG format [18].

Table 2. The camera control settings used during image acquisition.

Variable	Settings
Image Size	2160 x 4560
Magnification	1.0x
Flash	No Flash
Image Type	JPEG
Aperture	f/2.0

Table 3. The specifications of the LED Ring light used during image acquisition.

Variable	Settings
Brand	SANYK
Model	10 inches live fill light
Outer Ring Size	26cm
Light	Cold Light
Dimmable	Yes
Color Temperature	2700-7000K
Color Rendering Index	RA/CRI:80
Overall lumens	600-1300LM
Number of Lamp Beads	120PCSA
Working Power Supply	DC 5V/1A
Power	12W/24W
Lamp Bead Model	2835 LED
Light Angle	120

Table 4. Raw images of three *Musa acuminata x balbisiana* samples from each ripening stage (unripe, ripe, and overripe).

Samples	Unripe	Ripe	Overripe
1			
2			
3			

Projected Area Estimation. The bananas were cut into six planes in the longitudinal axis. Each perpendicular cut was measured using a Vernier caliper, while the internal and external lengths of the bananas were measured using a flexible ruler [10]. The area of the banana was calculated by solving for the summation of the individual elements: the mean value of the ring thickness, area of the sectoral frustum, and center of the curvature.

Pre-processing. The images were converted into the HSV colorspace. Afterwards, it was converted into grayscale and further converted into binary images which served as segmentation masks [19].

Image Segmentation. Using the segmentation masks, the RGB banana images were separated from the unwanted regions where only the regions of interest were kept [8] which are the areas of the images that were used for analysis [20].

Feature Extraction. The study focused on measuring the sample images' color and texture features. The HSV method was used to evaluate the color, amount of color, and brightness of the images. Afterwards, the HSV values were extracted and plotted into a histogram for each ripening stage where the data was analyzed [7]. The GLCM was used to investigate the texture, specifically, the contrast and homogeneity of the pixels [7,12].

Recognition. The SVM model was trained using 90 testing images with 30 from each ripening stage. The SVM was then used in order to predict the ripening stages of the Saba bananas based on the data sets from the feature extraction process [7].

Data Analysis. The classification of bananas based on their ripening stages was analyzed using the HSV and GLCM for color and texture features, respectively. For the HSV extraction, the data obtained were from the colors of the pixels generated from the HSV color space. These pixels were plotted on a histogram. The GLCM extraction focused on obtaining the value for the contrast [8] and homogeneity [12] using the following formulas:

$$\text{Contrast} = \frac{\sigma}{(\alpha_4)^{0.25}}, \text{ and } \alpha_4 = \frac{\mu_4}{\sigma^4}$$

Where μ_4 is the fourth moment about the mean, and σ^2 is the variance.

$$\text{Homogeneity} = \sum_{i=1}^{K}\sum_{j=1}^{K}\frac{P_{ij}}{1+|i-j|}$$

Where K is the size of the co-occurrence matrix, P_{ij} is the estimate of the probability of a pair of points having values that satisfy an operator, and i and j are values of intensity.

The contrast and homogeneity values were then placed on a matrix and were sorted into pairs according to their banana sample [21]. Using Microsoft Excel, the mean and standard deviation of the texture values were calculated. The SVM was used to compare its predictions with the actual ripening stages of the samples.

Safety procedure. The mandated safety protocols of the LGUs for the COVID-19 were followed during the conduct of the data gathering by the researchers.

Results and Discussion. - Figures 1, 2, and 3 show the average hue, saturation, and intensity values from the ten segmented unripe, ripe, and overripe banana images, respectively, which were obtained from the HSV color feature extraction process. The hue values for the unripe stage are between the range of 90 to 110, while the ripe and overripe stages have hue values in between the range of 50 to 70 with the ripe banana samples having the highest frequency of pixels and the overripe bananas having the lowest frequency of pixels. For the saturation, ripe bananas had the highest saturation value being 0.6 - 0.8 while unripe bananas had the lowest saturation ranging only from 0.4 - 0.6. Lastly, for the intensity, the unripe bananas have the most diverse range of brightness from 50 to 250 while the overripe bananas had the least diverse range of brightness from 150 to 200.

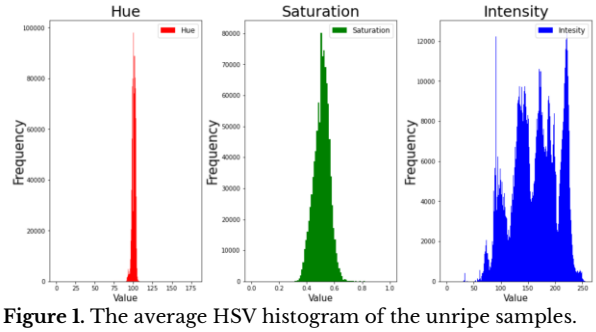

Figure 1. The average HSV histogram of the unripe samples.

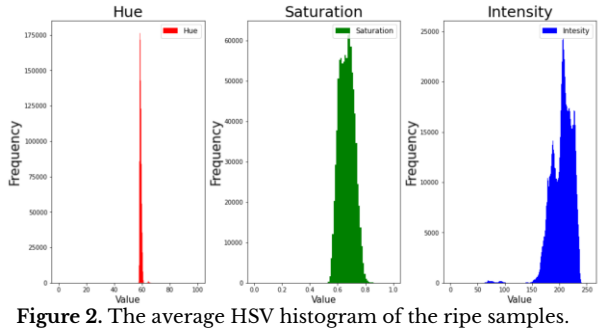

Figure 2. The average HSV histogram of the ripe samples.

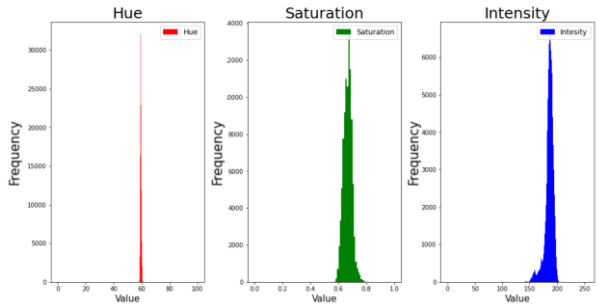

Figure 3. The average HSV histogram of the overripe samples.

The contrast and homogeneity values were obtained using Python in Google Colaboratory, meanwhile, Microsoft Excel was used to calculate the mean of the values and their standard deviation. Normalization of data was done to obtain the best performance for the system with values between zero and one [23]. From Table 4, the overripe bananas have obtained the lowest normalized texture feature value for contrast and homogeneity. The unripe and ripe bananas obtained the highest normalized values for contrast and homogeneity, respectively.

Table 5. The normalized feature vector for the unripe, ripe, and overripe Saba bananas using GLCM Feature Extraction.

Texture Feature	Contrast	STD. DEV	Homogene-ity	STD. DEV
Unripe	0.22	0.24	0.25	0.20
Ripe	0.21	0.25	0.29	0.12
Overripe	0.19	0.27	0.21	0.25

Figures 4, 5, and 6 are histograms that present the average red, green, and blue values of the ten unripe, ripe, and overripe banana samples that were analyzed during the HSV color feature extraction process, respectively. On the right side of the plots, the unripe samples have more green pixels than red pixels as evidenced by the higher peak around the 150-color range, while the ripe samples were the other way around having a stronger peak towards the 250-color range. On the other hand, the overripe samples have much more red, green, and blue pixels on the left side of the plot.

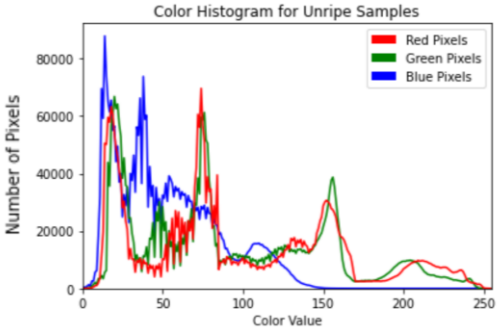

Figure 4. The average color histogram for the unripe samples.

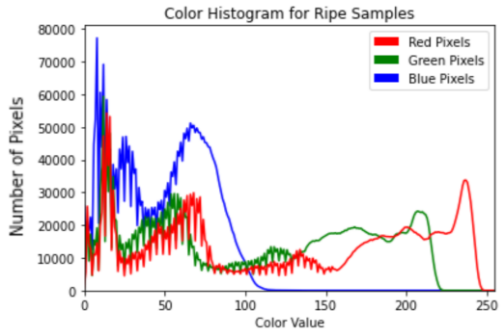

Figure 5. The average color histogram for the ripe samples.

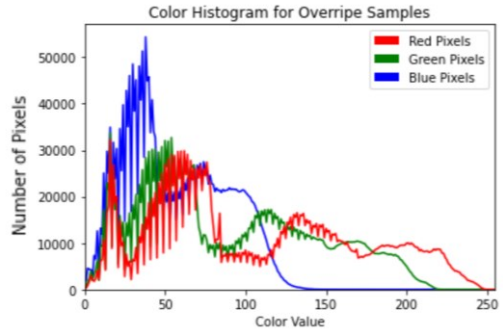

Figure 6. The average color histogram for the overripe samples.

The average values of the histograms in Figures 4, 5, and 6 have a high frequency of dark blue pixels as evidenced by the strong peaks of the blue line reaching over 50,000 pixels from the 0-50 range. This indicates that there may be high amounts of shadows that were included in the images during the HSV color extraction. However, the frequency of the blue pixels in all three histograms was reduced to zero as the color value rose, which means that there were no light blue pixels in the banana images. In contrast to the reduced amount of blue pixels, the right side of the histograms has higher amounts of red and green pixels.

Specifically, the unripe samples had more green pixels than the ripe and overripe samples while the ripe sample had more red pixels than the unripe and overripe samples. Moreover, the unripe samples have the least amount of red and green pixels on the ride side of the plot but have higher values of red, green, and blue pixels on the left side.

An SVM is a supervised learning method that analyzes data and recognizes patterns that are useful in data classification [24]. Random forest was used to

classify the images based on the SVM model. The classification was conducted in Colaboratory using python as a programming language.

Table 6. The confusion matrix resulting from the classification of the ripening stages of the Saba bananas using an SVM Classifier.

Actual Stage	Predicted Stage			Sensitivity (%)
	1	2	3	
Unripe	*5*	2	3	*50*
Ripe	0	**10**	0	100
Overripe	0	4	**6**	60
Precision (%)	100	62.5	66.7	Overall Correctness = **70%**

In Table *5*, the confusion matrix presented was used to evaluate the SVM system. The total samples that were processed in the system were 30 bananas, ten from each ripening stage. The system has an overall agreement of 70%. The system classified 10 out of the 10 samples of the ripe bananas correctly (100% sensitivity). Analyzing the errors, 4 out of 10 samples of overripe bananas were misclassified as ripe. This means that the banana samples between the ripe and overripe stages have a similar texture and color features. In a study conducted by Mazen and Nashat (2019), they had made an SVM that achieved an overall agreement of 96.6%. In their study, they used another image feature to differentiate between the different ripening stages—Ripening Factor (RF)—which was not included in this study. RF is the banana's ripeness factor where the total area of the brown spots is divided by the total area of the banana [10]. The maximum value of precision, which is a proportion of the predicted positive ripening stage that was correctly identified, in the classifier is from the unripe stage with 100%. The maximum value of sensitivity, which is the ability of the prediction model to select the instance of a certain ripening stage from the dataset, is reached by the ripe stage with 100%. Table *5* proves this fact because 10 out of 10 banana samples were classified in the correct stage.

Limitations. The limitations of this study include the color range threshold for the image segmentation as the study only used the visual chart provided by Soltani et al. (2019) due to the lack of previous literature involving Saba bananas. Furthermore, only the basic color values of yellow, green, and brown were used for the image segmentation process due to a lack of previous literature regarding the color ranges of Saba bananas.

Conclusion. - The color and texture features from the 90 images that were used to train SVM were able to achieve a 70% overall agreement in classifying the 30 Saba banana samples into unripe, ripe, and overripe classes. Nevertheless, the SVM was still able to garner a 100% accuracy rating for the ripe banana images. Hence, 2D-image analysis has the potential to be a non-destructive alternative in classifying the ripening stages of Saba banana as well as other similar fruits in the food industry, but can always be improved further in the future.

Recommendations. - It is recommended to use the official or actual color ranges of the different stages of bananas depending on their species, as this study was not able to find the color chart for the species used in this study -Saba banana. Moreover, it is recommended to apply more than two texture features for the GLCM analysis such as correlation, energy, entropy, dissimilarity, and other image features such as the Ripeness factor to achieve the best performance for the SVM [23]. Additionally, it is also advisable to use classifiers other than the SVM such as Artificial Neural Network [23] to attain a suitable classifier with the best performance depending on the research design process. Lastly, the researchers emphasize the importance of adding more samples to increase the number of images for the training dataset to also increase the performance of the system [24].

Acknowledgement. - The researchers would like to extend their gratitude to the OIC-Municipal Agriculturist for providing their knowledge in selecting a source for the saba bananas as well as the banana farmers who assisted us in the collection of the samples. The group also extends their appreciation to the external consultants for sharing their expertise in this research.

References

[1] [DA] Department of Agriculture. 2018 Dec. Philippine banana industry roadmap. Diliman (QC): DA. *52* p.

[2] Elmasry G, Wang N, Elsayed A, Ngadi M. 2007. Hyperspectral imaging for nondestructive determination of some quality attributes for strawberry. J Food Eng. 81(1): 98–107. doi: 10.1016/j.jfoodeng.2006.10.016.

[3] Calica GB, Lingbawan KR. 2019. Value chain analysis of processing Cardava banana chips in the Philippines: Luzon case. IJSRM. 7(1): 941–946. doi: 10.18535/ijsrm/v7i1.em01.

[4] Dadzie BK, Orchard JE. 1997. Routine post-harvest screening of banana/plantain hybrids criteria and methods. Rome: IPGRI. (INIBAP Technical Guidelines; No. 2).

[5] Drury R, Hörtensteiner S, Donnison I, Bird CR, Seymour GB. 1999. Chlorophyll catabolism and gene expression in the peel of ripening banana fruits. Physiol Plant. 107(1): 32–38. doi: https://doi.org/10.1034/j.1399-3054.1999.100105.x.

[6] Li M, Slaughter DC, Thompson JF. 1997. Optical chlorophyll sensing system for banana ripening. Postharvest Biol Tech. 12(3): 273–283.

[7] Nayak AM, Manjesh R, Dhanusha MS. 2019. Fruit recognition using image processing. IJERT. 7(8): 1–6.

[8] Mazen FMA, Nashat AA. 2019. Ripeness Classification of Bananas Using an Artificial Neural Network. Arab J Sci Eng. 44(8): 6901–6910. doi: 10.1007/s13369-018-03695-5.

[9] Soltani M, Alimardani R, Omid M. 2010. A New Mathematical Modeling of Banana Fruit and Comparison with Actual Values of Dimensional Properties. Mod Appl Sci. 4(8): 14–113.

[10] Mendoza F, Aguilera JM. 2006. Application of Image Analysis for Classification of Ripening Bananas. J Food Sci. 69(9). doi: 10.1111/j.1365-2621.2004.tb09932.x.

[11] Santoyo-Mora M, Sancen-Plaza A, Espinosa-Calderon A, Barranco-Gutierrez AI, Prado-Olivarez J. 2019. Nondestructive quantification of the ripening process in banana (Musa AAB Simmonds) using multispectral imaging. Sensors. 2019: 1–12. doi: 10.1155/2019/6742896.

[12] Shukla D. Recognition of fruits using hybrid features and machine learning. 2016. 2016 International Conference on Computing, Analytics and Security Trends (CAST). doi: 10.1109/cast.2016.7915046.

[13] Fachrurrozi EM, Fiqih A, Saputra BR, Algani R, Primanita A. 2017. Content based image retrieval for multi-objects fruits recognition using k-means and k-nearest neighbor. 2017 International Conference on Data and Software Engineering (ICoDSE). doi: 10.1109/icodse.2017.8285855.

[14] Yogesh, Dubey AK. 2016. Fruit defect detection based on speeded up robust feature technique. 2016. 5th International Conference on Reliability. Infocom Technologies and Optimization (Trends and Future Directions) (ICRITO).

[15] Tichkule SK, Gawali DH. 2016. Plant diseases detection using image processing techniques. 2016 Online International Conference on Green Engineering and Technologies (IC-GET).

[16] Mohapatra A, Shanmugasundaram S, Malm-athanraj R. 2017. Grading of ripening stages of red banana using dielectric properties changes and image processing approach. Computers and Electronics in Agriculture. 143(1): 100–110. doi: 10.1016/j.compag.2017.10.010.

[17] Saad H, Ismail AP, Othman N, Jusoh MH, Naim NF, Ahmad NA. 2009. Recognizing the ripeness of bananas using an artificial neural network based on histogram approach. 2009 IEEE International Conference on Signal and Image Processing Applications. 536–541.

[18] Miljković O. 2009. Image pre-processing tool. Kragujevac J. Math. 32: 97–107.

[19] Mande A, Gurav G, Ajgaonkar K, Ombase P, Bagul V. 2018. Detection of Fruit Ripeness Using Image Processing. Common Comput Inf Sci. 545–555. doi: 10.1007/978-981-13-1813-9_54.

[20] Verma M, Raman B, Murala S. 2015. Local extrema co-occurrence pattern for color and texture image retrieval. Neurocomputing. 165: 255–269. doi: 10.1016/j.neucom.2015.03.015.

[21] Olaniyi EO, Adekunle AA, Odekuoye T, Khashman A. 2017. Automatic system for grading bananas using GLCM texture feature extraction and neural network arbitrations. J Food Process Eng. 40(6). doi: 10.1111/jfpe.12575.

[22] Other crops: Volume of production, by region and by PROVINCE, by quarter and semester, 2010-2020. PX-Web.

[23] Burges CJC. 1998. A tutorial on support vector machines for pattern recognition. Data Min Knowl Discov. 2(2): 121–167.

[24] Zhu X, Vondrick C, Fowlkes CC, Ramanan D. 2015. Do we need more training data?. Int J Comput Vis. 119(1): 76–92. doi: 10.1007/s11263-015-0812-2.

Using a sssNet Convolutional Neural Network (CNN) with Support Vector Machine (SVM) algorithm to identify formalin presence in images of eyes of *Chanos chanos* (milkfish)

THOREENZ P. SOLDEVILLA, DOMINIC NATHANIEL ANTHONY A. REDANIEL, LANCE CHRISTIAN V. SY, and MARIA MILAGROSA A. NULLA

Philippine Science High School Western Visayas Campus - Department of Science and Technology (DOST-PSHSWVC), Brgy. Bito-on, Jaro, Iloilo City 5000, Philippines

Article Info

Submitted: Apr 30, 2021
Approved: Jun 21, 2021
Published: Aug 30, 2021

Keywords:
Chanos chanos
formalin
image processing
neural network
SVM

Abstract

Using image processing, eye turbidity of formalin-treated *Chanos chanos* (milkfish) was statistically proven to be significantly different from those untreated. However, automation of such processes was yet to be explored. This study aims to use a sssNet Convolutional Neural Network (CNN) with Support Vector Machine (SVM) algorithm to identify formalin presence in milkfish. Ninety percent of 420 formalin-treated milkfish images and 420 untreated images, each with an indicated day of image capture, were subjected to feature extraction and classification using sssNet-SVM. The remaining 10% of the dataset was used to validate the algorithm's performance. The algorithm garnered 98.16 to 99.15% validation accuracy for identifying formalin presence. However, seven-day feature map analysis reveals that the algorithm struggles to determine formalin presence in treated samples using their images that were captured one or two days after the samples' dousing in formalin.

Introduction. - The Philippines is a fish-producing country that ranks 11th in global fishing production [1]. The main aquacultural produce of the country, *Chanos chanos*, locally known as *bangus* or milkfish, accounts for 2.4% of the national fisheries production [2]. Fish are highly perishable food, with storage times for tropical species ranging from 6-40 days [3]. Due to this limitation, various preservation techniques have been devised to prolong its freshness in order for such to be marketable for longer periods of time. One of the chemicals used to preserve fish is formalin [4,5], a solution consisting of 37% formaldehyde, a known respiratory disease enabler [6]. Formalin can also cause early protein denaturation which compromises fish quality [7]. Several studies used chemical analysis methods to detect the early presence of formalin in meat and fish such as spectrophotometry [8] and formalin rapid testing [9].

However, methods regarding chemical analysis are labor-intensive and time-consuming, while rapid test kits are not readily available in the market. This limitation was addressed by Cadorna et al. [8]. that used computer vision techniques such as image processing to detect formalin presence in milkfish by evaluating its eye, a method similar to most computer vision techniques that measure fish freshness. Image analysis has implied that the eye of formalin-treated fish became cloudy after a seven-day period as opposed to untreated fish which almost retained its appearance. The study then quantified the eye turbidity by capturing the image of the fish, splitting the channels into HSV (Hue, Saturation, and Value) components, and determining the intensity of each color space using an image processing tool. The study then found out that with values below 0.05 level of significance, the value components of the eye images +-of formalin treated and untreated *C. chanos* are significantly different. Such has opened the possibility of utilizing eye turbidity to be used for automation of formalin detection using imagery.

Since automation of fish quality [11] and classification of eye appearance [12] is possible, formalin detection in *C. chanos* can be done using supervised machine learning. Algorithms for classifying fish samples according to their quality are using two distinct methods – feature extraction and classification. These are done by first enhancing the images using methods such as blob extraction and border smoothing [11], as well as eye masking [12]. Then, the processed images are loaded into algorithms such as *k*-Nearest Neighbor, Support Vector Machine (SVM), or Feed-forward Artificial Neural Network (ANN). Hence, it is implied that feature extraction and classification algorithm methods for machine learning are always interdependent of each other. However, feature extraction is a tedious process that requires enhancing images manually before being analyzed or loaded into an algorithm. To be able to overcome this limitation, an algorithm that unifies feature extraction and classification shall be utilized.

How to cite this article:
CSE: Soldevilla TP, Redaniel DNAA, Sy LCV, Nulla MMA. 2021. Using a sssNet Convolutional Neural Network (CNN) with Support Vector Machine (SVM) algorithm to identify formalin presence in images of eyes of *Chanos chanos*. Publiscience. 4(1): 99–104.
APA: Soldevilla, T.P., Redaniel, D.N.A.A., Sy L.C.V., & Nulla, M.M.A. (2021). Using a sssNet Convolutional Neural Network (CNN) with Support Vector Machine (SVM) algorithm to identify formalin presence in images of eyes of *Chanos chanos*. *Publiscience, 4*(1), 99–104.

For supplementary data, contact: publiscience@wvc.pshs.edu.ph.

One such algorithm unexplored in determining fish quality is the sssNet algorithm with SVM, developed by Nagata et al. [13]. It is a type of Convolutional Neural Network (CNN) that enhances the features of the images by filtering important pixels in the image and removing unwanted features. The sssNet-SVM algorithm was validated by testing it with images of 7000 resin articles, 6000 of which have defects such as cracks, while the remaining 1000 images are of good quality. The algorithm only misclassified three images of resins of good quality and 13 images of defects. By implementing an algorithm with a unified extraction and classification such as sssNet-SVM, the need for tedious operation of manually extracting the important features of fish for analysis is eliminated. This proposed machine learning model composed of the algorithm trained using a reliable dataset would help those in the aquaculture sector to detect such a hazardous preservative faster and cheaper than conventional chemical analysis methods.

The aim of this study was to use the sssNet-SVM algorithm in identifying formalin presence in *Chanos chanos* (Milkfish) and specifically aimed to:

(i) Preprocess images of a *C. chanos* dataset to be suitable for algorithm training,

(ii) Extract features from the images using sssNet and classify them into formalin-treated and untreated classes using sigmoid Support Vector Machine,

(iii) Evaluate the confusion matrix table and percent accuracy of the image classifications, and

(iv) Determine differences in features between images of formalin-treated and untreated classes extracted by the optimized algorithm using heatmap visualization.

Methods. — The dataset created by Cadorna et al. [10], which consists of 420 images of eyes of *C. Chanos* that were treated with formalin, and 420 images of eyes of *C. Chanos* that were untreated with formalin, were used for training the algorithm. Before the images were loaded into the algorithm, the images were preprocessed. Tensorflow (version 2.3.1) powered by the Python programming language (version 3.8) was used to execute the methodology. The Anaconda distribution for Python was used, along with Jupyter as the Integrated Development Environment. The methodology is then divided into three parts, namely (1) image preprocessing, (2) algorithm building, and (3) algorithm training. The specifications for the hardware and software used to run the algorithm is stated in table 1.

Image Preprocessing. Images from the dataset were loaded using the *os* library in Python. Python then reads the images as sets of arrays with hexadecimal values that correspond to each pixel. Since Cadorna et al. [10] used HSV (Hue, Saturation, and Value) color space for assessment of the images, the dataset was converted from RGB (Red, Green, and Blue) color space into HSV. The pixel values were then normalized by dividing each pixel value by 255 which is the maximum hexadecimal value. Image augmentation was then used to artificially enlarge the dataset size by providing multiple instances for each image. Manipulation methods such as resize fit, rotate, stretching, skewing, zooming, flipping, and filling were used for data augmentation.

Table 1. Specifications of hardware and software used for the algorithm training.

Item	Specifications
desktop computer	Windows 10 Operating System, AMD Ryzen 5 3600 3.6 GHz processor, AMD RX 5700-XT GPU, 512 GB SSD with 330 MB/S read and write speeds, 1 TB HDD with 175 MB/S read and write speeds, and 32GB of RAM clocked at 3000MHz DDR4
Python	Version 3.8
Anaconda*	Version 4.0.15
Tensorflow	Version 2.3.0
Jupyter	Version 6.0.3.

**open source version*

Algorithm Building. As previously mentioned, the study used the sssNet-SVM algorithm as the classification method for the *C. chanos* images. The algorithm is a type of Artificial Neural Network (ANN). A more specific type of ANN, the Convolutional Neural Network (CNN), is a multilayer perceptron that deals with grid-structured data. Used often in computer vision, CNN outputs an input image by using a two-dimensional filter with a set of weights that would be multiplied to each input [15]. The resulting output would be an image with amplified features, just like the expected outputs from feature extractions. The study used the sssNet algorithm as the classification layer, as seen in Figure 1. The input image is characterized as a normalized HSV image with dimensions of 330 by 330 pixels with a depth of three representing the three color space channels. The image then entered the algorithm through a feature layer structure that consists of three instances of weighted filters, or convolutional layers with filter size 5 followed by a max-pooling layer of filter size 3. After the final max-pooling layer, the pixel values are flattened, or the pixel values are lined side by side, then fitted into 32 sets of outputs, then summarized and fitted into the SVM, which is a sigmoid function.

The sigmoid function is described as:

$$(1)\quad \Phi(y) = \frac{1}{1+e^{-y}}$$

The sigmoid function fitted the summarized outputs y into the probabilistic values of 1 to 0, with 1 being close to the formalin treated value and 0 being close to the untreated value [15].

Algorithm Training. In order for the algorithm to learn, such was optimized using backpropagation, a process of relearning the receptive filters of the feature extracting layers by (1) finding the loss function, (2)

finding the gradient descent, and (3) using an optimization equation to revise the filters.

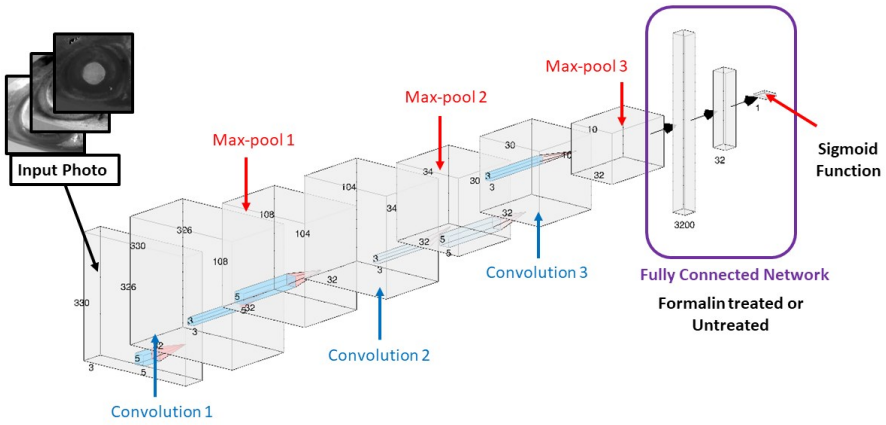

Figure 1. The sssNet-SVM algorithm diagram.

Furthermore, to expedite the training process, the images shall be fed to the algorithm in batches and shall automatically stop if training is sufficient using the callback function. Finding the loss function is done by plotting the loss values of the input data. The binary cross-entropy loss equation is used to find the difference between the calculated output value y and the actual label of the input images [15].

The cross-entropy loss equation is evaluated as:

$$(2)\ L = -\sum_{i=1}^{k} \quad y_i \log(\Phi y)$$

L as the negative summation of expected output data y_i multiplied by the logarithm of input data log Φy.

The loss values L are then plotted, in which a loss function is determined. Gradient descent method is then used to find the relative minimum of the loss [15]. The gradient method is noted as the derivative of loss L over the derivative of the filter weight w. After determining the gradient, the ADAM optimization equation takes note of the gradient then relearns the weights of the sssNet-SVM algorithm [15]. ADAM, short for Adaptive Moment Estimation, is an optimizer that tries to use learning decay rates characterized as ρ and momentum F_i in order for a model to find the minimum loss with accelerating speed. In the Keras module, ρ is initialized as 0.9.

$$(3.1)\ A_i \Leftarrow \rho A_i + (1-\rho)\left(\frac{\delta L}{\delta w_i}\right)^2 \forall_i$$

The first equation describes how the gradient descent is regulated with the learning decay rate.

$$(3.2)\ F_i \Leftarrow \rho_f F_i + (1-\rho_f)\left(\frac{\delta L}{\delta w_i}\right) \forall_i$$

The second equation, F_i is the momentum of the optimizer equation. Adding momentum to the optimizer increases the speed of the model approaching the minimum loss of the data. The learning decay rate ρ_f = 0.99 is also initialized with the Keras module.

$$(3.3)\ w_i \Leftarrow w_i - \frac{\alpha_t}{\sqrt{A_i}} F_i \forall_i$$

The last equation describes how a weight of a filter is adjusted according to A_i and F_i. w_i is replaced as the previous w_i subtracted by the ratio of learning rate a and the square root of A_i which is then multiplied by the momentum F_i. A_i in Keras is added with a stabilizer ε of 1 x 10^{-8} to avoid division by zero during the first model training with no pre-saved values.

Longer periods of training would result in fluctuating accuracy because the gradient descent value may be larger than a value's proximity to the relative minimum of the loss function. To cope with this limitation, a callback function, which detects when a model's accuracy is about to fluctuate or overfit, was implemented. In order for the algorithm to train faster, batches of images were fed in the algorithm, then the summation of the cross-entropy loss for each batch was evaluated instead of feeding the algorithm with images one-by-one then evaluating the loss values for each image. Ninety percent (90%) of the dataset consists of 756 images being fed into the algorithm. For each learning instance of the algorithm, or epoch, 18 batches of 42 images per batch were fed into the algorithm.

Data Analysis The data analysis part is divided into two parts, namely (1) AUROC analysis, and (2) heatmap visualization.

A Receiving Operating Characteristics curve or ROC is used by classification studies to assess the accuracy of the model. Once used in the medical field, ROCs are used to determine how deviant the values of the true positive and true negative values are. The computation of values shall be done using a Confusion Matrix Table [14]. Using training data obtained from the Cadorna et al. [10] dataset, an image's probability value as calculated by the sigmoid function was calculated by the algorithm if it is a false positive (FP), false negative (FN), true positive (TP) or true negative (TN). Next, the true positive rate was obtained by dividing TP by TP+FN. Then, the false-positive rate was obtained by subtracting the true positive rate from 1.0. A linear regression model of the true vs false positive rate was obtained to get the ROC curve. The Area Under ROC curve or AUROC for the epoch was then evaluated using the Riemann sum method as shown in Figure 2.

To test the ability of the optimal algorithm to identify formalin presence in *C. chanos* using unseen data, the remaining 10% of the Cadorna et al. [10] dataset was fed into the optimal algorithm. The confusion matrix table of the validation data was then evaluated.

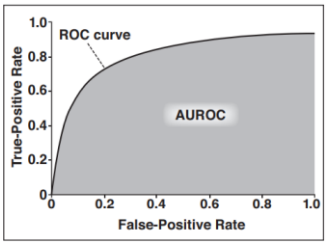

Figure 2. AUROC curve [14].

Lastly, to visualize how the convolutional and max-pooling layers of the optimal algorithm extract features from formalin-treated image classes and untreated image classes, the seven-day image capture of a randomly-picked sample from the formalin-treated class, as well as the seven-day image capture of a randomly-picked sample from the untreated class was obtained from the dataset. All images are then fed into the optimal algorithm, which were then visualized using a heatmap. The images are then compared to the heatmap of the unaltered HSV color spaces of the input image. The code for heatmap visualization was then used from a GitHub repository [16].

Results and Discussion. - Table 2 shows the accuracy for the sssNet-SVM algorithm tested in five trials using the same dataset showing a consistent accuracy above the 95% confidence threshold, ranging from 98.16 to 99.15%. AUROC curve percentage is calculated from the confusion matrix table, or evaluation of formalin-treated and untreated images which are either correctly classified or otherwise. Out of 84 validation images, trial 5 presents an askew confusion matrix with 13 images falsely classified as formalin-treated, unlike the other trials which falsely classified only 3 or 4 images as formalin-treated. For the untreated classes, all trials only falsely classified 0-4 images as untreated.

Table 2. Confusion matrix and AUROC curve percentages for each training trial of the sssNet-SVM algorithm

Trial	TF	FF	TU	FU	AUROC (%)
1	39	3	40	2	99.15
2	38	4	41	1	98.64
3	38	4	40	2	98.30
4	39	3	38	4	98.16
5	29	13	42	0	98.64

Legend:
TF: True Formalin-Treated class
FF: False Formalin-Treated class
TU: True Untreated class
FU: False Untreated class

Heatmap visualization is then applied into the feature extraction filters of the sssNet-SVM algorithm. Visualization of the extracted images is important in determining the receptive field that defines the significant difference between classes [17]. The receptive field in this algorithm pertains to the rectified pupils of the image samples. The pupils are said to be rectified if they are isolated from the eye of the fish and are then enlarged in the final layers of the algorithm.

The filter visualizations for the formalin-treated class and untreated classes were then compared with each other to see if differences in feature maps were exhibited by the algorithm in order for it to achieve high accuracy in classifying the dataset. Selection of feature maps for comparison used images taken from a single *C. chanos* sample which are captured daily, in a span of seven days. This is to examine if data for formalin-treated and untreated data are comparable irregardless of when the *C. chanos* sample was captured.

Figure 3 shows that regardless of the day the sample was taken, the pupil of the eye of untreated *C. chanos* is rectified. In contrast, Figure 4 shows that for images in day 1 and day 2 of the formalin-treated classes, the pupil is rectified. This is not the case for the few remaining filters in figure 4. Hence, we can say that irregardless of the onset of storage of untreated *C. chanos*, the algorithm easily determines it as an untreated class. On the other hand, formalin-treated fish can be easily determined by the algorithm as such if the fish was taken 3 days after the onset of treatment or later.

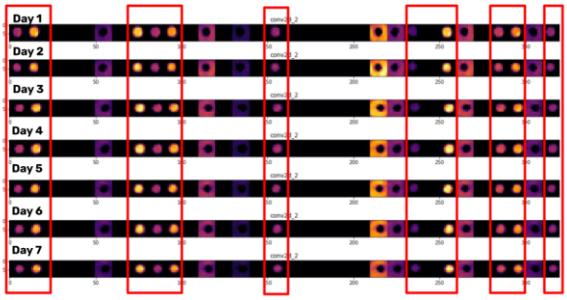

Figure 3. Final feature extraction layers of untreated *C. chanos* sample #28, left-eye, in seven days.

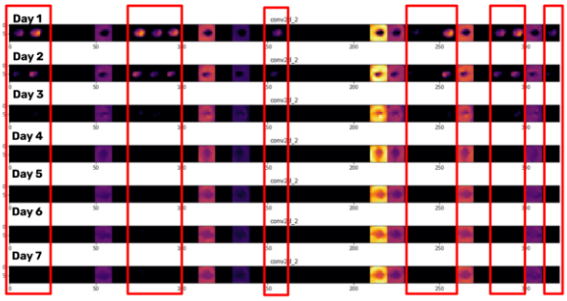

Figure 4. Final feature extraction layers of formalin-treated *C. chanos* sample #28, left-eye, in seven days.

Based on Figures 3 and 4, the framework of the algorithm, as shown in Figure 5, is generally described as starting from the input image is split into hue, saturation, and value channels. Then, the input image is augmented and extracted using the sssNet. If pupils are rectified, or present in the extracted image, the

fish sample in the picture is likely to be untreated with formalin; otherwise, the fish is likely to be doused with such substance. When training a CNN such as sssNet, the perception, or filter map of the algorithm is trained to focus on the specific parts of the image wherein classifications could produce significant differences between classes [17]. Eye turbidity of the image, the parameter that best describes the significant difference between the formalin-treated and untreated, is exhibited by the pupil, hence the algorithm focused on extracting features from the pupil.

Trials presented in Table 2 describe the algorithm training was run with the same process, however, the image augmentation is randomized for each trial. An image may be skewed 10% rightward or enlarged 5% before being fed in the algorithm. This is done to (1) artificially enlarge the limited dataset of 756 *C. chanos* images, and (2) take account of human bias in taking pictures. This randomized image augmentation affects the capability of the algorithm to detect formalin in fish samples if such algorithm is retrained, hence the study has done five trials to see the consistency of the algorithm.

While the samples consistently achieved above threshold AUROC curve of 95% confidence, the number of false classifications for the formalin-treated class greatly varied. This pertains to trial 5 classifying 13 out of 84 images falsely as formalin-treated as compared to trials 1-4 only having false classifications ranging from 3-4 images. Image augmentation is one of the reasons for such skewed results of trial 5 compared to other trials. Theoretically, if a formalin-treated image is randomly enlarged or skewed, its pupils would be beyond the bounds of the filter map of the algorithm. Hence, the pupil of an image is accidentally rectified or extracted by the algorithm. This implies that an algorithm's filter interpretability should be improved by training the filter to map the bounds of the region of interest [18], specifically of the pupil of the eye irrespective of how skewed, enlarged, or manipulated the image is.

Another reason for the false classifications that occurred was the presence of pupils. Days one and two of the untreated dataset exhibited rectified pupils. By basing on the framework in Figure 5, untreated images should not have pupils that are rectified. This is because the difference in the mean eye turbidity values for days one and two of formalin-treated and untreated classes of *C. chanos* is nearer as compared to the differences in these two classes observed beyond two days [10]. However, statistical analysis for each day of treatment is needed to support this claim.

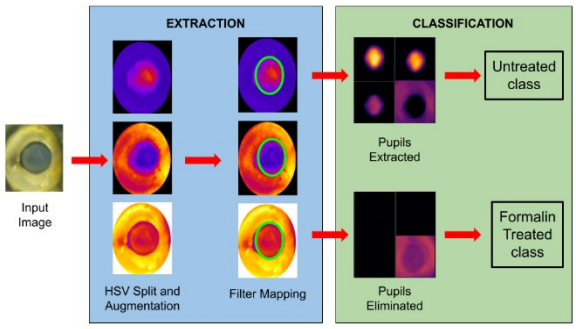

Figure 5. Framework of sssNet-SVM algorithm in classifying the *C. chanos* dataset.

Limitations. The qualitative description of describing the feature maps of the optimal algorithm partially supports the claim that the optimal algorithm is effective in classifying *C. chanos* images. A supposed quantitative assessment of the feature maps, such as calculating the receptive field of the algorithm's filters with respect to the training data [19] is beyond the capabilities of this study since such empirical method shall only be applicable if the sssNet-SVM algorithm was proven to be accurate. The researchers were unable to perform quantitative analysis for this claim.

Conclusion. - The sssNet-SVM algorithm developed by Nagata et al. [13] is accurate in identifying formalin presence in images of *Chanos chanos* with a 98.16-99.15% AUROC curve. However, due to the varied confusion matrix trials as well as pupils extracted found in feature maps of *C. chanos* images doused with formalin one or two days after immersion, the sssNet-SVM will be challenged to classify *C. chanos* doused with formalin if the image analyzed was captured one or two days after its supposed dousing. It is advised that the sssNet-SVM algorithm is to be used solely to delimit the number of commercially available *C. chanos* needed to be tested for formalin presence using spectro-photometry analysis.

Recommendations. - Using Grad-CAM analysis for quantification of feature maps is highly encouraged to measure the extent of feature maps between formalin-treated and untreated samples. A newer study may also want to integrate the algorithm into a mobile application to utilize a camera for in-site analysis.

Acknowledgment. - This study would not be done without the help of Mr. Rajo Christian G. Cadorna, Ms. Maxine P. Chan, and Mr. Juan Paulo Miguel I. Salmon, for the dataset that they provided was easily accessible and of high quality. We would also like to acknowledge their support in our research endeavors.

References

[1] [FAO]. Food and Agriculture Organization of the United Nations. 2020. The State of World Fisheries and Aquaculture 2020. Sustainability in action. Rome (Italy): FAO. Retrieved October 27, 2020, from: https://doi.org/10.4060/ca9229en.

[2] [PSA] Philippine Statistics Authority. 2020. Performance of Philippine Agriculture 2020. Manila (Philippines): Philippine Statistics Authority. [Internet]. Accessed October 20, 2020.

[3] Shawyer M, Pizzali AM. 2003. The use of ice on small fishing vessels (No. 436). FAO Fisheries.

[4] Uddin R, Wahid MI, Jasmeen T, Huda NH, Sutradhar KB. 2011. Detection of formalin in fish samples collected from Dhaka City, Bangladesh. Stamford Journal of Pharmaceutical Sciences. 4(1): 49–52.

[5] Villaflores RL. 2018. Effect of Formalin on the Sensory and Some Biochemical Attributes of Fish. IJHSS. 8(4): 82–85.

[6] [IARC] International Agency for Research on Cancer – Working Group on the Evaluation of Carcinogenic Risks to Humans. 2012. Chemical Agents and Related Occupations [Internet]. Lyon (FR): IARC; [cited 2021 May 15]. Available from: https://www.ncbi.nlm.nih.gov/books/NBK304416.

[7] Yeasmin T, Reza MS, Shikha FH, Khan MNA, Kamal M. 2010. Quality changes in formalin treated rohu fish (*Labeo rohita*, Hamilton) during ice storage conditions. Asian Journal of Agricultural Sciences. 2(4): 158–163.

[8] Jaman N, Hoque MS, Chakrabort, SC, Hoq ME, Seal HP. 2015. Determination of formaldehyde content by spectrophotometric method in some freshwater and marine fishes of Bangladesh. Intl. J. Fish. Aqua. Stud. 2(6): 94–98.

[9] Rahman S, Majumder MAA, Ahasan R, Ahmed SM, Das P, Rahman N. 2016. The extent and magnitude of formalin adulteration in fish sold in domestic markets of Bangladesh: a literature review. International Journal of Consumer Studies, 40(2): 152–159.

[10] Cadorna RCG, Chan MP, Salmon JPMI, Salazar GU. 2020. Measurement of eye turbidity of formalin-treated *Chanos chanos* (milkfish) using image analysis. Publiscience. 3(1): 84–89.

[11] Tolentino LKS, Orillo JWF, Aguacito PD, Colango EJM, Malit JRH, Marcelino JTG, Nadora AC, Odeza AJD. 2017. Fish freshness determination through support vector machine. Journal of Telecommunication, Electronic and Computer Engineering (JTEC). 9(2–5): 139–143.

[12] Navotas IC, Santos CNV, Balderrama EJM, Candido FEB, Villacanas AJE, Velasco JS. 2018. Fish identification and freshness classification through image processing using artificial neural network. ARPN Journal of Engineering and Applied Sciences. 13(18): 4912–4922.

[13] Nagata F, Tokuno K, Nakashima K, Otsuka A, Ikeda T, Ochi H, ... & Habib MK. 2019. Fusion Method of Convolutional Neural Network and Support Vector Machine for High Accuracy Anomaly Detection. In 2019 IEEE International Conference on Mechatronics and Automation (ICMA). pp. 970–975. IEEE.

[14] Yusuf M, Theophilous S, Adejoke J, Hassan AB. 2019. Web-Based Cataract Detection System Using Deep Convolutional Neural Network. In 2019 2nd International Conference of the IEEE Nigeria Computer Chapter (NigeriaComputConf) pp. 1–7. IEEE.

[15] Aggarwal CC. 2018. Neural networks and deep learning. Switzerland: Springer Nature Switzerland AG; [accessed October 21, 2020].

[16] Moroney L, Vanderplas J. 2019. Colabs for ML Day Tokyo. San Francisco (CA): GitHub; [accessed 2020 October 18]. Available from: https://bit.ly/3feOzBe.

[17] Teow MY. 2017. Understanding convolutional neural networks using a minimal model for handwritten digit recognition. In: 2017 IEEE 2ndInternational Conference on Automatic Control and Intelligent Systems *(I2CACIS)* pp. 167–172. IEEE.

[18] Zhang Q, Wu YN, Zhu SC. 2018. Interpretable convolutional neural networks. In: Proceedings of the IEEE Conference on Computer Vision and Pattern Recognition; 18-22 June 2018; Salt Lake City, UT, USA. Computer Vision Foundation. p. 8827–8836.

[19] Zhou B, Khosla A, Lapedriza A, Oliva A, Torralba A. c2015. Object detectors emerge in deep scene CNNs. In: IEEE International Conference on Learning Representation; 7-9 May 2015; San Diego, CA, USA. ICLR.

CLUSTER SEVEN

SPATIAL ANALYSIS

A glimmering white is representative of the light which guides humanity in a new direction. One on the path of progress and development, the culmination of various ideas in fields of science such as spatial analysis. These research studies employ computer-based systems and techniques in analyzing and mapping significant area coverage and geographical features. The top of the gem is representative of this because it depicts the earth in a virtual sense.

These studies fall under the Industry, Energy, and Emerging Technology (IEET) Research Development Agenda, as they are in line with the goal of increasing the usage of computer-based systems in research and development.

BASED ON: Harmonized National Research and Development Agenda (HNRDA)

Publiscience Vol. 4 Issue 1

Assessment of soil erosion risk within the Maasin Watershed Forest Reserve, Iloilo, Philippines using the Revised Universal Soil Loss Equation (RUSLE) and Geographical Information System (GIS)

FRANCE MATTHEW T. AGUILOS, FAYE ANDREA V. ENCANTO, GHELAI MARIE F. TOLENTINO, and MARIA DEANNA B. JOLITO

Philippine Science High School Western Visayas Campus - Department of Science and Technology (DOST-PSHSWVC), Brgy. Bito-on, Jaro, Iloilo City 5000, Philippines

Article Info

Submitted: May 05, 2021
Approved: Jun 28, 2021
Published: Aug 30, 2021

Keywords:
GIS
mapping
RUSLE
soil erosion
watershed

Abstract

Soil erosion is the leading cause of watershed degradation. It affects the Maasin Watershed Forest Reserve (MWFR), the main source of domestic water to Iloilo, as evidenced by reports of sedimentation that degrade the water supply of receiving communities. Hence, this study aims to assess the soil erosion risk within the MWFR using the Revised Universal Soil Loss Equation (RUSLE) and Geographical Information System (GIS) data. Geospatial data were processed to calculate the RUSLE factors using ArcGIS. The soil loss rates were determined by multiplying the factors, and were classified into erosion risk classes whose area covered was also measured. It was estimated that the erosion rate in the watershed is 40.7 tons/ha/yr. High to very severe soil erosion risks occur in 63.6% of the MWFR which accounts for the watershed degradation The erosion map can be used in monitoring the soil erosion within the MWFR.

Introduction. - Soil erosion is one of the primary causes of land degradation around the world [1]. It is generally defined as the deterioration of the topsoil by physical forces such as rainfall, flowing water, ice, wind, gravity, or other natural agents that deposit soil elsewhere [2]. Among these factors, high erosive rainfall and consequent runoff due to slope steepness play a role in the displacement of the fertile topsoil [3]. The Philippines is highly susceptible to this problem with its steep topography, deforested uplands, and heavy rainfall events [4]. It is one of the country's most pressing environmental issues and it has gravely threatened the sustainability of agricultural systems [5]. Watersheds sustain these systems by serving as a water source that farmlands receive in the form of irrigation [6]; however, soil erosion in watersheds has also become a widespread phenomenon [7].

Soil erosion causes significant changes in the water quality of watersheds [8]. It affects the hydrological cycle of watersheds through soil compaction, overground vegetation change, evapotranspiration change, infiltration change, and water holding capacity [9]. In addition, the continuous removal of the topsoil has led to soil degradation evidenced by the increasing sediment loads in rivers and water reservoirs [10]. Soil monitoring through mapping of soil erosion-prone areas has been identified to be an essential part of planning for dealing with environmental and natural resource management [11,12]. Through this, different model-based methods have been developed for soil erosion assessment. One of the most widely accepted empirical models for estimating soil erosion rate is the Universal Soil Loss Equation (USLE) developed by Wischmeier and Smith [13] due to its relative simplicity and standardized approach; however, an improved version of this has been developed, the Revised Universal Soil Loss Equation (RUSLE). The RUSLE [14] was developed due to the added availability of data and resources with a deeper understanding of the erosion process since the publication of USLE. It retains the equation of its predecessor with modifications in several of its factors. The factors of RUSLE are rainfall erosivity (R), soil length and steepness (LS), soil erodibility (K), cover management (C), and conservation practice (P).

Previous studies have been conducted to map soil erosion with the use of RUSLE and GIS. The studies of Belayneh et al. [1] and Da Cunha et al. [15] both used RUSLE and GIS techniques to estimate the soil loss due to water erosion in the Gumara Watershed in Ethiopia and the watershed stream Indaia in Brazil, respectively. They were able to identify areas within the watersheds that had the highest risk of soil erosion making these areas possible priorities for soil erosion prevention programs. Mapping soil erosion-prone areas through RUSLE and GIS is an efficient way to help the local governments monitor and prevent watershed

How to cite this article:
CSE: Aguilos FMT, Encanto FAV, Tolentino GMF, Jolito MD. 2021. Assessment of soil erosion risk within the Maasin Watershed Forest Reserve, Iloilo, Philippines using the Revised Universal Soil Loss Equation (RUSLE) and Geographical Information System (GIS). Publiscience. 4(1): 106–111.
APA: Aguilos F.M.T., Encanto F.A.V., Tolentino G.M.F., & Jolito M.D. (2021). Assessment of soil erosion risk within the Maasin Watershed Forest Reserve, Iloilo, Philippines using the Revised Universal Soil Loss Equation (RUSLE) and Geographical Information System (GIS). *Publiscience*, *4*(1), 106–111.

For supplementary data, contact: publiscience@wvc.pshs.edu.ph.

degradation [7,16].

The Maasin Watershed Forest Reserve (MWFR) is the main supplier of domestic water to Iloilo City and adjacent municipalities, as well as irrigation to agricultural lands within Central Iloilo, therefore it is urgent to address problems caused by soil erosion within the watershed such as siltation which may affect the water supply of the receiving communities. However, no published studies have been done to assess the soil erosion-prone areas within the MWFR even with its location, being at high risk for soil erosion [17].

With this, the research aimed to identify soil erosion risk areas within the MWFR using RUSLE and GIS. It specifically aimed to:

(i) collect data on the RUSLE factors of rainfall erosivity (R), soil slope and length (LS), soil erodibility (K), cover management (C), and conservation practice (P) within the MWFR;

(ii) estimate the annual soil erosion rate within the MWFR using the RUSLE based on available GIS data from 2010–2020; and

(iii) assess the spatial distribution of soil erosion risk areas within the MWFR using the estimated annual soil erosion rates.

Methods. - The data gathering procedure was divided into four parts: (1) collection of geospatial data for the RUSLE factors from online sources from 2010–2020, (2) calculation of the RUSLE factors by processing the geospatial data, (3) calculation of the soil erosion rates and, (4) classification of soil erosion rates into erosion risk classes and assessment of its spatial distribution.

Study Area. The site studied was the Maasin Watershed Forest Reserve (MWFR) which is found in an aggregate of two critical watersheds found in Iloilo, the Tigum-Aganan Watershed, and is located within the municipalities of Maasin, Alimodian, and Janiuay, Iloilo. The MWFR is found at the UTM coordinates from 422,690 m to 435,800 m East and 1,203,730 m to 1,214,480 m North with an area of 6,539.352 ha.

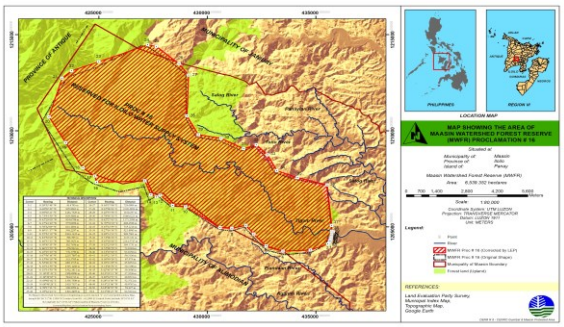

Figure 1. Boundary of MWFR from City Environment and Natural Resources Office (CENRO) Region 6.

Geospatial Data Collection. The data for the mean monthly rainfall were collected from WorldClim, an online database. The Shuttle Radar Topography Mission (SRTM) digital elevation model (DEM) for the Philippines was downloaded from the United States Geological Survey (USGS) database. The soil type map and boundary shapefile of MWFR were obtained from CENRO Region 6. The 2010 land cover map from the PhilGIS website was also downloaded. The files were then clipped in ArcGIS, version 10.4 to focus on the MWFR. To ensure uniformity, all the raster layers were ensured to have pixel sizes of 30 m by 30 m through resampling by bilinear interpolation and were aligned with each other with the on-the-fly projection of ArcGIS.

Calculation of RUSLE Factors. For the R factor, the mean annual precipitation was first calculated by adding the raster layers for the mean monthly precipitation in the raster calculator before being clipped and resampled. The R factor was then calculated following the model by El-Swaify et al. [18] where P is the mean annual precipitation in mm and the R factor is measured in MJ·mm·(ha·h·year)$^{-}$.

$$R = 38.5 + 0.35\,P$$

Equation 1. Formula for the R factor.

For the LS factor, the model by Moore and Burch [19] was followed. The clipped SRTM DEM raster layer was processed to calculate the flow direction, flow accumulation, and slope in degrees which were required as inputs for the model.

Table 1. Representative values of soil erodibility (K) for various Philippine Soils (David 1988).

Soil Texture	K Value
Clay loam	0.30
Clay	0.26

For the K, C, and P factors, the categories within the soil type map and land cover map were assigned corresponding K, C, and P values obtained from previous studies. The K values taken from the study of David [20], shown in Table 1 above, were assigned to each soil type present. The C values assigned to the different land cover categories were based on the study of David [20] in Table 2 while the P values were based on the study of David [20] and Delgado and Canters [21].

Table 2. Estimated crop cover coefficient or C values for the common cover conditions of Philippine watersheds [18].

Land Cover	C Value
Bare soil	1.0
Primary forest with dense undergrowth	0.001
Second growth forest with good undergrowth and mulch cover	0.006
Perennial crops	0.1–0.3
Grassland, moderately grazed, burned occasionally	0.2–0.4
Shrubs with open, disturbed grassland	0.15
Built-up	1.00
Inland water	0.00

Calculation of Soil Erosion Rates. The soil loss empirical model RUSLE is shown by Equation 1 below with A being the average soil loss per unit area measured in ton ha^{-1} yr^{-1} and the rainfall erosivity (R), slope length and steepness (LS), soil erodibility (K), land cover (C) and conservation practice (P) factors being the key parameters of the model. ArcGIS was used to multiply all the raster layers of the RUSLE factors to obtain a single raster file where the rates of soil loss within MWFR were shown.

$$A = R \; x \; LS \; x \; K \; x \; C \; x \; P$$

Equation 2. Formula for the RUSLE model.

Erosion Risk Classification and Spatial Distribution. The soil erosion rates were classified into low to very severe erosion risk classes following the classification from the study of Singh et al. [22] as reported by Salvacion [23] as shown in Table 3.

Table 3. Classification of soil erosion rates into classes of soil erosion risk.

Soil erosion rates (ton ha^{-1} yr^{-1})	Erosion risk class
0 – 5	Low
5 – 10	Moderate
10 – 20	High
20 – 40	Very high
40 – 80	Severe
> 80	Very severe

To find the area covered by each erosion risk class, the raster layer of the soil erosion rates was first digitized into a vector layer. Polygons belonging to the same risk class were merged and their area covered in sq. km. was then determined using the field calculator feature in ArcGIS which calculates the polygon areas for each soil erosion class. The percentage of the area covered by each class was also calculated following Equation 3 below.

$$\% \text{ area covered} = \frac{area \; of \; soil \; erosion \; risk \; class}{land \; area \; of \; MWFR}$$

Equation 3. Formula for percentage of area covered by soil erosion risk class.

Results and Discussion. - The collected geospatial data were used to determine the RUSLE factors needed in calculating for the soil erosion rates within the boundary of the MWFR. The raster layers containing pixel values embedded and assigned for all the RUSLE factors were multiplied to generate the estimated soil erosion rates. These rates were then used to determine the erosion risk classes and their spatial distribution within the watershed.

RUSLE Factors. For the R factor, the annual rainfall data had values which ranged from 2,265–3,088 millimeters within the MWFR. Using the model by El-Swaify et al. [18], it was found that the R factor had values ranging from 831.25–1,119.3 $MJ{\cdot}mm{\cdot}(ha{\cdot}h{\cdot}year)^{-1}$. The R factor within the MWFR generally increases from the south to the north of the watershed. Higher rainfall erosivity, which is due to higher annual rainfall, was observed in the mid or mountainous portion of the watershed as seen on Figure 2.

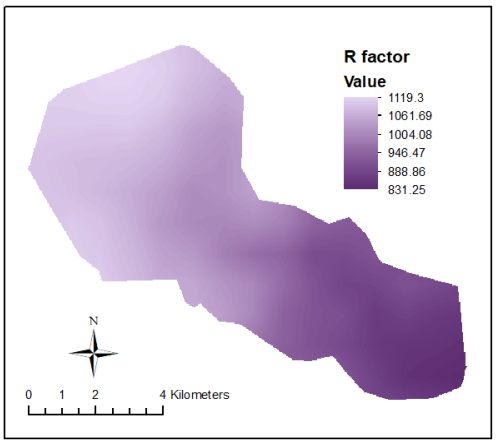

Figure 2. Rainfall erosivity (R) factor for the MWFR.

For the LS factor, the DEM file was found to have values ranging from 97–1,583 m above sea level. Following Moore and Burch [19], the calculated LS factors were found to range from 0–38.4307 with a mean of 1.04 as seen in Figure 3. The highest LS values were found in areas near the river, especially in the northwestern region of the MWFR where the elevation is relatively higher than the southeastern region of the MWFR.

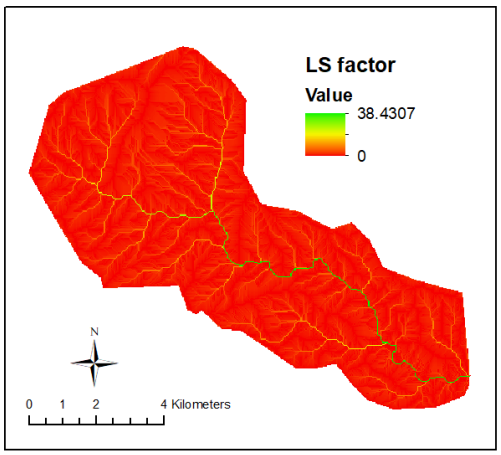

Figure 3. Slope length and steepness (LS) factor for the MWFR.

The soil types present in the MWFR were identified to be the following: Alimodian clay loam, Alimodian soil, Umingan clay, and Mountain soil as seen in Figure 4. Undifferentiated soil types such as those of Alimodian and Mountain soil were also classified as clay loam. The values assigned were 0.3 for the clay loam and undifferentiated soil, and 0.26 for clay. In terms of soil textural class, the watershed is highly dominated by clay loam as seen in Figure 5.

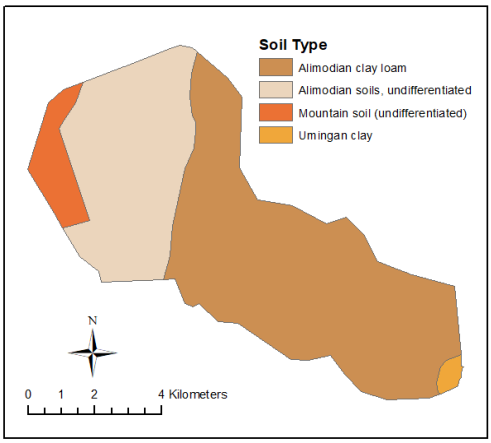

Figure 4. Soil types within the MWFR.

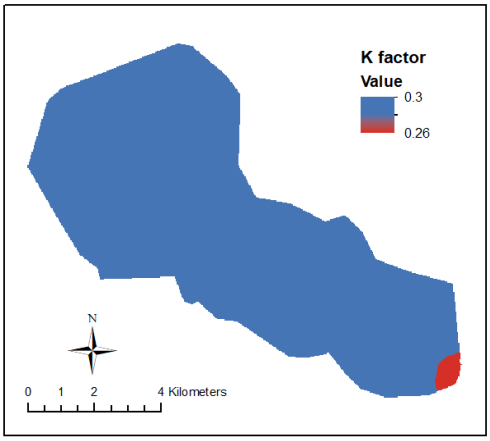

Figure 5. Soil erodibility (K) factor within the MWFR.

The C factor values were assigned to each of the land cover categories. The vegetation cover found within the MWFR are of the following: annual crop, built-up, closed forest, inland water, mangrove forest, open forest, open or barren, perennial crop, shrubs, and wooded grassland as seen in Figure 6. The values assigned ranged from 0–1 based on Table 2. Based on the acquired land cover map, the northern areas and some areas at the south of the watershed are occupied by open forests which have a very low C value of 0.001, thus its presence can greatly reduce the soil erosion rates within these areas.

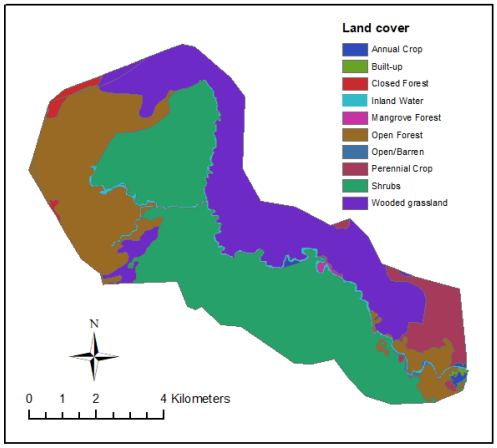

Figure 6. Land cover within the MWFR.

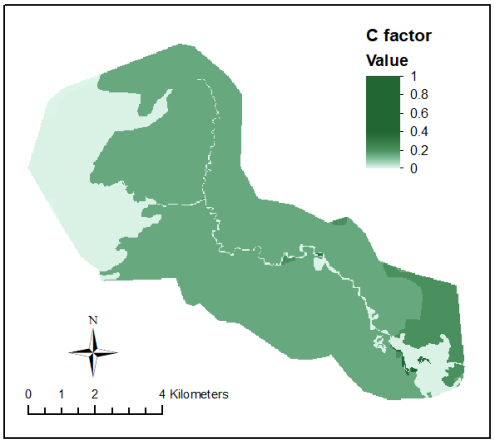

Figure 7. Land cover management (C) factor for the MWFR.

Due to the lack of information and data on the conservation practices within the MWFR, the P factor values were set to 1 for the land cover categories with the exception of the areas classified as inland water, which along with the C factor, were assigned the value 0.

Soil Erosion Rates. The estimated soil loss rates found within the MWFR ranged from 0–9,406.37 tons/ha/yr with a mean of 40.74 tons/ha/yr. After classifying the soil erosion rates, it was observed that all the erosion risk classes were present within the boundary of the MWFR as reflected in Figure 8. This data coincides with the raw geospatial data of each RUSLE factor multiplied to yield the soil erosion rates. Low erosion rates in the boundary of MWFR were mainly due to the presence of forests as based on its land cover map. According to the study of Gharibreza et al. [24], the absence of forests in the land cover management of catchments or watersheds hastens land degradation. Meanwhile, high to very severe soil loss rates were mostly found in mountain sides and around rivers where the slope is long and steep.

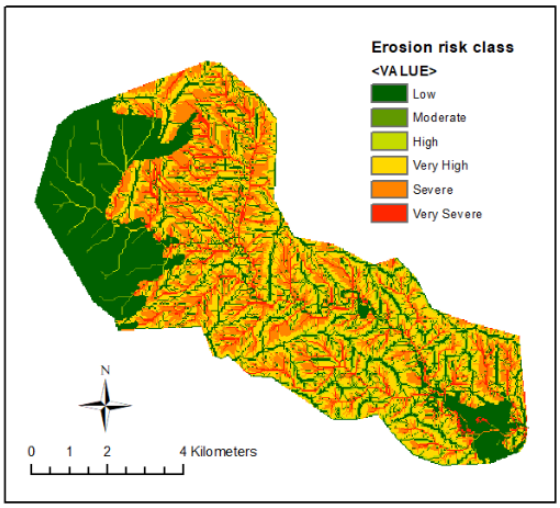

Figure 8. Soil erosion rates and classes within the MWFR.

Spatial Distribution of Erosion Risk Classes. The area covered by each erosion risk classification was also determined. Using the area of the MWFR which is 65.39 sq. km., the percentage of the area covered by each erosion risk class was found to be 35.49% for low

risk, 0.50% for moderate risk, 4.80% for high risk, 31.43% for very high risk; 20.38% for severe risk; and 6.99% for very severe risk. The remaining 0.42% were the areas set to zero which are areas classified as inland water such as the river.

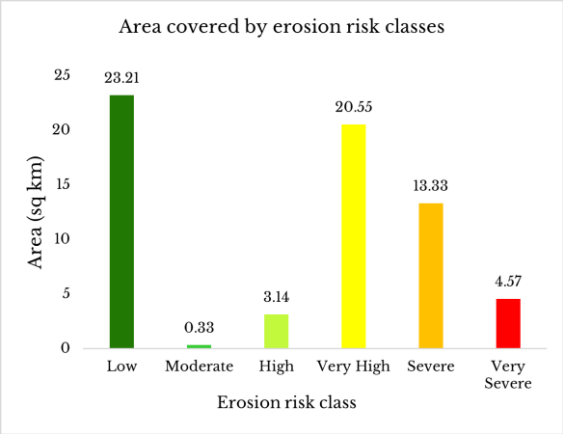

Figure 9. Area covered by each soil erosion risk class in sq. km.

It was found that the majority of the area within the boundary of the MWFR is at low risk of erosion with 35.49%; however, soil erosion is still imminent with the combined areas having high to very severe erosion risk composing 63.60% of the MWFR as shown in the graph in Figure 9. The mean soil erosion rate for the MWFR also falls under the severe erosion risk class which means that the MWFR generally experiences severe soil erosion. The severity of the soil erosion within the MWFR coincides with the information about its location according to recent hazard assessment reports and studies. The MWFR is found within an aggregate of two critical watersheds, the Tigum-Aganan watersheds. The presence of MWFR in these two critical watersheds explains the prevalence of soil erosion within the MWFR. Additionally, findings of a study by Bito-onon [17] identified the municipality of Maasin as having a very high hazard index when it comes to typhoons, floods, and soil erosion, while Alimodian and Janiuay, have high and moderate hazard indices, respectively. The high hazard index to soil erosion of Maasin, the location of the MWFR, supports the presence of severe soil erosion risk within the watershed.

Limitations. The study used the most recently updated data available from different online sources and databases, and government agencies, and coming from different years between 2010–2020. The researchers mainly relied on information that is available online. Furthermore, the soil erosion rates are only estimations which rely on the available data online without any on-site inspection of the MWFR due to the COVID-19 pandemic. Moreover, due to the absence of any recorded data on the conservation practices of the watershed, the values assigned for the P factor were only based on the C factor. Another limitation is the use of RUSLE which only accounts for soil loss through sheet and rill erosion, while ignoring the possibility of gully erosion and dispersive soils in a certain area. There is also no accounting for the deposition of sediment before reaching a waterway; hence, RUSLE is only a predictor of erosion for topsoils [25].

Conclusion. - This study demonstrates the utilization of RUSLE with GIS to model soil erosion rates within the MWFR. The MWFR was found to have a mean soil erosion rate of 40.74 tons/ha/yr, which generally classifies the MWFR as having severe soil erosion risk. Based on the soil erosion map and the spatial distribution for the erosion risk classes, 63.6% of the MWFR was found to be at high to very severe risk of soil erosion and this may account to the degradation of the watershed. The results emphasize the urgent need to address the soil erosion in the watershed. The geological location of Maasin may contribute to the watershed degradation since the municipality has a high hazard index making it susceptible to natural disasters. Although the erosion rates are estimations, this soil erosion map can help the local government get a gist of priority areas in monitoring the soil degradation of the MWFR to prevent its adverse effects on the ecosystem and water quality. It can also show what causes the soil erosion in the area and provide visualization as to which parts of the MWFR may have high to very severe cases of erosion. With this, the government can be guided in preventing and addressing any rising problems within the watershed.

Recommendations. - For further studies involving the soil erosion rates within the MWFR, an on-site inspection may be conducted for the cross-referencing of the estimated soil erosion rates generated from the use of RUSLE and GIS data. A survey with the locals may also be conducted to verify the data for the RUSLE factors and identify the areas that experience severe soil erosion. This is to take note of essential information on the factors of soil erosion within the watershed which are not available online such as the conservation practices. Other sources of GIS data aside from those mentioned in the study may also be used. The application of the RUSLE model with readily available GIS data should be utilized more in monitoring the occurrence of soil erosion in critical watersheds in the country. Using the same methodology, comparisons may also be made between the soil erosion rates within the MWFR and other critical watersheds.

Acknowledgement. - The researchers would like to thank the involvement of Mr. Paul Caesar M. Flores from the University of the Philippines, Marine Science Institute for promptly responding to our queries and assisting us during the conduct of the study, and CENRO Region 6 for providing the work unit the needed information and data for the MWFR.

References

[1] Belayneh M, Yirgu T, Tsegaye D. 2019. Potential soil erosion estimation and area prioritization for better conservation planning in Gumara watershed using RUSLE and GIS techniques. Environ Syst Res. 8(20): 1–17. doi: 10.1186/s40068-019-0149-x.

[2] Efthimiou N, Evdoxia L, Karavitis C. 2014. Soil erosion assessment using the RUSLE model and GIS. EWRA European Water. 47: 15–30.

[3] Ganasri BP, Ramesh H. 2016. Assessment of soil erosion by RUSLE model using remote sensing and GIS—a case study of Nethravathi Basin. Geosci Front. 7(6): 953–961. doi: 10.1016/j.gsf.2015.10.007.

[4] Olabisi LS. 2012. Uncovering the root causes of soil erosion in the Philippines. Society & Natural Resources. 25: 37–51. doi: 10.1080/08941920.2011.563435.

[5] Puno GR, Marin RA, Puno RCC, Toledo-Bruno AG. 2021. Geographic information system and process-based modeling of soil erosion and sediment yield in agricultural watershed. Global Journal of Environmental Science and Management. 7(1): 1–14.

[6] Lantican MA, Guerra LC, Bhuiyan SI. 2003. Impacts of soil erosion in the upper Manupali watershed on irrigated lowlands in the Philippines. Paddy Water Environ. 1(1):19–26. doi: 10.1007/s10333-002-0004-x.

[7] Bouguerra H, Bouanani A, Khanchoul K, Derdous O, Tachi SE. 2017. Mapping erosion prone areas in the Bouhamdane watershed (Algeria) using the Revised Universal Soil Loss Equation through GIS. Journal of Water and Land Development. 32: 13–23. doi: 10.1515/jwld-2017-0002.

[8] Pimentel D. 2000. Soil erosion and the threat to food security and the environment. Ecosyst Health. 6(4): 221–226.

[9] Koralay N, Kara Ö. 2018. Effects of Soil Erosion on Water Quality and Aquatic Ecosystem in a Watershed. 1st International Congress on Agriculture Structures and Irrigation. 26-28 September 2018. Antalya, Turkey. doi: 10.13140/RG.2.2.26247.39841.

[10] Clark EH, Haverkamp JA, Chapman W. 1985. Eroding soils: the off farm impacts. The conservation foundation, Washington, DC. 252.

[11] Thilagavathi N, Subramani T, Suresh M. 2015. Land use/land cover change detection analysis in Salem ChalkHills, South India using remote sensing and GIS. Disaster Adv. 8: 44–52.

[12] Minaei M and Kainz W. 2016. Watershed land cover/land use mapping using remote sensing and data mining in Gorganrood, Iran. ISPRS International Journal of Geo-Information. 5(5): 57.

[13] Wischmeier WH and Smith DD. 1978. Predicting rainfall erosion losses: a guide to conservation planning. U.S. Department of Agriculture, Agric Handbook. 537.

[14] Renard KG, Foster GR, Weesies GA, Porter JI. 1991. Revised universal soil loss equation (RUSLE). J Soil Water Conserv. 46(1): 30–33.

[15] Da Cunha ER, Bacani VM, Panachuki E. 2016. Modeling soil erosion using RUSLE and GIS in a watershed occupied by rural settlement in the Brazilian Cerrado. Natural Hazards. 85(2): 851–868. doi: 10.1007/s11069-016-2607-3.

[16] Renard KG, Foster GR, Weesics GA, McCool DK, Yorder DC. 1997. Predicting soil erosion by water: A Guide to conservation planning with the revised universal loss equation (RUSLE). U.S. Department of Agriculture, Agric Handbook. 703: 404.

[17] Bito-onon JB. 2020. Climate risk vulnerability assessment: Basis for decision making support for the agriculture sector in the province of Iloilo. Risk, 13(3).

[18] El-Swaify SA, Gramier CL, Lo A. 1987. Recent advances in soil conservation in steepland in humid tropics. In: Tay, T.H., Mokhtaruddin, A.M., & Zahari, A.B. (eds) Proceedings of the International Conference on Steepland Agriculture in the Humid Tropics. Kuala Lumpur, MARDI, 87–100.

[19] Moore ID, Burch GJ. 1986. Modelling Erosion and Deposition: Topographic Effects. Transactions of the ASAE. 29(6): 1624–1630. doi: 10.13031/2013.30363.

[20] David WP. 1988. Soil and Water Conservation Planning: Policy Issues and Recommendations. J Philipp Dev. 15(1): 47–84.

[21] Delgado MEM, Canters F. 2012. Modeling the impacts of agroforestry systems on the spatial patterns of soil erosion risk in three catchments of Claveria, the Philippines. Agrofor Syst. 85(3): 411–423. doi: 10.1007/s10457-011-9442-z.

[22] Singh G, Babu R, Narain P, Bhushan LS, Abrol IP. 1992. Soil erosion rates in India . Journal of Soil and Water Conservation 47: 97–99.

[23] Salvacion AR. 2020. Delineating soil erosion risk in Marinduque, Philippines using RUSLE. GeoJournal. 7. doi: 10.1007/s10708-020-10264-7.

[24] Gharibreza M, Zaman M, Porto P, Fulajtar, E, Parsaei L, Eisaei H. 2020. Assessment of deforestation impact on soil erosion in loess formation using 137Cs method (case study: Golestan Province, Iran). Intl Soil and Water Cons Res. 8(4): 393–405. doi :10.1016/j.iswcr.2020.07.006.

[25] Rowlands L. 2019. Erosion and Sediment Control—WSUD During the Construction Phase of Land Development. In Approaches to Water Sensitive Urban Design. Woodhead Publishing. 163–176.

Publiscience Vol. 4 Issue 1

Mapping and calculation of the shoreline change in selected areas in Tigbauan, Iloilo, Philippines using remote sensing and geographic information systems (GIS) techniques

MAXINNE LOUISE DOMINIQUE L. CO[1], TRISHA MARIE A. LUCIDO[1], GABRIEL DAX P. AGURA[1], ARIS C. LARRODER[1], and PAUL CAESAR M. FLORES[2]

[1]*Philippine Science High School Western Visayas Campus - Department of Science and Technology (DOST-PSHSWVC), Brgy. Bito-on, Jaro, Iloilo City 5000, Philippines*
[2]*The Marine Science Institute, University of the Philippines, Diliman, Quezon City 1101, Philippines*

Article Info

Submitted: Apr 30, 2021
Approved: Jul 21, 2021
Published: Aug 30, 2021

Keywords:
shoreline change
coastal vulnerability
remote sensing
satellite imagery
GIS techniques

Abstract

Shoreline change poses a significant threat to coastal environments and is exacerbated by climate change, hence, it should be monitored for better coastal management. This study aimed to determine the shoreline change in Tigbauan, Iloilo using remote sensing and GIS techniques. Eighteen Landsat 5 and 8 images from 1993 to 2020 were obtained using Global Visualization Viewer and processed in Quantum GIS. Shorelines were extracted from processed images and analyzed using the Digital Shoreline Analysis System (DSAS) in ArcGIS by calculating the net shoreline movement, shoreline change envelope, endpoint rate, and linear regression rate. Results showed that from 1993 to 2020, erosion had greater magnitude, rates, and occurrences than accretion. The average rate was -1.022 m per year and erosion was forecasted for most areas in 2030 and 2040. The results can help the government mitigate shoreline erosion risks and methods can be extended to other shorelines.

Introduction. - The rapid changing of shorelines caused by their high vulnerability to natural hazards such as floods, storm impacts, sea-level rise, and coastal erosion, pose a significant threat to coastal environments. With climate change accelerating the occurrence of these natural hazards, shoreline conditions are worsening and better coastal management is needed [1]. Shoreline data is fundamental for coastal management and thus, studies have investigated methods for the accurate detection, mapping, and monitoring of shorelines.

Among the shoreline mapping methods, three main categories have emerged: field testing, aerial photography, and remote sensing [2]. Among the three mapping methods, remote sensing is preferred due to its ability to analyze small changes in the coast as a result of its very long spectral bands and good spatial resolutions. It is also cheaper and can be done through more convenient and accurate methods, such as satellite imagery [3]. To handle satellite data, geographic information system (GIS) programs were utilized with satellite imagery to extract shorelines and calculate parameters through computer-aided tools and methods that reduce manual errors and give researchers full control [4].

Hence, several researchers have studied shoreline change using both remote sensing and GIS techniques. Louati et al. [5] and Sutikno et al. [6] utilized Landsat images and the United States Geological Survey Digital Shoreline Analysis System (USGS DSAS) extension for ArcGIS Copyright© 1995-2015 Esri. [7], Foti et al. [8] used Google Earth Pro and QGIS, while Flores and Siringan [9] utilized Landsat and QGIS. It is notable that among the satellite data used for shoreline studies, the Landsat series images have been proven to offer the best combination of performance and availability due to its open access, large coverage, and long-term data record features [10]. Among the GIS programs for shoreline studies, it was concluded that QGIS is more suitable for editing and georeferencing [11], while the DSAS extension of ArcGIS makes it a better program for shoreline change calculations [7].

Various statistical methods have also been studied and applied to quantify shoreline change, with the most common being the endpoint rate (EPR), average of rates (AOR), and linear regression rate (LRR) [1,12]. However, it is notable that EPR and LRR are more effective [13]. Thus, Landsat images, ArcGIS-DSAS, QGIS, and EPR and LRR were chosen for the analysis of the selected shoreline.

Climate Central [14] identified Tigbauan, Iloilo as one of the many Philippine municipalities that will submerge by 2040. This finding, along with

How to cite this article:
CSE: Co MLDL, Lucido TMA, Agura GDP, Larroder AC, Flores PCM. 2021. Mapping and calculation of the shoreline change in selected areas in Tigbauan, Iloilo, Philippines using remote sensing and geographic information systems (GIS) techniques. Publiscience. 4(1): 112–118.
APA: Co M.L.D.L., Lucido T.M.A., Agura G.D.P., Larroder A.C., & Flores P.C.M. 2021. Mapping and calculation of the shoreline change in selected areas in Tigbauan, Iloilo, Philippines using remote sensing and geographic information systems (GIS) techniques. *Publiscience*, *4*(1), 112–118.

For supplementary data, contact: publiscience@wvc.pshs.edu.ph.

parameters such as land area, shoreline length, and anthropogenic activities, led to the selection of the Tigbauan Shoreline as the study area. It was verified by the local government unit that there is no data on the Tigbauan shoreline positions and changes. More effective coastal management is necessary for these areas, which requires shoreline data [15,16]. Thus, the study aimed to determine the shoreline change in selected areas in Tigbauan, Iloilo using remote sensing and GIS techniques [10,12].

This study will provide the municipality with important data on shoreline positions, change values, and rates that can help improve their coastal management. Moreover, the methods can also be replicated to determine shoreline change in other areas. Specifically, this research study aimed to:

(i) gather suitable Landsat 4-5 and 8 images from 1993 to 2020 of the selected shoreline using the USGS Global Visualization Viewer (GloVis);

(ii) apply cropping and image enhancement to Landsat images using QGIS 3.10.10 A Coruña;

(iii) trace and extract the shorelines using QGIS;

(iv) calculate the net shoreline movement (NSM) and shoreline change envelope (SCE) using the DSAS extension in ArcGIS 10.4;

(v) calculate the shoreline change rate using the endpoint rate (EPR) and linear regression rate (LRR) methods in DSAS; and

(vi) evaluate the shoreline change over the years.

Methods. - The methods were divided into three main phases: (1) georeferencing of satellite images, (2) digitization of georeferenced images, and (3) shoreline analysis by calculating the shoreline change values and rate statistics.

Study Area. The study area was chosen using four parameters based on previous shoreline change studies: (1) coastal risk projection of Climate Central [14], (2) land area, (3) shoreline length, and (4) locality and infrastructure risk [1,12,16]. The first parameter identified areas that will be submerged by 2040 [14]. The affected land areas were ranked since selecting larger areas would benefit more people. The shoreline lengths were ranked to minimize zoom and increase calculation accuracy. Settlements and infrastructure were also considered. Thus, as seen in Figure 1, the shoreline bordering Barangay 7 and Baguingin in Tigbauan, Iloilo was chosen. It faces the Panay Gulf near the Sibalom River and the observed nearby infrastructures are residential areas and vegetation approximately 15 m from the shoreline.

Figure 1. (a) The study area in the Philippines. (b) The areas in Tigbauan, Iloilo projected to be below the annual flood level in 2040. (c) The shoreline in Tigbauan, Iloilo selected based on the set criteria.

Satellite Image Georeferencing. Landsat 5 and 8 images of the study area from 1993 to 2020 were obtained using GloVis. The images were chosen based on image clarity, cloud coverage, and time and date of image acquisition. The selection process involved scanning all the available images that were taken during the equinox, specifically within the months of August to September. Due to the lack of clear images during these months from 1993 to 1998, images from February and March were used instead. The images with a clear view of the study area, minimal to no cloud cover, and acquisition times ranging from 9:00 AM to 10:30 AM MPST were selected. Those not satisfying the criteria were excluded, resulting in non-uniform intervals. The primary image acquisition date criterion was based on March 20 and September 23 due to the presence of equinoctial tides. A total of 18 Landsat images were used in the study, with five from the March equinox and 13 from the September equinox since during these months, the tidal amplitudes are at a maximum [17]. All images were subjected to visual comparisons and were ensured to have been georeferenced correctly, as determined by the lack of shifts in road alignment.

Image Processing and Shoreline Extraction. The acquired Landsat 4–5 and 8 images underwent image processing using QGIS. The raster images were first uniformly cropped to focus on the identified shoreline. The cropped images were then subjected to geometric and atmospheric corrections using the Semi-automatic Classification Plugin in QGIS [18], DOS1 atmospheric correction, and panchromatic image sharpening. Raster calculation was then performed on the Landsat bands using the Modified Normalized Difference Water Index (MNDWI) with the formula to extract the shoreline positions [19].

$$MNDWI = (Green\ Band - MIR\ Band)/(Green\ Band + MIR\ Band)$$

Where:
Green Band = green band number depending on Landsat type
MIR Band = middle infrared band depending on the Landsat type

Land and water features were further differentiated by utilizing a threshold value of zero in the raster calculator to produce a binary raster image which was then polygonized for shoreline tracing.

Data Analysis. The NSM, SCE, EPR, and LRR were calculated using DSAS in ArcGIS 10.4. Three sets

of shoreline data were calculated and the separation of shoreline images was based on the image acquisition dates. The set 1 and 2 images were acquired near the March and September equinox respectively, while set 3 contained only the earliest and most recent shoreline. The shorelines included in each set are shown in Table 1.

Table 1. Shoreline data used in each calculation.

Set	Shoreline Data (in years)	# of shorelines	Calculations
1	1993, 1996-1998	4	NSM, SCE, EPR, and LRR
2	2004, 2006, 2008, 2009, 2011, 2013-2020	13	NSM, SCE, EPR, and LRR
3	1993, 2020	2	NSM and EPR

The calculation of NSM, SCE, EPR, and LRR values was conducted using the calculate function in DSAS with a 90% confidence interval. ArcGIS-DSAS generated reports for the three sets.

The NSM is the distance between the oldest and earliest shoreline data identified by DSAS based on the exact shoreline dates parameter inputted in ArcGIS. SCE is the greatest distance between each transect. For NSM, positive and negative values mean accretion and erosion respectively, while the SCE is always positive. Both NSM and SCE are in meters. For the EPR, DSAS divided the NSM by the time elapsed between the two shorelines but the variation of the rate over time was not considered. The LRR is the slope of the line generated by a least-squares regression fit to all available shoreline points for each transect. The regression line is the minimum sum of the squared residuals. The squared residual for a data point is the square of the offset distance from the regression line. Both rates are in meters per year.

Results and Discussion. - The results and discussion were divided into six parts namely: acquired satellite images, processed satellite images, traced and extracted shorelines, shoreline change values, shoreline change rates, and shoreline forecasting. All values were generated using the ArcGIS-DSAS function and can be seen in the raw data tables found in the supplementary data section of the journal. Sets 1 and 2 each had a total of 283 transects while set 3 had 294 transects in total.

Acquired Satellite Images. There were 18 Landsat images gathered in total, with nine Landsat 4-5 images from 1993 to 2011, and another nine Landsat 8 images from 2013 to 2020. The images obtained all had spatial resolutions of 30 m, contained clear views of the shoreline, and were captured near the two equinoxes during times ranging from 9:00 AM to 10:30 AM MPST. The tide conditions varied with heights ranging from -0.03 m to 1.67 m. It was determined that three images in set 1, eight images in set 2, and one image in set 3 were taken during low tide. The lack of uniform conditions contributed to increased positional change due to the comparison of shorelines during high and low tides. The images from set 1 and set 2 were also taken in different monsoon seasons, which may affect the tidal conditions. No visible deviations were observed during the conduct of visual analyses, thus, the georeferenced images were concluded to be correct.

Processed Satellite Images. All satellite images were successfully subjected to image processing techniques starting with uniform cropping, atmospheric correction, and RGB enhancement. The enhanced images increased shoreline definition due to the color contrast in the land and water areas and the use of the water index enhanced the open water features and suppressed the built-up land noise. This enabled the creation of binary raster images with clearly defined separations of the land and water features for easier shoreline extraction.

Traced and Extracted Shorelines. All vector images were cropped and traced based on the study area coordinates. The x-components were the same for all images. However, the y-components of the traced endpoints varied, showing that the shoreline changed over the years. The traced shoreline vectors had sharpened edges due to the 30 m x 30 m pixels, but were not subjected to smoothing to preserve the defined geographical accuracy of the shorelines. Three datasets, shown in Table 1, were then created where images taken near the same equinox were grouped together to ensure uniform conditions for shoreline analysis.

Shoreline Change Analysis. The shoreline change experienced in the study area was analyzed using the SCE and NSM values generated by ArcGIS-DSAS and can be found in the supplementary data section.

Shoreline Change Envelope. The SCE represents the greatest distance among all intersecting shorelines in a given transect. This alone does not indicate if the change is erosional or accretional since it is always positive. The SCE calculations involved set 1 and set 2 shoreline data, shown in Figures 2.a and 2.b, respectively.

The shorelines in set 1 had an average SCE distance of 30.50 m. The greatest distance of 96.24 m in transect 146 showed that the shoreline eroded from 1993 to 1996. For set 1, 55 null values or transects with no observed shoreline position changes were generated, resulting in a minimum distance of 0. These null values were attributed to the low Landsat 4-5 resolution which prevented the detection of changes below 30 m [20].

For set 2, the 13 shorelines were calculated to have an average SCE distance of 61.54 m which is approximately two times greater than that of the previous set or an increase of 101.77%. The greatest distance observed in transect 61 showed that the shoreline accreted by 113.77 m from 2013 to 2020. In set 2, no null values were generated and a minimum distance of 30.01 m was observed in transect 8.

The SCE values show that in the period from March 1993 to 1998, shoreline changes ranged from 0 m to 96.24 m while from September 2004 to 2020, changes ranged from 30.01 m to 113.77 m. These results do not indicate whether the observed changes are mostly erosional or accretional and thus, require

supplemental data from the NSM values. However, it can be said that the greatest changes observed in sets 1 and 2 are erosional and accretional respectively.

Net Shoreline Movement. The NSM represents the distance between the oldest and most recent shorelines for each transect. The NSM values of the 3 sets were generated and analyzed in relation to the SCE values and contained both the negative or erosional and positive or accretional values. The NSM calculations involved all three sets of shoreline data, shown in Figures 3.a for set 1, 3.b for set 2, and 3.c for set 3.

For set 1, among the 283 transects, 47% or 133 were erosional, 25.09% or 71 were accretional, while 27.9% or 79 were null. The maximum negative value of -64.16 m at transect 146 also had the greatest SCE of 96.24 m from 1993 to 1996. This suggests that from 1996 to 1998, transect 146 accreted by 32.08 m. The shoreline changes from March 1993 to 1998 ranged from -64.16 m to 63.17 m. The average distances indicate that despite having greater accretion in terms of magnitude, the presence of more erosional transects led to an average distance of -6.04 m, which is considered erosional.

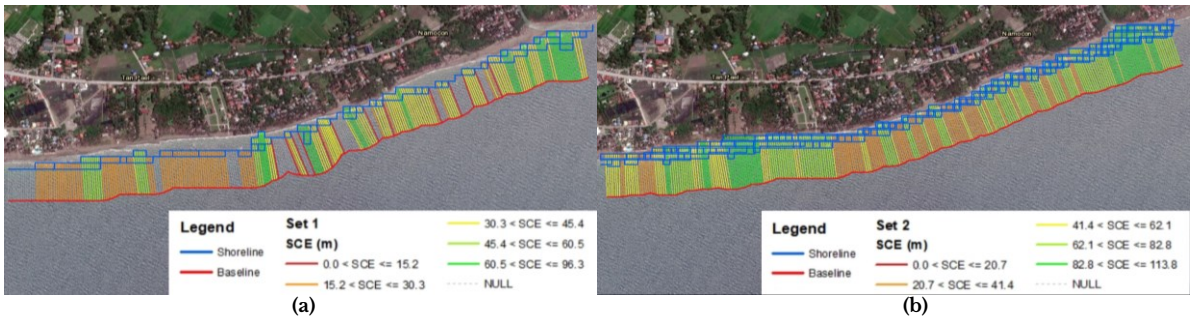

(a) (b)

Figure 2. The shoreline change envelopes of (a) set 1, and (b) set 2.

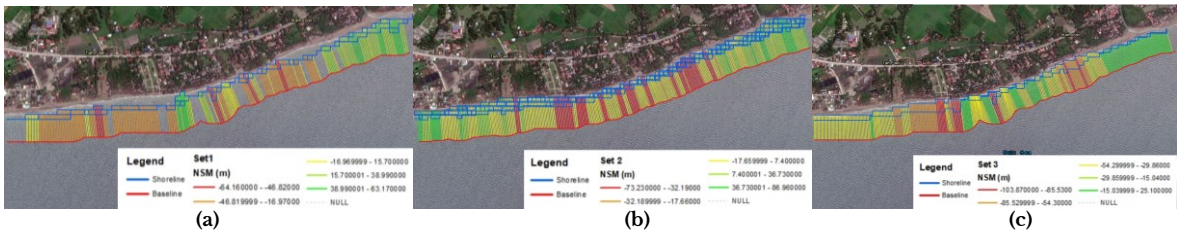

(a) (b) (c)

Figure 3. The net shoreline movements of (a) set 1, (b) set 2, and (c) set 3.

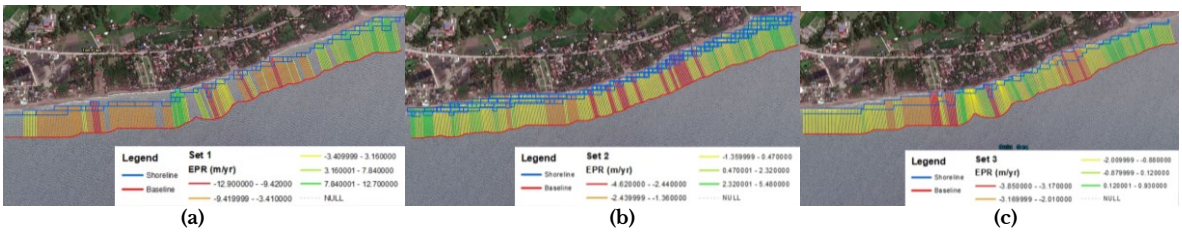

(a) (b) (c)

Figure 4. The endpoint rates of (a) set 1, (b) set 2, and (c) set 3.

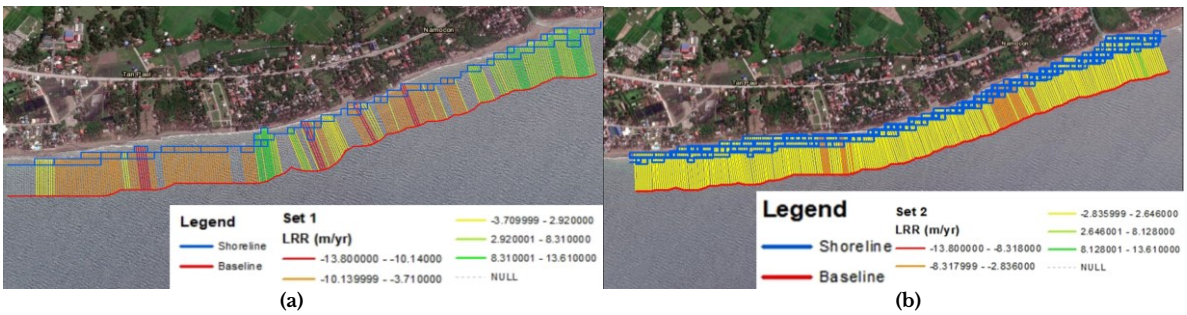

(a) (b)

Figure 5. The linear regression rates of (a) set 1, and (b) set 2.

Relative to set 1, the average erosion in set 2 decreased by 13.58 m while the average accretion decreased by only 3.22 m.The positive distances were also greater than the negative distances. These show that from 2004 to 2020, more parts of the shoreline eroded but the accretional areas had greater changes resulting in an average of only -1.99 m, which is 67.05% less than that of set 1.

Set 3 had the most and least number of erosional and accretional transects with 90.82% and 9.18% of the total, respectively. The shoreline changes ranged from -103.37 m to 25.1 m. The high maximum erosion and number of erosional transects contributed to a high average erosion of -41.3 m, while the average accretion was only 19.25 m. Thus, the average NSM from 1993 to 2020 was -35.74 m.

The average NSM in set 3 is significantly greater than that of sets 1 and 2. This high average can be attributed to the high shoreline erosion from 1998 to 2004 since the changes during this period were not investigated due to image availability.

Shoreline Change Rate Analysis. The rate of change experienced by the shoreline was calculated using the EPR and LRR methods in ArcGIS-DSAS and can be found in the supplementary data section.

Endpoint Rate. The EPR calculates the shoreline change rate based on only two shorelines. The average NSM distances were divided by the time elapsed between the oldest and most recent shorelines to generate the EPR values. The EPR calculations involved all three sets of shoreline data, shown in Figures 4.a for set 1, 4.b for set 2, and 4.c for set 3.

For set 1, the null transects prevented DSAS from determining the average CI associated with rates, reduced n, uncertainty, and transects with statistically significant erosion or accretion. The maximum rates for set 1 are significantly greater than that of the other sets while the average rates lowered to values closer to that of the other sets, leading to an EPR of -1.21 m per year.

For set 2, 35.94% of the 192 erosional transects and 96.70% of the 91 accretional transects were statistically significant. Accretional rates were also greater than the erosional rates. These explain why despite having more erosional transects, the average NSM and EPR of this set are low, leading to set 2 having the least EPR of -0.13±0.89 m per year.

Set 3 had the lowest maximum erosion rate and an average erosion rate that is only 50.83% of set 1. However, it had the lowest accretion rates, leading to set 3 having the highest average EPR of -1.32±0.52 m per year.

Linear Regression Rate. The LRR used all available shorelines to determine the change rate and was performed for sets 1 and 2, shown in Figures 5.a and 5.b, respectively.

The LRR of set 1 had fewer null transects than the EPR, showing that more changes occurred in 1996 and 1997. The maximum rates increased by less than 1 m per year with the addition of the 1996 and 1997 shorelines, but the average rates significantly increased by more than 100% of the EPR rates. This showed that the shoreline experienced more changes in 1996 and 1997 compared to just 1993 and 1998. However, the LRR of -1.23 m per year differed from the EPR by only 0.02 m, suggesting that despite having more changes, the erosion and accretion rates still balanced out to result in a similar average rate.

The LRR of set 2, shown in Figure 5 (b), had more erosional and less accretional transects than the EPR. This was also true for transects with statistically significant erosion and accretion. These can be attributed to the shorelines that were not included in the EPR calculations. The average erosion and accretion rates were greater and lesser, respectively, than the EPR. The LRR of -1.22±0.72 m per year is nine times the EPR which also indicates that despite the few differences in the 2004 and 2020 shorelines, the shorelines between them experienced more erosion and less accretion, resulting in the high erosional LRR.

Shoreline Forecasting. Using the LRR of set 2, the DSAS forecaster predicted that in 2030 and 2040, erosion will occur in most transects while accretion is observed in areas near the shoreline ends but are mixed with erosional transects. The part of the shoreline from 10° 40' 7.413" to 10° 40' 19.7292"N latitude and 122° 23' 27.4266" to 122° 24' 12.4158"E longitude is expected to erode by 2030 and 2040 and these areas contain most of the human settlements in the study area.

Figure 6. The forecasted shoreline positions for 2030 and 2040.

Limitations. The study utilized shorelines from years with Landsat images that fit the set criteria, thus, not all years from 1993 to 2020 were included in the calculations. Due to availability, low-resolution images were utilized resulting in the presence of null transects which prevented the calculation of certain values. No physical investigations were conducted due to safety concerns amidst the pandemic. Further investigation of the factors affecting the identified shoreline changes, as well as the verification of the predicted shoreline positions, was not performed.

Conclusion. - The shoreline change values showed that more parts of the shoreline eroded from 2004 to 2020 but a greater magnitude of erosion was observed from 1993 to 1998. The erosion from 1993 to 2020 was significantly greater than that of the other sets, suggesting that most occurred from 1998 to 2004. This was supported by the EPR and LRR calculations which showed that the 1993 and 2020 shorelines also had the least accretion rates and the most and least transects with statistically significant erosion and accretion respectively. It can be concluded that the

shoreline in Tigbauan, Iloilo experienced more erosion than accretion in both occurrence and magnitude from 1993 to 2020. The average shoreline change rates ranged from -0.13 to -1.32 m per year, showing that the shoreline is eroding at an average change rate of -1.022 m per year. The average LRR from September 2004 to 2020 was used to forecast that erosion will continue in 2030 and 2040 for the majority of the shoreline. These data can be used to improve the municipality's coastal management by identifying which areas are vulnerable to shoreline erosion and coastal area loss.

Recommendations. - More shoreline images with better resolutions are recommended to provide more accurate shoreline change rates. An effective smoothing function with a clearly defined accuracy may also be applied to extracted shoreline vectors prior to shoreline calculation. Moreover, adding the tidal level and monsoon season to the image criteria and considering the digitization uncertainty will enable more uniform shoreline conditions and accurate calculations. Physical shoreline inspection should be conducted to obtain more information that could contribute to the analysis. Supplementary data such as daily rainfall, typhoon tracks, and conducted human activities are recommended to understand the factors affecting shoreline change. Lastly, the shoreline change rate should be verified further so it can be utilized to accurately predict future shoreline positions.

Acknowledgment. - The authors would like to extend their gratitude to the external panelists and reviewers who, through imparting their wisdom, have helped improve the quality of the study.

References

[1] Armenio E, Serio FD, Mossa M, Petrillo AF. 2019. Coastline evolution based on statistical analysis and modeling. Natural Hazards and Earth System Sciences. 19(9): 1937–1953.

[2] Aryastana P, Ardantha IM, Candrayana KW. 2018. Coastline change analysis and erosion prediction using satellite images. MATEC web of conferences. 197: 13003.

[3] Parthasarathy KSS, Deka PC. 2019. Remote sensing and GIS application in assessment of coastal vulnerability and shoreline changes: a review. ISH Journal of Hydraulic Engineering. 1–13.

[4] Kostecki R. 2018. Application of the spatial database for shoreline change analysis and visualisation: Example from the western polish coast, southern Baltic sea. Quaestiones Geographicae. 37(3): 25–34.

[5] Louati M, Saïdi H, Zargouni F. 2014. Shoreline change assessment using remote sensing and GIS techniques: a case study of the Medjerda delta coast, Tunisia. Arabian Journal of Geosciences. 8(6): 4239–4255.

[6] Sutikno S, Sandhyavitri A, Haidar M, Yamamoto K. 2017. Shoreline change analysis of peat soil beach in bengkalis island based on GIS and RS. IACSIT International Journal of Engineering and Technology. 9(3): 233–238.

[7] Thieler E, Himmelstoss E, Zichichi J, Ergul A. 2017. Digital Shoreline Analysis System (DSAS) version 4.0—An ArcGIS extension for calculating shoreline change. U.S. Geological Survey Open-File Report. 2008–1278.

[8] Foti G, Barbaro G, Bombino G, Fiamma V, Puntorieri P, Minniti F, Pezzimenti C. 2019. Shoreline changes near river mouth: case study of Sant'Agata River (Reggio Calabria, Italy). European Journal of Remote Sensing. 52(4): 102–112.

[9] Flores PC, Siringan F. 2020. Shoreline Change in Response to the Construction of a Flood Canal in Jaro, Iloilo City, Philippines. IEEE India Geoscience and Remote Sensing Symposium (InGARSS). 134-137.

[10] Liu Y, Wang X, Ling F, Xu S, Wang C. 2017. Analysis of coastline extraction from Landsat-8 OLI imagery. Water. 9(11): 816.

[11] Friedrich C. 2014. Comparison of ArcGIS and QGIS for Applications in Sustainable Spatial Planning [thesis]. [Masterarbeit]: University of Vienna.

[12] Deepika B, Avinash K, Jayappa KS. 2013. Shoreline change rate estimation and its forecast: remote sensing, geographical information system and statistics-based approach. International Journal of Environmental Science and Technology. 11(2): 395–416. doi:10.1007/s13762-013-0196-1.

[13] Foster ER, Savage RJ. 1989. Methods of Historical Shoreline Analysis, in: Proc. Coastal Zone '89, ASCE, New York, USA.

[14] Climate Central Organization. Coastal Risk Screening Tool: Sea level rise and coastal flood risk maps. Climate Central. [accessed 2020 December 12]. Available from: https://coastal.climatecentral.org/map.

[15] Department of Environment and Natural Resources, Bureau of Fisheries and Aquatic Resources of the Department of Agriculture, and Department of Interior and Local Government. 2001. Philippine Coastal Management Guidebook No. 8: Coastal Law Enforcement. Coastal Resource Management Project of the Department of Environment and Natural Resources, Cebu City, Philippines, 164 p.

[16] Bañas JCC, Subade RF, Salaum DN, Posa CT. 2019. Valuing vanishing coasts: The case of Miagao coastline in Southern Iloilo, Philippines. Ocean & Coastal Management.

[17] Sridharan S. 2017. Solar and lunar tidal variabilities in GPS-TEC and geomagnetic field variations: Seasonal as well as during the sudden stratospheric warming of 2010. Journal of Geophysical Research: Space Physics. 122(4): 4571–4587.

[18] Congedo L. 2020. Semi-Automatic Classification Plugin Documentation Release 7.0.0.1.

[19] Xu H. 2006. Modification of Normalized Difference Water Index (NDWI) to Enhance Open Water Features in Remotely Sensed Imagery. International Journal of Remote Sensing. 27. 3025–3033.

[20] White K, Asmar HME. 1999. Monitoring changing position of coastlines using Thematic Mapper imagery, an example from the Nile Delta. Geomorphology. 29(1-2): 93–105. doi: 10.1016/s0169-555x(99)00008-2.

Research Events

The Research Events circuit is the series of research-related activities prepared by the Research Unit and/or the scholars with the aim of bringing their studies to the community. The logo to the left is the overarching symbol of the events circuit. The multicolored flame represents the multitude of activities the scholars undertake as embodied in each of the event logos. The interwoven circles represent the infinite possibilities in research. The logo itself is reminiscent of the PSHS logo, representing the values of truth, excellence, and service.

START OF SCHOOL YEAR

BANTALA
Hiligaynon
"to inform"
G12

PAGBANTALA
VIRTUAL RESEARCH CONGRESS

PAGBANTALA is the first event in the circuit. It is a virtual research congress where scholars present their studies to a panel of experts. The logo therefore features a caricature of the main scene in Pagbantala: a panel of three, sitting behind the table facing the scholars and their presentation – collectively represented by the incomplete frame. As the first event, Pagbantala is colored red, symbolizing the flames igniting the Research Circuit.

PAGBALANDRA
VIRTUAL POSTER PRESENTATION

PAGBALANDRA is where scholars present their posters to an audience. The logo therefore features a caricature of an individual presenting his/her poster. Scholars prepare and showcase three materials: a technical poster for professionals, a community poster for elementary school students, and a headline poster to capture their audience's attention.

BALANDRA
Hiligaynon
"to show"
G12

HINUNAN-ANON
Hiligaynon
"to inquire"
G11

PAGHINUN-ANON
GRADE 11 RESEARCH SEMINAR

PAGHINUN-ANON is an event for Grade 11 scholars. As in Pagbantala, the logo features the main scene in Paghinun-anon: the work unit, a group of scholars, and a three-man panel meet virtually to discuss the research proposal, with the panel guiding the scholars in their proposed study. The logo is yellow – a joyful color – as this is a time of celebration, the first step towards realizing a research study in the research curriculum.

PAHISAYOD
RESEARCH WORKSHOPS & GIMMICKS

PAHISAYOD is among the largest events in the circuit. This year's version had scholars present their study to elementary studies in the form of interactive games and gimmicks. The logo therefore shows two individuals: one representing the scholars, the other the students they are presenting to, and the white matter being the knowledge shared in this event. The green marks a transition in energy, as events move from being school-based to community-based.

HISAYOD
Hiligaynon
"to announce"
G12

Cont'd

Cont'd

PAGWARAGWAG
COMMUNITY-BASED RESEARCH CONGRESS

WARAGWAG
Hiligaynon
"to broadcast"

G12

PAGWARAGWAG is Pagbantala, Pagbalandra and Pahisayod combined into one virtual congress, with students from different schools in attendance. This is represented in the logo's caricature which shows a group of individuals facing a group of three: the scholars. The incomplete frame that represented the scholars in Pagbantala are now complete researchers in Pagwaragwag with the ability to communicate science in an elementary and secondary level.

PAINDIS-INDIS
JOURNAL COVER PAGE COMPETITION

INDIS-INDIS
Hiligaynon
"to compete"

G12

PAINDIS-INDIS is a campus-wide cover page competition. This is how the cover of Publiscience is decided. Hence, the logo shows multiple panels that showcase each submission and two individuals which are shown holding similar panels, as if they were issuing a vote. Several of Batch 2021's work units submitted an entry, the number of which is reduced in every stage of voting with the teachers issuing the final vote.

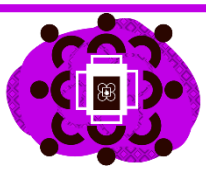

PAGPABALHAG
RESEARCH JOURNAL PUBLICATION

PABALHAG
Hiligaynon
"to publish"

G12

PAGPABALHAG is the event that formally launches this year's Publiscience issue. Through the journal, the audience of the scholars' studies is expanded, networking through various individuals or groups that possess a copy. This is represented in the logo by caricatures of individuals surrounding the journal, giving it the collective shape of an atom, which can diffuse through borders and catalyze the exchange of knowledge. The atom is reminiscent of the PSHS logo, a symbol of the institution which nurtured the scholars up to this point.

PAGSUGIDADON
GRADE 10 RESEARCH CONGRESS

SUGUID
Hiligaynon
"to report"

G10

PAGSUGIDADON is the culminating event for Grade 10 scholars. Work units composed of five scholars present their study to a panel. In the logo, the five scholars are shown, the descending white matter representing their initiation into the research process. The white-grey color represents a blank slate, scholars that are ready to be molded, brimming with unknown potential.

END OF SCHOOL YEAR

KEYWORD INDEX

A
acrolein, 20, 21, 22, 23, 24, *25*
adsorption, 67, 68, 69, 70
Aedes aegypti, 14, *15*, 16, 17, 18, 19
agar well diffusion method, 39, 40
algal growth, 82, 84, 86
antibacterial gel, 39, 40, 42
artificial intelligence, 88, 89, 90, 92
Artocarpus heterophyllus, 14, *15*, 16, 17, 18

B
banana, 93, 94, *95*, 96, 97, 98
biolarvicide, 14, *15*, 16, 17, 18
bunker fuel, 67, 68, 69

C
calcium, 63, 64, *65*, 66
carbon dioxide, 88, 89, 90, 91, 92
cellulose, 27, 28, 29, 30, 31
Chanos chanos, 99, 100, 101, 102, 103, 104
climatological analysis, 2
coastal vulnerability, 112, 117
COI gene, 77, 78
cooking oil fumes, 20, 21, 22, 24
corn husks, 67, 68, 69, 70
Crassostrea iredalei, 8, 9, 10, 11, 13
cyanobacteria, 82, 83, 84, *85*, 86

D
data science, 90, 91, 92
desalination, 32, 33, 34, *35*, 36, 37
DNA, 77, 78, 79, 80, 81
DNA barcoding, 77, 78, 80, 81

E
extraction, 27, 28, 29, 30

F
formalin, 99, 100, 101, 102, 103, 104
freshwater gastropods, 77, 78, 80
FTIR, 8, 9, 11, 12

G
GIS, 106, 107, 108, 110, 111
GIS techniques, 112, 113, 117
graphene oxide, 32, 33, 34, 35, 36, 37
green mussels, 72, 76

H
habagat, 2, 3
humic acid, *52*, *53*, *54*, *55*, *56*, *57*
hydropriming, *58*, *59*, 60, 61

I
image analysis, 93, 96, 97, 98
image processing, 99, 104
induction time, 20, 21, 22, 23, 24
inhibitor, *45*, 46, 47, 48, *50*
Ipomoea reptans, *52*, *53*, *54*, *55*, *56*, *57*
Irradiance, 82, 83, 84, *85*, 86

J
Jalaur River, 77, 78, 80, 81

K
KOH digestion, 8, 9, 10

L
larvicidal bioassay, 14, *15*, 16
Lyngbya majuscula , 82, 83, 84, *85*, 86

M
mapping, 106, 111
microplastic, 8, 9, 10, 11, 12, 13
microwave-assisted, 27, 28, 30
molecular docking, *45*, 46, 47, 49

N
nanoporous membrane, 32, 36
natural antioxidants, 20, 23, 24, *25*
neural network, 88, 89, 90, 91, 99, 100, 104

O
oil spill, 66, 68, 69
Oryza sativa, 32, 33, *35*
Oryza sativa L., *58*, *59*, 60, 61
oxidative stability, 20, 21, 22, 23, 24, *25*
oyster, 8, 9, 10, 11, 12, 13

P
Perna viridis, 72, 73, 74, *75*, 76
phytochemical analysis, 14, *15*, 17
phytochemicals, *45*, 46, 47, 48, 49
plant extract, 39
plant growth and yield, *52*, *55*
powdered eggshells, 63, 64, *65*
precipitation, 2, 3, 6
preservation, 72, 73, 74, *75*
Pseudomonas aeruginosa, *45*, 46, 47, 48, 49, *50*
Python, 93, 94, *95*, 96

R
rainfall, 2, 3, 4, *5*, 6
randomized complete block design, *52*, *53*, *57*
remote sensing, 112, 113, 117
rice husks - 67, 68, 69, 70
ripening stage, 93, 94, *95*, 96, 97, 98
RUSLE, 106, 107, 108, 109, 110, 111

S
salt stress, *58*, *59*, 60
satellite imagery, 88, 90, 92, 112
seedling vigor index, *58*, *59*, 60, 61
shelf life, 72, 76
shoreline change, 112, 113, 114, *115*, 116, 117
sodium chloride, *58*, *59*, 60
sodium lactate, 72, 73, 74, *75*, 76
soil amendment, 63, 64
soil erosion, 106, 107, 108, 109, 110, 111
southwest monsoon, 2, 3, 6
specific growth rate, 82, 83, *85*
Stachytarpheta jamaicensis, 39, 40, 42, 43
Staphylococcus aureus, 39, 40, 41, 42
SVM, 93, 94, *95*, 96, 97, 99, 100, 101, 102, 103

T
Tour method, 32, 33, 34, *35*, 36, 37
trehalose-6-phosphate phosphatase, *45*, 46, 47, 48, 49, *50*

U
urea, *52*, *53*, *54*, *57*

V
Vigna radiata, 63, 64, *65*, 66

W
watershed, 106, 107, 108, 109, 110, 111

Y
yield, 27, 28, 29, 30

Z
Zea mays var. ceratina, 27, 28, 29, 30

INSTITUTIONAL PARTNERS

The authors of this volume would like to recognize the unequivocal contribution of the following institutions for opening its facilities to the researchers, and extending consultative and technical support in the conduct of their studies:

Colorado School of Mines

Department of Agriculture - Region VI (DA-VI)

Department of Agriculture– Western Visayas Integrated Research Center (DA-WESVIARC)

Department of Environment and Natural Resources – Region VI (DENR-VI)

Department of Science and Technology – Industrial Technology Development Institute (DOST-ITDI)

Department of Science and Technology – Regional Standards and Testing Laboratories Region VI (DOST-RSTL VI)

Local Government Unit of Calinog

National Institute for Environmental Studies, Japan

Pharma GalenX Innovations Inc.

Philippine Coast Guard

Public Safety and Transportation Management Office

Southeast Asian Fisheries Development Center (SEAFDEC)

Science Integrated Direction for Highschool Investigators (SIDHI) Mentorship Community

University of the Philippines – Visayas Regional Research Center (UPV-RRC)

ACKNOWLEDGMENT

The authors of the studies in this journal extends their warmest appreciation, first and foremost, to the institution of Philippine Science High School - Western Visayas Campus for nurturing their scientific abilities and technical capabilities for the pursuit of the untarnished truth. In addition, this publication would not have been possible without the continuous support, patience, and guidance of the Research Committee of the aforementioned institution.

Finally, the authors would like to express their deepest gratitude to the science research assistants (SRA), research teachers, research advisers, faculty and staff, and families and friends who provided counsel and support, and served as an inspiration in pursuing their aspirations.